Metals and superoxide dismutase-1 proteinopathy in progressive supranuclear palsy

Jessica Louise Billings

BSc (Hons), MSc (Neuroscience)

A thesis submitted in the fulfilment of the requirements of the degree of Doctor of Philosophy

2024

ORCID: 0009-0006-4317-1397

The department of Anatomy and Physiology

Faculty of Medicine, Dentistry and Health Sciences

The University of Melbourne

Declaration

I, Jessica Louise Billings hereby certify that;

i. this thesis comprises of my own original work is submitted into the total requirement of the degree of Doctor of Philosophy.

ii. Acknowledge the contribution of the various peoples

iii. The thesis is fewer words than 100,000 in length (excluding, figures, tables, references and appendices)

COVID-19 impact statement

The barriers I have faced to my research have been significant since I began my PhD candidacy in 2020. My first year began with lockdowns due to the COVID-19 pandemic, which began shortly after my enrolment. My initial supervisor was relocating laboratories on university campus at the beginning of the year, which had to cease because of lockdown restrictions. Our laboratory facilities were not operational and had little to no access to other sites after the notice of essential work could begin, including studies to resume onsite under strict guidelines. In addition, I lost valuable time for training for my necessary experiments using a chemical imaging system, the core analytical technique that was the foundation of my thesis. Due to the on-and-off lockdowns that occurred across Melbourne (Australia) in 2020, I spent most of my time working from home and operating at different times of the day or night while homeschooling my two children. By the end of the year, my primary supervisor had lost his funding and position at the university. Consequently, I was put in a position at the end of the first year of my candidacy where I needed to find a new supervisor. I was fortunate to find new supervisors on campus with similar research interests. The foundational aim of my PhD project was aimed to develop novel imaging applications combining histology and analytical chemical imaging analysis to help diagnose and classify subcases of progressive supranuclear palsy. However, my thesis was completely restructured since I transferred to a new supervisory panel, removing the analytical chemical imaging component, and deemphasising the histological component, and replacing these methods with biochemical methodologies related to copper biology. Consequently, I had to rewrite my human ethics applications for obtaining new tissues, specifically frozen tissues for biochemical analysis. In 2022, my new supervisor was moving laboratories within the campus which meant there was some down time to help relocate and recommission the lab in a new facility. This new laboratory was also within another department and therefore required me to change my enrolment again to another department. In spite of all the obstacles I encountered over the years, I am grateful for the opportunity to complete my doctorate.

Preface

This thesis presents work that has been published with co-authors for Chapter 1 (including the abstract) have been peer-reviewed and published as described in publications arising from this thesis sections.

The contribution of others is recognised and is stated below.

I acknowledge the following people have contributed to the experiments described in this thesis:

- Ms Celeste Mawal (The Florey Institute Neuroscience and Mental Health) and mental health for running homogenates and tissues samples for ICPMS.
- A/Professor David Bishop (University of Technology, Sydney) for running human brain tissue sections for LA-ICPMS.
- A/Professor Peter Crouch (University of Melbourne) help with perfusion and taking animal tissues.
- Ms Fairlie Hilton (Victorian Brain Bank, The Florey Neuroscience Institute and Mental Health) for suppling the human frozen samples.
- Dr Geoff Pavey (Victorian Brain Bank) for sectioning the human frozen samples.
- Ms Heather McCann (University of Sydney, Sydney Brain Bank) for sectioning and suppling the human paraffin and frozen samples.
- Professor Catriona McLean (University of Melbourne/The Florey Institute of Neuroscience and Mental Health, Victorian Brain Bank) for neuropathological and clinical expertise for case diagnosis.
- Professor Glenda Halliday (University of Sydney, Sydney Brain Bank) for their neuropathological and clinical expertise for case diagnosis.
- Dr Nichollas Scott (The Peter Doherty Institute/University of Melbourne) for preparing and running the proteomics experiments.
- Ms Tina Cardonme (Phenomics Australia Histopathology and Slide Scanning Service /University of Melbourne) for scanning the human frozen brain sections.
- Ms Amelia Sedjahtera (The Florey Institute of Neuroscience and Mental Health) for helping with microscope troubleshooting and making PFA buffer.

- Dr Ian Birchall (Histology and Neuropathology scientific service, The Florey Institute Neuroscience and Mental Health) for the staining human frozen sections with H&E.
- Dr Vicky Perreau (University of Melbourne) for her consult service for proteomic analysis.

Acknowledgments

To begin with, I want to express my gratitude to my supervisors A/Prof Peter Crouch, Dr Jeff Liddell and Dr James Hilton. In a time that was most precarious, I received a lifeline where I could continue my studies in a nurturing, supportive and professional environment. The decision to take on a new student in trying times was not an easy one, especially with the COVID-19 pandemic still ongoing. However, I will be forever grateful at their generosity in welcoming me to their lab and sharing new ideas, concepts and teaching me new methods. I have had the genuine pleasure of working with Peter, Jeff and James, your contribution to medical research embodies integrity, humility, and a high level of dedication. Besides all the hinderances that we have endured, the lockdowns and the stops and starts with experiments, I have had a wonderful experience, and I cannot thank you all enough.

I would also like to acknowledge my original primary supervisor Dr Dominic Hare to whom I have known since doing my Masters degree way back when. Thank you, Dominic for always believing in me and challenging me to go further in my career. Even though you were not there with me to the end, you were the match that lit the fire in me to continue and that is something that cannot be taken away.

I would like to extend my gratitude to my PhD advisory committee, A/Prof Isabelle Rouieller (Chair), Prof. David Finkelstein and A/Prof. David Bishop. Thank you all for your support throughout my candidature and always being in my corner. My sincere thanks go out to you for guiding me through such an uneasy time, including supporting me through the Covid-19 pandemic (and all the paperwork included) as well as giving me advice to move on from such instability.

To the many people who I have worked with throughout the years and who were also there for me during the last 4 years of my candidature, I would like to thank you for your help with experiments and bouncing ideas with but to also thank you for your friendship, wisdom and advice (Amelia, Lydia, Lisa, Ian, Celeste). To my work colleagues over at The Florey Institute of Neuroscience and Mental Health and the University of Melbourne, thank you all for being a wonderful bunch of scientists who really want to make a difference in the world. You all inspire me every day.

Lastly, to my family who have ridden every bump in this journey with me. I really couldn't have continued without you. You all have been my rock and my source of inspiration to pursue a career in helping people and to better understand the world. Thank you to my mum Wendy and my dad Geoff, for your encouraging words to keep me on track and your love and support throughout this time. To my amazing husband Shay, words cannot thank you enough for the sacrifices, the amount of washing you had to fold, dinners you had to prepare, kids parties you had to go to and for looking after our beautiful children during the times when I could not. I am so thankful for you in my life, you are wonderful and are everything to me. Thank you for being you. To my 2 beautiful children, Livinia and Lachie. Thank you for your unconditional love and support throughout my life. You have motivated and inspired me every day, always cheering me on with those happy faces and beautiful smiles. I am sorry I haven't there for you all and I know these last 4 years have been extremely hard on you and I have missed so many parts of your life. I dedicate this thesis to you because of you both having taught me to be resilient, to keep going even though it is tough and uncertain and that it will be all alright in the end. I love you all.

Publications arising out of this thesis

Billings, J. L., Hilton, J. B. W., Liddell, J. R., Hare, D. J. and Crouch, P. J. (2023) Fundamental Neurochemistry Review: Copper availability as a potential therapeutic target in progressive supranuclear palsy: Insight from other neurodegenerative diseases. *J Neurochem*. 167(3):337-346.

Author contribution statement to the above publication: JLB conceived the idea for this review, conducted the initial literature searches, and wrote the first draft. JBWH, JRL, DJH and PJC conceived the idea for this review and edited the first draft. All authors read and approved the final version.

List of Scholarships and awards

Scholarships

Australian Government Research Training Program Scholarship	2020 - 2023
COVID-19 Stipend extension (University of Melbourne)	2023 - 2024
Agilent Technologies Pty Ltd Studentship	2020 - 2022

Other sources of funding

Parkinson's Victoria Argrou Grant	2018 - 2020

Awards

Journal of Neurochemistry-ISN Trainee Merit Award	2023

Table of Contents

List of Figures

List of Tables

Abbreviations

AAS	atomic absorption spectrometry
AD	Alzheimer's disease
AGC	automated gain control
ALS	amyotrophic lateral sclerosis
ALDH1L1	aldehyde dehydrogenase 1 family member L1
AQP4	aquaporin 4
ATOX1	antioxidant chaperone 1
ATP	adenosine 5'-triphosphate
ATP7A	ATPase 7A
ATP7B	ATPase 7B
BA17	Brodmann's area17; primary visual cortex
BBB	blood brain barrier
BCS	bathocuproinedisulfonic acid
BSA	bovine serum albumen
CCS	copper chaperone for SOD1
CNS	central nervous system
COMMD1	copper metabolism murr1 domain
COX5A	cytochrome c oxidase Subunit 5A
COX5B	cytochrome c oxidase Subunit 5B
COX6B	cytochrome c oxidase Subunit 6B
COX6C	cytochrome c oxidase Subunit 6C
COX11	cytochrome c oxidase 11 chaperone
COX17	cytochrome c oxidase 17 chaperone
CSF	cerebrospinal fluid
CSFB	cerebrospinal fluid barrier
CTR1	copper transporter related 1
CX3CR1	CX3C motif chemokine receptor
DAB	3,3'-diaminobenzidine
DAPI	4',6-diamidino-2-phenylindole

DβH	dopamine beta hydroxylase
DDA	data-dependent acquisition
DIA	data-independent acquisition
DBS	deep brain stimulation
DOPAL	3, 4 dihydroxyphenylacetaldehyde
DMT1	divalent metal transporter 1
EDI	exposed dimer interface
ESD	esterase D / S-formylglutathione hydrolase
FDR	false discovery rate
FTDP-17	frontal-dementia with parkinsonism linked to chromosome 17
GABA	gamma-aminobutyric acid
$GABA_{A1}$	gamma-aminobutyric acid receptor A1
GAPDH	glyceraldehyde 3-phosphate dehydrogenase
GFAP	glial fibrillary acidic protein
GSK-3β	glycogen synthase kinase-3 beta
GPI	glycosylphosphatidylinositol-anchored
GSTP1	glutathione S-transferase Pi 1
GO	gene ontology
IBA-1	ionises calcium-binding molecule
KEGG	Kyoto Encyclopedia of Genes and Genomes
ICPMS	inductively coupled mass spectrometry
INA	intermediate filament protein alpha
LA-ICPMS	laser ablation inductively coupled mass spectrometry
LC MS/MS	liquid chromatography with tandem mass spectrometry
LFQ	label free quantification
MAOB	monoamine oxidase B
MAPT	microtubule associated protein tau
MFT1	metal regulatory transcription factor 1
MFT2	metal regulatory transcription factor 2
μPIXE	Micro-particle induced emission
MPTP	1-methyl-4-phenyl-1,2,3,6-tetrahydropyridine
MRI	magnetic resonance imaging

m/z	mass to charge
NADH	nicotinamide adenine dinucleotide + hydrogen
Nano-SIMS	nano-secondary ion mass spectrometry
NDUFA5	NADH:Ubiquinone Oxidoreductase Subunit A5
NDUFA9	NADH:Ubiquinone Oxidoreductase Subunit A9
NDUFS1	NADH:Ubiquinone Oxidoreductase Core Subunit S1
NDUFS8	NADH:Ubiquinone Oxidoreductase Core Subunit S8
NDUFV1	NADH:Ubiquinone Oxidoreductase Core Subunit V1
NEFH	Neurofilament heavy chain
NFS1	iron-sulfur cluster assembly proteins cysteine desulfurase
NFT	neurofibrillary tangles
NINDS	national Institute of neurological disorders and stroke
PBS	phosphate-buffered saline
PBS-T	phosphate-buffered saline tween
PD	Parkinson's disease
PET	positron emission tomography
PMI	post-mortem interval
PSP	progressive supranuclear palsy
PSP-P	progressive supranuclear palsy - Parkinsonism variant
PSP-RS	progressive supranuclear palsy - Richardson's syndrome variant
qPCR	quantitative polymerase chain reaction
RBFOX3	RNA binding fox-1 homolog 3
ROS	reactive oxygen species
SCO1	synthesis of cytochrome c oxidase 1 chaperone
SCO2	synthesis of cytochrome c oxidase 2 chaperone
SDB-RPS	styrenedivinylbenzene resin
SDS	sodium dodecyl sulphate
SLC31A1	solute carrier family 31 member 1
SOD1	superoxide dismutase 1
SP3	single-pot, solid-phase-enhanced sample-preparation
Sp1	specificity factor 1

STEAP	six transmembrane epithelial antigen of the prostate
TFA	trifluoracetic acid
TMEM119	transmembrane protein 119
TBS	tris-buffered saline
TBST	tris-buffered saline tween
TH	tyrosine hydroxylase
TUBB3	tubulin Beta-III
VIM	vimentin
XANES	X-ray absorption near edge structure
XFM	X-ray fluorescence microscopy

Abstract

Progressive supranuclear palsy (PSP) is a rare complex neurodegenerative condition which presents with clinical indicators resembling Parkinson's disease (PD). The challenge to this disease is to diagnose PSP in its early stages and this requires the identification of molecular pathways that underlie the disease and its progression.

To this end, examination of other neurodegenerative diseases has provided some insight to the pathways to neuronal death that may be important in PSP, with oxidative stress and dysregulation of metal availability implicated. The brain has a capacity to combat the formation and build-up of reactive oxygen and nitrogen species, but this capacity is diminished in the last few decades of human life [1]. Oxidative damage to proteins, lipids and nucleic acids is a pervasive feature of neurodegenerative disease and this extends to PSP [1-16]. This is likely because the brain has a high composition of fatty acids, is rich in metals, requires more energy than other organs to fuel neurotransmission, and has generally low concentrations of antioxidants [6]. The basal ganglia are illustrative of this, where neurons and glia in these regions are suggested to have a higher metabolic load and are more energy-intensive [17, 18]. ATP levels, metal concentrations, and antioxidant levels are significantly altered in the regions implicated in PSP as compared to non-neurological controls [19-22].

Recent reports indicate disrupted availability of copper to the copper-dependent frontline antioxidant superoxide dismutase 1 (SOD1) is an aberrant feature shared by idiopathic forms of PD and some forms of amyotrophic lateral sclerosis (ALS). Renamed in 1969 to reflect its enzymatic activity towards superoxide [23], SOD1 is essential, with genetic deletion resulting in cell death caused by ROS accumulation [24, 25]. As SOD1 has direct links with ALS, its role in this disease context has been extensively researched [26-38]. Mutations spanning the gene for SOD1 lead to protein aggregation and disease onset in familial forms of ALS and SOD1 aggregates are also evident in neurodegenerative diseases that do not involve mutant SOD1. Copper deficient SOD1 can misfold and form aggregates.

Herein, we used SOD1 specific antibodies to probe and quantify pathological changes in SOD1 in disease-affected regions with unabated neurodegeneration and gliosis of PSP. The accumulation and misfolding of SOD1 that was found in astrocytes in PSP brain tissue suggests

that there is a potential dysfunction in astrocytes. In order to better understand the factors that might be involved in SOD1 misfolding, we investigated the copper levels in the substantia nigra of PSP cases, one of the most affected regions with elevated levels of SOD1 pathology. The substantia nigra demonstrated low copper levels, with copper deficiency in subcellular regions containing SOD1 and other important cuproenzymes that require copper for their function. The decrease in copper availability did not affect SOD1 levels and activity within the substantia nigra in PSP. However, the copper-dependent ferroxidases ceruloplasmin and hephaestin levels had increased in parallel with iron levels in PSP; however, their activity did not change, suggesting a disconnect between expression and activity. Alterations in copper homeostasis were seen when the overall copper handling mechanisms were changed in PSP with 9 out of 20 genes significantly upregulated in PSP.

In order to determine if decreased copper availability influences pathological changes reminiscent of those observed in PSP, a mouse model with lower CNS copper levels was constructed with a partial genetic knockout of the primary copper importation mechanism (*Slc31a1*; encoding copper related transporter 1; Ctr1). Mice were aged to 9-10 months old and the substantia nigra samples were collected and assessed to observe changes in copper handling, accumulation of Sod1 and loss in neuronal cell numbers. It was found that, unlike what was observed in PSP, the substantia nigra did not show evidence of Sod1 accumulation or other pathological changes including gliosis, despite a significant decrease in copper levels within the substantia nigra and a modest loss of neuronal cells within the substantia nigra *pars compacta*. With no overall shift in copper handling, this suggests that these mice have the ability to maintain copper homeostasis despite a significant decrease in CNS copper levels.

Proteomic analysis of the PSP substantia nigra tissue provided a comprehensive assessment of disrupted cellular pathways contributing to pathogenesis. Using label free quantitation, 3146 proteins were identified within the substantia nigra proteome and of those proteins, 191 were differentially expressed in PSP. These proteins were involved in pathogenic pathways including dysfunction in the mitochondria, metabolism and within the cytoskeleton and not just limited to oxidative stress. These proteins were enriched within the Parkinson's disease pathway. Further characterisation showed that mitochondrial based copper

dependent oxidoreductases, monoamine oxidase b and the subunits for complex IV are altered in PSP implicating copper and its involvement in many of the disease pathways.

In conclusion to this thesis, our findings suggest a role for copper in PSP pathogenesis which could be a factor in the misfolding of SOD1 and causing dysfunction in astrocytes which help provide support to neurons and supply the necessary copper to other cells within the CNS. A closer examination of copper changes in PSP within specific CNS cells might determine where copper may be distributed and might provide a novel target for future drug development.

Chapter 1. Introduction to progressive supranuclear palsy

Progressive supranuclear palsy (PSP), an atypical Parkinson syndrome, is now considered to be the second most common parkinsonism, after idiopathic Parkinson's disease (PD) [39]. It was recognised as its own syndrome by Richardson, Steele and Olszewski in 1963 through observation of characteristics uncommon in most PD patients, including unexplainable falls, supranuclear gaze, furrowed brow, pseudobulbar palsy, axial rigidity, and mild dementia [40]. PSP is still frequently misdiagnosed as PD due to broad overlap in clinical features, making the prevalence of PSP (approximately 7.1 per 100,000 pooled global figure) a likely underrepresentation [41]. Clinical symptoms are the result of rapid loss of neurons within the basal ganglia, brainstem, and cerebellum. The progression of neuronal cell loss after diagnosis is rapid and there are no reliable biomarkers or treatments currently available.

The aetiology of PSP is unknown, with age and environmental factors, along with common genetic variability in *MAPT* (tau gene) being the only known risk factors [42-44]. Tau pathology in glia and neurofibrillary tangles in surviving neurons within affected regions of the brain provide cardinal hallmarks of PSP pathology confirmed post-mortem [39, 45-55]. Outside of tau pathology, however, the understanding of other molecular mechanisms involved in the propagation and progression of the disease is relatively limited.

1.1 Aetiology, genetic and environmental contributions to PSP

PSP is typically diagnosed at an average age of 65 years and lasts an average of 6 years since diagnosis, but it is unknown what causes the disease [56]. Unlike other neurodegenerative conditions, PSP cases are all sporadic, most likely arising from complex gene-environment interactions.

1.1.1 Genetic contributions

PSP is traditionally considered a sporadic disease, notwithstanding evidence of familial clustering [57-60]. Having been considered a tauopathy, it is not surprising that *MAPT* mutations have been a focal point of genetic contributions to PSP. While there have been reports of familial and sporadic cases with de novo mutations in *MAPT* [58, 61] and another

parkinsonian gene, leucine-rich repeat kinase 2 (PARK8 gene), these patients present with PSP-like characteristics but are not definitively confirmed as PSP [62]. The risk of developing PSP is elevated with a 5.6-fold increase if H1/H1 haplotype is present [63] and is more commonly associated with typical PSP cases [54]. Two extensive whole genomic-based screening studies have identified other possible gene loci associated with PSP, including myelin-basic binding protein, syntaxin 6, and eukaryotic translation initiation factor 2 alpha kinase 3 [64, 65]. It is reasonable to associate myelin-basic binding protein, syntaxin 6, and eukaryotic translation initiation factor 2 alpha kinase 3 with PSP as demyelination, abnormalities in tau secretion, and accumulation of misfolding proteins are all, respectively, systemic pathological features of PSP [66, 67]. There is a need for further research into the role that these genes and proteins play in the development of PSP.

1.1.2 Environmental contributions

Several studies have investigated a wide range of environmental factors that increase the risk of developing PSP. The ENGENE study, one of the largest case-control studies incorporating a 284 cohort of PSP patients and aged-matched controls, focused on environmental toxins known to cause mitochondrial inhibition through occupational or locality exposure [43]. Increased risk of developing PSP was seen in many factors, including; residential history (living in a lower educational and socio-economical region or living in proximity to an agricultural region), drinking well water for many years, and occupational exposure to industrial waste (agriculture toxins and metal exposure) [43]. Clusters of PSP illnesses have also been identified in Northern France, where cases reside near a textile-dying plant allowing arsenic and heavy metals like nickel and chromium to run off into waterways and absorb into the surrounding soil [68].

The consumption of indigenous fruits from the Annonaceae family, and the use of leaves from the same plants in herbal teas and medicines has been associated with clusters of PSP in Guadeloupe, Guam, New Caledonia, and the Kii Peninsular of Japan [69-72]. Neurotoxins annonacin (pubchem ID 354398), benzyl-tetra-isoquinoline (pubchem ID 98468), reticuline (pubchem ID 439653), corexamine (pubchem ID 7037179) and tetrahydroprotoberberine (pubchem ID 101707) are found within fruits from the Annonaceae family [69] and are known to inhibit mitochondrial function, cause tau pathology and cell death in dopaminergic neurons

[73, 74]. The Annonaceae genus have an aliphatic chain with 35-37 carbon atoms, a terminal α,β-unsaturated γ-lactone ring with the presences of tetrahydrofuran and tetrahydropyran rings [75]. Due to their lipophilic properties, they can readily cross into the brain parenchyma [73]. Unlike the PD neurotoxin 1-methyl-4-phenyl-1,2,3,6-tetrahydropyridine (MPTP; pubchem ID1388), annonacin does not only target the dopamine transporter [74] but can cause a widespread degeneration in the basal ganglia and brainstem [73]. Considering its effects on tau, neurotoxins like annonacin may provide insight into the pathogenesis of PSP and its associate tau pathology.

1.2 Clinical manifestations of PSP

PSP is often colloquially referred to as the 'drunken sailor disease' because postural instability, gait disturbances and unexplainable falls are the common symptoms associated with the disease (**Figure 1.1**). The progressive nature of the illness shows severe deterioration in neurological systems which include oculomotor paresis (supranuclear gaze), worsening parkinsonism, dysarthria, dysphasia and cognitive impairment. Supranuclear gaze, which is often a cardinal symptom of PSP, does not always present until later stages of the disease. This often makes PSP indistinguishable from parkinsonian disorders in the early stages of the disease [56]. Efforts into early diagnosis are important given that once an initial clinical presentation is evident, the disease would have already progressed to a halfway point **[76]**. The clinical diagnosis is challenging as more phenotypical subvariants of PSP have now been identified (see **Table 1.1**). The clinical phenotypes are divided into "typical variants" and "atypical variants" which represent the prevalence in the population. The diagnostic criterion established by the PSP study group from the International Parkinson and Movement disorders Society was updated to include the wide spectrum of clinical variants of PSP. However, it is often delayed or only retrospectively diagnosed and does not capture the wide spectrum of PSP. Achieving a diagnosis is multifarious, particularly in the early stages of the disease, therefore we need to appreciate the complexity of PSP and find a sensitive method to detect PSP and its clinical phenotypes. This understanding will help with designing therapies to modulate the disease pathology.

1.2.1 Clinical variants

Since the time when PSP was first described, several subvariants with varying array of clinical symptoms have emerged (**Table 1.1**). Neuropathologies appear to be heterogeneous in both severity and distribution with disparity in symptomologies. Tau pathology is a measure of disease surrogacy and its distribution pattern within typical predominate regions such as the subcortical and brainstem (typical variants) and cortices (atypical).

1.2.1.1 Typical variants of PSP

Named after a founder of PSP, PSP-Richardson's syndrome (PSP-RS) is the most common variant, representing up to 50% of the total PSP cases [77, 78]. The spectrum of PSP has expanded since Steel *et al*. [79] first described it, with various variants emerging as additional phenotypes were recognised. PSP-RS characteristically presents with postural instability, together with abnormal gait leading to falls usually backwards without loss of consciousness. Due to the subtly of some of the early features of PSP, most cases of PSP-RS are often delayed but manifest within the first two years after the initial symptom [47]. Clinical features of PSP-RS include cognitive impairment and oculomotor dysfunction, which are also key indicators of the disorder (**Table 1.1**). These symptoms usually develop in the later stages of the disease and may not present at all during the disease course [56]. In the majority of patients with PSP-RS, there are subtle changes in personality (apathy, depression) and cognition [80], which can also be an initial early phenotypical marker of the disease [56]. Other typical features are the slurred and slowed speech (dysphagia) in the early stages followed by problems with swallowing and chewing food (dysarthria). PSP patient's functional capabilities diminish quickly after becoming dependant within 3-4 years of diagnosis. PSP-RS has a shorter median expected survival of 5 - 8 years [56, 81] and typically the primary cause of death is asphyxiation via choking or neurogenic respiratory failure [82].

The second most common subtype is the parkinsonian variant (PSP-P), making up to 30% of the total of PSP cases [54, 83]. Patients usually present with limb asymmetry bradykinesia, rigidity, and tremors (**Table 1.1**). It is suggested that true numbers of PSP-P variants might perchance be an underestimate due to misdiagnosis with PD and exclusion of features that overlap with PSP-RS [54]. Unfortunately for PSP-P, the diagnosis is often after the fact given

the clinical similarities with PD but PSP-P is a rapid deterioration compared to PD with only small clues of early eye abnormalities, dysphagia and dysarthria as potential phenotypic markers [47]. PSP-P has a longer expected survival compared to PSP-R with the median disease duration of 9 - 12 years [39] and symptoms can be slightly moderated by parkinsonian treatments such as dopamine supplementation (levodopa/madopar) for a few years [54, 82, 83].

1.2.1.2 Atypical clinical PSP variants

Atypical PSP subgrouping was described as a scheme to encompass the variance of severity and distribution of both clinical tau pathology together with symptomology (**Table 1.1**). Currently there are number of phenotypic variants that have been defined including; PSP-Pure akinesia freezing gait (PSP-PAGF), PSP-cortico-basal syndrome (PSP-CBS), PSP-behavioural variant of frontal temporal dementia (PSP-bvFTD), PSP-postural instability (PSP-PI), PSP-primary lateral sclerosis (PSP-PLS) and PSP-cerebellar ataxia (PSP-C). The atypical PSP variants are listed in **Table 1.1**, where they show both clinical and phenotypical features. Differences in these atypical PSP subtypes are most likely a reflection on the both the distribution and severity of tau pathology within the cortical regions.

Chapter 1. Introduction to progressive supranuclear palsy

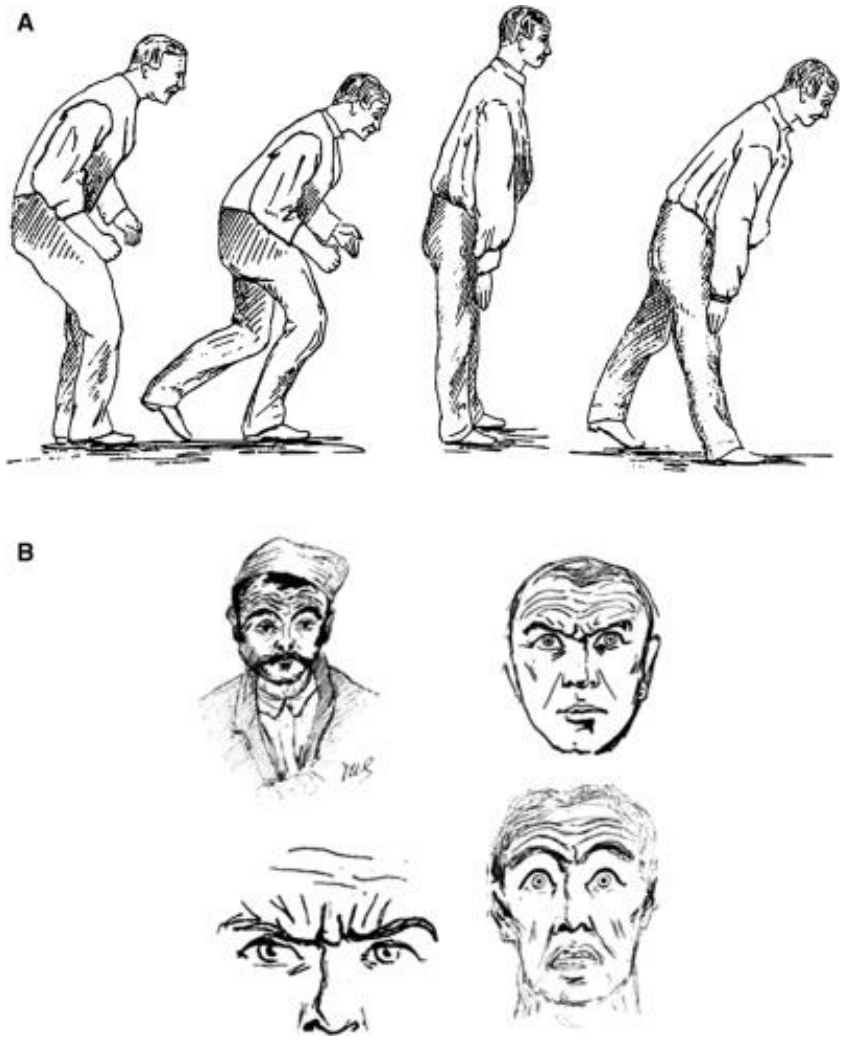

Figure 1.1. The early description of atypical parkinsonism suggests features characteristic of progressive supranuclear palsy (PSP)

Early observations and drawings made by Charcot in 1888 by which he contrasted (**A**) a stooped posture of a typical Parkinson's Disease (PD) patient (left) and the stiff and broad base gait and with an extended trunk, from an atypical PD case which is most likely to be a PSP (right). (B) Charcot's original drawings of atypical PD cases showing distinct facial features such as a furrowed brow and a frightened expression due to contraction of the corrugator supercilii muscle [84, 85].

Chapter 1. Introduction to progressive supranuclear palsy

Table 1.1. Characteristics of PSP clinical variants

Clinical variant	Dominant region	Region affected	Dominant phenotype	Disease duration	Clinical features
PSP-Richardson's Syndrome (PSP-RS)	Classic	Mid-brain: SN, striatum, GP, STN, pons, DN	Fall, ocular motor impairment	5-8 years	Early onset falls with postural instability, oculomotor paresis; vertical gaze initial onset, pseudobulbar palsy, axial rigidity, cognitive dysfunction
PSP-Parkinsonism (PSP-P)	Brainstem predominant	Mid-brain: SN, striatum, GP, STN, pons, DN	Parkinsonism	9-12 years	Early onset asymmetrical onset of limb bradykinesia, rigidity, tremor, and moderately levodopa responsive. Late onset falls, cognitive dysfunction and oculomotor paresis can present
PSP-Progressive gait freezing (PSP-PAGF)	Brainstem predominant	Motor cortex, cerebellum, pons	Gait freezing	11-13 years	Early onset unsteadiness on feet, axil rigidity, gait abnormalities; progressive gait freezing and initiation of gait, Parkinsonian features of micrographia and hypophonia develop (no other PD symptoms), late onset oculomotor paresis – vertical gaze and postural instability
PSP-Primary lateral sclerosis (PSP-LS)	Cortical predominant	Corticospinal tracts, upper motor neurons	Lateral sclerosis	3-12 years	Gradual onset of spasticity, Pseudobulbar features, dysphagia, and dysarthria, late onset Parkinsonian features
PSP-Corticobasal syndrome (PSP-CBS)	Cortical predominant	Parietal and frontal cortices	CBS	7 years	Asymmetric dyspraxia, cortical sensory loss, alien limb, akinesia, bradykinesia, late onset of falls, late onset postural instability and oculomotor paresis; latency in eye movements
PSP-Progressive non-fluent aphasia/ataxia of speech (PSP- PNF/AOS)	Cortical predominant	Frontal, temporal, and parietal cortices	Progressive apraxia or aphasia	< 10 years	Early onset apraxia of speech (non-fluency in speech) but can present with ataxia, which is slow and segmented in effortful speech, late onset postural instability and oculomotor paresis; vertical gaze, akinesia and behavioural changes
PSP-Behavioural variant-Frontal temporal dementia (PSP-bvFTD)	Cortical predominant	Frontal and temporal cortices	Behavioural/personality and cognitive impairment	5-8 years	Cognitive and behavioural impairments; lack of empathy, aggregative outburst, inappropriate social awareness and disinhibited, late onset of falls and oculomotor paresis can present
PSP-Cerebellar ataxia (PSP-C)	Cortical predominant	Deep cerebellar nuclei	Cerebellar ataxia	7 years	Cerebellar limb and gait ataxia, losing balance, develop parkinsonism, Late onset of fall and oculomotor paresis

1.3 Neuropathology of PSP

Pathological accumulation of misfolded or aggregated proteins is evident in many vulnerable regions in diverse CNS disorders. It is a feature that can be used as a means of differential diagnosis, with the classification of disease determined in part by disease-specific deposition of aggregation-prone proteins such as tau, amyloid-β, α-synuclein and TAR DNA binding protein 43. Histological assessment of post-mortem brain tissue is the definitive method of diagnosis using antibodies against these proteins to detect associated abnormalities within the brain. The varying distribution of pathological lesions across multiple brain regions seen in PSP make it a complex condition to pathologically delineate from other extrapyramidal disorders. Pathological lesions in the PSP-affected brain are found within key neuroanatomical regions that control motor function, balance, visuo-spatial awareness, emotion, and memory. Initial studies by Steel *et al.* (1964) presented evidence from seven cases of PSP and all histological results showed neuronal loss, the presence of tau pathology (neurons and glia), and demyelination in several neuroanatomical regions, including the midbrain, brainstem, and cerebellum [79] (**Figure 1.2**).

1.3.1 Tau pathology

Tau, also known as tubulin-associated unit, is predominately found within neurons and plays an essential role in the assembly and stabilisation of microtubules for axonal transport, neuronal integrity and neurite growth. The tau protein presents six different isoforms due to alternative splicing events, with equal ratio repeat domains (3R-4R) in healthy adults. A biochemical characteristic of PSP is the dominance of the 4R isoform of tau found within protein aggregates caused by the ratio equilibrium shift in tau exon splicing [51, 86]. Histological approaches using chemical enhancement like silver staining and antibodies raised against tau have been the gold standard for detecting the pathology. Tau enrichment is selectively distributed in the PSP, and therefore it is essential to examine multiple neuroanatomical regions at post-mortem as stated by the established guidelines for determining PSP by the National Institute of Neurological Disorders and Stroke (NINDS) [55]. Given the large number of regions affected, the NINDS requires three areas of the basal ganglion (substantia nigra, subthalamic nucleus, globus pallidus) and the pons to have high densely of tau found within neurons or neuropil threads for diagnosis (**Figure 1.2a**).

Microscopic tau appears in neurons as neurofibrillary tangles (NFT) and neuropil threads in neuronal processes containing hyperphosphorylated tau (**Figure 1.2b**) [48, 53, 87]. The distribution and severity of tau pathology within various neuroanatomical structures found by Williams *et al.* (2009) suggest that deposition of abnormal tau could be used to differentiate PSP subtypes, including the typical variants of PSP-RS and PSP-P [78] see **Figure 1.2c.**

Appearing to be globose, these aggregates of tau filaments intertwined with beta-sheet arrangements resemble a ball of yarn when viewed under an electron microscope [88]. The generalised pattern of tau pathology is relatively consistent across all subtypes, with the subthalamic nucleus, substantia nigra and globus pallidus most heavily burdened with deposition of abnormal tau and neuronal loss (**Figure 1.2a**)[50]. Despite tau expression being lower in glia than neurons [89], tau fibrils are also found in non-neuronal cells like astrocytes (tufted astrocytes) and oligodendrocytes (coiled bodies) (**Figure 1.2b**). A star-shaped tau pathology devoid of amyloid cores, later termed as tufted astrocytes with the astrocytic markers glial fibrillary acidic protein (GFAP) and homing cell adhesion molecule (CD44), suggests that PSP has elements of glial dysfunction [45, 46]. Tau is densely distributed throughout the cytoplasm radiating to the distal processes of astrocytes when stained with anti-phosphorylated tau, AT8 antibody [90]. Morphological features of glial tau fibres show discrepancies in size, particularly within in the proximal processes [90, 91]. Tufted astrocytes are distributed abundantly within the premotor/motor cortex, striatum, substantia nigra, palladium, brainstem and cortices [50, 92, 93] and seem to be distributed in close proximity to blood vessels [94]. Additional to tufted astrocytes, thorn-shaped astrocytes have also been reported in PSP cases, however these are suggested to form incidentally since these aggregates lack ubiquitin [95] and could result from the reactive astrocytes process [96]. Typically and consistently found in PSP, coiled bodies are coil-like branches of fine tau filaments [93] found within the cytoplasm and within the processes that shield the injured axons [97]. Tau within coiled bodies has a tubular structure that is observed in perikarya and interfascicular threads with fuzzy contours in oligodendrocytes in white and grey matter [98]. Coiled bodies are consistently found in PSP and are observed within substantia nigra, globus pallidus, subthalamic nucleus, striatum, thalamus, brainstem, cerebellum (white matter), and even have been detected in the spinal cord [99].

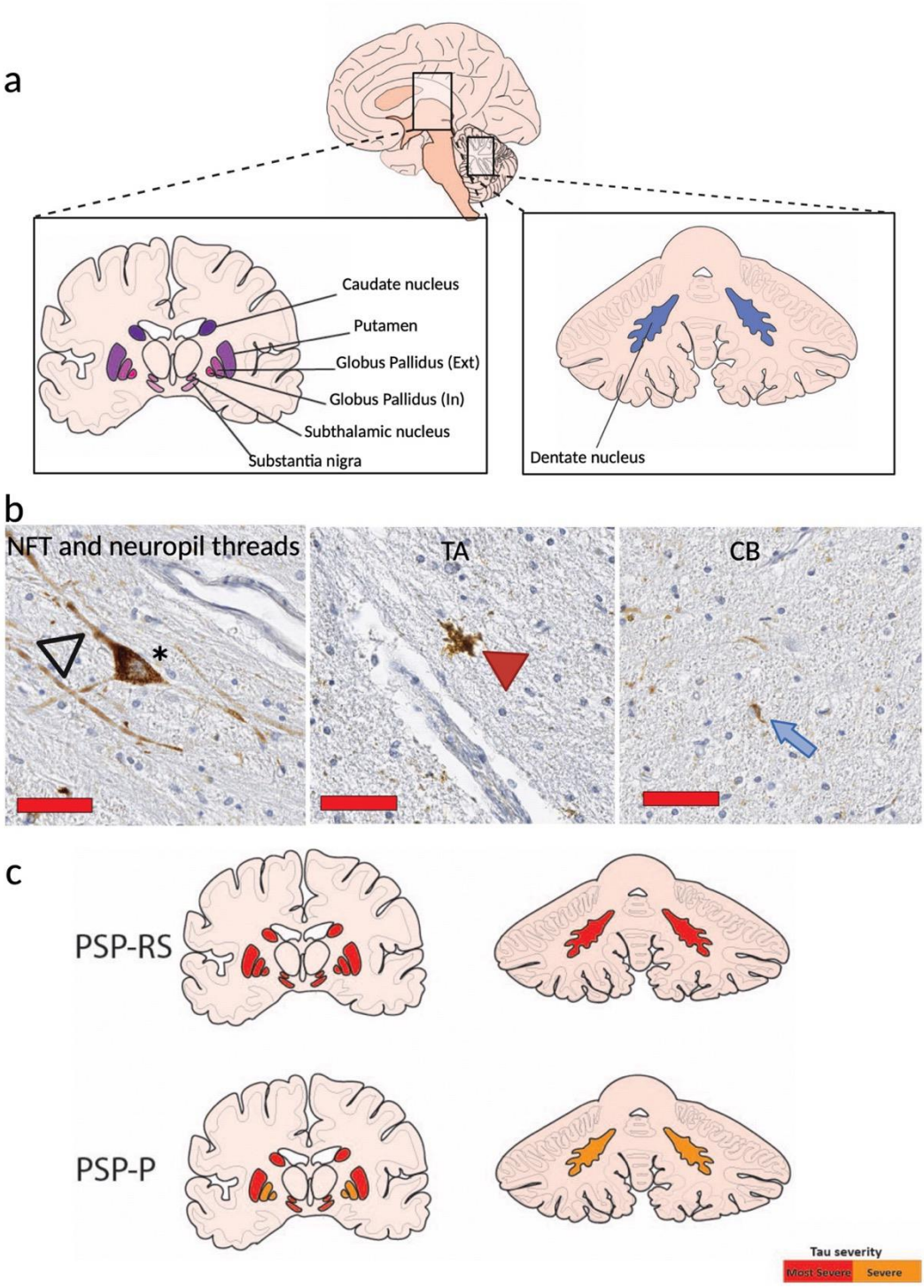

Figure 1.2. Neuropathology seen in PSP

Neuroanatomical regions that are affected in PSP. **a**) Map of regions in the brain that are affected in PSP. **b**) Tau pathology seen in the substantia nigra *pars reticulata* of a PSP case in neurons as neurofibrillary tangles (NFTs; asterix) and neuropil threads (open arrowhead); astrocytes (Tufted astrocytes, TA; red arrowhead) and oligodendrocytes (coiled bodies, CB; blue arrow). **c**) Tau pathology severity within subcortical and cerebellum regions based on Williams *et al*. 2007 and Kovacs *et al*. 2020 in PSP-Richardson's syndrome (PSP-RS) and PSP-Parkinsonism (PSP-P) Tau scores are based on tau NFTs, coiled bodies and tufted astrocytes pathology with orange to red being the most severe [47, 50, 78]. Red scale bars 25 µm.

1.3.2 Neuronal cell loss

In PSP, the most common pathological finding is neuronal cell loss in the subcortical and cortical nuclei. Gross pathological findings show that atrophy is most prominent in the midbrain, cerebrum, and superior cerebral peduncle with loss of pigmented neurons. As with PD, PSP shows the same loss of melanin pigmented neurons in substantia nigra *pars compacta* that occurs in PD with a loss of over 70% of these neurons [100, 101]. Unlike PD, PSP involves substantial loss of neurons throughout the substantia nigra, including the *pars reticulata*, which is associated with the clinical feature of gaze palsy [102]. The loss of neurons in other key subcortical nuclei such subthalamic nucleus and globus pallidus is consistently seen in PSP [103] suggests that together with the substantia nigra, the loss pallido-nigro-luysian axis could be an early event in the disease [104]. Other slightly less prominent regions that show neuronal loss include, dentate nucleus, caudate nucleus, pontine tegmental area (pons), locus coeruleus, periaqueductal grey, pretectal regions, and the super colliculi [105]. The degeneration of pre and post synaptic neural circulatory in the PSP brain leads to neurochemical changes, whereby loss of dopamine, produced by the substantia nigra *pars compacta* neurons is abnormally depleted in the striatum [106-108]. In addition, loss of neurons in the substantia nigra *pars reticulata* decreases the neurotransmitter gamma-aminobutyric acid (GABA) and its receptors [101, 109], resulting in motor and oculomotor dysfunction in PSP. Other neurotransmitters like glutamine, serotonin, norepinephrine and acetylcholine are also decreased but inconsistently across the PSP brain and require a larger cohort study to fully evaluate their loss [109-111].

1.3.3 Neuroinflammation - Gliosis

Gliosis is a pathological feature seen in the PSP brain that is extensively seen in the basal ganglia accompanying tau pathology and neuronal loss [99, 112-115]. Markers of gliosis including both reactive astrocytes (vimentin; VIM and GFAP) and reactive microglia (human leukocyte antigen-dr type; HLA-DR and ionised calcium-binding molecule 1; IBA-1) are known to be increased and triggered in response to injury, stress and built-up levels of accumulated proteins [116]. The expression levels of total GFAP and VIM are reported to be increased by 80% and 373%, within the substantia nigra *pars compacta* found in PSP post-mortem tissue respectively [117]. The caudate nucleus showed a similar result with a significant elevation of

GFAP (79%) and VIM (105%) expression [117]. The highest burden of reactive microglia was seen in the substantia nigra and the subthalamic nucleus [118]. The secretion of proinflammatory factors by reactive microglia under pathological conditions have been detected in elevated levels in both the PSP brain regions (substantia nigra, globus pallidus and subthalamic nucleus) and in biofluids [114, 117, 118]. Chronic and sustained neuroinflammation, that is driven by aberrant activation of glia is considered an early event in the neurodegenerative disease process [119, 120] and it seems the glia play an important role in PSP pathogenesis.

1.3.4 Demyelination

Gross macroscopic examination of a PSP brain shows discolouration of various nuclei due to the loss of myelinated fibers in the areas of the subthalamic nucleus, globus pallidus and dentate nucleus, regions that are severely affected with tau pathology [121]. Clinical symptoms of PSP have also been associated with white matter degeneration and may be a strong predictor of disease severity [122]. Demyelination is an inherent feature of PSP, with white matter tracts that project from the cerebellar dentate nucleus via the superior peduncle and within the longitudinal fasciculus show severe axonal degeneration, loss of myelin and loss of oligodendrocytes, the glial cells that regulate these processes [122, 123]. Oligodendrocyte dysfunction leads to the degeneration of white matter tracts, demyelination and failure in its repair. In addition, oligodendrocytes secret trophic factors for both axonal growth and maintenance and neuronal survival [124]. It is unknown what causes oligodendrocytes to degenerate in PSP, but tau and inflammation may play a role in the pathogenesis.

1.4 Lessons learned from neurodegenerative disease regarding the molecular basis of neurodegeneration

Neurodegenerative diseases such as Alzheimer's disease (AD), amyotrophic lateral sclerosis (ALS) and PD share overlapping clinicopathologic features with PSP (see **Figure 1.3**). After establishing tau being the primary pathological contributor to PSP, the understanding of involvement of other molecular mechanisms that are suggested to propagate the disease and its progression has fallen short. Inferences from other important studies from across the

neurodegenerative umbrella have given clues as to what pathways maybe involved in the disease. The empirical evidence on pathways that would most likely be shared across these diseases highlights oxidative stress. The brain has the capacity to combat the formation and build-up of reactive oxygen species (ROS). However, this capacity is lost in the last few decades of human life, and oxidative damage to proteins, lipids and nucleic acids is a pervasive feature of neurodegenerative disease [1]. Previous studies have linked this feature of neurodegenerative disease to an imbalance in essential metals such as copper, iron and zinc that accumulate or shift in availability over the lifetime of humans and could lead to the observed increases in oxidative stress [7, 9, 125-128]. This is supported with well-documented changes in proteins that regulate or require metals in neurodegenerative disease [129-131].

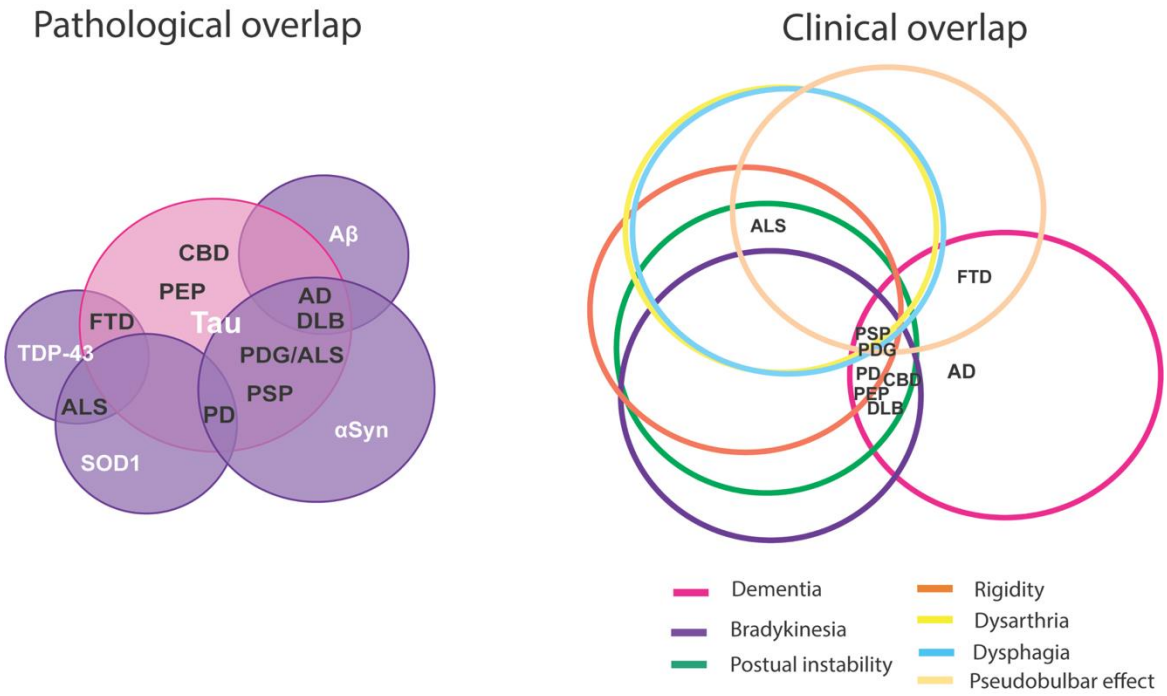

Figure 1.3. Clinicopathological overlap of neurodegenerative diseases
A diagram showing the overlap between some of the pathological and clinical manifestations of neurodegenerative diseases. Proteinopathies are used as a form of classification based on the histopathological distribution within the CNS (left). Tau is central and is repeatedly observed across multiple neurodegenerative conditions (including Alzheimer's' disease; AD, Dementia with Lewy bodies; DLB, Parkinson's dementia complex with Guam/amyotrophic lateral sclerosis; PDG/ALS, progressive supranuclear palsy; PSP, Parkinson's disease; PD, Frontotemporal dementia; FTD, Post encephalitic parkinsonism; PEP and corticobasal degeneration; CBD). Presentation of heterogeneity of clinical phenotypes (right) that overlaps across neurodegenerative diseases that reflect the affected regions of different neuroanatomical structures.

1.4.1 Oxidative stress

Common if not to all neurodegenerative diseases, is a shift or imbalance of redox equilibrium also known as oxidative stress. For the cell to be under oxidative stress conditions, the cell must be producing ROS beyond the threshold of intrinsic antioxidant capabilities. In healthy conditions, cells are well equipment to defend themselves from excessive ROS by neutralising ROS using many different frontline antioxidants. These include glutathione, α-tocopherol, and a family of metalloenzymes the superoxide dismutases which utilise forms of reduced copper or manganese to perform their antioxidant function. The persistent production of ROS from vicious cycles of oxidative stress is accelerated when reactive amine neurotransmitters such as dopamine are available to participate in the reaction with free metal ions such as copper and iron [132-135]. Copper and iron are key players in redox chemistry due to the ability to transfer electrons and shift redox states (cuprous to cupric and ferrous to ferric). If unbound, copper and iron can cause catastrophic damage to cells via the generation of oxidative stress. Free or "labile" iron can contribute to iron-mediated ROS production, generated through Fenton and also Haber-Weiss chemistries [136]. Unlike iron, however, copper rarely exists in a free or unbound state [137] due to specific chaperones that ensure its 'free' concentration is kept at a minimum level. Redox chemistry is dependent on the ligand (oxidative and reducing agents) that are present and are within close proximity, together with the physiological environmental conditions [138]. What is firmly established is that increases in oxidative stress has been seen in many brain regions and bio-fluids across many neurodegenerative diseases [14]. Identification of many oxidative stress biomarkers including products of lipid peroxidation (4-hydroxynoneal and malonaldehyde) [12, 13], DNA/RNA oxidation (8-hydroxyguanine/8hydroxy-deoxyguanosine) [3] and protein oxidation (carbonyls, addition of adducts to cysteine residues) [139, 140] are elevated in post-mortem in diseased brain tissue. Inversely, what has also been seen in these common forms of neurodegenerative conditions is that the levels of active superoxide dismutase 1 (SOD1) [141] and glutathione [142] are decreased within these vulnerable regions.

Oxidative stress also has a significant impact on protein aggregation and in particular tau NFT formation. The presence of metals that are unusually altered in aged and diseased brains also have a significant impact on hyperphosphorylation and aggregation of tau. Chronic exposure

to oxidative stress by inhibiting glutathione production in cultured neurons increases tau susceptibility to be hyperphosphorylated and form aggregates [143]. Additionally, the lipid peroxidation product, 4-hydroxynonenal, promotes the assembly of phosphorylated tau in NFTs [144] and modifies the conformation of phosphorylated tau to induce its aggregation [11]. Oxidative stress also has a direct impact on upregulating glycogen synthase kinase-3 beta (GSK-3β), one of a few kinases that phosphorylates tau on residues Thr321, Ser396, Ser404 [145]. Aggregates extracted from PSP brains show up to 16 phosphorylated residues [48, 53, 87]. Hyperphosphorylation at specific but multiple sites in the tau microtubule binding domain seems to disturb the ability to bind to microtubules causing disruption in axonal transport, promoting a demise in cellular architecture and synaptic dysfunction [146]. Copper ions are enriched in pathological inclusions in AD-affected brain tissue, including amyloid plaques and within NFTs [147]. This accumulation of copper potentially contributes to tau pathology through several mechanisms. Not least of which, copper binding sites are present within the pseudo-repeat units R1-R4 within tau [148, 149]. When tau is exposed to copper, these coordination R1-R4 sites result in a conformational change in the microtubule binding domain, resulting in destabilisation of microtubules and thus an increase its aggregation propensity [149]. Additionally, destabilisation of microtubules is also seen when tau is hyperphosphorylated by GSK-3β [150], the activity of which is also regulated by intracellular copper levels [151]. Copper has shown to potentially be an allosteric regulator of protein kinase (ARK1) [152], that phosphorylates GSK-3β on serine 9 causing its inactivation [153, 154]. In the presence of intracellular copper, a dose-dependent inhibition of GSK-3β is seen with small copper modulating compounds designed to either remove copper from tau aggregates and or inhibit tau phosphorylation via GSK-3β [151, 155-157]. A small number of *in vivo* and *in vitro* experiments have shown that the inhibition of GSK-3β by these copper modulating compounds, decreases tau phosphorylation and reduces cognitive decline in AD transgenic mice [151, 156, 157]. The expression of GSK-3β is reportedly increased in PSP tissue, with GSK-3β deposits apparent in both neurons and glia [158]. While it is known that copper is found in neuronal pathology as seen in AD cases, copper and its contribution to glial tauopathy, particularly in PSP remains unclear.

1.4.2 Disrupted copper availability in neurodegenerative diseases

As described further in Section 1.5, copper is an essential element due to its requirement in iron homeostasis [159], diverse cuproenzymes [160-164], neuronal myelination [165], and lipid and neurotransmitter biosynthesis [166, 167]. The natural distribution of copper within the brain is variable in terms of concentration within specific regions [168] and over the course of development and aging [125, 126, 168-172]. Regional distributions of copper reflect the highly organised cytology of the neuroanatomy with distinct grey and white matter compositions. Grey matter regions enriched with neuronal soma have a higher copper content than neighbouring white matter regions enriched with myelinated axons [173]. The neuroanatomical regions that contain high levels of copper are the basal ganglia, locus coeruleus, red nucleus, and the dentate nucleus [21, 173-176]. Astrocytes play an important role in bringing copper into the CNS via their proximity to neurons and to endothelial cells that line the brain capillaries [177]. The sequestration of copper by astrocytes is essential to both regulate the distribution of copper to various other cells in the CNS and to protect the CNS from toxicity caused by copper that is in excess to requirement [178, 179].

The impact of disrupted copper availability on neurological function is seen in diseases where copper levels are altered, with copper overload the hallmark of Wilson's disease [180] and copper deficiency the hallmark of Menkes disease [181]. Wilson's disease (OMIM 277900) is caused by mutations affecting the copper transporter *ATP7B* and is associated with neurological symptoms that include tremors, ataxia, rigidity, dystonia, dysphagia and dysarthria, and these often manifest late in the third decade of life [180, 182]. Menkes disease (OMIM 309400), conversely, is caused by mutations that affect the copper transporter *ATP7A* and prevent systemic copper uptake from the gut and result in decreased copper availability. Menkes disease is a systemic depletion of copper and subsequent dysfunction of cuproenzymes first described by Joh Menkes in 1962 [183]. The neurological consequences of Menkes disease include demyelination and progressive neurodegeneration [184, 185], with the overall impact being fatality in children 3 years and under [181]. This impact is driven by insufficient supply of copper to mitochondria, where it is required for incorporation into cytochrome c oxidase also known as complex IV for the generation of ATP. This disproportionately impacts the brain because of its high metabolic demand [128]. Being one

of the most described genetic copper depletion models, mutations in *Atp7a* gene result in severe copper deficiencies in the brain as it is involved in copper uptake at the blood-brain barrier (BBB) and loading copper onto cuproenzymes, which impairs CNS as well as bone, skin, and vascular systems [186]. Mice with mutations in *Atp7a* are known as mottled mice due to their "mottled" appearance in their coat due to the reduced pigmentation [187, 188], closely resemble Menke's disease phenotype, with lethality. There are several mouse strains with *Atp7a* mutations that cause gestational lethality in hemizygote males, emphasizing the importance of ATP7A in development (strains *Atp7a*^{moca}, *Atp7a*^{modp} *Atp7a*^{11H} *Atp7a*^{mo1pub}, Atp7a^{mo2btl}, *Atp7a*^{mob2t} and *Atp7a*^{mo3btl}). These severe phenotypes are caused by mislocalisation of this protein in the endoplasmic reticulum from where its suppose to function at the trans Golgi network [189]. The less severe mutants (brindled-mobr; *Atp7a*^{mobr}, macular; *Atp7a*^{moml} and mosaic; *Atp7a*^{moms} strains have partial Atp7a function [190] and therefore can survive past 15 days postpartum with intraperitoneal delivery of copper. In spite of their widespread use in studies of copper trafficking, these mutant mice succumb to their disease phenotype due to loss of lysyl oxidase activity, and they develop aortic lesions and weakening of vascular walls before dying from capillary rupture [191]. Upon histological examination of a brain from a brindled hemizygote male, severe neurodegeneration in the thalamus, brainstem and the cerebellum is evident [192, 193], and could be a likely result in the reduction in complex IV and SOD1 activity [194]. Untreated *Atp7a* brindle-mobr mutants, suffer from neurological symptoms such as ataxia, tremors, unsteady gait, clasping and hindlimb paralysis [186], with treatment of copper chloride in utero delays the onset of neurological symptoms [195].

Further to Menkes and Wilson's diseases which exhibit neurological deficits with established molecular connections to copper availability, changes affecting copper availability are also reported in more common neurodegenerative disease such as AD, PD and ALS, with changes in copper concentration seen within vulnerable areas of the CNS [21, 175, 196-198]. Some studies indicate no changes in copper within these diseases [199, 200], but variations in detection and preparation methods need to be considered. Specifically, assessing total tissue copper content can potentially mask detection of changes that occur within particular regions of interest, as indicated by the accumulation of copper in AD within regions with pathological hallmarks of NFTs and amyloid plaques [147, 198].

1.4.3 Evidence of oxidative stress and disrupted copper homeostasis in PSP

The analysis of PSP brains at post-mortem has shed light on the possible mechanisms underlying the disease. Immunohistochemistry has been used to showed biomarkers of oxidative stress in post-mortem tissue of PSP patients [10, 142, 201]. Pathologically affected regions have higher levels of oxidative stress with lipid peroxidation markers 4-hydroxynonenal and malondialdehyde found in the pons and the subthalamic nucleus respectively [10, 201]. These products of lipid peroxidation are known to cause direct damage to the activity of antioxidant glutathione peroxidases and increase the expression of GFAP [9, 49]. A disparity exists between antioxidant expression and activity patterns in PSP as a result of changes in frontline defenses such as SOD1 and glutathione. For example, glutathione, another important antioxidant, is reduced in the caudate nucleus [142] but increased within the subthalamic nucleus and globus pallidus [20]. SOD1 activity is evident within regions that show higher levels of tau pathology and neuronal cell loss, however SOD1 activity is also found to be elevated within the calcarine [20], a region that shows no tau deposits [202]. Due to the absence of universal procedures for tissue collection, preparation, and antioxidant extraction, each factor impacts activity directly and therefore may have effect on specific activity.

The basal ganglion is an area of the brain that is highly enriched in copper [173, 176] and iron [22, 173, 203]. The reason copper and iron are increased in basal ganglion is thought to be related to their high metabolic demand to modulate movement, although it is not fully understood why this is the case. Heightened recognition of altered copper availability within the CNS therefore comes with methodologies that move beyond total tissue content and begin to inform on changes that can occur within anatomical regions and biochemical fractions of interest. With this consideration in mind, reports on neurodegenerative disease-associated changes in brain copper already extend to PSP. The first publication on copper concentrations in brain tissue from cases of PSP reported total tissue copper content for five anatomical regions of interest [21]. All indicated a decrease in total copper content, with the cerebellum reaching a statistically significant change (**Table 1.2**). A subsequent study that also assessed total tissue copper content provided results that were overall corroborative [22], with the caudate nucleus in this study highlighted as the region of interest with a statistically significant decrease (**Table 1.2**).

Decreased copper levels in the PSP-affected brain reported by these two studies suggests that the activities of cuproenzymes is likely to be affected. However, reports on the activity and expression profiles of cuproenzymes in PSP is rather limited with only one study reporting on ceruloplasmin, a predominately astrocytic cuproenzyme that utilises six bound copper atoms to exert its ferroxidase activity [204-207]. Decreased copper associated with increased iron is reported in the PD-affected substantia nigra where, importantly, copper-dependent ferroxidase activity required for iron export is decreased [208]. A similar association between copper availability affecting iron accumulation may be present in PSP. However, elevated levels of ceruloplasmin in PSP [22, 209] may appear inconsistent with this possibility. But as an acute phase protein, delineating between ceruloplasmin changes in an inflammatory context from its role as a cuproenzyme responsible for regulating cellular iron requires measurement of its ferroxidase activity. Reports on the copper-dependent ferroxidase activity of ceruloplasmin in the PSP-affected brain do not yet exist. Notably, however, one of the studies that reported a decrease in copper in PSP also reported elevated iron levels in regions of the PSP affected brain [21].

Table 1.2. Copper changes detected in various neuroanatomical structures in human PSP

Sample size	Neuroanatomical region	Change compared to age-matched controls	(Reference) detection method
Control = 13, PSP = 11	Cerebellar cortex	16%↓	
Control = 14, PSP = 11	Caudate nucleus	13%↓	
Control = 13, PSP = 11	Putamen	8%↓	[21]
Control = 8, PSP = 7	Substantia nigra *pars compacta*	13%↓	ICPMS
Control = 12, PSP = 7	Cerebellum	26%↓*	
Control = 7, PSP = 11	Caudate nucleus	54%↓*	[22]
Control = 7, PSP = 11	Putamen	33%↓	AAS
Control = 7, PSP = 11	Substantia nigra	39%↓	

Direction of change indicated (↓) represents a decrease compared to non-neurological control cases. * Denotes $p<0.05$ when compared to controls (stated by authors). PSP: progressive supranuclear palsy; AAS: atomic absorption spectrometry; ICPMS: inductively coupled plasma mass spectrometry.

1.5 Copper biology

1.5.1 Copper

Copper is an essential metal important for several fundamental biological processes including antioxidant activity [161], iron homeostasis [159], catalytic centres for enzymes [160-164] and specific to neurons myelination [165] and neurotransmitter biosynthesis [166]. Copper is acquired through dietary intake, where once absorbed it is distributed to the body's copper abundant areas the liver and the brain [210, 211]. The importance of copper to the body is seen in diseases where copper being deficient in Menkes disease and in overload, Wilson's disease, highlights the fine balance between too much versus too little (described in Section 1.4.2).

1.5.2 The body's acquisition of copper

The body's stores of copper are acquired through the diet of naturally enriched in copper foods and through supplementation. The gastrointestinal system can absorb up to 40% of copper from dietary consumption [212]. In early life, copper is obtained through breastfeeding, with human breast milk having a higher copper content when compared to other mammals (i.e., cows) [213]. During development, copper expressed in human breast milk has the is highest peak in colostrum [214] and then declines over time during the course of lactation [215]. Since essential elements like copper are required to strengthen immunity and brain development, copper is also supplemented in infant formula to support age development [216]. In adults, it is through dietary consumption where humans received their daily doses of copper with recommendations of 1.2 mg (females) and up to 1.7 mg (males) based on Australian standards. Rich copper foods are shellfish (oysters), nuts, organ meats, vegetables (potatoes, spinach, mushrooms) and chocolate [217], with low range detection of copper found in tap water [218]. Copper deficiency although being rare in the adult population is now being more recognised, given that its symptoms present with similarly to anaemia. The risks that are common to copper deficiency are stomach surgery [219], malabsorption diseases (Celiac's disease and Crohn's Disease) [220] and inadequate dietary intake. There are limited studies on food choices and their effect on the body's physiological copper concentrations. However, it has been shown that copper depletion could also be a

result of competitive absorption of other elements like zinc [221], with zinc smelter workers [222, 223] and use of denture adherents [224] are prone to causing a depletion in serum copper levels. Copper depletion is seen in rodent studies where a copper deficient diet was used to measure the impacts on the body. Impairment in motor coordination [225] and sensorimotor functions [226] are seen in aged mice after deprivation of copper only during neonatal development. Restorations of copper levels can be achieved by supplementation, but this seems to only be specific to peripheral copper levels and more permanent and persisting copper depletion is seen the brain [225]. Copper, essential to the enzyme dopamine beta hydroxylase (DβH) to breakdown dopamine to norepinephrine, is not restored even after a transient deprivation of copper to neonatal mice [227]. Therefore, dietary copper, particularly during the critical stages of human development, is important to the acquisition of brain copper levels for later in life.

1.5.3 Copper uptake and handling machinery in the brain

Researchers have used a radioactive copper tracer to study how copper is absorbed into the bloodstream and is transported via albumin and transcuprein to the liver and kidneys and eventually the brain by other copper-handling proteins [228]. Copper enters hepatocytes to deliver copper to the trans Golgi network via chaperone proteins. The radioactive copper tracers then confirms copper is added to ceruloplasmin, the main copper transport protein and a cuproenzyme, which is responsible for over 90% of the body's copper transport [229]. Ceruloplasmin can sequester up to 6 - 8 copper atoms per protein [230] delivering copper to the plasma membrane for cellular importation. For copper to enter the brain, there is a stringent mechanism that allows the entry of small molecules to cross the BBB (**Figure 1.4**). Transportation into the brain requires copper to cross the BBB and the cerebrospinal fluid barrier (CSFB) via a lining of endothelial cells of the cerebral capillaries into the brain parenchyma [231] (**Figure 1.4**). Excess copper is released into the CSF via epithelial cells in *choroid plexus* then cycling back into the blood [231] all to be accepted again by ceruloplasmin. Located next to capillary endothelial cells and widely distributed throughout the brain, astrocytes take up copper via copper transporter 1 (CTR1) and divalent metal transport 1 (DMT1) and other metals like iron and zinc to redistribute to other types of cells like neurons and oligodendrocytes [232-234]. Astrocytes have a high capacity to accumulate

copper because they express abundant levels of copper cellular handling proteins and antioxidants like glutathione, metallothionine and SOD1 [232, 235] allowing for protection against copper induced toxicity. Copper must be as a cuprous ion (Cu+) upon entry to any cell. It is unknown which cuproreductase is found on the plasma membrane of astrocytes and or neurons although it is possible that STEAP proteins (six transmembrane epithelial antigen of the prostate; STEAP 1-4) which are classed as metalloreductases, could facilitate this role as they are known to stimulate copper uptake upon expression [236]. Copper transporting mechanisms are ubiquitously expressed across different cell types to maintain the flux of intracellular copper (**Figure 1.5**). CTR1, is abundant in cerebral capillaries and within choroid plexus to capture copper from the blood and CSF respectively [237, 238]. CTR1 is one of the primary mechanisms of copper uptake given that the homozygous mutants are embryonic lethal [239]. CTR1 is ubiquitously expressed and requires no ionic gradient or ATP hydrolysis for importation of copper into the cell [240]. Upon its entry into the cell, unbound copper must be maintained at low concentrations and this is performed by copper chaperone proteins and/or intermediary shuttling to glutathione and metallothionines [241, 242] which are all are sensitive in regulating the bioavailable pool of copper. The uptake rate of 5 to 15 copper atoms per second [243], millimolar concentrations of glutathione [244] and metallothionein [241, 242] are engaged to not only receiving copper, but to keep its unbound concentration at a minimum [245]. Copper homeostasis also plays a significant role in mitochondrial function since there are two important cuproenzymes located within the intermembrane space that both require copper for protein maturation; complex IV and superoxide dismutase 3 (SOD3). Localisation of copper within the mitochondrial matrix ensures that there is a minimum level of copper in the matrix pool to sustain cuproenzyme activity even when the cells are copper deficient [246]. The delivery of copper to various cuproenzymes requires specific protein chaperones to ensure copper is transported within the cytosol and to specific organelles that require it (**Figure 1.5**). Copper chaperone to SOD1 known as CCS, is a small homodimer chaperone which directly binds to SOD1 through its domain III for both ion transfer and SOD1 activation [247, 248]. CCS is essential for SOD1 activity since its loss seen in knockout mice shows a dramatic reduction in SOD1 activity [249, 250].

Other organelle specific proteins that require copper have designated chaperones like cytosolic COX17, COX19, COX23 coordinating with mitochondrial intermembrane space SCO1, SCO2, and COX11 for delivery of copper to complex IV. Newly synthesised cuproenzymes in the trans Golgi network are in an un-metallated state and require the delivery of copper via chaperone Antioxidant-1 (ATOX1). ATOX1 not only facilitates the transport of copper to the trans Golgi network for cuproenzymes (ceruloplasmin, lysyl oxidase, DβH and tyrosinase) but also distributes copper to ATP copper pumps ATP7A and ATP7B for intracellular removal [251]. Energy is required for ATPases to transport copper from the cell across the plasma membrane and it is an important step for the successive incorporation of copper to cuproenzymes [252-256]. ATP7A and 7B expression in human tissue show that they are most prominently found in the cerebellum, anterior cingulate cortex, visual cortex, caudate nucleus, putamen, cerebellum and the substantia nigra [176]. The ATPases 7A and 7B possess a role in also the removal of copper from cells and may play an important role in copper distribution from astrocytes to neurons [178, 257]. Most functional experiments involving these ATPases and copper are performed using peripheral based cells. However, it is understood that copper regulation by both ATPases is similarly seen in astrocytes and neurons. ATPases regulate copper by its subcellular localisation within cells. Under conditions of high intracellular copper levels, both ATPases trafficked from the trans Golgi network to the plasma membrane for copper removal [258] which is also mediated by another protein chaperone copper metabolism MURR domain 1 (COMMD1). COMMD1 is involved in copper transport and in animals [259, 260] its deletion results in excessive copper levels in the liver. However, COMMD1 is ubiquitously expressed in various tissues so it suggests that its copper handling abilities are not limited to hepatocytes [261]. The histidine residues in the COMMD1 domain, located in the C-terminal of COMMD1 bind copper [262] and act as a protein scaffold for ATPases (ATP7A/B), which facilitates the secretion of copper [263, 264]. COMMD1 is known to promote proteolysis of many misfolded proteins including the ATPases 7A and 7B, Parkin (PD associated protein) and SOD1 [263, 265, 266]. Despite the direct association between copper handling and PD, there have been no studies investigating whether copper handling mechanisms have changed in PSP. Further investigation is needed.

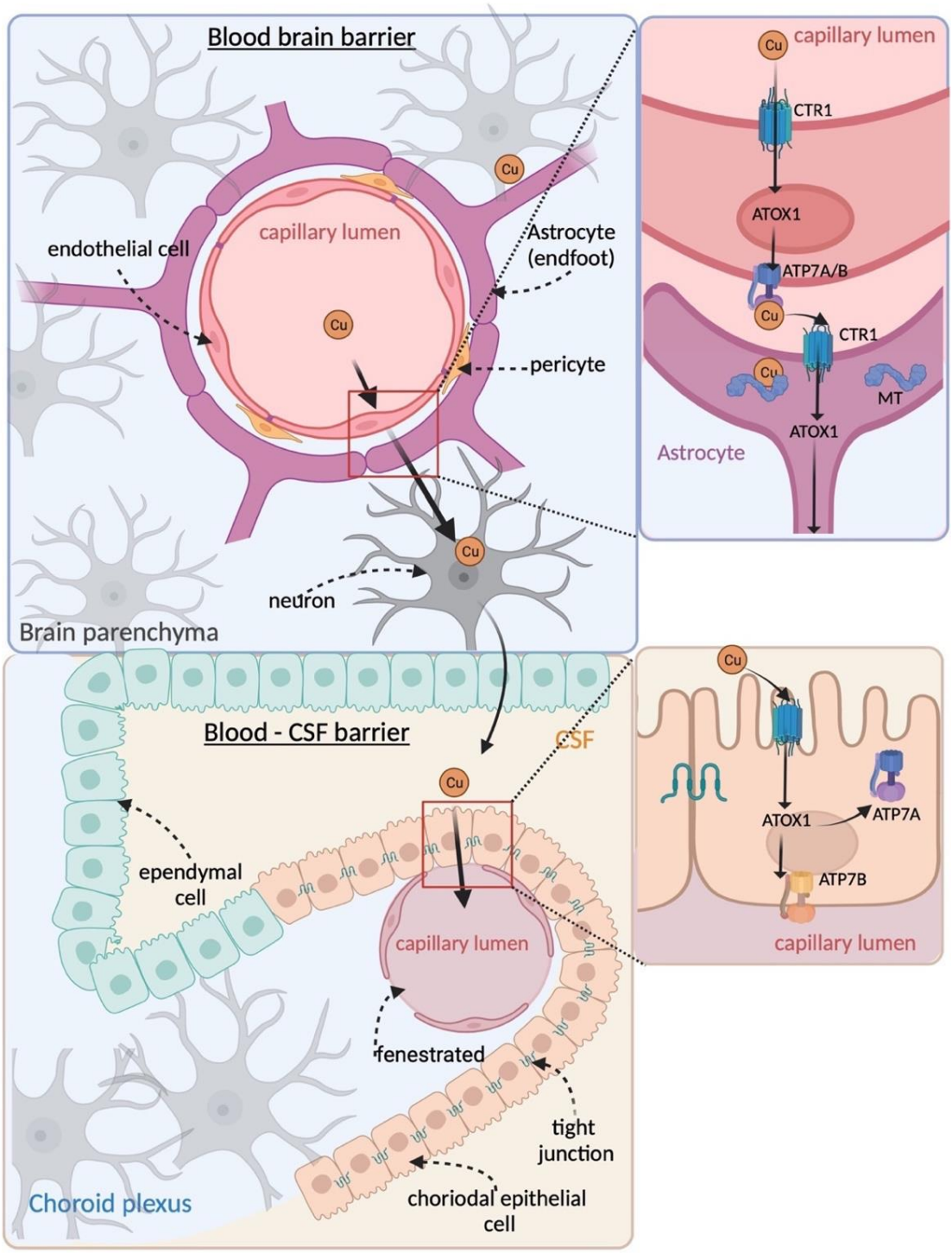

Figure 1.4. Facilitation of copper transport across the blood-brain and CSF barriers
The blood-brain-barrier (BBB) transports peripheral copper (Cu) into the brain. Endothelial cells located near capillary lumens take up copper using copper transporter 1 (CTR1), which transports it from chaperone antioxidant 1 (ATOX1) to ATPase 7A (ATP7A) before it is taken up by astrocytes (via the astrocytic endfoot), stored in metallothionein (MT), or transported to neurons. Copper ions readily flow through the ependymal cells into the CSF and are taken up by choroidal cells via CTR1, ATOX1, and recycled back into the blood by ATP7A/B. This figure was created using Biorender and adapted from Wen *et al*. (2021) [267].

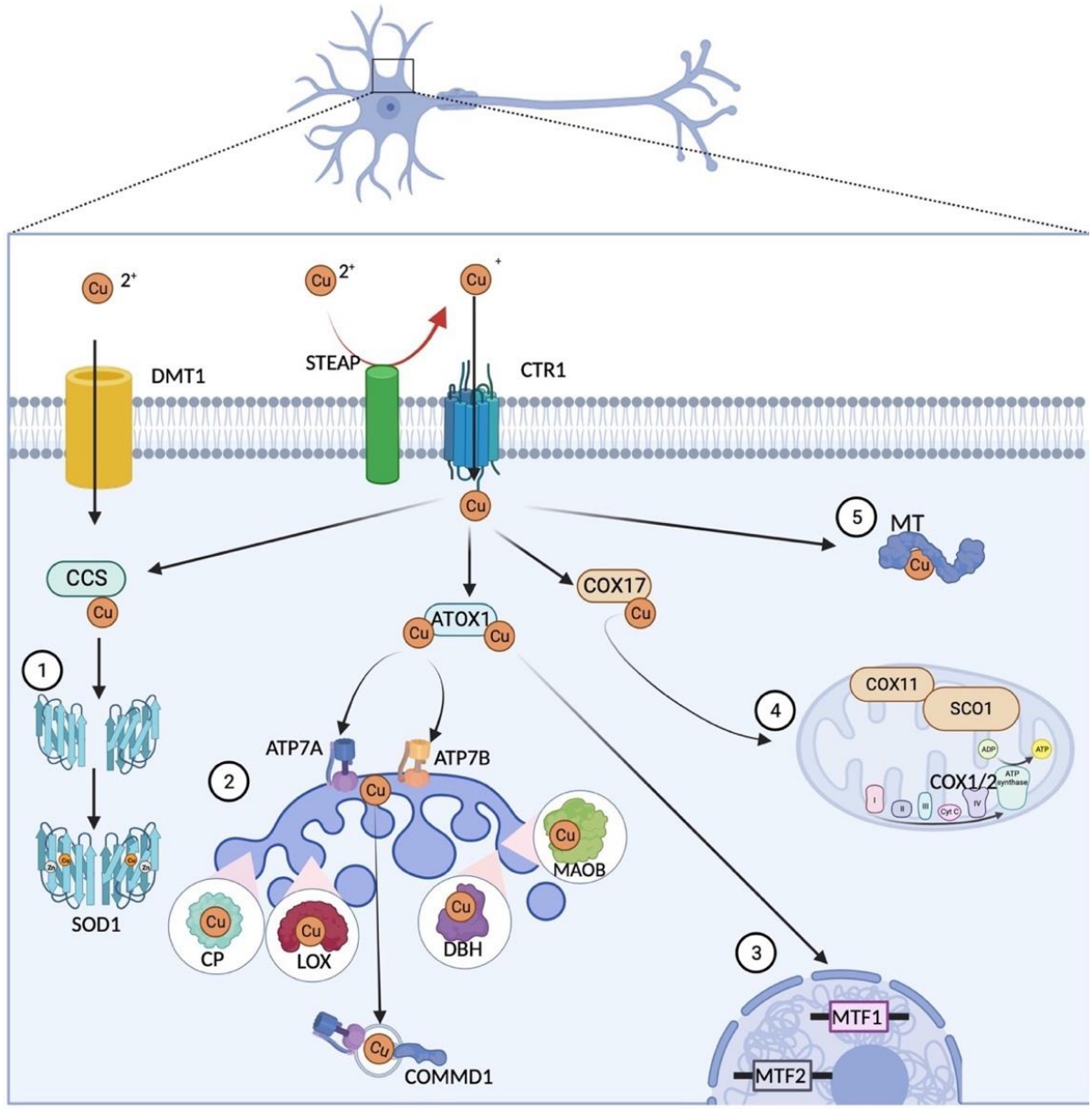

Figure 1.5. Copper transport and handling within cells

Extracellular copper in the oxidase form (Cu^{2+}) is reduced by metalloreductase, STEAP proteins before it enters the cells via copper related transporter 1 (CTR1). Copper can also enter the cell by divalent metal transporter 1 (DMT1). Copper can be bound by chaperones and shuttled to various pathways including; **1**) incorporation into superoxide dismutase 1 (SOD1) within the cytosol via its chaperone for SOD1 (CCS); **2**) bound to antioxidant chaperone 1 (ATOX1) and shuttled to ATPases, ATP7A and ATP7B to be incorporated into cuproenzymes (like ceruloplasmin; CP, lysyl oxidase; LOX, dopamine beta hydroxylase; DBH and monoamine oxidase B; MAOB) through the trans Golgi network (TGN) and excess is released via vesicle-mediated exocytosis that is facilitated by ATP7A and copper metabolism murr1 domain (COMMD1) with ATP7A is recycled back to the TGN; **3**) Excess copper levels stimulate the expression of metallothionines via metal regulatory transcription factors (MTF1/2); **4**) transported via chaperones Cytochrome C oxidase 17 (COX17) into the mitochondria and through inner membranes via Cytochrome C oxidase 11 (COX11) and synthesis of cytochrome c oxidase 1/2 (SCO1) to be delivered to Complex IV and **5**) storage into metallothionines (MT). This figure was created using Biorender.

1.5.4 Cuproenzymes

Integral to various metabolic pathways, copper is essential for the function of several of the body's cuproenzymes as outlined in **Table 1.3**. Many of these copper handling and cuproenzymes genes are regulated by the intracellular availability of copper and iron, through a transcription factor specificity protein 1, known as Sp1. With its three zinc finger domains Cys_2-his-Cys domains which recognises CG box in DNA sequences [268], Sp1 is affected by excess copper as it displaces the zinc ions, resulting in confirmational change and compromising the binding to DNA promoters [269, 270]. Many of these cuproenzymes are expressed ubiquitously and are also there are exclusively expressed within certain cell types within the CNS. Here we describe a few important of these copper-dependent and how they are regulated in mammalian cells.

Human cytochrome c oxidase also known as complex IV, is the terminal copper-dependent enzyme in the electron transport chain. Copper delivery from the cytosol into the mitochondria is performed by a series mitochondrial specific chaperones (COX11, COX17, SCO1 and SCO2). Human complex IV is composed of 14 subunits for the assembly within the intermembrane space, with two of the three catalytic subunits COX1p and COX2p requiring both copper and haem for electron transfer. While the exact mechanism of copper transfer to COX1p being unknown, it is suggested that the supply of copper to a nascent COX1p is a transient interaction within the intermembrane space [271, 272]. Copper delivery to the COX2p subunit is shared by initially by COX17, then by SCO1 within the inner membrane of mitochondria [273]. Copper deficiency has a significant impact on the assembly and biosynthesis of complex IV, which causes repression of respiration and reduced ATP levels [274, 275]. The activity of complex IV is reduced significantly in a variety of different tissue matrices including the brain when there is lack of dietary copper [276], in genetic altered copper-deficient models [194, 277] and in neurodegenerative diseases [278, 279].

Within glycosylphosphatidylinositol-anchored (GPI) astrocytes and in circulation within neurons, ceruloplasmin catalyses ferrous to ferric iron for binding into apo-transferrin for its immediate removal from the cell [280-282]. Based on its various functions other than iron export, the expression of ceruloplasmin is thought to be regulated by various factors including

iron, inflammation, and ROS [283-285]. The translation of ceruloplasmin is not reliant on the availability of copper but the copper deficient form, apo-ceruloplasmin requires copper for its correct folding [286]. Apo-ceruloplasmin degrades rapidly with a short life of 5 hours [281]. The delivery of copper to ceruloplasmin is thought to arise from ATP7B after synthesis of apo-ceruloplasmin in the trans Golgi network, which requires six copper atoms that occupy six ligand binding sites [286, 287]. Copper deficiency in cells has an enormous impact on the activity of ceruloplasmin whereby its alteration leads to intracellular iron accumulation, oxidative stress and cellular death [208, 288-290]. The alterations in its ferroxidase activity provides the link between iron accumulation and the loss of copper that is seen in many neurodegenerative conditions like AD, PD, ALS [119, 196, 208, 291], genetic defects in aceruloplasminaemic patients [281] and also within many their associated aberrant genetic animal models [292].

As a neurotransmitter rate limiting enzyme, the copper-dependent DβH is involved in the biosynthesis from the catalytic breakdown dopamine to form norepinephrine. Found within the adrenal medulla, heart and the CNS [293-295], the enzyme activity requires not only copper but requires oxygen, and an additional cofactor ascorbic acid, as an exogenous electron donor [296]. In SH-SY5Y cells, the levels of soluble DβH in secretory vesicles are associated with the intracellular copper levels [297]. DβH is subject to strict transcriptional regulation and many inhibitors and enhancers have been discovered, including copper-sensitive transcription factor Sp1 [298]. Lower levels of copper alter both the enzymes activity and its expression levels in both mice [299] and patients with Menkes disease [181]. The delivery of copper is performed by ATP7A within the lumen of the Golgi, and with the lack of copper, causes the retention of DβH, and an increased to dopamine to norepinephrine ratio [300]. Dopamine, which is highly reactive and can undergo spontaneous oxidation to produce toxic dopamine-quinones intermediates can induce oxidative stress, and toxicity when excess levels are present in the cytosol.

Homologous to ceruloplasmin, hephaestin is also part of the oxidase family, where its primary role is to facilitate the export of intracellular iron. Hephaestin has similar characteristics to ceruloplasmin, with a high 68% sequence homology, conserved copper binding site, disulfide bond formation [301] and copper acquisition through ATP7B [287, 302]. Tethered to

membranes, hephaestin is expressed within the entire gastrointestinal tract, pancreas at lower levels in the brain with expression mainly seen within oligodendrocytes [303, 304]. Hephaestin being an essential component of iron homeostasis in the brain, is transcriptionally regulated by copper and iron levels, but does not appear to be dependent on an iron response element. Transcription of hephaestin is co-ordinately upregulated in both iron deficient and higher copper conditions in concert with DMT1 and iron exporter protein ferroportin [304, 305]. Chen *et al*. (2006) found that hephaestin levels were lower when mice were fed a copper-deficient diet and when HT29 cells were treated with copper chelator bathocuproinedisulfonic acid (BCS) [306]. Studies of double mutants of ceruloplasmin and hephaestin show that both astrocytes and oligodendrocytes accumulate more iron in the brain than with one mutant alone [307, 308]. It was shown that in gray matter, hephaestin knockout mice not only showed iron and oxidative stress levels was elevated within oligodendrocytes, but these mutant mice exhibited motor deficits [206, 309].

Within the brain and the periphery, monoamine oxidase b (MAOB), is an enzyme that catalyse the breakdown of biogenic amines including dopamine, through oxidative deamination, leading to the production of norepinephrine. While expression is seen in the liver and kidney, MAOB is highly expressed in the brain particularly within both astrocytes located in the mitochondria's outer membrane and within serotonin containing neurons [310]. The activities of MAOB also shown to regulate the biosynthesis of GABA in diseased astrocytes in a mouse model of AD [311]. MAOB is also a target for PD, with its inhibition using deprenyl (selegiline) conferring a treatment for PD to retain dopamine supply within an ailing dopaminergic system [312]. MAOB activity is dependent on copper together with the additional cofactor, flavin adenine dinucleotide [313] with its regulation reliant on early growth response element 1, cAMP response-element binding protein and Sp1 [314, 315]. Altered levels of MAOB have been associated with motor-related neurodegenerative conditions including PSP [316].

Table 1.3. Mammalian copper dependent enzymes

Cuproenzymes	Abbreviation	Cellular location	Function
Cytochrome c oxidase (EC 1.9.3.1)	complex IV	Mitochondria - inner membrane space	Electron transport chain, energy production
Ceruloplasmin (EC 1.16.3.1)	CP	Plasma membrane-based	Ferroxidase, iron transport (astrocytic)
Superoxidase dismutase 1 (EC 1.15.1.1)	SOD1	cytosolic	Antioxidant; dismutase superoxide radical
Superoxidase dismutase 3 (EC 1.15.1.1)	SOD3	Extracellular	Antioxidant; dismutase superoxide radical
Dopamine beta hydroxylase (EC 1.14.17.1)	DβH	Neurosecretory vesicles	Catecholamine synthesis; conversion of dopamine to norepinephrine
Hephaestin (EC 1.16.3.1)	HEPH	Membrane	Ferroxidase, iron transport (astrocytic)
Lysyl oxidase (EC1.4.3.1)	LOX	Extracellular	Cross linking of collagen and elastin by the deamination lysine and hydrolysine.
Monoamine oxidase b (EC 1.4.3.4)	MAOB	Mitochondria	Breakdown of biogenic amine using dopamine as a substrate.
Myeloperoxidase (EC 1.11.2.2)	MPO	Cytoplasmic granules, vesicles, mitochondria and nucleus	Antimicrobial present in phagocytes
Tyrosinase (EC 1.14.18.1)	TYR	Cytosol	Conversion of tyrosine to melanin
Peptidylglycine monooxygenase (EC 1.14.17.3)	PAM	Membrane-based within secretory granules	Synthesis of amindation of neuroendocrine peptide
Tyrosinase (EC 1.14.18.1)	TYR	Cytosol	Conversion of tyrosine to melanin

1.5.5 Disrupted copper availability promotes SOD1 pathology

The superoxide dismutases are a family of a metalloenzymes that provide frontline defence against the intracellular production of oxidative metabolite superoxide that is produced by cells. Among the SODs, SOD1 is the most abundantly expressed, residing within the cytosol, as well as subcellular compartments such as the nucleus, mitochondria, and lysosomes [317-320]. Renamed in 1969 to reflect its enzymatic activity towards superoxide [23], SOD1 is essential, with genetic deletion resulting in cell death [24, 25]. Ubiquitously expressed, SOD1 is a highly abundant and stable enzyme in its mature form. The immature form of SOD1 must undergo posttranslational modifications to form a fully active and functional enzyme (**Figure 1.6**). This includes dimerisation, metalation, and tertiary folding to form a stable homodimer [321-325]. The supply of copper to nascent SOD1 involves the copper chaperone for SOD1 [247, 326, 327] which provides one copper atom to each SOD1 monomer subunit (**Figure 1.6a**). This facilitates the formation of a disulphide bridge that brings together two monomer subunits [322]. Without copper, SOD1 is less stable under physiological conditions [328]. Moreover, copper-deficient SOD1 monomers provide a precursor to the formation of SOD1 aggregates [321] and copper insufficiency causes the protein to misfold in a fashion similar to other amyloidogenic proteins associated with neurodegenerative disease [329, 330].

As SOD1 has direct links with ALS [27], its role in this disease context has been extensively researched [28, 331]. Mutations within the disulphide bridge and within the copper binding domain of SOD1 can promote the formation of insoluble cytoplasmic aggregates within glia and motor neurons in some cases of ALS [332] and mouse models of the disease [333]. Despite ubiquitous expression of mutant SOD1 in ALS and animal models thereof, accumulation of the protein in an aberrant copper-deficient state is most evident within the CNS [31, 334]. Moreover, promoting the physiological copper state of mutant SOD1 *in vivo* through pharmacological and genetic interventions is associated with neuroprotection and improved indications of neuronal function [32, 335, 336]. Aggregates of SOD1 in ALS-affected spinal cord contain less copper than the surrounding gray matter that contain no SOD1 pathology [36] and, like ubiquitin, the copper chaperone for SOD1 is also a constituent of protein aggregates found in cases of ALS [337, 338]. **Table 1.4** provides a list of protein constituents found within SOD1 aggregates.

Notably, mutations in SOD1 are not required for aggregation of the protein in neurodegenerative disease. Disruption of copper handling mechanisms and SOD1 pathology are evident in the disease-affected tissue of sporadic cases of ALS which do not involve mutant SOD1 [36, 196, 339]. Moreover, data illustrative of decreased copper availability in PD [208] are accompanied by histological and biochemical data for SOD1 aggregation in the human, PD-affected brain [141, 340]. This includes evidence derived from use of conformation specific antibodies raised against epitopes that are naturally inaccessible when buried within the physiological structural fold of SOD1 (e.g., B8H10 and EDI). Immunoreactivity for these antibodies indicates destabilised forms of SOD1 are present in over 70% of substantia nigra *pars compacta* cells in PD [141]. Significantly, SOD1 pathology in PD is reported to be a strong correlate of neuronal loss in PD [141] even though the cases of PD examined were confirmed free of SOD1 mutations [341].

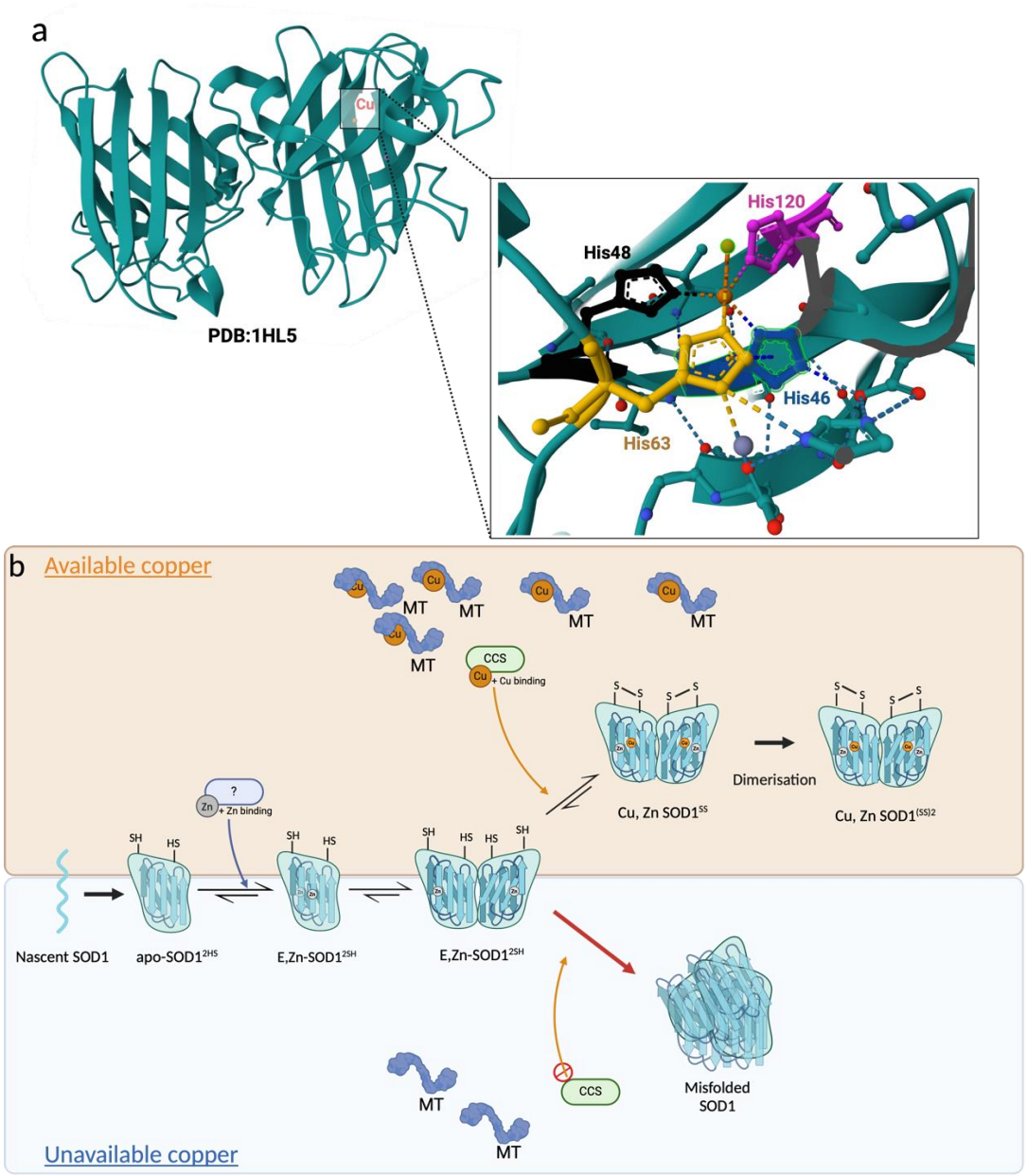

Figure 1.6. Copper coordination sites and the effect of copper availability on the maturation of SOD1

a) Local coordination sites of copper within SOD1 (Protein database; PDB;1HL5) insert showing the 4 histidine sites that are involved in copper binding when copper is oxidised (His46; blue, His48; black, His63; yellow, His120; pink and copper Cu^{2+} in orange) **b**) Schematic representation of the normal maturation process is SOD1 which is still not completely understood. Nascent SOD1 peptide undergoes successive folding, into a monomeric metal deficient SOD1 (apo-SOD12HS). Zinc is thought to be delivered to metal deficient SOD1 (apo-SOD1) first by an unknown process to initiate the metalation process to form weak dimeric bonds (E, Zn-SOD12SH) and can interchange between monomer and dimer (bidirectional arrows). If copper is available, with a large pool bound to metallothionines (MT), within the cytosol, copper chaperone for SOD1 (CCS) is able to deliver copper to SOD1. Transfer of copper into metal binding sites induces oxidation of (Cys57, Cys146) [329] and forms a stable dimeric enzyme once the disulphide bridge is formed (SOD1SS). If copper is unavailable, the lack of copper delivery to SOD1 induces SOD1 to misfold and can recruit nascent, monomeric SOD1 and copper deficient SOD1 to misfold and form protein aggregates in the cytosol.

Table 1.4. Identification of protein constituents in SOD1 aggregates

Protein		Function	Reference
Superoxide dismutase 1	(SOD1)	Cytosolic antioxidant	[338, 342]
Nitric oxide synthase	(NOS)	Enzyme catalysing the formation of nitric oxide	[343]
Ubiquitin	(Ub)	Post-translation tag to degrade proteins	[38]
14-3-3 proteins		Multi-functional phosphor-binding proteins that regulate cellular functions	[344]
Copper chaperone for SOD1	(CCS)	A chaperone to delivery copper to SOD1	[338]
Cathepsin D		Aspartate protease	[29]
Glucose-regulated protein 78-kDa	(GRP78/BiP)	ER chaperone protein	[38]
Lys-Asp-Glu-Leu	KDEL	Target signalling peptide	[38]

1.6 Measurement of metals

Measuring metal content in biological tissues is important for understanding the biology of metals including the alterations seen in health and disease. It is imperative to find a method for measuring metals in a certain state that reflects their complexity in biological tissue that is reliable, accurate and valid. Metals are complex because they are present as multiple chemical species, oxidation states and are bound to diverse molecular structures. Both the isotopic speciation and oxidation state of metals can influence the bioavailability, absorption, ability to cross membranes, biological activity, and toxicity properties [345]. Traditionally, histochemical methods were used to determine copper abundance in various tissues and cell types. This approach has a semi-qualitative ideology but was a valuable method at detecting high levels of copper in astrocytes compared to neurons particularly close to the ventricular regions [127]. Analytical technologies are now widely used to measure trace elements in biological samples, such as brain samples, using methods such as atomic absorption spectrometry (AAS) and inductively coupled plasma mass spectrometry (ICPMS), which are the most commonly used and described methods for detecting metallo-biological changes within the brain. Several factors must be considered when choosing an analytical technique that can accurately measure metals in complex matrices, including sample type, sensitivity, speed, element of interest, cost, and availability of the technology (see **Table 1.5** for a description of the advantages and limitations of each method). AAS was the first tool for spectrometric metal analysis in samples and is widely used in many industries [346]. The sample is atomised using a graphite or flame furnace atomiser, which the atoms once free and upon exposure to light (hollow-cathode lamp) transition from ground to excited energy states with radiation of energy states absorbed is measured [347]. To ensure only the element of interest is detected, monochromators are employed to select the wavelength of the light to minimise interference with the intensity of the beam measured by a detector. The advantages of AAS include its high throughput, sensitivity, and low cost per analysis. However, this method does not have the ability to measure multiple elements in complex samples unlike newer technologies (**Table 1.5**).

Based on the Mössbauer effect, Mössbauer spectroscopy measures the atomic nucleus and is primarily used to study iron metabolism in samples [348-351]. In accordance with its

principles, a sample is exposed to radiation (in the form of gamma-rays), where the gamma-rays excite the atomic nucleus. In order to maintain its energy, the nucleus must move with equal and opposite momentum, and the intensity of the beam of energy transition is measured and analysed by a detector [350]. While this technique is non-destructive to the sample, it has a poor sensitivity as it measures only subtle differences in molecular structure and nuclear species (oxidation states) [351, 352]. Its application is limited to detecting specific isotopes and requires specific operation conditions (temperature/pressure)[351, 352] (**Table 1.5**).

Synchrotron X-ray based absorption and emission techniques have been developed over the last decade to characterise materials in complex matrices. While these tools are both versatile and powerful, they are restricted in terms of both their availability and accessibility in beamtime, and experimental timeframes can take longer than the granted access (**Table 1.5**). One of these techniques, X-ray absorption near edge structure (XANES), is where photons produced by X-ray beam are at an energy above its absorption edge (~50eV), and are absorbed by core electrons of a sample [353]. This change in energy across the edge is due to a hole within the inner shell and an electron from a higher energy state falling into this vacancy. The energy that is released can have the effects of 1) cause fluorescent emission to release photons or 2) can excite and eject electrons from a higher energy state. The absorption edges reveal the elements that absorb within X-ray absorption spectra [353]. Only until recently, XANES is used as a imaging tool to map speciation of metals in complex biological tissues in situ [354]. XANES provides further evidence for metal speciation shifts and changes in metal-complexes in neurodegenerative diseases [355]. Complementary to the speciation information from XANES, X-ray fluorescence microscopy (XFM) that is often in conjunction as XANES, can facilitate the location and quantification of elements down extremely low detection limits [353]. *In situ* mapping of elements using XFM does not require the destruction of the sample which can alter the endogenous metal concentration and chemistry. The emitted X-ray fluorescence signals from XFM, aids in the resolution of elements at a subcellular level and can reveal information about the cells metal homeostasis. Importantly, XFM has determined a significant shift in the copper to zinc signal in ALS CNS tissue with a lower copper level (12%) within SOD1 aggregates within ALS compared to the surrounding tissue [36].

Micro-particle induced emission (µPIXE) is another synchrotron-based technique to identify and determine concentration of various elements in a sample. Using a particle accelerator (2-4MeV), a sample is irradiated, and energy is released as photons as electrons in higher shells fill the gaps, giving off excess energy [356]. An ion beam is concentrated on a small spot size and is sampled across the sample's surface. The X-ray spectra is collected for each of the rastered points to create an elemental map. Each element has its own characterisation based on its X-ray energies it emits and the intensity of these X-ray lines can determine its concentration [356].

Nano-secondary ion mass spectrometry (nano-SIMS) is a new generation of ion-microprobes that acquire nanoscale resolution to measure elements within scales. Nano-SIMS is commonly used to detect cellular structures, organelles and proteins in tandem with rare biological isotypes or newly synthesised fluorescent probes with rare isotopes to increase resolution [357, 358]. With nano-SIMS, a rastered ion beam is used to ablate the surface of a solid sample, and metal is detected with a mass spectrometer [359]. The focus of a small spot size ion beam enables nanoscale spatial resolution to give both cellular differentiation [360]. In addition, isotypes can be distinguished within the sample since nano-SIMS utilised the separation of ions by mass [359].

While having a small primary ion beam allows for greater sensitivity and larger dynamic range, it is also its nano-SIMS greatest hinderance. As the beam size gets smaller, so too does the interaction volume and the number of secondary ion from the surface is reduced [361]. This also increases the time for imaging acquisition. Furthermore, the secondary ion yields of different elements change with the complexity of the matrix making both calibration of the instrument and determining concentration very difficult [361].

Due to its lower detection and higher sensitively limits, ICPMS is the method of choice for most laboratories for determining metal content in a variety of different tissue matrices including the brain. The principle of ICPMS is the plasma generates and converts the sample into positively changed ions. The liquid sample after digestion are introduced into the system by neubilisation, with the aerosol being transferred to argon gas (plasma). The element spectra are generated by the ionisation of plasma (argon) that is heated to 7000K [362]. The biological sample is therefore undergoing ionisation and atomisation and with each element passing through ion optics then separated by mass to charge using a mass

spectrometer (quadrupole) please see review for detailed description [362]. ICPMS is the most common method for determining total metal content due to its low interference from tissue sources, higher dynamic range (5-7 orders), and the ability to detect multiple elements in a single sample (**Table 1.5**) [334].

With the advantage of being fast and sensitive than AAS, ICPMS does have drawbacks with spectral interference cause by polyatomic, or isobaric species that arise from sample matrices, solvents and surrounding plasma [362, 363] (**Table 1.5**). However, these interfering species often affect lighter elements and there have been newer strategies and technologies that have attenuated these spectral interferences [364, 365].

To effectively evaluate normal and pathological effects of metals including copper, it is essential to understand *in vivo* copper concentrations in biological systems. When it comes to measuring changes in copper in neurodegenerative diseases, to date there is no standard method for sample collection, preparation and analytical tool used determine changes in copper which make evaluating data across multiple studies extremely challenging. In addition, there is limited data on copper distribution across organs, tissues, biofluids, cell types and subcellular compartments. These studies have a heavy focus on measuring total copper within a tissue sample with no reflection of the subcellular partitioning of copper within the cell. The use of differential centrifugation to separate subcellular components of cells has given a greater understanding of copper changes that have been observed across many diverse neurodegenerative diseases [196, 366, 367]. The redistribution of copper in cellular fractions has revealed copper pools deficient in cytosolic fractions, enriched within subcellular compartments [196, 366, 367] or within insoluble protein aggregates [147] in brain tissue from cases with neurodegenerative diseases. Using this knowledge, we can adopt and develop drugs that can act to divert redistribution and supply deficiencies as needed. Due to the complexity of the brain, a certain cytoarchitecture exists within each sample and region, which explains how chemical imaging technologies have developed to visualize copper changes within different types of brain cells. A bulk sample of brain tissue taken at the time of post-mortem extraction would likely contain multiple neuroanatomical structures and, therefore, dilute the copper concentration. These days, traditional methods, like ICPMS are now complemented with the advent of more advanced metal imaging such as laser ablation -inductively coupled plasma mass spectrometry (LA-ICPMS). LA-ICPMS is a sensitive analytical

technique used to determine the chemical and isotopic compositions of a solid-based sample. The mounted tissue is ablated using a pinpoint laser with a spatial resolution of 30 µm, while the analyte is carried through using an inert gas, argon into the mass detector. LA-ICPMS, like ICPMS discussed above, can detect elements down to the parts per trillion but without the need to physically dissect the tissue. *In situ* quantification of copper using LA-ICPMS has the spatial resolution to discriminate distribution patterns of metals within important neuroanatomical regions. Moreover, the potential to identify cell-type specific disturbances could help identify metabolic disturbances between neurons, astrocytes and oligodendrocytes. A combination of *in situ* imaging and bulk ICP-MS has not been used to determine region specific changes and copper distributions in post-mortem tissues from PSPs to date. In tandem, these techniques may shed light on the copper distribution changes in PSP across specific regions, cell types, and subcellular structures that have been overlooked in previous studies.

Table 1.5. Comparative table of analytical techniques for detecting metals in biological tissues

Analytical technique	Detection/resolution	Strengths	Limitations	References use in human CNS tissue
Atomic absorption spectroscopy (AAS)	**Detection limits** (0.1 μg mL^{-1}) **Resolution** (0.02–2 nm)	High throughput High sensitivity (ppm/ppb) Inexpensive Minimal inter-element interference	Solution samples only Can only measure one analyte at a time Cannot detect non-metals	AD [368] ALS [369, 370] PD [22]
Inductively coupled plasma mass spectrometry (ICPMS)	**Detection limits** (10 pg ml^{-1}) **Resolution** (<1 amu)	High throughput High sensitivity (ppm/ppb) Multi-element analysis Isotopic analysis	Destructive of tissue sample Liquid samples only	AD [371, 372] ALS [196] PD [175, 208, 366] PSP [373]
Laser ablation - Inductively coupled plasma mass spectrometry (LA-ICPMS)	**Detection limits** (0.01 μg g^{-1}) **Resolution** (5-150 μm)	High sensitivity (ppm/ppb) Solid, liquid samples Multi-element analysis Spatial distribution of elements Isotopic analysis	Destructive of tissue/sample Longer scan times for large tissue Low throughput Cannot map subcellular distribution	AD [374-376] ALS [196] PD [21, 377-379] PSP [112]
Mössbauer spectrometry	**Detection limits** (20 μg g^{-1}) **Resolution** (100 μm)	Analyse delicate samples (Non-destructive) Metal species differentiation (oxidative states)	Low sensitivity Limited to certain isotopes (Fe^{157}) Limited to operational environment (temperature/pressure)	AD [380] ALS PD [380-382] PSP [380]
Nano-scale secondary ion mass spectrometry (nano-SIMS)	**Detection limits** (0.1 μg g^{-1}) **Resolution** (50–100 nm)	High sensitivity (sub-μm scale) Distinguishes different isotopes Creates 2D - 3D elemental maps	Destructive of tissue/sample Imaging acquisition is slow (small beam size) Difficulties in absolute quantification	AD [355, 383, 384]
Micro particle induced X-ray emission spectroscopy (μPIXE)	**Detection limits** (1–10 μg g^{-1}) **Resolution** (100 μm)	High spatial resolution, low detection limits Multi-element analysis High sensitivity (ppm)	Can only probe a small region of sample (10-50 μm)	AD [385-387] ALS [388] PD [389]
X-ray absorption near-edge structure (XANES)	**Detection limits** (1 μg g^{-1}) **Resolution** (1 μm)	High spatial resolution, low detection limits Analyse delicate samples (Non-destructive) Solid, liquid samples Metal species differentiation (oxidative states) Determine a number of properties (coordination environment, complexes)	Accessibility and availability are limited Cannot determine relative concentration of elements	AD [355] ALS [355] PD [355, 390, 391]
X-ray fluorescence microscopy (XFM)	**Detection limits** (0.1-1 μg g^{-1}) **Resolution** (0.1-1 μm)	High spatial resolution, low detection limits Multi-element analysis Analyse delicate samples (Non-destructive)	Accessibility and availability are limited Tissue handling (histological staining) required before/after XFM which may change metal concentration/distribution	AD [368, 385] ALS [36, 392] PD [393-395]

Table adapted from [396, 397].

1.7 Therapeutic strategies for PSP

Currently, there is no effective treatment available for PSP. It is important to note that in suspected cases of PSP, the treatments are primarily focused on relieving the symptoms associated with the disease, rather than treating the underlying pathology. Cases that present with parkinsonian variant PSP are generally supplemented with the pharmaceutical agents levodopa-carbidopa (dopamine precursor together with a DOPA decarboxylase inhibitor) with little benefit. The use of other parkinsonian treatments such as rasagiline (a dopamine breakdown inhibitor) [398] and deep brain stimulation are not recommended for PSP as they do not address significant symptoms such as falls, altered gait, and postural instability [399]. Disease-modifying therapies investigated to date for PSP include the antioxidant coenzyme Q10 [400], riluzole (a glutamate antagonist) [401], and therapies that focus on tau specific interactions and pathology such as Davunetide [402] and Tideglusib [403]. Clinical studies examining these treatment options did not meet primary endpoint outcomes related to reducing disease progression [404-406].

Microtubule stabilising compounds have been effective in improving axonal transport, reducing motor and cognitive impairments, and decreasing tau pathology in transgenic tauopathy models [407]. To date, however, these treatments have failed to translate from efficacy in preclinical trials using tau-based animal models to positive outcomes in clinical trials. Outcomes from an assessment of TPI-287, for example, indicated worsening of signs of disease in patients with AD, PSP, and corticobasal degeneration [408] despite the reversal of cognitive decline, attenuation of neuronal cell loss and enhanced clearance of tau by the similar taxane-based compound BMS-241027 in tau transgenic mice [409].

The development of tau-directed vaccines has resulted in new approaches to modulating tau in a variety of tauopathies such as PSP, including blocking its protein-protein interactions or promoting its clearance. Active immunotherapies that target microtubule binding regions of tau, including the active vaccine AADvac1 [410], show to reduce the truncated form of tau in rodents [411]. In human clinical trials, AADvac1 [410], have been shown to decrease total and phosphorylated tau in CSF samples from AD patients, and antibodies also showing proof of principle with strong tau immunoreactivity in PSP brains [412]. While AADvac1 demonstrated safety and tolerability, there was no improvement seen in clinical dementia

[413, 414]. Tau clearance is promoted by passive immunotherapies such as BBIIB092, an antibody that targets tau's N-terminal [415]. Repeated intravenous treatments for up to 2100mg doses in PSP patients showed that not only was well tolerated, but by day 85 unbound N-terminal tau was reduced within the CSF [416, 417]. A 52-week follow-up study of 490 PSP patients did not show clinical benefits, including reduced falls and no differences in gait or balance compared to placebo, despite a 98% reduction in N-terminal unbound tau within the CSF [418]. The strategy of targeting tau may not translate into clinical benefits, implying that therapies aimed at neutralising tau may be challenging.

Therapeutic strategies for neurodegenerative disease based on modulation of metal availability have been proposed for the treatment of neurodegenerative disease [419-421], with several translating to clinical trials [422-426]. PBT2 for example, is a cell and blood-brain barrier-permeant copper/zinc chaperone that has been shown to decrease tau pathology and cognitive deficits in tau transgenic mice [157]. A mechanism of action for PBT2 involves facilitating the transport of copper and zinc across plasma membranes to elicit a cell signalling response that inhibits tau phosphorylation [156]. Corroborative evidence for mitigation of tau phosphorylation through a mechanism involving copper is derived from studies involving the copper-delivery compound Cu^{II}(gtsm) which increases intracellular levels of available copper [427] and decreases tau phosphorylation *in vitro* and *in vivo* [151, 428]. Whether the tau response is primarily attributable to inhibitory phosphorylation of GSK-3β or stimulation of protein phosphatase 2A is yet to be resolved [151, 428]. Nonetheless, improvements in tau phosphorylation after administration of treatments that modulate available copper support a potential role for copper availability in tau pathology.

Structurally related to Cu^{II}(gtsm), the blood-brain barrier-permeant copper containing compound Cu^{II}(atsm) is neuroprotective in mouse models of ALS and PD [32, 429, 430]. A protective mechanism of action related to tau pathology is not yet reported. However, Cu^{II}(atsm) is confirmed to increase levels of physiologically copper-replete SOD1 within the CNS via copper delivery [335, 336] and the compound targets disease-affected regions of the CNS when administered to patients with neurodegenerative disease [431-433]. The neuroprotective activity of Cu^{II}(atsm) has been ascribed in part to regulated release of available copper from the atsm ligand via disease-associated changes in redox conditions and

the presence of a pool of apo-cuproproteins [427, 434, 435]. Collectively, these studies indicate that compounds capable of safely modulating available copper within the CNS have capacity to improve pathological features of neurodegenerative disease that involve tau and SOD1. With tau accumulation being the primary pathological hallmark of PSP and evidence beginning to emerge for the involvement of SOD1 pathology and altered copper availability, it is possible that therapeutic modulation of copper may be a plausible strategy for treating PSP. Direct experimental and analytical verification of this is required.

1.8 Experimental outline and rationale

1.8.1 Project summary and rationale

Metals are essential to human life as they are involved in many biological functions in the brain including neurotransmitter biosynthesis, metabolism, mitochondrial oxidation phosphorylation and antioxidant activity. Copper is a co-factor for many different proteins and enzymes in which it is static and buried within active sites with the flexibility to shift redox state during catalysis. As copper is tightly regulated within cells, any unbound copper like iron can induce oxidative stress by the generating ROS through reactions of Fenton and Harber-Weiss redox chemistry [136, 436, 437]. The excessive generation of ROS causes damage to many macromolecules within cells and can induce metal-mediated toxicity. Alterations in copper are observed along with increases in oxidative stress biomarkers in areas exhibiting neuronal cell loss, gliosis, and tau pathology in PSP [10, 21, 22, 201]. The dysfunction of copper handling mechanisms that regulate copper can impact the availability of copper for various cellular compartments and can also cause the aggregation of proteins such as tau which are pathological hallmarks of PSP.

One of the most commonly affected brain regions in PSP is the basal ganglion, a region that has a high metabolic demand and regulates motor movement and is also abundantly copper-rich [168, 173, 438]. Copper is decreased within key anatomic regions in the PSP brain which suggests that there could be a disruption in many cuproenzymes that require it for their function. Disrupted bioavailability of copper is a common feature seen in neurodegenerative conditions such as AD, ALS and within PD, with copper unavailable to be delivered to the important cellular antioxidant SOD1. Failure to load copper onto the active site of SOD1, which is seen as an early event in ALS, triggers its misfolding and leading to its aggregation. The antioxidant activity of SOD1 with the lack of copper within its active site, becomes impaired with the build-up of toxic ROS inside the cell ultimately causing its demise. The perturbed levels of copper that is seen in PSP could also have profound effects on other various cuproenzymes with selective distribution of copper that has been shown in ALS [196]. Multi-copper ferroxidases that aid in the removal of excess iron from cells, like ceruloplasmin are shown to be severely affected in neurodegenerative conditions of PD and ALS where together its activity is decreased [196, 208] and iron accumulates [21, 439, 440]. In PSP,

changes in expression of ceruloplasmin [22] and accumulation of iron is shown in various nuclei in the brain [21, 439, 440] which potentially links aberrant changes of both copper and iron to PSP pathogenesis.

The diversity of roles that copper plays in biology shows that there are multiple pathways that could be affected in PSP. Thus, one goal is to identify metal-associated mechanisms of neurodegeneration that can be one of many targets during the early stages of the disease in order to prevent cell death. In this thesis, immunohistochemistry, biochemical analysis, and proteomics were used to examine neurodegenerative mechanisms seen in PSP human post-mortem tissue. The overarching focus of this thesis is to investigate whether the disruption of copper availability is a feature of PSP whereby we observe SOD1 misfolding and pathology, changes in copper handling mechanisms and cuproenzymes together with various cellular pathways that may contribute to disease pathogenesis. The hypothesis of this project is that there are decreased copper levels in neuroanatomical regions in PSP that show high levels of pathological changes. The lower levels of copper in these regions have a profound impact on a diverse range of cuproenzymes that facilitate many different functions within the cell that lead to protein misfolding including SOD1.

The specific aims of this current study are as follows:

Aim 1. Assess SOD1 in specific brain regions from human cases of PSP.

Aim 2. Determine if SOD1 metal status and activity is perturbed in human cases of PSP.

Aim 3. Determine the molecular signature for copper availability in PSP brain samples relative to controls.

Aim 4. Assess copper-dependent functionality of additional cuproenzymes in PSP brain samples relative to controls.

Aim 5. Proteomic analysis to quantitate protein changes and pathways that are disrupted in PSP brain tissue.

Aim 6. Examine the relationship between copper availability and neuronal survival in vivo by partially knocking out the gene for copper transporter (*Slc31a1*).

1.8.2 Study design

In this study, we used both human samples from cases diagnosed with PSP together with aged-matched controls with no history of neurological illness and an animal model of copper deficiency. From the studies using human tissue, two tissue sources were used, paraffin embedded brain sections and fresh frozen tissue. Samples from cases, together with their demographics, are shown in **Table A1** in **Appendices**. Paraffin embedded sections were used for the histopathological analysis and the frozen samples were used for biochemical analysis as stated in each chapter methods section. The one frozen substantia nigra sample per case was used across a number of different biochemical assays and a uniform sample that consisted of the whole substantia nigra was prepared and described (**Figure 1.7**). We also obtained fresh frozen midbrain sections to perform LA-ICPMS that encompassed the two subregions of the substantia nigra to determine spatial distribution of copper within the substantia nigra *pars compacta* and substantia nigra *pars reticulata* (**Figure 1.7**). From the animal model of copper deficiency, (involving partial knockout of *Slc31a1*, the gene encoding CTR1), we used the substantia nigra dissected from mouse brain to perform similar experiments to determine if there was a similar histological and molecular phenotype that resembles that of PSP (**Figure 1.8**).

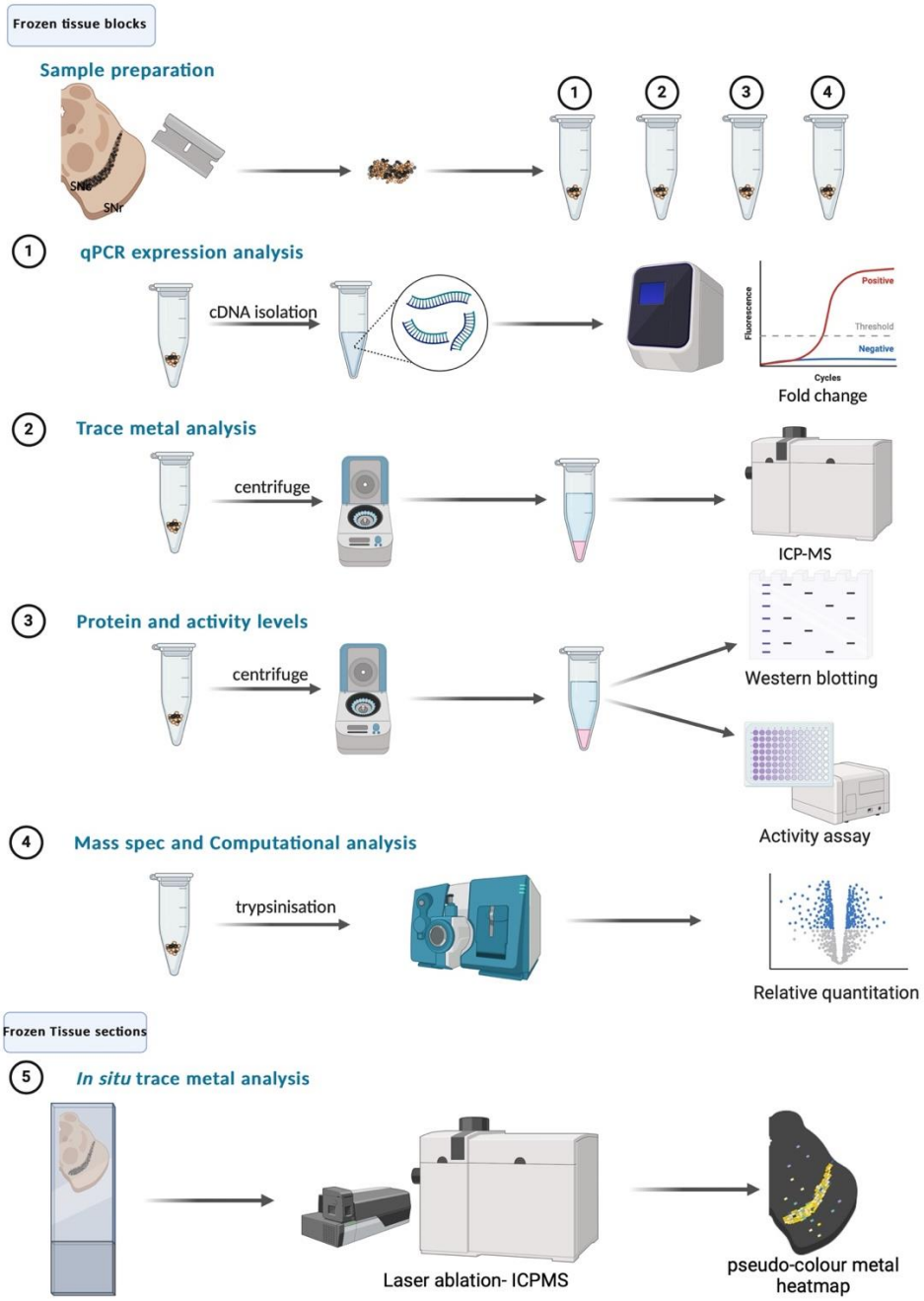

Figure 1.7. Workflow of frozen tissue from human PSP and control cases

A whole substantia nigra sample that contains both subregions *pars compacta* (SNc; dark pigmented region) and *pars reticulata* (SNr; sits adjacently below SNc). A uniform sample that combines both SNc and SNr was produced to keep the sample consistent across all assays. The substantia nigra sample were left to acclimatise on dry ice for 40 minutes, before the chunk of sample was powdered into small fragments using a warm fresh blade and combined before dividing up the sample into systematic tissue aliquots of ~10mg each. These samples were pre-weighed and snapped frozen in the -80°C until future until subsequent assays of **1**) quantitative PCR analysis **2**) trace metal analysis using Inductively coupled plasma mass spectrometry; ICPMS, and **3**) Protein levels measured by western blotting and activity assays and **4**) proteomic mass spectrometry analysis.

Frozen midbrain section which encompasses both of the subregions *pars compacta* and *pars reticulata of* substantia nigra were used to quantify **5**) trace metals *in situ* using laser ablation using Inductively coupled plasma mass spectrometry. A Pseudo-colour map of metal abundance is used to quantify the metal concentration within a region of interest.

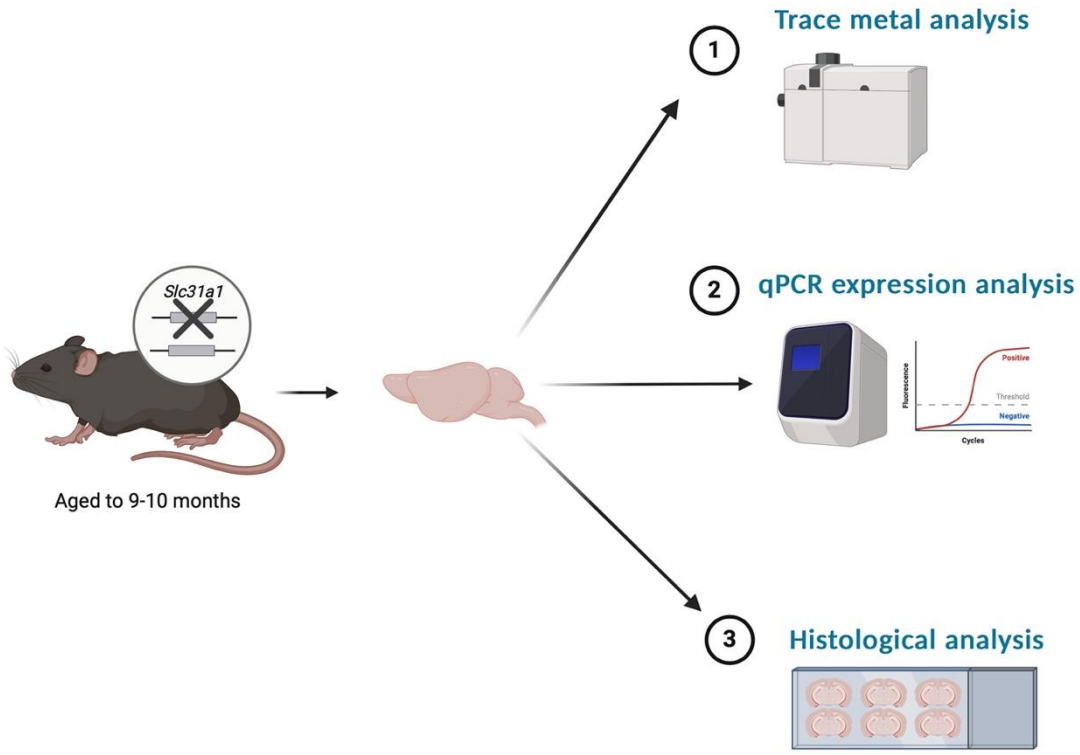

Figure 1.8. Workflow of mouse tissue from copper deficient animal model Scl31a1$^{-/+}$
Slc31a1$^{-/+}$ and littermate wildtype controls were bred to 9 - 10 months of age. Mouse brain samples were next collected and the substantia nigra was microdissected from the rest of the brain and used in biochemical and molecular analyses. Histological samples were prepared for cyrosectioning and were frozen once sectioned prior to Nissl and immunohistochemical staining. The microdissected samples were pre-weighed and snapped frozen in the -80°C until future until subsequent assays of quantitative PCR (qPCR) analysis and trace metal analysis using Inductively coupled plasma mass spectrometry (ICPMS).

Chapter 2. Investigating superoxidase dismutase 1 pathology in progressive supranuclear palsy

Commonalities among neurodegenerative conditions were discussed in Chapter 1 where proteinopathy and altered availability of essential metals were highlighted as features consistently evident across different conditions that result in diverse cognitive and physical symptoms of neuronal demise. Moreover, connections between altered metal availability and proteinopathies were described. Generally, distinct proteinopathies are described in terms of their specific neurodegenerative condition (e.g., amyloid plagues in AD). However, some proteinopathies appear to occur in several neurodegenerative conditions. Some of these have been recognised for some time (e.g., tauopathy in AD and Dementia with Lewy bodies) whereas others are only beginning to gain recognition. In the present Chapter, we examined SOD1 pathology in PSP. SOD1 is a copper-dependent enzyme mostly described in terms of ALS [27, 441, 442] but more recently described as a pathological feature of PD [141]. We examined SOD1 pathology in PSP because of disease commonalities shared with PD [39, 54, 78], prior reports on altered SOD1 in PSP [20], and prior indications that copper availability is disrupted in PSP.

2.1 Introduction

The characterisation of neurodegenerative diseases, and in some instances their confirmation of diagnosis, relies heavily on immunohistochemical detection of specific proteinopathy at post-mortem [443]. For PSP, this has primarily focussed on tau pathology. PSP brains show a distinct accumulation of aggregated tau in neurons, astrocytes, and oligodendrocytes, which correlates with neuronal cell loss and disease severity [444, 445]. However, multiple proteinopathies are now being identified in a large range of neurodegenerative diseases [141, 443] (as shown in Chapter 1, **Figure 1.3**), indicating that although some proteinopathies may be more conspicuous than others in certain diseases, the dysfunctional processes associated with neurodegeneration are not necessarily restricted to pathological alteration of one key protein. As therapeutic strategies for neurodegenerative diseases have to date tended to focus on preventing specific and readily detectable proteinopathies (e.g., tau in PSP), the implication herein is that on-going therapy development may need to incorporate poly-

therapy strategies that target multiple proteins and/or target mechanisms more broadly involved in maintaining proteostasis. Illustrative of the expansion in understanding of multiple proteinopathies in neurodegenerative disease, a study by Trist *et al*. (2017) showed that in PD, a primary synucleinopathy, SOD1 aggregates were evident within regions of degeneration regions in the PD brain [141]. In the absence of mutations within the SOD1 gene, SOD1 misfolding and dysfunction are features of the PD-affected brain [141]. SOD1 alone has been strongly linked to neuronal loss, with a level eight-fold higher in substantia nigra *pars compacta*, an area with severe neuronal cell death [141].

SOD1 is a frontline antioxidant whose physiological function involves formation of a homodimer in which each protein subunit acquires one copper atom and one zinc atom. Destabilisation of SOD1 and its potential subsequent aggregation can arise from post-translational modifications that affect the protein's correct folding and quartnery structure [321-325]. Notably, these include incomplete acquisition of copper and oxidative modification of the protein, factors that are implicated in PSP. Key areas in the brain that are vulnerable to tau pathology and neuronal cell loss in PSP are also associated with decreased copper levels [21, 22] and have indications of abnormal SOD1 accumulation [20]. This chapter further explores the potential role of SOD1 proteinopathy in PSP through direct examination of human, PSP-affected brain samples

Chapter 2. Investigating superoxidase dismutase 1 pathology in progressive supranuclear palsy

2.2 Hypothesis and aims

Considering that PSP has substantial biochemical and clinical overlap with PD, including decreases in copper, elevated brain iron and motor symptoms, as well as increased SOD1 expression, this chapter will investigate if SOD1 proteinopathy is present within PSP diseased-affected tissue.

Hypothesis: In regions where tau pathology and neurodegeneration are most prominent in the PSP brain as previously described [47], which is where copper depletion is most common, causing SOD1 to misfold and form pathological inclusions. The specific aims as per outlined in section 1.8.1:

Aim 1: Assess SOD1 in specific brain regions from human cases of PSP using immunohistochemistry.

.

2.3 Materials and methods

2.3.1 Post-mortem human brain tissue

Human ethics was approved for this project by the University of Melbourne (ID #21178, University of Melbourne Office of Research Ethics, and Integrity). Post-mortem brain tissue was obtained from Sydney Brain bank (New South Wales, Australia). PSP cases were clinically diagnosed with classic variant PSP-Richardson's (PSP-R) or parkinsonian variant PSP (PSP-P). Brain tissue from control cases involved and aged-sex matched individuals who died without any confirmed neurological condition. All case details are provided in **Table A1** (see in **Appendices**)**,** with **s**ample demographics for this chapter provided in **Table 2.1**.

Paraffin embedded sections were used for all histopathological analyses in this study. These were obtained from neuroanatomical regions that showed neurodegeneration, gliosis and mild to severe pathological tau distribution in the PSP brain according to Williams *et al.* (2007) [47]. Specifically, the substantia nigra *pars compacta*, substantia nigra *pars reticulata*, subthalamic nucleus, globus pallidus *externus*, caudate nucleus and the dentate nucleus (**Figure 2.1**). Sections were also obtained from visual cortex (Brodmann's area primary visual cortex; BA17) and these brain regions were assessed as regions not normally associated with PSP pathology (**Figure 2.1**). All brain regions were sectioned at 7 µm in a coronal plane with the exception of the substantia nigra *pars compacta*, substantia nigra *pars reticulata* and dentate nucleus which were sectioned on a transverse plane and mounted on superfrost slides (**Figure 2.1**).

Table 2.1. Descriptive demographics of PSP cohort

Group	N	Males	females	Age (years)	PMI	Disease duration (years)[#]
PSP	13	7	6	77.08 ± 1.62*	26.08 ± 5.44	7.15± 1.43
Control	9	5	4	83.0 ± 2.25	26.89 ± 4.90	N/A

Control cases were pathologically confirmed free of neurological disease. [#]Period from diagnosis to death. PSP: Progressive supranuclear palsy; PMI: Post-mortem interval; n/a: not applicable; significance is indicated when *P<0.05 (two-tailed t-test)

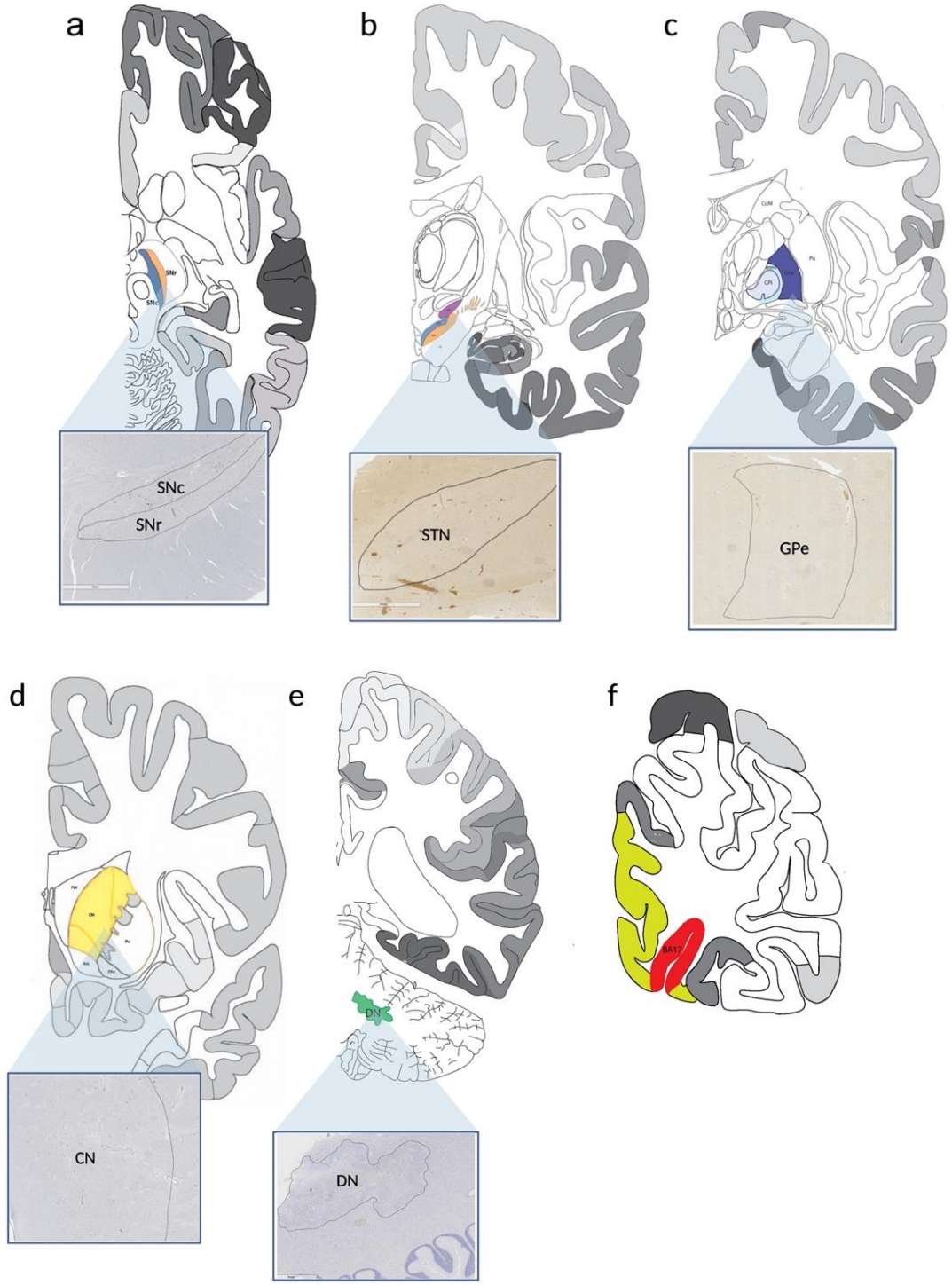

Figure 2.1. Human sections were immunostained for SOD1 in the neuroanatomical regions of the brain

Regions were selected based in tau distribution pattern observed by Williams et al. (2007) [47]. Each region was paraffined embedded, sectioned and mounted on glass slides. Regions examined were the **a**) substantia nigra *pars compacta* (SNc; blue) and substantia nigra *pars reticulata* (SNr; orange); **b**) subthalamic nucleus (STN; purple) **c**) globus pallidus *externus* (GPe; dark blue), **d**) caudate nucleus (CN; yellow) **e**) dentate nucleus (DN; green) and the **f**) sampled region from the visual cortex (Brodmann's area A17; red).

2.3.2 Immunohistochemical staining for SOD1

One designated slide from each region was immunohistochemically stained for SOD1 pathology. Validated by the Human Protein Atlas, the SOD1 antibody is capable of detecting physiological as well as aggregated forms of SOD1 (refer to **Table A2** in **Appendices** for antibody details). A known PD midbrain section (contains both the substantia nigra *pars compacta* and the *pars reticulata*) was used as a positive control for detection of aggregated SOD1 whereas negative controls involved omission of primary antibody on the same slide (each slide contained multiple sections from the same case). Samples were deparaffinised using xylene, exposed to a series of decreasing ethanol concentrations, then rinsed in ddH_2O. The sections underwent heat mediated antigen retrieval using a pressure cooker (Retriever 2100, Electron Microscopy Sciences) to boil in sodium citrate buffer (pH 6.0) for 10 min. Samples were then allowed to cool in the solution for an hour. Due to extreme melanin brown pigmentation of substantia nigra *pars compacta* obscuring 3,3'-diaminobenzidine (DAB) positivity [446], sections were rinsed in ddH_2O, then bleached for 21 hours overnight by immersion in a 10% H_2O_2 (H1009-500ML, Merck, USA) diluted in TBS (pH 7.4). Sections were washed with TBS-T (pH 8) three times for 5 min each and incubated with endogenous blocking solution (K802321-2Dako/Agilent) for 10 min at room temperature. Blocking solution was removed then sections incubated with primary rabbit anti-SOD1 (1:400, HPA001401, Merck) in diluent (3% NGS, 0.1% Triton-x100 and TBS (pH7.4)) for 10 min at room temperature. Sections were washed three times using TBS-T (pH 8.0). Sections were probed with secondary antibody IgG (K802321-2, Dako/Agilent) for 10 min at room temperature, then washed using TBS-T (pH 8.0) three times for 5 min each. For visualisation, DAB, together with chromogen substrate, was incubated on the sections for 5 min as per manufacturer's instructions (Dako/Agilent). Excess DAB was tipped off into bleach and sections rinsed three times for 5 min in ddH_2O. Tissue sections were counter stained using Hematoxylin (CS70030-2, Agilent) and Dako bluing agent (CS70230-2, Agilent) for 11 sec each, dehydrated in ethanol gradient and xylene, mounted in DPX and cover slipped.

2.3.3 Stereological quantification of accumulated SOD1

Quantification of accumulated SOD1 was performed using a microscopic design-based technique, stereology, which estimates the number of objects within a 2- or 3-dimensional region of interest. A physical fractionator (Stereo investigator version 11, MBF Bioscience) was employed as a probe to dissect thin sections for histological approximation using a stereological microscope (DMLB2, Leica, Germany). At least 100 sampling sites were assessed across x and y axes for all regions of interest except for the substantia *nigra pars compacta* due to its smaller area (**Table 2.2**). Neurons and glia within a counting frame of 110 x 110 µm across a delineated region with a superimposed grid based on Bokulic *et al*. (2021) with the grid size being adapted to the region's area (**Table 2.2**)[447]. Cell counting was performed whilst blinded to sample identification numbers and diagnostic group. DAB brown positive (accumulated SOD1) and negative (hematoxylin stained) cells were discriminated and counted under a 63X oil objective lens (1.4 numerical aperture; NA). Neurons and glia were distinguished from each other separately by their size, the presence of clear and visible nuclei, and their nucleolus to cytoplasm ratio (**Figure 2.2**). Endothelial cells were excluded based on their rectangular shape [447, 448]. The extent of SOD1 pathology within each region of interest was determined based on the number of cells counted for showing SOD1 accumulation (glial or neuronal) per mm^2.

Table 2.2. Stereological parameters relative to brain region of interest

Region of interest	Average number of sampling sites	Grid size (µm x µm)	Counting frame (µm x µm)
Substantia nigra pars compacta	78	300 x 300	110 x 110
Substantia nigra pars reticulata	140	300 x 300	110 x 110
Subthalamic nucleus	166	600 x 600	110 x 110
Globus pallidus externa	180	400 x 400	110 x 110
Caudate nucleus	142	900 x 900	110 x 110
Dentate nucleus	126	600 x 600	110 x 110

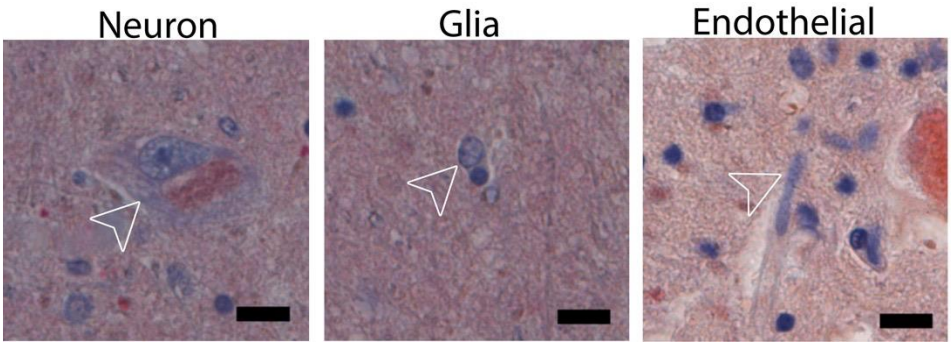

Figure 2.2. Morphological criteria for cellular discrimination of neurons, glia and endothelial cells

Neurons, glia and endothelial cells were distinguished by their individual cellular characteristics (nuclei, size and shape) under 63X magnification. Neurons have a prominent nucleus and nucleolus with a spherical shape and size (25-30 µm) as indicated in neuron panel with white arrowhead. Glial cells are sometimes multinucleated and size and shape are much smaller size of (10 µm) than neurons without processes as indicated glia panel with white arrowhead. Endothelial cells as indicated by the white arrowhead in endothelial panel are elongated and parallel to vessels. Black scale bar 25 µm.

2.3.4 Accumulated SOD1 pathology relative to neuronal and glial cell numbers

To explore the association between aggregated SOD1 pathology in PSP and neuronal loss, an index value for neuronal loss was calculated per case within the substantia nigra *pars compacta* and substantia nigra *pars reticulata* as described by Trist *et al.* (2017). In brief, the neuronal index was calculated by normalising the total number of neurons remaining in each case to the mean number of cells found in the control samples within the same region. This was performed to reduce the natural variation across samples. Once established, the neuronal index for each case/region was compared to the previously determined quantification of accumulated SOD1 (as described in methods Section 2.3.3). Similarly, an index value for gliosis was determined by normalising the total number of glial of each case to the mean number of glial cells found in the control samples within the same region and the relationship between glial index was also compared to the quantification of accumulated SOD1.

2.3.5 Detecting misfolded confirmation of SOD1

As forementioned in section 2.3.2, despite the antibody's ability to detect accumulated SOD1, it would be unable to distinguish what proportion of the total SOD1 is misfolded or aggregated and what is physiological levels. For this reason, we probed a small subset of PSP and control sections with a misfolded confirmation specific antibody called SOD1-exposed dimer interface (SOD1-EDI). The use of antibodies to detect confirmation specific and misfolded forms of SOD1 has been valuable in distinguishing natively folded from misfolded forms of the enzyme [35, 449, 450]. The antibodies recognised misfolded forms or epitopes that are buried within but are exposed when SOD1 misfolds [35, 449, 450]. In SOD1, the dimer interface is located at residues 145 to 151aa and the sequence RLACGVIGI is recognisable and is exposed as an aberrant monomer or an oligomer and not as a dimer [450]. Of the commercial misfolded antibodies, SOD1-EDI is the most sensitive antibody that can detect the early forming oligomers [449]. SOD1 forms the stable homodimer upon the metalation events of copper and zinc [322] as is rarely found in monomeric state. We employed the use of SOD1 exposed dimer interface (EDI) antibody to determine if SOD1 is found misfolded form in PSP tissue (refer to **Table A2** in **Appendices** for antibody details).

2.3.5.1 Triple immunofluorescent staining for GFAP and IBA-1, and accumulated SOD1 or SOD1-EDI

To identify which glial cells contain accumulated SOD1 or SOD1-EDI (misfolded), we performed triple labelling immunofluorescence. Using fluorophore conjugated secondaries as visualisation aids, the three antigens (GFAP, IBA-1 and SOD1/SOD1-EDI) were multiplexed with a secondary conjugated fluorophore with its own excitation and emission spectra for differentiation (see **Figure 2.3**). To increase specificity and limit cross-reactivity, accumulated SOD1 and SOD1-EDI antibodies were each incubated with different species of antibodies raised against common glial marker for astrocytes (GFAP) and fluorophore conjugated marker for microglia (IBA-1). An additional section with the omission of primary antibodies was used as a negative control to determine if there was non-specific binding of primary antibodies. Sections of substantia nigra regions (additional slides from Section 2.3.2) from each case (N = 6 PSP cases and N = 6 control cases) were deparaffinised using xylene then rehydrated using a sequential decreasing dilution of ethanol followed by ddH_2O. Using a pressure cooker (Retriever 2100, Electron Microscopy Sciences, PA), the sections were boiled in sodium citrate buffer (pH 6.0) for 10 min, then allowed to cool in the solution for over an hour. Sections were rinsed in ddH_2O, followed by a block step of 5% H_2O_2 (H1009-500ML, Merck, USA) diluted in TBS (pH 7.4) for 5 mins and a rinse in TBST (pH 8). Sections were blocked using donkey serum blocking solution (10% donkey serum, 0.3% Triton X-100 in Tris buffer, pH 7.4) overnight at 4°C with rocking. One section was incubated with primary antibodies goat anti-GFAP (1:500, Ab53554, Abcam) and rabbit anti- SOD1 (1:200, SOD1, HPA001401, Merck) and the other section with primary antibodies goat anti-GFAP (1:500, Ab53554, Abcam) and rabbit anti-SOD1-EDI (1:200, SPC-206, Stressmarq) made in antibody diluent (0.1% donkey serum, 0.3% Triton X-100, Tris buffer pH 7.4) for 1 hour at room temperature (see **Figure 2.3**). Sections were thoroughly washed three times for 10 min each using TBST (pH 8). Under dark conditions, fluorophore conjugated secondary antibodies donkey anti-goat Alexa 488 (Ab150177, Abcam) and donkey anti-rabbit Alexa 594 (150064, Abcam) were then applied to the sections, with both diluted to 1:1000 in antibody diluent (0.1% donkey serum, 0.3% Triton X-100, tris buffer pH 7.4) for 1 hour at room temperature. Sections were rinsed three times for 10 min using TBST (pH 8). Samples were reblocked with 3% bovine serum albumen (BSA) 0.3% Triton X-100, tris buffer pH 7.4) for 30 min at room temperature followed by incubation with IBA-1 (ab225261, Abcam) diluted to 1:100 in antibody diluent 0.1% BSA (0.3% Triton X-

100, tris buffer pH 7.4). Sections were rinsed three times for 10 min using 0.1M PBS (pH 7.4), counterstained with DAPI for 2 min, then rinsed for 10 min using 0.1M PBS (pH 7.4). Quenching of autofluorescence by lipofuscins was performed using 1x Trueblack solution made in 70% ethanol (Trueblack, Biotum) for 1 min, rinsed in 0.1M PBS (pH 7.4) mounted in aqueous mounting medium Fluroshield (F6182, Sigma-Aldrich) and sealed.

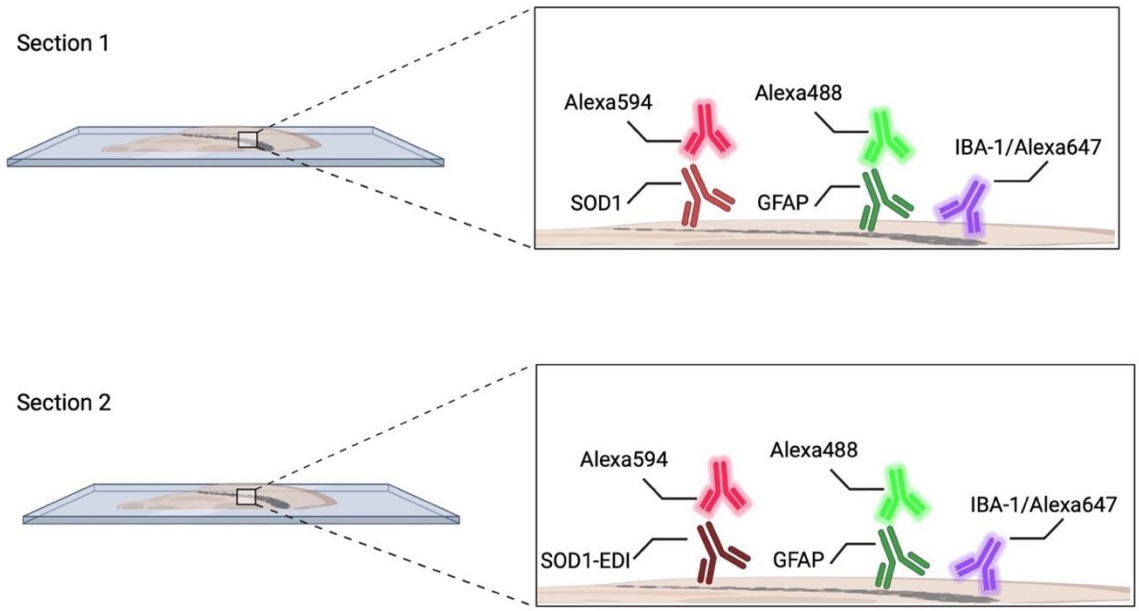

Figure 2.3. Triple immunofluorescence labelling of accumulated SOD1 and SOD-EDI in glia
Two midbrain sections per case (total of control; N = 12, PSP; n = 12) that contain the substantia nigra *pars compacta* and *pars reticulata* were immunostained to determine which glial cells, astrocytes (glial-fibrillary acid protein; GFAP) or microglia (Ionized calcium-binding adaptor molecule 1; IBA-1) the accumulated SOD1 and (exposed dimer interface) SOD1-EDI are located in. Section 1 was labelled with accumulated SOD1 antibody, GFAP and lastly conjugated IBA-1 Alexa647. Section 2 was labelled with SOD1-EDI, GFAP and then followed by conjugated IBA-1 Alexa647 outlined in section 2.3.5.1 Schematic diagram was created in Biorender.

2.3.6 Quantification of accumulated and SOD1-EDI immunofluorescence

Multiple antibody targets were visualised using fluorescence detection, with each fluorophore having a unique emission and excitation spectrum. Multispectral fluorescence images were captured on a Zeiss upright microscope (M2 Imager) using the Zen software (Zeiss) with an area size of 40.136 mm^2 calculated from a 20 µm scale bar. Individual images of four channels with filter-sets for DAPI (Ex 358 nm, Em 463nm), Alexa488 (Ex 493 nm, Em 520 nm), Alexa594 (Ex 590 nm, Em 619 nm) and Alexa647 (Ex 653 nm, Em 669 nm) were taken at 20X objective with four independent adjacent images from the ventral substantia nigra *pars compacta* and substantia nigra *pars reticulata* regions (total of 32 images per case) see **Figure 2.4**. Four channel images were merged using photoshop software (Adobe Photoshop) and the number of GFAP positive cells, GFAP positive cells with SOD1 within cytosol/nucleus, IBA-1 positive cells and IBA-1 positive with SOD1 within nucleus/radial arms were counted and averaged across the 4 individual images per region and case and were normalised by the area of the image.

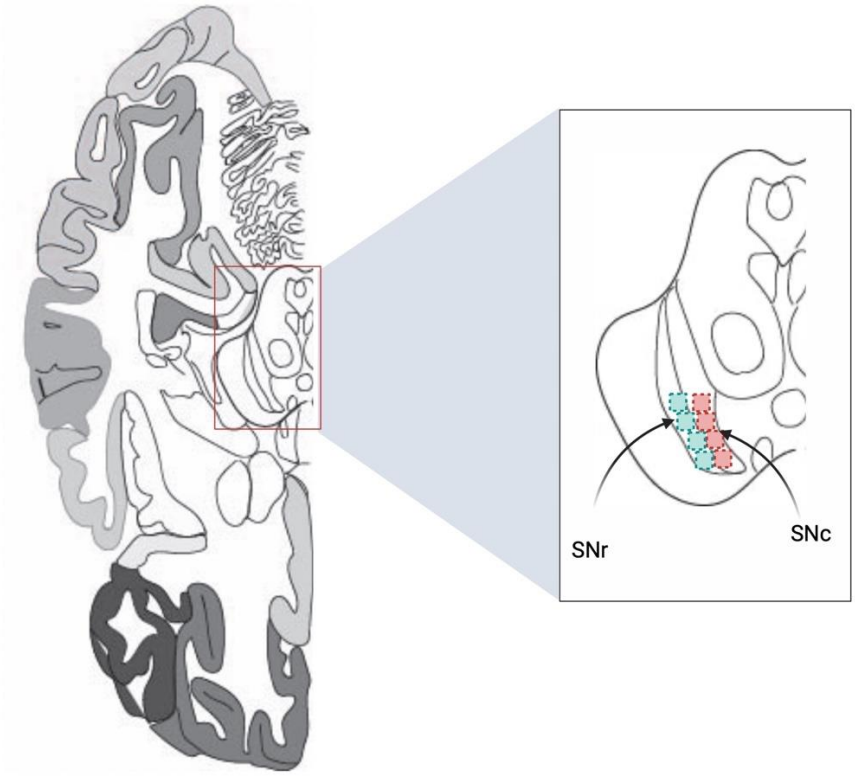

Figure 2.4. Schematic diagram of human midbrain with images obtained to quantify SOD1 and SOD1-EDI in glial cells in the substantia nigra *pars compacta* and *pars reticulata*

Four individual locations (dotted squares) were sampled images were taken across the ventral substantia nigra *pars compacta* (SNc; red dotted squares) and the adjacent substantia nigra *pars reticulata* (SNr; green dotted squares). At 20X magnification, the four locations were imaged across the four channels; DAPI (Ex 358 nm, Em 463 nm), Alexa488 (Ex 493 nm, Em 520 nm), Alexa594 (Ex 590 nm, Em 619 nm) and Alexa647 (Ex 653 nm, Em 669 nm) and merged to quantify accumulated SOD1 and misfolded SOD1-EDI. Image created in Biorender.

2.3.7 Gene expression

RNA was isolated from fresh-frozen tissue using TriReagent as per manufacturer's instructions (T9424, Sigma-Aldrich). Genomic DNA contamination was removed from isolated RNA samples using the Turbo DNA-Free kit (Thermo Fisher Scientific) before measuring the concentration and quality of the samples using a Nanodrop. cDNA was synthesised using High-capacity cDNA reverse transcript kit (#4368814, Thermo Fisher Scientific) before being pre-amplified (TaqMan Preamp Master mix, #4488593, Thermo Fisher Scientific) using probes for all genes of interest (see **Table A3** in **Appendices** for full list of probes). The pre-amplified cDNA was diluted 20-fold in water then aliquoted in triplicate into a 384 well microamp plates together with Taqman Fast master mix (#4444554, Thermo Fisher Scientific) and probes for genes of interest (see **Table A3** in **Appendices**). The samples were run on a Viia 7 Applied Biosystems qPCR system with hot start 50°C (2 min), 95°C (20 sec), 60°C (30 sec) and 40 cycles of 95°C (3 sec) and 60°C (30 sec). Relative expression was calculated using the ΔΔct method when correcting to housekeeper gene *GAPDH*, with results presented as fold-change relative to controls (bar graphs) or as gene expression z-scores (heatmaps).

2.3.8 Statistical analyses

All statistical analyses were performed using GraphPad Prism version 10.0. Results generated are presented as mean values $\pm$ SEM in bar graphs or as mean values with linear regression and 95% confidence intervals in correlation plots. Histopathological comparisons were performed using t-tests comparing controls and PSP groups with F tests used to determine equal variances. In the instance of unequal variances, a Welsch's correction was used. Correlation analyses were performed using Pearson *r* upon meeting parametric assumptions. A two-way ANOVA was used to compare the levels of SOD1 and accumulated SOD1 with Sidak multiple comparisons to test differences between both levels. Significance was indicated when p value was $p<0.05$ *, $p<0.01$ ** and $p<0.001$***.

2.4 Results

2.4.1 Neuronal loss in PSP is associated with gliosis

Neuronal loss and gliosis are characteristic features of the PSP-affected brain, particularly within substantia nigra *pars compacta*, substantia *pars reticulata*, subthalamic nucleus, globus pallidus *externus*. Our initial assessment of the tissue samples used for this study quantified neuronal loss and gliosis to confirm these salient features in our tissue samples and therefore their suitability for subsequent analyses. Histological examination confirmed significant neuronal loss (**Figure 2.5a**) and gliosis (**Figure 2.5b**) in our PSP samples. Neuronal loss was most evident in the substantia nigra *pars reticulata* (60% neuronal cell loss compared to controls), globus pallidus *externus* (48% neuronal cell loss) and the caudate nucleus (31% neuronal cell loss). A trend towards neuronal cell loss was evident within the substantia nigra *pars compacta (28*% neuronal cell loss), subthalamic nucleus (16% neuronal cell loss) and dentate nucleus (30% neuronal cell loss) (**Figure 2.5a, c**). Gliosis was most apparent within the substantia nigra *pars compacta*, subthalamic nucleus, and globus pallidus *externus*, within increases in glial cell numbers in these regions measured at 80%, 63% and 56% above controls respectively (**Figure 2.5b, d**).

To gain greater insight to the histological results generated, particularly the types of glial cells likely contributing to the observed gliosis, we performed gene expression analyses targeting genes enriched in neurons, astrocytes, microglia and oligodendrocytes. In contrast to histological examination which enables direct observation of individual cells within known neuroanatomical regions, the gene expression analysis methodology we used necessitates homogenisation of tissue samples. Thus, all gene expression results presented here are for tissue homogenates enriched for substantia nigra *pars compacta* and substantia nigra *pars reticulata*. Overall, the expression of genes associated with neurons was decreased in PSP. An RNA binding protein *RBFOX3* regulates alternative splicing of exon 10 in pre-mRNA tau transcript [451] is significantly reduced in the PSP brain. Other neuronal based cytoskeletal proteins *NEFH* and *TUBB3* are significantly decreased in PSP (**Figure 2.12a** and **b**). Among the neurotransmitter-specific genes, *GABRA1 (encodes* $GABA_{A1}$) and not *TH*, is significantly altered in PSP. GABA neurons are abundant in the substantia nigra *pars reticulata*, however

in PSP these neurons are lost [452, 453]. Notably, the expression of *MAPT*, the gene that codes for tau, was significantly higher in substantia nigra of PSP tissues.

Expression of the astrocytic markers *ALDH1L1* and *GFAP* were significantly elevated in the substantia nigra of PSP cases (**Figure 2.12a** and **b**). A solute carrier gene called aquaporin 4 (*AQP4)*, which facilitates astrocytic migration in response to neural injury and inflammation in the nervous system [454, 455], is found to be elevated in PSP. *TMEM119*, the microglial marker, is shown to be elevated in expression, whereas oligodendrocyte markers are not altered (**Figure 2.12a** and **b**).

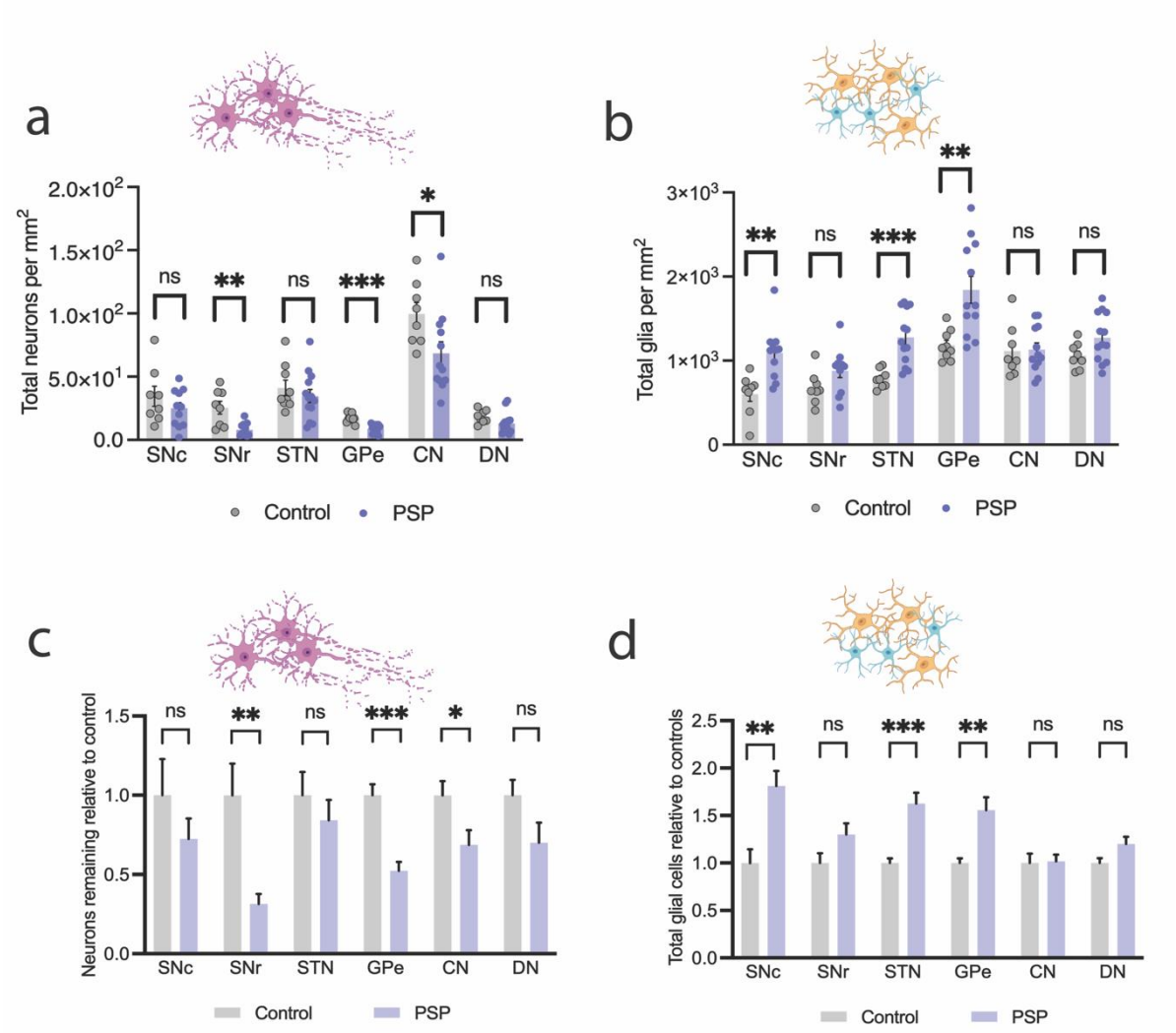

Figure 2.5. Quantitative assessment of pathological changes in PSP using stereology
Several pathologies were assessed in post-mortem tissue sections from PSP and controls including **a**) neuronal cell loss and **b**) gliosis, together with relative numbers of **c)** neurons remaining and **d)** total number of glial cells to controls. The pathological evaluation on various neuroanatomical regions of substantia nigra *pars compacta* (SNc), substantia nigra *pars reticulata* (SNr), subthalamic nucleus (STN) globus pallidus *externus* (GPe), caudate nucleus (CN) and the dentate nucleus (DN). Data are expressed as the mean ± SEM, with non-significance (ns) and significance being indicated when *p<0.1, **p<0.01 and ***p<0.001.

2.4.2 SOD1 accumulation is seen at higher levels in the glia in PSP

Histological examination of the brain samples revealed that accumulated SOD1 pathology was present in all brain regions of interest in PSP cases (**Figure 2.6a-e**) and controls (**Figure 2.6f-j**). Accumulated SOD1 was not detected in visual cortex (**Figure 2.6e,j**), a region of the brain that is suggested to show no tau pathology, neuronal cell loss or gliosis in PSP [47]. When comparing PSP cases to controls, accumulated SOD1 pathology appeared more abundant in PSP within neurons of the substantia nigra *pars compacta* and the substantia nigra *pars reticulata* (**Figure 2.6k)**, although neither of these results were statistically significant. By contrast, accumulated SOD1 pathology within glial cells of these same brain regions was significantly higher in PSP compared to controls (**Figure 2.6l**). In addition, accumulated SOD1 pathology within glial cells was also higher in the subthalamic nucleus of PSP cases compared to controls (**Figure 2.6l**). Abnormal accumulation of SOD1 within glial cells in the PSP affected brain but not neuronal cells is consistent with a previous report [20]. The presence of accumulated SOD1 in control cases indicates that SOD1 pathology may be a feature of the aged brain, but its higher abundance in PSP cases overall shows a proteinopathy that is more pronounced in the presence of neurodegenerative disease. Glial SOD1 pathology has been reported in ALS cases, where an immunohistochemical study showed SOD1 aggregates found in CNS tissue are comprised of up to 75% of the glial population in patients that carry a SOD1-mutation using a mutant specific antibody [332]. In addition, families that carry a non-SOD1 familial mutation and even in sporadic ALS cases showed between 75 - 100% of glia contained SOD1 aggregates [332]. Interestingly, the majority of these aggregates were found in association with astrocytes (using GFAP co-staining), with a few positively stained microglia and oligodendrocytes [332]. The more extensive change of accumulated SOD1 is seen in the glia within the basal ganglion (SNc, SNr and STN see **Figure 2.6l**). As previously reported, SOD1 staining is particularly prominent in the substantia nigra of the PSP brain, followed by a SOD1 staining in the subthalamic nucleus. (**Figure 2.6l**). The DAB chromogen was intensely stained within glial cells that are an average size of 10-20 µm, a size that makes it hard to distinguish specific glial cells. In addition to accumulated SOD1, a pathology similar to the Lewy bodies more commonly associated with PD was detected in PSP cases (**Figure 2.7a**). Lewy body like hyaline inclusions positive with SOD1 were observed and distinguished from SOD1 positive cells due

to the eosinophilic round halo (glass like) within the soma (**Figure 2.7b**). The Lewy body like hyaline inclusions had a homogenous intense staining of the entire inclusion body and were also detected in the control cases. Similar SOD1 positive Lewy body like hyaline inclusions are also present in mutant SOD1 cases of familial ALS [38, 338, 342, 344] in both motor neurons and astrocytes. The SOD1 positive Lewy body like hyaline inclusions detected in cases of PSP appeared to be localised within astrocytes since there was an absence of contorted nuclei which are associated with neuronal Lewy body like hyaline inclusions. We observed that the Lewy body like hyaline inclusions present in PSP were associated with a swollen cytoplasm, with a range of these cells measuring between 20 and 50 µm in diameter (**Figure 2.7b**). In addition, the presence of Lewy body like hyaline inclusions in PSP appeared in all regions of the brain however the levels were elevated in the substantia nigra *pars reticulata*, subthalamic nucleus and the globus pallidus *externus* (**Figure 2.7a**).

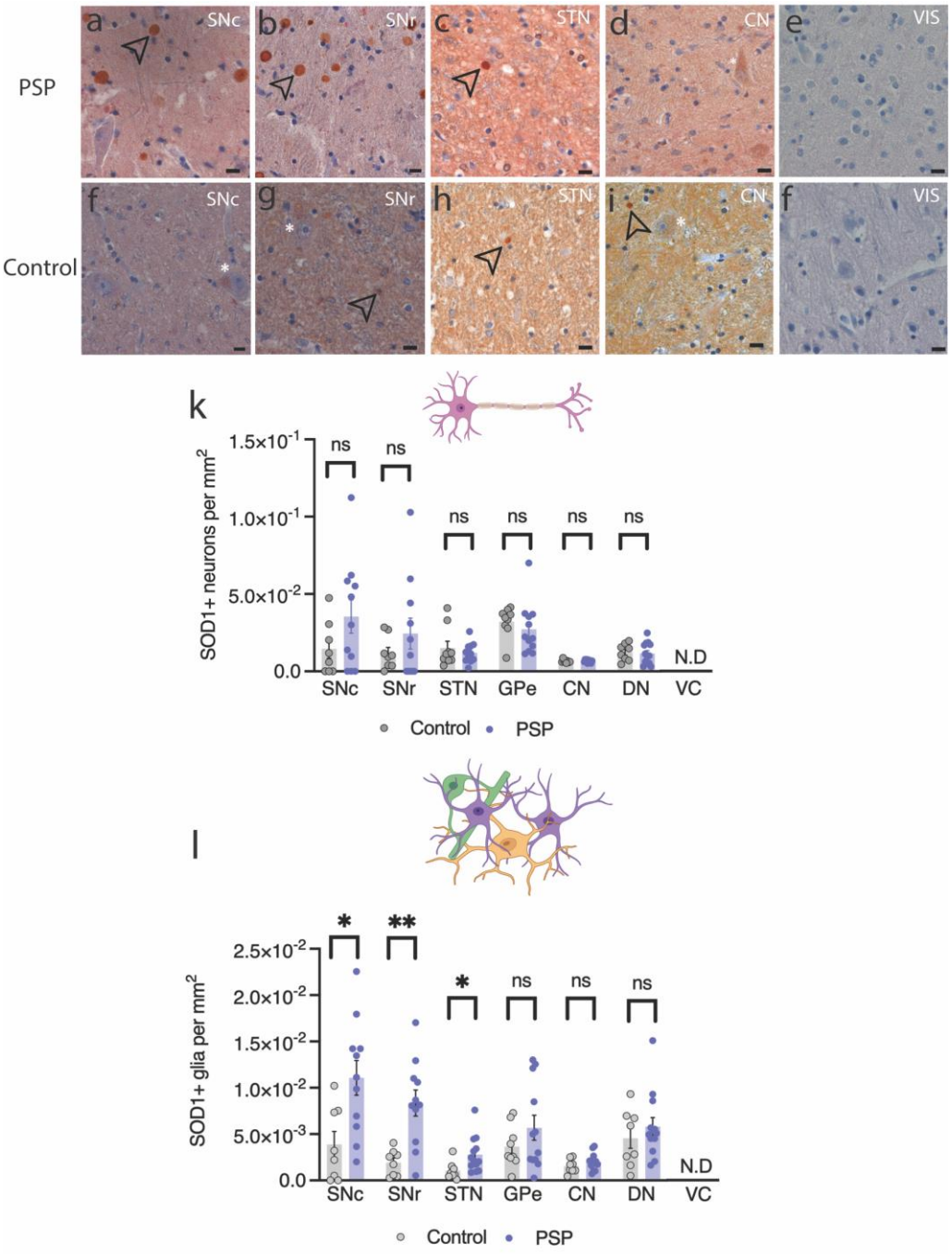

Figure 2.6. Accumulation of SOD1 is seen in glia within PSP tissue

Representative images of tissue sections from PSP (**a, b, c, d** and **e**) and control (**f, g, h, i, j)** stained with SOD1 (brown DAB) and counterstained with hematoxylin (blue) and pathological negative control (Visual cortex; VIS). Images showing the staining patterns in the substantia nigra *pars compacta* (SNc), substantia nigra *pars reticulata* (SNr), subthalamic nucleus (STN) and the Visual cortex (Vis) with the regions not shown (globus pallidus *externus* and dentate nucleus. Arrow heads and white asterisks indicate SOD1 positive staining for glia and neurons respectively. Black scale bars 25 µm. Stereological quantification of accumulated levels of SOD1 in **k**) neuronal cells and within **l**) glial cells in neuroanatomical regions; substantia nigra *pars compacta* (SNc), substantia nigra *pars reticulata* (SNr), subthalamic nucleus (STN) globus pallidus *externus* (GPe), caudate nucleus (CN) and the dentate nucleus (DN) and visual cortex (VC) with none detected ;N.D. Data are expressed as the mean ± SEM with non-significance (ns) and significance being indicated when *p<0.1 and **p<0.01.

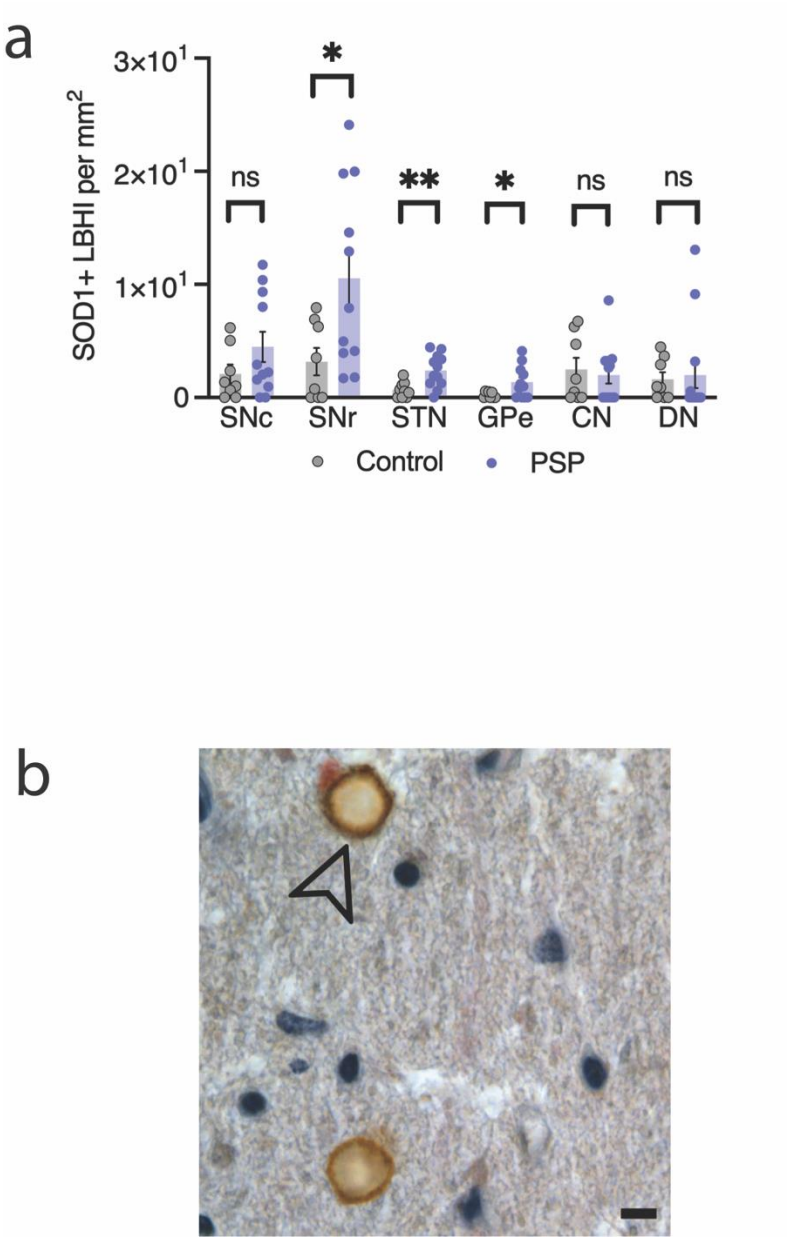

Figure 2.7. SOD1 positive Lewy body like hyaline inclusions found within PSP tissue
Accumulated SOD1 found within Lewy body like hyaline inclusions (LBHI) **a**) in neuroanatomical regions; substantia nigra *pars compacta* (SNc), substantia nigra *pars reticulata* (SNr), subthalamic nucleus (STN) globus pallidus *externus* (GPe), caudate nucleus (CN) and the dentate nucleus (DN). Data are expressed as the mean ± SEM with non-significance (ns) and significance being indicated when *p<0.1 and **p<0.01. Represented picture micrograph of a **b**) PSP case with Lewy body like hyaline bodies found the in substantia nigra *pars reticulata*. Arrowhead indicates SOD1 positive Lewy body like hyaline inclusions. Black scale bar 25 µm.

2.4.3 Associations between neuronal cell loss, gliosis and SOD1 aggregation in PSP

Due to the involvement of neuronal cell loss, gliosis, and SOD1 accumulation in the substantia nigra *pars compacta* and substantia nigra *pars reticulata*, we examined these regions further to determine whether any associative correlations exist between these factors. In the substantia nigra *pars compacta*, gliosis (**Figure 2.8a**), accumulated SOD1 in neurons (**Figure 2.8b**), accumulated SOD1 in glia (**Figure 2.8c**) and accumulated SOD1 in the Lewy body like hyaline bodies (**Figure 2.8d**) did not have any association with neuronal cell loss. In addition, accumulated SOD1 in neurons (**Figure 2.8e**) and the glia showed no relationship with gliosis (**Figure 2.8f**). However, the presence of accumulated SOD1 in the Lewy body like hyaline inclusions correlated significant with gliosis ($r = 0.4768$, $p = 0.0390$, **Figure 2.8g**). In the substantia nigra *pars reticulata*, a relationship between neuronal cell loss and glia is indicated but not statistically significant ($r= -0.4540$, $p = 0.0509$ see **Figure 2.9a**). There was no correlation seen between neuronal cell loss and the amount of accumulated SOD1 in neurons (**Figure 2.9b**), or within Lewy body like hyaline bodies (**Figure 2.9d**). However, there was a trend in neuronal loss and with accumulated SOD1 in glia ($r= -0.4471$, $p = 0.0550$ **Figure 2.9c**). Additionally, there was no association between gliosis and the accumulation of SOD1 in neurons (**Figures 2.9e)**, or in glia (**Figures 2.9f**) and a positive trend was seen within Lewy body like hyaline inclusions ($r= 0.4363$, $p = 0.0618$, see **Figure 2.9g**).

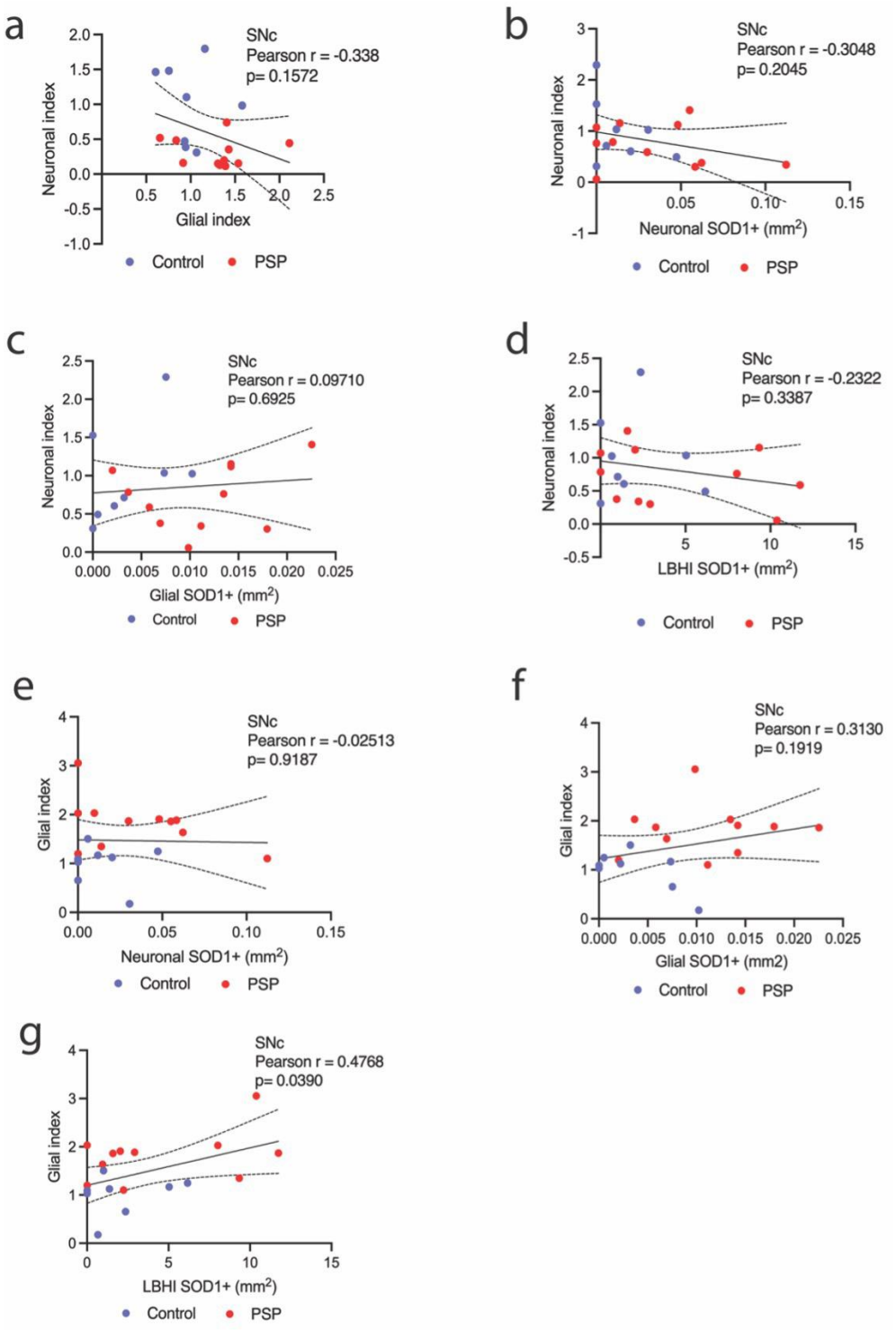

Figure 2.8. Relationships between neuronal cell loss, gliosis and SOD1 within the substantia nigra *pars compacta*

Linear regression (line of best fit together with the 95% confidence intervals) between **a**) neuronal loss and gliosis, **b**) neuronal loss and accumulation of SOD1 in neurons, **c**) neuronal loss and accumulated SOD1 in glia, **d**) neuronal loss and accumulated SOD1 in Lewy body like hyaline inclusions (LBHI), **e**) gliosis and accumulated SOD1 in neurons, **f**) gliosis and accumulated SOD1 in glia and **g**) gliosis and accumulated SOD1 in Lewy body like hyaline inclusions. Data points represent individual control samples (blue) and PSP samples (red). Pearson's r coefficient was calculated to measure the linear relationships between the pathological variables, with p values (two-tailed) indicating significance.

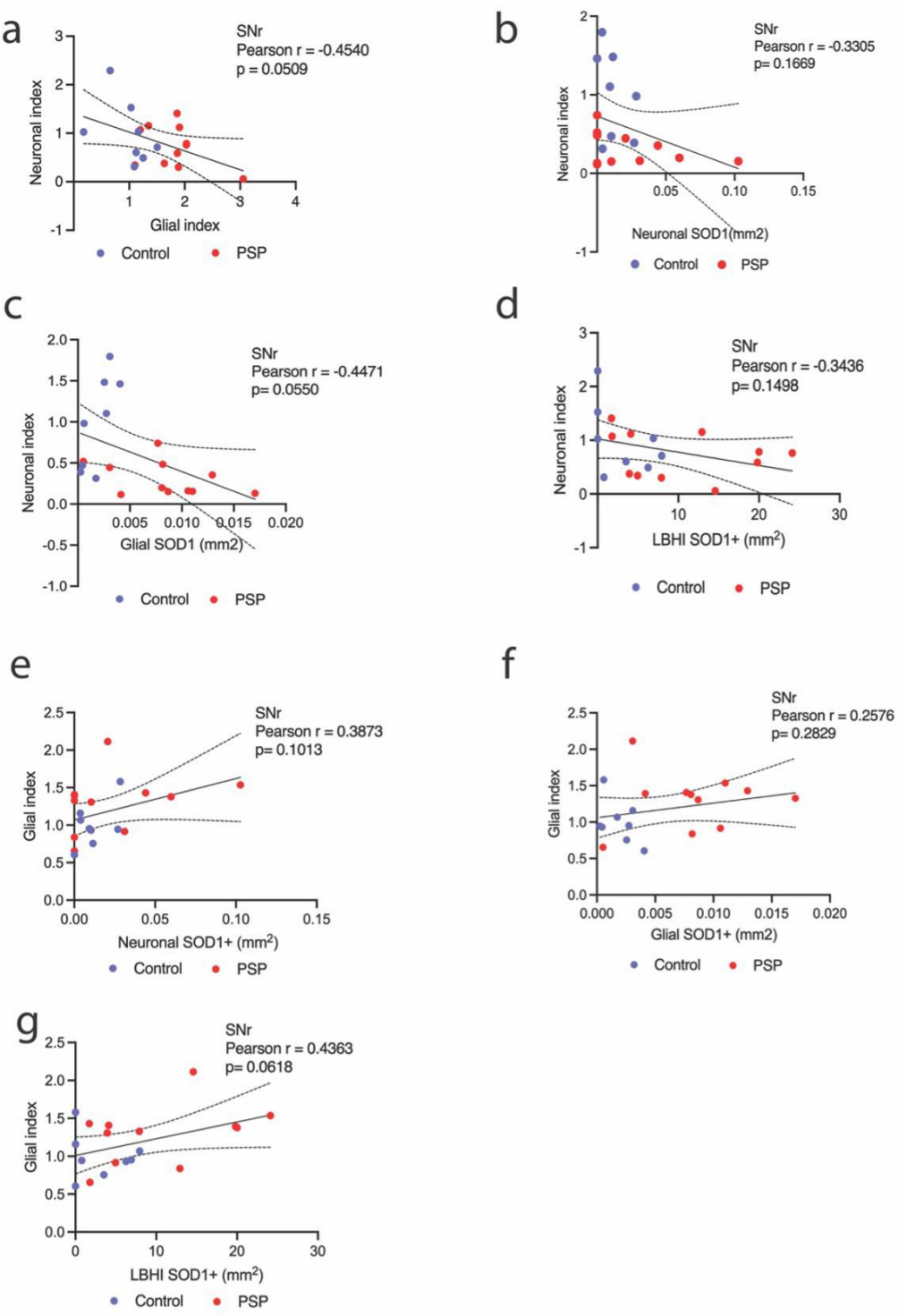

Figure 2.9. Relationships between neuronal cell loss, gliosis and SOD1 within the substantia nigra *pars reticulata*

Linear regression (line of best fit together with the 95% confidence intervals) between **a**) neuronal loss and gliosis, **b**) neuronal loss and accumulation of SOD1 in neurons, **c**) neuronal loss and accumulated SOD1 in glia, **d**) neuronal loss and accumulated SOD1 in Lewy body like hyaline inclusions (LBHI), **e**) gliosis and accumulated SOD1 in neurons, **f**) gliosis and accumulated SOD1 in glia and **g**) gliosis and accumulated SOD1 in in Lewy body like hyaline inclusions. Data points represent individual control samples (blue) and PSP samples (red). Pearson's r coefficient was calculated to measure the linear relationships between the pathological variables, with p values (two-tailed) indicating significance.

2.4.4 SOD1 accumulation in PSP is localised to astrocytes

We performed triple immunofluorescent labelling to examine the glial cells (astrocytes and microglia) within which SOD1 accumulation occurs in PSP. Quantification of the triple labelling images showed that accumulated SOD1 is present at higher levels in astrocytes (GFAP) than microglia (IBA-1) in both the substantia nigra *pars compacta* (**Figure 2.10a**) and the substantia nigra *pars reticulata* (**Figure 2.10b**), regardless of whether the cases were PSP or controls. In PSP cases, the accumulated SOD1 seen in astrocytes was 40% and 79% higher than controls within substantia nigra *pars reticulata* and substantia nigra *pars compacta* respectively. We also observed that the GFAP expressing cells show a hypertrophic morphology with increase thickness and length of processes (**Figure 2.10k** and **m**). GFAP and IBA-1 expressing cells were elevated in the PSP brain (**Figure 2.10c, d**) and this is in line with the elevated levels gliosis detected (using immunohistochemistry in methods 2.3.2) and as presented in **Figure 2.5b** and **c**.

As opposed to DAB chromogenic labelling of the whole cell (**Figure 2.6**), accumulated SOD1 deposits were observed mainly in the cytosol of GFAP expressing cells when using immunofluorescence (**Figure 2.10i-n**). Fluorophores as visualisation aids provide sensitive detection methods that can simultaneously detect the compartmentalisation of target antigens while multiplexing multiple targets of interest [456-458]. DAB as a chromogen, has been the gold standard visualisation agent in diagnostic histopathology, however DAB has a poor dynamic range with up to 99% of the light being blocked by the DAB substrate [457] which is a limiting factor to resolving small abundant proteins and could explain the difference in staining profiles.

Lewy body like hyaline inclusions, which were identified by their spherical shape, stained positively for both GFAP and SOD1 (**Figure 2.10n**) indicating that this pathological feature is present within astrocytes. Positive IBA-1 staining indicates microglia (purple) surrounding GFAP positive Lewy like hyaline inclusions for engulfment through phagocytosis (**Figure 2.10n**). The GFAP expression in these cells showed a circular ring which would indicate that this region would be the cytosolic compartment, given GFAP is an intermediate filament that is involved in the cytoskeletal structure of astrocytes [459].

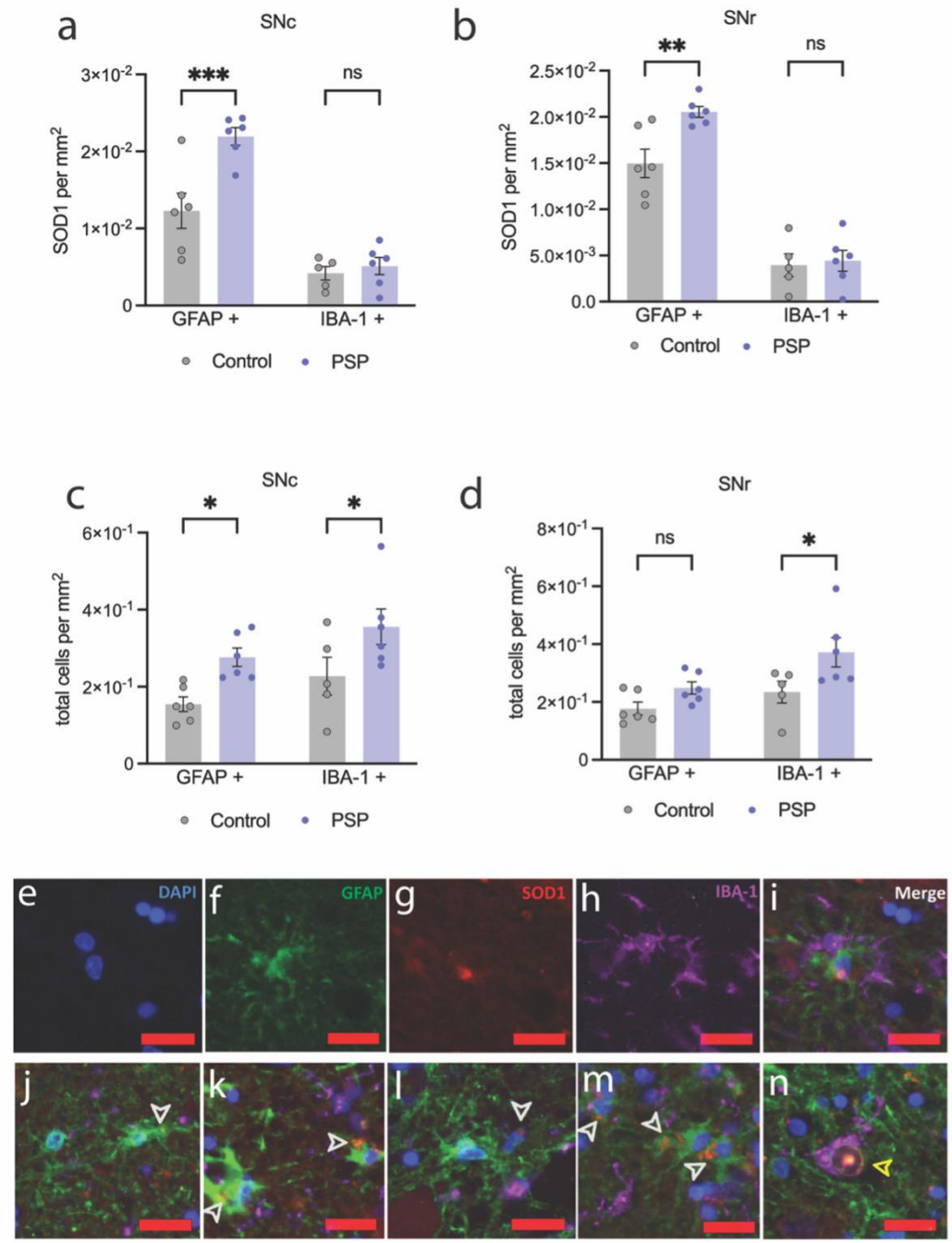

Figure 2.10. SOD1 accumulation is seen within astrocytes found within substantia nigra in PSP compared to control

Quantification of accumulated SOD1 within glial cells; astrocytes (GFAP) and microglia (IBA-1) **a)** in the substantia nigra *pars compacta* (SNc) and **b**) the substantia nigra *pars reticulata* (SNr). Total number of GFAP and microglia within **c**) substantia nigra *pars compacta* (SNc) and the **d**) substantia nigra *pars reticulata* (SNr). Representative images of individual filter channels **e**) DAPI - nuclei, 358 nm **f**) GFAP – 488 nm, **g**) SOD1- 594 nm, **h**) IBA-1- 647 nm and **i**) all merged channels. Representative images of accumulated SOD1 (red), GFAP (green), IBA-1 (purple) and DAPI (blue) within the substantia nigra *pars compacta* in **j)** controls and in **k)** PSP and within substantia nigra *pars reticulata* (SNr) in **l)** controls and in **m)** PSP with accumulated SOD1 within astrocytes as indicated by white arrowheads. Accumulated SOD1 was found to be co-localised within a GFAP expressing **n**) Lewy body like hyaline inclusion as indicated by the yellow arrowhead. Data are expressed as the mean

± SEM with non-significance (ns) and significance being indicated when *p<0.1 and **p<0.01. Red scale bars 20 μm.

2.4.5 SOD1 proteinopathy in PSP astrocytes involves misfolded SOD1

An antibody that recognises the solvent exposed dimer interface (EDI) of SOD1 was used to determine if SOD1 accumulating in PSP is of a misfolded conformation. The antibody recognises an epitope that is normally inaccessible within the physiologically folded homodimer and therefore recognises monomeric and misfolded forms of SOD1, particularly when there is a lack of bound copper [450] (**Figure 2.11a**). SOD1-EDI was detected in both control and PSP cases, and the staining pattern was similar to accumulated SOD1 (**Figure 2.10i-n**) whereby SOD1-EDI was seen in the cytosol of GFAP positive astrocytes (**Figure 2.11b-g**). It is unsurprising that SOD1-EDI was present in control cases given that 35% of the total pool of SOD1 in humans exists as a metal-deficient form [460]. Interestingly, Lewy body like hyaline inclusions, positive for GFAP had very limited and less intense misfolded SOD1 staining (**Figure 2.11f, g**). It could be suggested that these aggregates are highly insoluble and therefore mask the potential epitope that the EDI antibody recognises.

Quantification of these images, using the same methodology used for immunofluorescent labelled accumulated SOD1, revealed SOD1-EDI was elevated by 116% in the substantia nigra *pars reticulata* and 67% within the substantia nigra *pars compacta* of PSP cases compared to controls (**Figure 2.11h, i**). Relatively little SOD1-EDI was seen in the microglia and there was no difference between PSP cases and controls for microglial SOD1-EDI. Levels of SOD1-EDI in PSP cases and controls were similar to but slightly lower than accumulated SOD1 levels (**Figure 2.11j, k**). In the substantia nigra *pars reticulata* where we see most neuronal cell death in PSP (**Figure 2.5a, c**), there is a larger proportion of SOD1 is found to be misfolded (**Figure 2.11k**).

Chapter 2. Investigating superoxidase dismutase 1 pathology in progressive supranuclear palsy

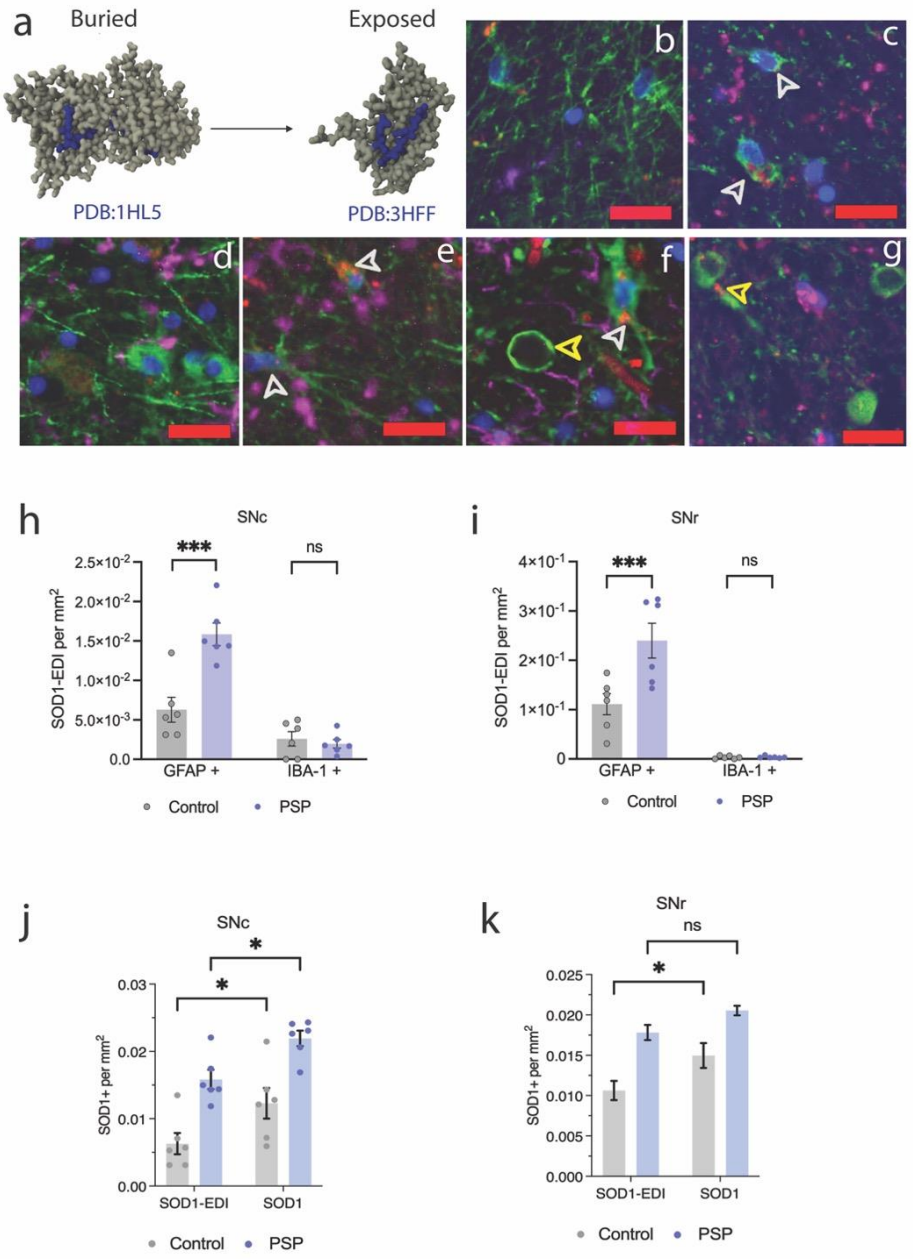

Figure 2.11. Elevated levels of misfolded SOD1 are seen within astrocytes found within substantia nigra in PSP compared to control

a) The epitope shown in blue of exposed dimer interface (EDI) antibody is buried deep inside the folds of SOD1 structure. Representative images of SOD1-EDI (red), GFAP (green) and IBA-1 (purple) found in **b**) control and in **c**) PSP within the substantia nigra *pars compacta* and in **d**) control and in **e**) PSP within the substantia nigra *pars reticulata* as indicated by white arrowheads. Within substantia nigra *pars reticulata* **f, g**) Lewy body like hyaline inclusions staining positive for GFAP showing little SOD1-EDI staining within the cytoplasm as indicated yellow arrowheads. Quantification of SOD1-EDI in glial within the **h**) substantia nigra *pars compacta* (SNc) and **h**) substantia nigra *pars reticulata* (SNr). A comparison of the staining levels of accumulated SOD1 and SOD1-EDI within the **j**) substantia nigra *pars compacta* (SNc) and **k**) substantia nigra *pars reticulata* (SNr). Data are expressed as the mean ± SEM with non-significance (ns) and significance being indicated when *p<0.1 and **p<0.01. Red scale bars 20 µm.

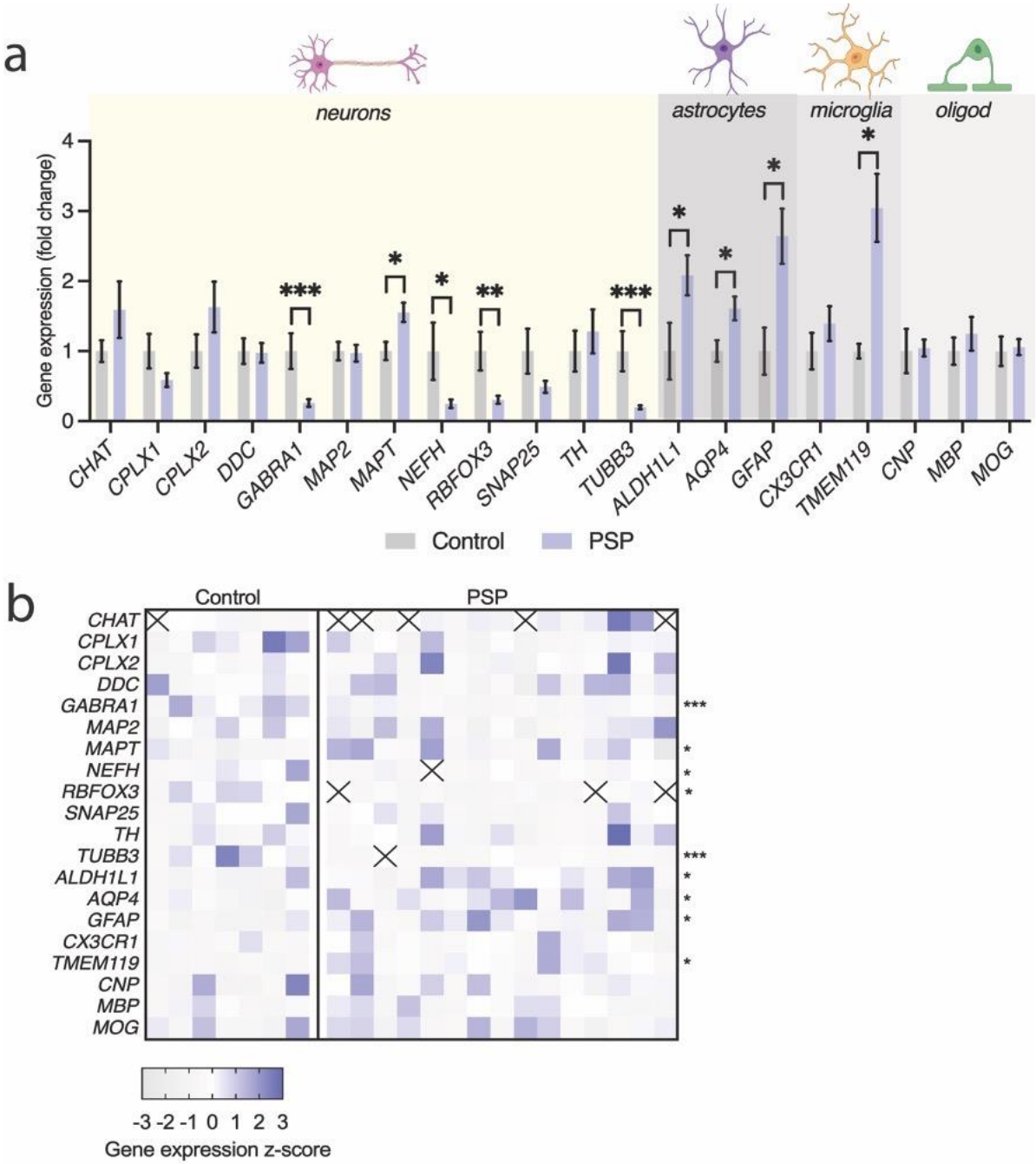

Figure 2.12. Molecular signature of cell specific gene markers in the substantia nigra of patients with PSP

Gene expression profiles using qPCR from tissue homogenates from the substantia nigra; **a**) relative gene expression fold change in cell specific markers in PSP case with data expressed as the mean ± SEM, **b**) standardised Z- score heatmap of cell specific gene markers. Multiple t-test (two sided) were used to determine non-significance (ns) and significance being indicated when *p<0.1 and **p<0.01.

2.5 Discussion

We demonstrated that SOD1 proteinopathy is present in PSP by probing tissue sections with antibodies directed against SOD1 and its misfolded form. A comprehensive assessment of multiple regions in the brain showed that the basal ganglia was the region that was severely damaged in PSP using an unbiased method of pathological assessment. Obtaining tissue from both case and control specimens from tissue biobanks is a major barrier to stereological evaluations because serial section sampling is required in order to accurately assess the region as a 3D structure [461, 462]. Due to limited tissue availability, we used a representative section. Although not entirely sampled throughout each region, this representative section is a standard sample that is used for diagnostics across many neurodegenerative diseases. Of these regions in the basal ganglia, we found that the substantia nigra *pars compacta* and the *pars reticulata* seemed to be the most affected regions with higher levels of neuronal cell loss, gliosis and SOD1 intracellular staining. The stereological assessments commonly used to assess PSP pathology focus on neuronal loss and tau deposition [463, 464] which, in varying degrees, have been found to affect the substantia nigra consistently [101, 102]. Here, we also evaluated the levels of glia within these sub-structures. The glia showed significant changes in SOD1 cell positivity despite cytosolic SOD1 being detected in neurons. This phenomenon has also been seen in a similar study in PSP tissue [20] and also within another closely related tauopathy, frontal temporal lobar dementia [465]. There is extensive evidence to implicate the involvement of glial cells in the pathogenesis of neurodegenerative diseases [466, 467], suggesting glial dysfunction is an early event [204, 468, 469] that propagates the neuronal degeneration cascade. The study of astrocyte functions has mainly been performed using cell culture experiments where the support and protection of neighbouring neurons is through the supply of metabolites required for antioxidant synthesis to defend against rising ROS levels [470, 471]. Consequently, astrocytes may have lost their antioxidant abilities, since the greatest accumulation of SOD1 is found in the area where the greatest loss of neurons is observed, the substantia nigra *pars reticulata*.

Interestingly, we identified proteinaceous inclusions which stained positive for SOD1, resembling Lewy body pathology that was seen at elevated levels in PSP tissue. Lewy body like hyaline inclusions were first identified by Hirano *et al.* (1967) in a family with ALS and

unlike Lewy bodies these do not stain positive for α-synuclein [472]. While Lewy body like hyaline inclusions were detected in cases with long-term ALS illness, some early formations of Lewy body like hyaline inclusions have SOD1 positivity [473]. In our case, several individuals of our control group did have Lewy body like hyaline inclusions present in different brain regions and given that our control cohort used for histopathological analysis was significantly older than our PSP cohort (**Table 2.1**) there could be a possible age-related accumulation of SOD1. Lewy body like hyaline inclusions have been commonly associated with sporadic and familial ALS cases by which their presence is noted within neuronal soma and within astrocytes in CNS tissue [474, 475]. Lewy body-like hyaline inclusions in astrocytes and neurons share similar features with granular-fibrils ranging from 10 – 25 nm in length and are positive for various proteins and enzymes including S100, αB-crystallin, ubiquitin, tau, tubulin, metallothionein, SOD1, and CCS, the copper chaperone for SOD [338, 342]. A previous study by Yamagishi *et al*., (2007) demonstrated that *in vitro* ER dysfunction leads to Lewy body like hyaline inclusion formation [38], although the mechanism of their formation is not entirely understood. Based on our initial immunohistochemical stain for SOD1 (**Figure 2.6**), we speculated that these positive inclusions were located within the glia and this was subsequently supported using the astrocytic marker GFAP, which stained all Lewy body like hyaline inclusions present in the sampled images (**Figure 2.10n**). We have not excluded the possibility that SOD1 could also be accumulated within oligodendrocytes since we did not stain for oligodendrocytes and tau pathology is also seen in these glial cells. It appears however, that the morphology of Lewy body like hyaline inclusions observed in PSP cases is characterised by an enlargement of the cytosolic compartment, a feature that is not evident in published Lewy body like hyaline inclusions images. We recognised that Lewy body like hyaline inclusions pathology seen in this study may overlap with another astrogliosis pathology given that astrocyte cell bodies, which measure normally between 10-20 µm (without processes) appear swollen like Alzheimer type I astrocytes [476]. Alzheimer type I astrocytes are characterised by staining strongly for GFAP with voluminous cytoplasm and also have thickened glial processes, and these types of abnormal astrocytes are generally found in white matter unlike Alzheimer type II, which do not stain positive for GFAP [477]. These types of abnormal astrocytes have featured in many neurological diseases such as multiple sclerosis, brain trauma, epilepsy, hereditary ferritinopathy, aceruloplasminemia and

Wilson's disease and two independent studies showing these unusual cells in PSP [45, 46, 478-482].

What is evident in the relationship between SOD1 Lewy body like hyaline inclusions and glia that is seen in PSP is that Lewy body like hyaline inclusions looks to induce gliosis in the substantia nigra *pars compacta* and to a lesser extent the *pars reticulata*. Accumulated SOD1 staining within neurons had no effect on gliosis or neuronal survival. Since the Lewy body like hyaline inclusions are found within astrocytes this could suggests the abnormal astrocytes might play a role in the disease pathogenesis. Bondi *et al*. (2023) found that there are more GFAP-expressing astrocytes in the *pars reticulata* than in the *pars compacta* [483], and a combination of these abnormal astrocytes observed in PSP might explain why the there is substantial loss of neurons within substantia nigra *pars reticulata*.

Furthermore, we found that there is a large portion of misfolded SOD1 (SOD-EDI) within the astrocytic cytosol that is significantly elevated in both of the substantia nigra *pars compacta* and *pars reticulata* in PSP (**Figure 2.11j** and **k**), suggesting that although misfolded SOD1 may be associated with neurodegeneration in PSP, the aged brain has some capacity to tolerate a certain level of misfolded SOD1 without involving both gliosis and neurodegeneration. The substantia nigra *pars reticulata* is one of the regions that undergoes significant pathological changes in PSP and degeneration of the substantia nigra *pars reticulata* results in gaze palsy, a cardinal symptom of PSP [102]. It is reported that misfolded proteins including SOD1 are known to trigger neuronal cell death [16, 329, 484-487], induce gliosis and cause disruptions in cross talk communications with glia and neurons [488]. The EDI antibody used to identify the destabilised structure of SOD1 recognises a large portion that is usually hidden within the native dimer interface but can become exposed as a result of monomer-misfolding or oxidative modification of a SOD1 intermediate [450]. Given there are different staining patterns for many conformation-specific SOD1 antibodies, it is an important consideration that there is no standardised immunohistochemical methods for misfolded SOD1 [35]. Here, although our complementary use of an antibody and methodology that is not dependent upon SOD1 conformation facilitated interpretation of results obtained from the conformation specific antibody for misfolded SOD1, only one conformation specific SOD1 antibody was

used. The use of additional conformation specific SOD1 antibodies would likely give additional insight to the role of misfolded SOD1 in PSP.

What causes the elevated SOD1 misfolding seen in PSP tissue in this study is still unknown and further experiments are required to identify these factors. PSP is generally not associated with genetic mutations in SOD1 [489] and therefore we postulate that an aberrant post translational modification event during its maturation process is a likely cause of destabilisation in leading to its misfolding. Oxidative modification of SOD1 is shown to induce its destabilisation and promote its aggregation in a similar fashion to mutant forms of SOD1 [490] and lead to toxicity as seen *in vitro* and *in vivo* studies [491, 492]. Indications of oxidative stress have been reported with the identification of biomarkers, 4-hydroxynoneal and malondialdehyde that are found in increased levels in the PSP brain [8, 10, 49, 201], and also seen to be present within type I astrocytes [493]. Several residues in SOD1 are known to be targets of oxidative modification including Lys3, Lys9 and Arg115 which impact the folding and the dimerisation of SOD1 at its native interface [490]. The histidine residues that coordinate the copper binding site, are susceptible to H_2O_2 oxidation, and SOD1 loses its affinity to bind copper [494]. Copper insertion into each monomer by its chaperone CCS, induces its structural stability by forming a disulphide bridge, resulting in dimerisation and ultimately its dismutase activity [326, 495]. The lack of available intracellular copper implicated in neurodegenerative conditions can result in a pool of copper-deficient SOD1 which is a template for its self-assembly within the cytosol [496, 497]. There are also indications of copper dyshomeostasis in PSP, where some regions in the brain have significantly decreased copper levels [21, 22]. Considering that neuronal copper is supplied by astrocytes [178, 232], either dysfunction or degeneration of these cells may affect their copper supply. Genetically inherited disorders characterised by copper accumulation (Wilson's disease) or deficiencies (Aceruloplasminemia) are known to have Alzheimer type I astrocytes [477, 481, 493], which suggests the glial machinery responsible for regulating neuronal copper availability is also dysfunctional. As astrocytes have an abundance of copper storage molecules such as glutathione and metallothionines, they have the ability to protect neurons and themselves from copper-induced toxicity. Interestingly, metallothionines highly enriched in Alzheimer type I astrocytes and Lewy body like hyaline inclusions [342, 481], which suggests the two astroglioses could be synonymous. The upregulation of many

metallothionines is seen in many neurodegenerative conditions like PD and AD [498, 499] and it would be of benefit to stain for metallothionines in PSP to further characterise these pathologies. There is evidence that metallothionine-1 is produced following neuronal damage, oxidative stress and neuroinflammation [500]. It has been shown that the overexpression of metallothionine -1 in mutant SOD1 mice attenuates the copper levels in cells, preventing Lewy body like hyaline inclusion formation and increasing the animal's longevity [501]. Metallothionine being taken up into insoluble aggregates could presumably exacerbate copper dyshomeostasis and contribute to oxidative stress and protein aggregation. Studies that have used bulk metal analysis of tissue is not sensitive enough to detect copper levels needed for cytosolic cuproenzymes such as SOD1 [502], it would be recommended to separate and measure the soluble cytosolic fraction from tissues to determine if is copper availability and is a factor that contributes to SOD1 misfolding [196, 366].

Our immunohistochemistry studies confirmed that the PSP tissues samples used in our study are characterised by salient pathological changes, so we explored further cell specific changes in the brain to determine which cells are most affected in PSP. Using qPCR, we measured mRNA levels for targeted neuron and glial markers within the substantia nigra of PSP cases. First, we investigated changes in *MAPT* mRNA since PSP is a tauopathy. Although *MAPT* is expressed only in neurons [89], its protein product tau can exit neurons and be taken up by neighbouring glial cells, suggestive of a prion-like spreading [503]. We observed that there was an increase *MAPT* levels in the substantia nigra from cases of PSP. This increase in *MAPT* mRNA occurred despite significant decreases in markers of neuronal abundance (*RBFOX3, TUBB3* and *NEFH*) (**Figure 2.12**). *RBFOX3* is a transcriptional factor as well as a well-known mature neuron nuclei marker (known as NeuN). In addition to its decreased levels being a marker of neuronal loss in PSP, its decreased levels in PSP could influence the splicing of exon 10 isoform in *MAPT* [504, 505].

The neuron-specific changes that were seen in PSP tissue, were genes that were associated with *TUBB3* and *NEFH*. *TUBB3* encodes a III class member, β-tubulin which is a core protein that assembles to form microtubules with actin. Mutations in *TUBB3* are associated with neurological conditions as distinct tubulinopathies, and result in axonal neuropathy due to a

defect in protein trafficking [506]. Since microtubules are destabilised in PSP, it is possible that reduction of *TUBB3* seen in the substantia nigra of PSP cases could be a consequence of tau overexpression and aggregation [507]. Together with microtubules, microfilaments like NEFH crosslink within the mature neuron cytoskeletal architecture to provide support within myelinated axons [508]. Dysfunctions in NEFH has been associated with neurodegenerative conditions such as ALS and Charcot-Marie-Tooth disease [509] and are also constituents in many aggerates including tau inclusions [510, 511]. In PSP, NEFH is detected at higher levels in the CSF measured by ELISA [512]. Considering that neurofilaments are broken down and released from degenerating neurons or after axonal damage, they are cleared from the brain into the interstitial fluid and diffuse into the CSF [513]. *NEFH* levels were significantly decreased in substantia nigra of PSP cases and a decrease in neurofilaments could act as a marker of demyelination and axonal damage [514].

The sparse neurons in the substantia nigra *pars reticulata* are predominantly GABA-dependent with intermixing of a small number of dopaminergic neurons [515]. These GABA-expressing neurons project out to inhibit structures such as the motor/intralaminar thalamus, superior colliculus, and pedunculopontine, but there may also be other projections to diencephalon and brainstem [516-519]. The substantia nigra *pars reticulata* is therefore rich in *GABRA1* which encodes GABA receptor A1 ($GABA_{A1}$) and in PSP there is a significant decrease in *GABRA1* mRNA transcript, indicating a loss of GABA and GABAergic neurons, which we reported in our PSP cohort (**Figure 2.5a** and **c**). Given that this sample consisted of dopaminergic neurons and from what was observed in **Figure 2.5a** and **c**, there being a small loss of neurons from the substantia nigra *pars compacta*, it was intriguing that there was no decrease in *TH* levels. There is a possibility that the sample didn't contain similar amounts of substantia nigra *pars compacta* to detect changes between non-neurological controls and PSP with the majority of the sampling being the substantia nigra *pars reticulata*.

Glia have an important role in maintaining brain homeostasis and in disease we understand that aberrant activation and changes in glia drive disease progression. We observed significant changes were seen in the markers for astrocytes and microglia, with no alterations seen in the oligodendrocytes (**Figure 2.12**). Astrocytes have a complex role in the brain and they can become reactive in pathological conditions, with astrogliosis being a common

significant feature of diverse neurodegenerative conditions [520]. We assessed the astrocytic markers, *GFAP*, *ALDH1L1 (*aldehyde dehydrogenase 1 family member) and *AQP4* (aquaporin 4). GFAP is frequently used to measure astrogliosis in neurodegenerative disorders [521] and its up-regulation is a previously reported prominent feature found within the substantia nigra in PSP post-mortem tissue [522]. In addition the cellular morphology of GFAP expressing astrocytes in PSP we observed to have a hypertrophic phenotype (**Figure 2.10k** and **m**) also indicating these cells are undergoing reactive gliosis [523]. Together with our histology results for GFAP (**Figure 2.10** and **Figure 2.11**), our gene expression analyses complement and support these prior findings (**Figure 2.11**). To our knowledge and prior to this study, the astrocyte markers *ALDH1L1* and *AQP4* had not been assessed in PSP. *ALDH1L1* is not a widely used marker in neurodegenerative conditions, however it is now considered a broader marker for astrocytes as it labels more astrocytes than GFAP itself [524]. ALDH1L1 functions as a metabolic folate enzyme that is expressed within fibrous and protoplasmic astrocytes [525]. The observed increase in *ALDH1L1* levels in the substantia nigra of PSP tissue could suggest that there is a large number of proliferating astrocytes within the substantia nigra, which often leads to glial scaring as a means to stimulate repair and regrowth of axons [526].

Within the astrocyte-facing neurons and within the perivascular end feet, AQP4 controls fluid exchange from the CSF and interstitial fluid in the brain parenchyma in a bidirectional manner [527, 528]. In addition to this function, it is also found to regulate K^+ reuptake [528] and its transcriptional expression is altered in pathological conditions. Altered AQP4 expression is seen in many CNS disorders like ischemia, cerebral edema, glioblastoma, astrocytoma, neuromyelitis optica, AD, ALS and PD [529-535]. In our study, *AQP4* was seen to be upregulated in PSP post-mortem tissue. AQP4 has a role in the glymphatic system which facilitates the removal of waste and prevents toxic protein build-up in the brain. The glymphatic system is impaired within aged people and within the cortex of AD cases [536]. The immunohistochemical staining pattern of AQP4 is similar to that of GFAP, where it is present around amyloid plaques and tau inclusions [536, 537]. In addition, several metals are shown to cause inhibition of AQP4 *in vitro* studies [528, 538].

Microglia play a dual role of neuroprotection and neurotoxicity in neurodegenerative conditions [539, 540] and therefore we assessed if there were any alterations to other

microglia genes in PSP. As part of our immunofluorescence experiments, we used an IBA-1 antibody to determine whether SOD1 accumulated and misfolded within microglial cells (**Figures 2.10** and **2.11**) and get a first impression of microglial changes in PSP. IBA-1, which we used as a widely utilised marker for detecting microglia [541], was altered in PSP (**Figures 2.10c** and **d**) and though it is thought to detect activated microglia, IBA-1 can also detect resting microglia and also infiltrating myeloid cells [541, 542]. We measured two additional microglial activation markers: CX3C motif chemokine receptor (CX3CR1) and transmembrane protein 119 (*TMEM119*). The internalisation of tau into microglia via phagocytosis is regulated by CX3CR1 [543]. We did not detect any changes in *CX3CR1* expression which like IBA-1, can be detected within other resident tissue macrophages and circulating monocytes [544]. By contrast *TMEM119* levels increased significantly. It is known that the transmembrane microglial marker, TMEM119, can distinguish between resident brain microglia and infiltrating myeloid cells, however the function of TMEM119 is unknown [542, 545]. TMEM119 is upregulated in a variety of neurodegenerative diseases, but there is conflicting evidence that it is unchanged in the cerebellum [546] or that it increases in PSP as seen in purified extracellular vesicles from inferior parietal gyrus of PSP patients [547]. TMEM119 is also differentially expressed across regions, with some regions like the midbrain having a microglia transcriptome profile that indicates greater immune vigilance [548]. In ALS SOD1 (G93A) mutant mice with SOD1 pathology in their spinal cords, RNA-seq analysis of myeloid cells showed that resident microglia in the CNS like TMEM119 were increased [549]. Our analyses indicate a strong up-regulation of *TMEM119* in the PSP-affected substantia nigra (**Figure 2.12ab**).

Here, we provide results that show SOD1 proteinopathy is a feature of PSP that involves accumulation of SOD1 and its misfolding. While both tau pathology and neurodegeneration are pathological hallmarks of the disease, our results confirm that pathological processes in PSP extend beyond neuronal tau, supporting the assertion that effective therapeutic inventions for PSP will likely need to extend beyond tau as a protein target and also address non-neuronal factors.

Chapter 3. Molecular signature of copper bioavailability in PSP

Results presented in Chapter 2 provided evidence for SOD1 proteinopathy in cases of PSP whereby the protein accumulates and misfolds in regions that have severe neurodegeneration and gliosis. This proteinopathy was most evident within astrocytes, the glial cells that provide trophic support for neurons under physiological conditions but can directly cause neuronal death if provoked into an aberrant activated state. As the propensity for SOD1 to misfold and accumulate is in part determined by its acquisition of copper, and as evidence exists to implicate altered copper availability in PSP, experiments reported in the present chapter were undertaken to gain further insight to the role that copper availability may play in the SOD1 proteinopathy of PSP.

3.1 Introduction

Among the six transition metals, copper serves as a cofactor for many proteins and enzymes that are essential to human health, which is why copper deficiency and overload are closely related to disease. Aside from the liver, the brain has one of the highest concentrations of copper in the body and of all the neuroanatomical structures, the basal ganglia, cerebellum, and hippocampus contain the highest amounts of copper [176, 550]. Though it is unclear why these areas are particularly high in copper, it is known that these regions also tend to be more susceptible to pathological lesions and degeneration in PSP. The disruption of copper homeostasis is a prominent feature of neurodegenerative disorders, being implicated in pathological protein misfolding and oxidative stress. Most pertinent to PSP, the tau protein, which is associated with more than twenty different neurodegenerative clinicopathologies [551], is known to possess copper binding sites that lay within the histidine residues in the pseudo-repeat regions of the microtubule-binding domain [149]. The reason for their existence is unknown. A meta-analysis study by Schrag *et al.* (2011) indicated significant depletion of copper in regions is associated with tau pathology in patients diagnosed with AD [552]. Similarly, as described in Chapter 1 (Section 1.3.1), PSP has a hallmark pathology of misfolded tau seen within neurons, astrocytes, and oligodendrocytes. The PSP-affected brain exhibits regional copper changes within several nuclei, including the most severe decrease in copper seen in the cerebellum [21] and caudate nucleus [22]. It appears, therefore, that

disrupted copper availability may be involved in PSP and that it may be associated with the disease's characteristic tau pathology. However, detailed examination of copper in PSP and its potential role in causality is lacking. Not least of which, consideration is yet to be given to biochemical partitioning of copper in PSP, the molecular machinery involved in its cellular handling, and whether the natural anatomical distribution of copper may be altered within brain substructures or even between different cell types.

The only reports of copper in PSP (see **Table 1.2**) show the cerebellum and basal ganglion regions caudate nucleus being significantly decreased in copper levels with trends in substantia nigra and putamen [21, 22]. Even though these studies have been useful for identifying copper changes in neuroanatomical regions, they have been unable to identify changes at the cellular and subcellular levels. By determining the cellular and subcellular changes, you not only determine the potentially underlying cause of the changes, but also the pathological effects in the subcellular environment. We reported that SOD1 is found to accumulate and also misfolded in some of the key degenerative regions in the post-mortem tissue of the PSP brain especially within astrocytes (Chapter 2). SOD1 is known to misfold and form aggregates when there is no binding of copper within its active sites seen in *in vitro* and *in vivo* studies [31, 497]. Additionally, copper loss decreases the ability of SOD1 to regulate the basal oxidative stress load within cells, resulting in decreased antioxidant capacity [553]. Thus, it is critical to understand the metal status to determine whether the loss of metals like copper could be a factor as to why SOD1 is found to be aggregated in PSP particularly when astrocytes are the key cell type that regulates the copper homeostasis in the brain [178, 232].

3.2 Hypothesis and aims

Although the reports described above show copper changes in post-mortem brain tissue from cases of PSP, the amount of insight provided for copper handling and cuproenzyme activities in PSP remains limited. Therefore, the aim of this study is to investigate the copper related changes in the regions affected in the substantia nigra of PSP cases, the region that was most vulnerable to SOD1 pathology, neurodegeneration, and gliosis (as described in Chapter 2).

Hypothesis:

Indications of disrupted copper availability are present in the PSP-affected brain, particularly in the vulnerable substantia nigra where neuronal loss is most prominent.

The specific aims of this current study as per Section 1.8.1 are as follows:

Aim 2. Determine if SOD1 metal status and activity is perturbed in human cases of PSP.

Aim 3. Determine the molecular signature for copper availability in PSP brain samples relative to controls.

Aim 4. Assess copper-dependent functionality of additional cuproenzymes in PSP brain samples relative to controls.

3.3 Methods

3.3.1 Fresh frozen post-mortem human samples

Post-mortem substantia nigra tissue used in this study was obtained from the Sydney Brain Bank and the Victorian Brain Bank under the approval of the University of Melbourne (ID #21178, University of Melbourne Office of Research Ethics, and Integrity). Fresh frozen substantia nigra tissue from clinically diagnosed classical Richardson's syndrome (PSP) and controls were used in this experimental chapter (see **Table A1** in **Appendices** for the full list of case details). Frozen tissue was prepared at outlined in **Figure 1.7** and removed from -80°C and kept on ice for subsequent biochemical and molecular assays (**Table 3.1**), with fresh frozen samples cryosectioned for LA-ICPMS (**Figure 1.7**, **Table 3.2**). The tissue samples used for qPCR, solution ICPMS and protein/activity levels encompassed both the substantia nigra *pars compacta* and the *pars reticulata* and all results derived from these samples are therefore collectively termed substantia nigra (See study design in Section 1.8.2).

Table 3.1. Descriptive demographics of PSP cohort used for qPCR, ICPMS, protein/activity levels

Group	N	Males	females	Age (years)	PMI	Disease duration (years)[#]
PSP	15	8	7	74.73 ± 1.26	22.53±2.55**	5.526 ± 0.79
Control	7	5	2	74.71 ± 3.183	40.57 ± 5.71	N/A

Control cases were pathologically confirmed free of neurological disease. [#]Period from diagnosis to death. PSP: Progressive supranuclear palsy; PMI: Post-mortem interval; n/a: not applicable; significance is indicated when **P<0.01 (two-tailed t-test)

Table 3.2. Descriptive demographics of PSP cohort used for LA-ICPMS

Group	N	Males	females	Age (years)	PMI	Disease duration (years)[#]
PSP	3	2	1	66.67 ± 3.21	43.0 ± 4.04	9.00 ± 3.00
Control	3	2	1	70.33 ± 2.97	45.83 ± 7.59	N/A

Control cases were pathologically confirmed free of neurological disease. [#]Period from diagnosis to death. PSP: Progressive supranuclear palsy; PMI: Post-mortem interval; n/a: not applicable.

3.3.2 Preparation of fresh-frozen CNS tissue samples for biochemical assays

Pre-weighed tissue samples were thawed on ice then homogenisation buffer (See **Table A4** in **Appendices**) added with a 1 mg to 10 µL tissue:buffer ratio. Using a motorised tissue homogeniser, the tissue was homogenised twice for 20 sec with a 20 sec delay in between. Samples were centrifuged at 21,000 RCF for 30 min at 4°C. The supernatant (soluble fraction) was removed and placed into a separate tube and stored at -80°C. The pellet fraction was resuspended in 20 times volume of homogenisation buffer, centrifuged (21,000 RCF, for 30 min at 4°C) and the supernatant discarded. The pellet was resuspended again in 20 times volume of homogenisation buffer, then this 'insoluble fraction' stored at -80°C. This tissue processing protocol, when applied to CNS tissue samples, separates cytosolic material (soluble fraction) from other cellular material such as the nucleus, plasma membrane and myelin (insoluble fraction) [554].

3.3.3 Inductively Coupled Plasma-Mass Spectrometry

Soluble and insoluble material prepared from human brain samples (Section 3.3.2; 50 µL aliquots) was transferred to 1.5 mL microfuge tubes then lyophilised. After lyophilisation, each sample was digested in nitric acid (65% Suprapur, Merck) overnight at room temperature then for a further 20 min at 90°C. An equal volume of H_2O_2 (30% Aristar, BDH chemicals) was then added in the samples via incubation at room temperature for 30 min then at 70°C for 15 min. A final addition of 1% nitric acid was added to each sample. Multiple elemental measurements were made using a 7700 series ICPMS (Agilent) under routine operating conditions with a helium reaction gas cell. Certified multiple element calibration solutions at 0, 5, 10, 50, 100 and 500 parts per billion (ICPMS-CAL2-1, ICPMS-CAL-3 and ICPMS-CAL-4, Accustandard), together with an internal standard containing 200 ppb of Yttrium (Y89), were used. Results for copper, iron and zinc were adjusted for inter-sample differences in the high abundance elements magnesium, phosphorous, potassium. This involved calculating concentrations of these high abundance elements in each sample then using these concentrations to determine a correction factor for each sample, akin to using total protein abundance on a western blot to correct for abundance of a protein of interest on a western blot. The resulting corrected values for elements of interest where then expressed as µg element per g tissue.

3.3.4 Laser Ablation Inductively Coupled Plasma Mass Spectrometry (LA-ICPMS)

Frozen, unfixed tissue sections from clinically diagnosed cases of PSP (N = 3) and non-neurological controls (N = 3) were sectioned at 30 µm in a coronal plane using a cryostat and mounted on superfrost slides for *in situ* elemental analysis using laser ablation ICPMS (LA-ICPMS). The images were generated using an ESL imageBIO laser ablation unit (Kennelec Scientific) coupled to an Agilent 7900 ICP-MS (Agilent). Adapted from a method previously described [555, 556], data were collected from brain samples that contained substantia nigra *pars compacta*, substantia nigra *pars reticulata*, and cerebral peduncle. We identified these regions using another section stained with hematoxylin and eosin and the neuromelanin pigmented cells of the *pars compacta* as a reference [557]. We annotated the regions of interest using Caseviewer and the Human Brain Atlas [557].

Intensity values for all elements of interest as ppm were collected for ablation spots of 30 µm and these values, relative to x and y co-ordinates of the section, saved as csv files. Heatmap images for all elements analysed within each sample were generated by importing csv file data into ImageJ. Mean values for copper, iron and zinc were calculated within each anatomical region of interest, were subtracted for background levels and normalised to potassium, magnesium and phosphorous levels, then expressed as a concentration of µg per g^{-1}.

3.3.5 Gene expression

For complete methods please refer to section 2.3.7 (Chapter 2). The list of genes of interest and assays used for measuring their expression is presented in **Table A3**, in **Appendices**). Relative expression was calculated using the ΔΔct method when correcting to housekeeper gene *GAPDH*, with results presented as fold-change relative to controls (bar graphs) or as gene expression z-scores (heatmaps).

3.3.6 SDS-PAGE and immunoblotting

SDS-PAGE and immunoblotting was used to investigate the abundance of cuproenzymes in TBS soluble and insoluble fractions prepared from PSP brain samples and controls (Section

3.3.2). The TBS insoluble fraction was further processed by the addition of Triton X-100 (1% v/v, Calbiochem) and vigorous vortexing, followed by centrifugation (18,000 RCF for 3 min, 4°C). The resultant supernatant was collected ,then the protein concentration of each sample determined using the BCA assay (Pierce BCA Protein assay Kit, Thermo Scientific) and all samples subsequently normalised to a consistent protein concentration by diluting with TBS. Protein-normalised samples were prepared in 4x sample buffer (Nupage LDS sample buffer, NP0007, Invitrogen) and loaded onto 4-12% Bis-Tris Midi gels (Thermo Scientific) and run in MES SDS buffer (1x, Life Technologies) at 200 volts for 40 min. Proteins were transferred to PVDF membrane (Invitrogen) using the iBlot as per manufacturer's instruction (Invitrogen). Membranes were blocked in blocking buffer consisting of PBS-T (0.05% v/v Tween-20 Chemsupply) and 4% v/w Skim milk for 1 hour at room temperature followed by the incubation of primary antibody overnight at 4°C prepared in blocking buffer. Primary antibodies used were raised to detect SOD1 (1:100,000, Abcam), ceruloplasmin (1:1000, DAKO) or hephaestin (1:500, SantaCruz Biotechnology). All antibody details are provided in **Table A2** in **Appendices**. Blots were rinsed 3x in PBST for 10 min then incubated with secondary IgG HRP (1:5000, Cell Signaling) for 1 hour. The membranes were rinsed 3x in PBST for 10 min then visualised using ECL reagents (GE Healthcare) and an LAS-3000 image capture system (Fujifilm). Membranes were re-probed for the loading controls GAPDH (1:5000, Cell Signaling) or β-actin (1:2000, Cell Signalling). Quantitation of proteins were performed using ImageJ software and proteins expression levels normalised to the loading controls GADPH (soluble fraction) or β-actin (insoluble fraction).

3.3.7 SOD1 activity

Cytosolic SOD1 activity in the substantia nigra was measured in the TBS soluble fraction using a colourimetric assay as described by [31]. As pyrogallol is autoxidized in the presence of superoxide, a chromophore is formed which can be measured at 325 nm. The presence of active SOD1 prevents this reaction. In a 96 well plate that is preloaded with blank (ddH_2O) or with the SOD1 inhibitor potassium cyanide (10 mM made in ddH20, #20710, Sigma-Aldrich), TBS soluble fractions were added to the plate in duplicate. The pyrogallol (#254002, Sigma-Aldrich) was prepared in a buffer containing 50 mM Tris, 1 mM EGTA and with a pH of 7.4, and was added into each well after a 1 min pre-incubation period. The reaction was

monitored in a plate reader (Enspire, Perkin Elmer) by measuring absorbance at 325 nm in 30 sec intervals for 30 min at 25°C. Using the initial linear phase, SOD1 activity was calculated relative to controls [31].

3.3.8 Ferroxidase activity

Ferroxidase activity in PSP brain tissue was measured using an established method [31], in which oxidation of ferrous iron (Fe^{2+}) into ferric iron (Fe^{3+}) and its subsequent incorporation into apo-transferrin is measured by an increase in absorbance at 460 nm. Human substantia nigra tissue (see sample list in **Table A1**, in **Appendices**) was prepared as outline in the method in section 3.3.2 however in this homogenisation buffer contained detergent Triton X-100 with a final volume of 1% (v/v) to increase the solubilisation of the membrane-bound ferroxidases. The assay utilised the Triton X-100 extracts of the TBS insoluble fraction (Section 3.3.2). The use of TBS-based homogenisation buffer in preference to a PBS-based homogenisation buffer for original tissue homogenisation was critical to avoid interference in the ferroxidase assay introduced by the presence of phosphate [558]. Fresh solutions of human apo-transferrin (250 µM product, Sigma-Aldrich) and 1 mM $FeSO_4$ were made in N_2-purged ddH_2O to prevent the oxidation of iron. In a 96 well plate, HEPES-buffered saline (50 mM HEPES, 150 mM NaCl, pH 7.2) was loaded into the wells followed by apo-transferrin to a final concentration of 50 µM and with 20 µL of the substantia nigra samples (final concentration of 60 µg of sample was loaded). In a plate reader (Enspire, Perkin-Elmer), $FeSO_4$ was added to each well to a final concentration of 150 µM and the absorbance at 460 nm measured every 10 sec for 5 min at 25°C. This assay does not discriminate the different ferroxidases (predominantly ceruloplasmin and hephaestin in CNS tissue). The calculation of total ferroxidase activity was performed using the initial linear phase.

3.3.9 Statistical analysis

Compared to controls, this study examined whether there are disease-associated changes in copper availability and its homeostatic regulation in post-mortem human brain tissue. The data collected across a variety of assays was graphed in GraphPad Prism (version 10) and expressed as the mean ± SEM (unless stated otherwise). All statistical analyses were calculated using Graphpad Prism (version 10) and statistical outliers were determined using

ROUT method as previously described [559]. Significant differences in the mean scores between PSP group and control were tested using two-sided t-tests. F tests used to determine equal variances and in the instance of unequal variances, a Welsch's correction was used.

3.4 Results

3.4.1 Alterations in nigral metals levels in PSP diseased tissue

The substantia nigra contains naturally high levels of metals, particularly copper, iron, and zinc [168, 173, 174, 176, 375]. Our understanding from previous studies is that changes in metals is an underlying feature across diverse neurodegenerative diseases in regions that have severe tau pathology, gliosis and neuronal cell loss. Results presented in Chapter 2 indicate that the substantia nigra in PSP had the highest levels of gliosis, SOD1 pathology, and neuronal cell loss. Based on this, we performed a more comprehensive biochemical analysis on the substantia nigra. Using analytical methods to measure metal concentrations in the brain, we observed that there were significant alterations in metals levels in the substantia nigra of a PSP-diseased brain (**Figure 3.1** and **Figure 3.2**). While changes in these metals have been observed in previous studies using PSP tissue, there is little known about potential changes within subcellular fractions within the substantia nigra as copper is associated with various compartments inside the cell. Therefore, we separated tissue samples into two fractions, the soluble fraction and the insoluble fraction to represent both the cytosolic and the membrane-associated compartments respectively [554]. The concentration of copper in the nigra showed a significant decrease of 37.0% in the soluble and 27.5% decrease in the insoluble fraction (**Figure 3.1a)** (**Table A5** in **Appendices**). Conversely, a non-significant increase in iron (54.4%) in the soluble fraction and increased by 78.7% in the insoluble fraction. Note that only the latter did reach statistical significance (**Figure 3.1b)** (**Table A5** in **Appendices**). Although the trends in zinc were similar to those in iron, there was only a modest 23.2% increase in soluble zinc and slight but significant increase in zinc within the insoluble (27.4%) (**Figure 3.11c)** (**Table A5** in **Appendices**).

LA-ICPMS is a sensitive tool to investigate the spatial distribution of elements, with the ability to resolve distinct regions in biological tissues. The application of this technology enabled the discrimination between the concentration of metals within the subregions of the substantia nigra (**Figure 3.2a, b**). Total copper levels were significantly decreased in the substantia nigra *pars compacta* and a similar trend was seen in the substantia nigra *pars reticulata* (**Figure 3.2c**) (see **Table A6** in **Appendices**). The white matter tracks of cerebral peduncle that encapsulate the midbrain and the brainstem, showed a non-significant decreased in copper.

Iron levels detected in all regions, substantia nigra *pars compacta*, *pars reticulata* and the cerebral peduncle showed large variation in the datasets, with no significance changes in iron or zinc concentration detection within the substantia nigra *pars compacta* or *pars reticulata* with a small decrease in zinc seen in the cerebral peduncle (**Figure 3.2d, e**) (see **Table A6** in **Appendices**).

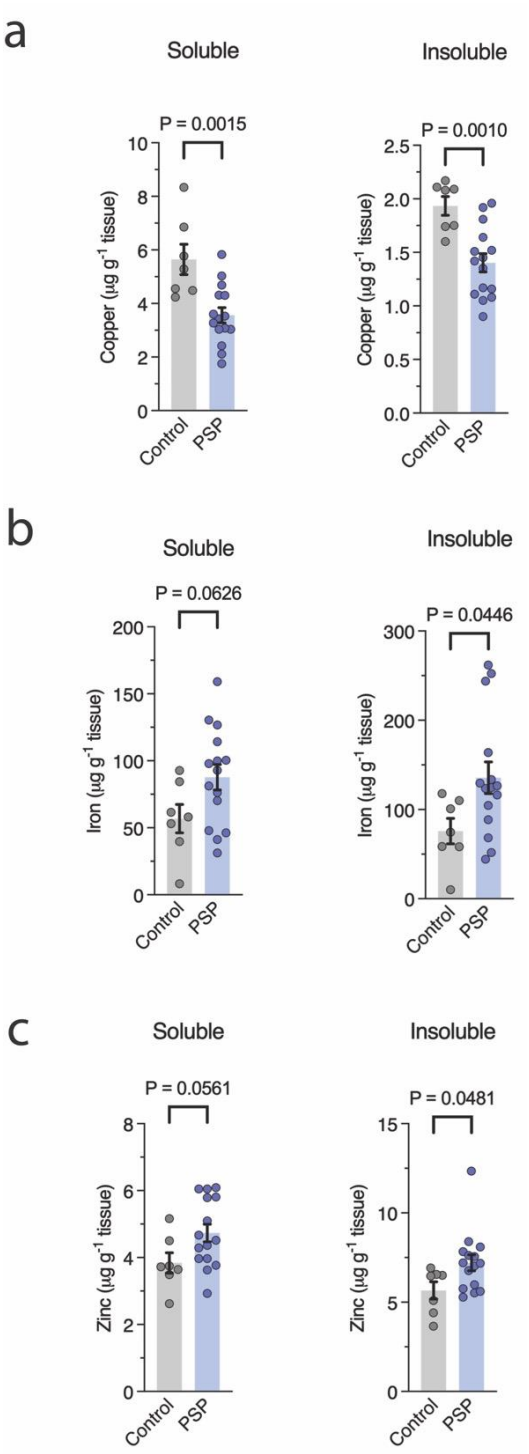

Figure 3.1. Trace metal levels within soluble and insoluble fractions of the substantia nigra in PSP cases detected using solution ICPMS

Comparison of cytosolic (soluble) and membrane-associated compartments (insoluble) metals levels in nigral tissue homogenates in PSP. Using solution ICPMS, metals **a**) copper, **b**) iron and **c**) zinc were measured in the sample fractions. Data expressed as mean ± SEM expression relative to control. Two tailed t-tests were used to test significance.

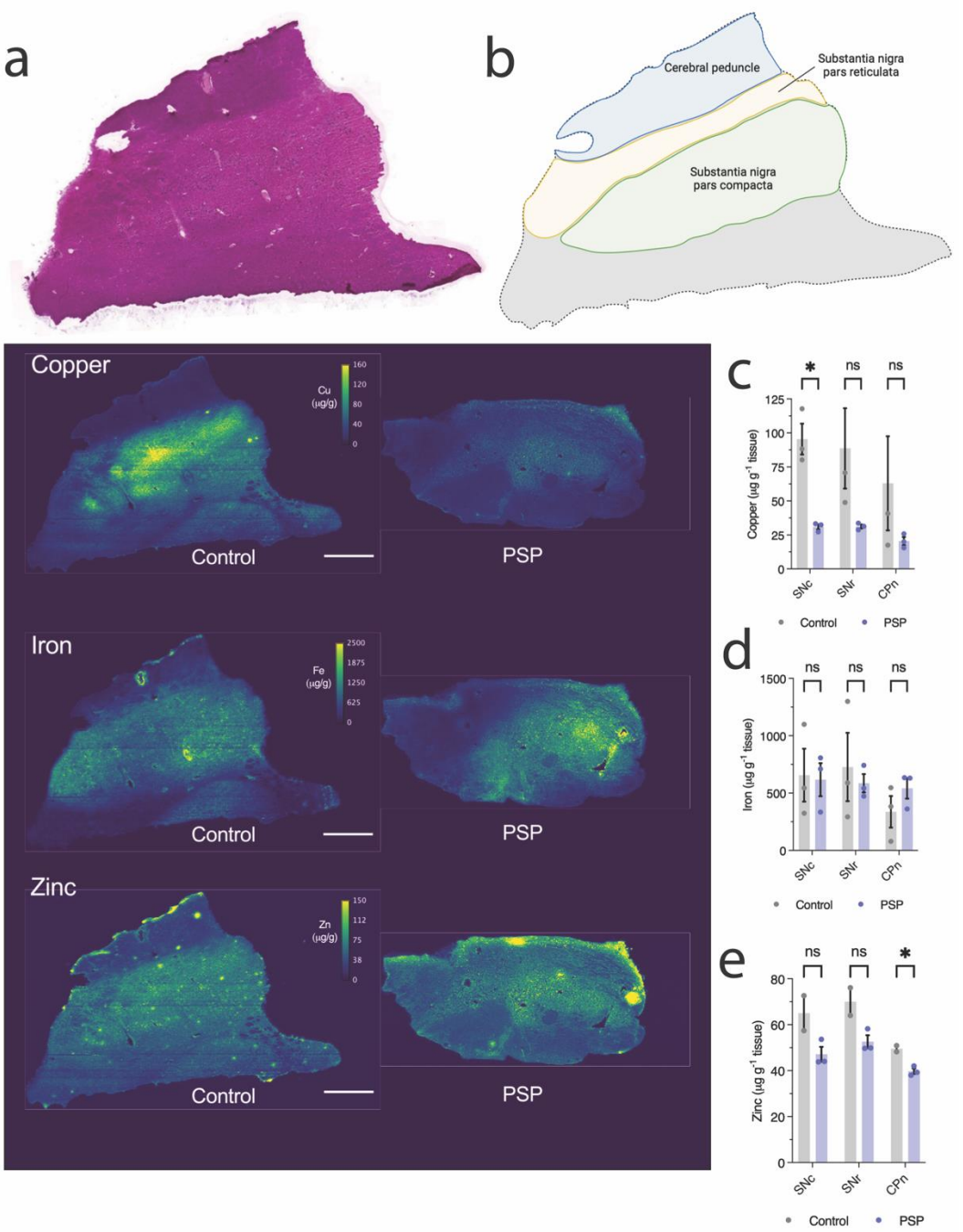

Figure 3.2. Trace metal concentration within subregions of the substantia nigra of PSP cases detected LA-ICPMS

An example of **a**) H&E-stained midbrain section and **b**) the corresponding superimposed annotated regions of interest defining areas of substantia nigra *pars compacta* (SNc), substantia nigra *pars reticulata* (SNr) and surround region of the cerebral peduncle (CPn). Comparison trace metal content within sections measured by LA-ICPMS; **c**) copper, **d**) iron and **e**) zinc. Representative LA-ICPMS pseudocolour heatmaps of copper. Iron and zinc in control midbrain section and PSP midbrain section. Data expressed as mean ± SEM expression relative to control. Multiple t-tests (two-sided) were used to test significance. Significance indicated ** P<0.01, * P<0.05 compared to control.

3.4.2 Expression of genes related to copper handling is changed in PSP

The regulation of intracellular copper involves a variety of copper transporters and chaperones that coordinate the delivery of copper to various subcellular compartments and its cellular extrusion. To explore mechanisms that may be involved in the alterations in copper observed in PSP (**Figures 3.1a**, **3.2c**), we measured the expression of 20 genes related to copper handling (**Figure 3.3**). We observed that of the 20 copper handling genes measured, 9 were increased in expression in the substantia nigra of PSP brain (**Figure 3.3**) with an overall change in copper handling (**Figure 3.3c**). While copper deficiency in PD may be due to decreased levels of *SLC31A1* encoding CTR1 [175], *SLC31A1* levels were not altered in the substantia nigra in PSP (**Figure 3.1**). In contrast to *SLC31A1*, the metalloreductases (STEAP family 1-4) that facilitate copper entry into the cell and its transport inside the cell were altered in PSP. In addition, expression levels of the ATPase *ATP7A* were significantly increased in PSP as well as the mitochondrial specific chaperones *COX11* and *SCO1* (**Figure 3.3**). Factors that sense metals and regulate metal homeostasis at the transcription level *MFT1* and *MFT2* were significantly elevated in PSP (**Figure 3.3**). We examined the relationship between copper concentration and copper handling genes significantly altered in PSP (**Table 3.3**). There was a strong relationship between the copper levels and *STEAP1* and *STEAP3*, whereby as copper levels decreased, the *STEAP1* and *STEAP3* gene expression increased (**Table 3.3**). There was a moderate negative correlation between *ATP7A, COX11* gene expression and copper levels, although it was not statistically significant (**Table 3.3**).

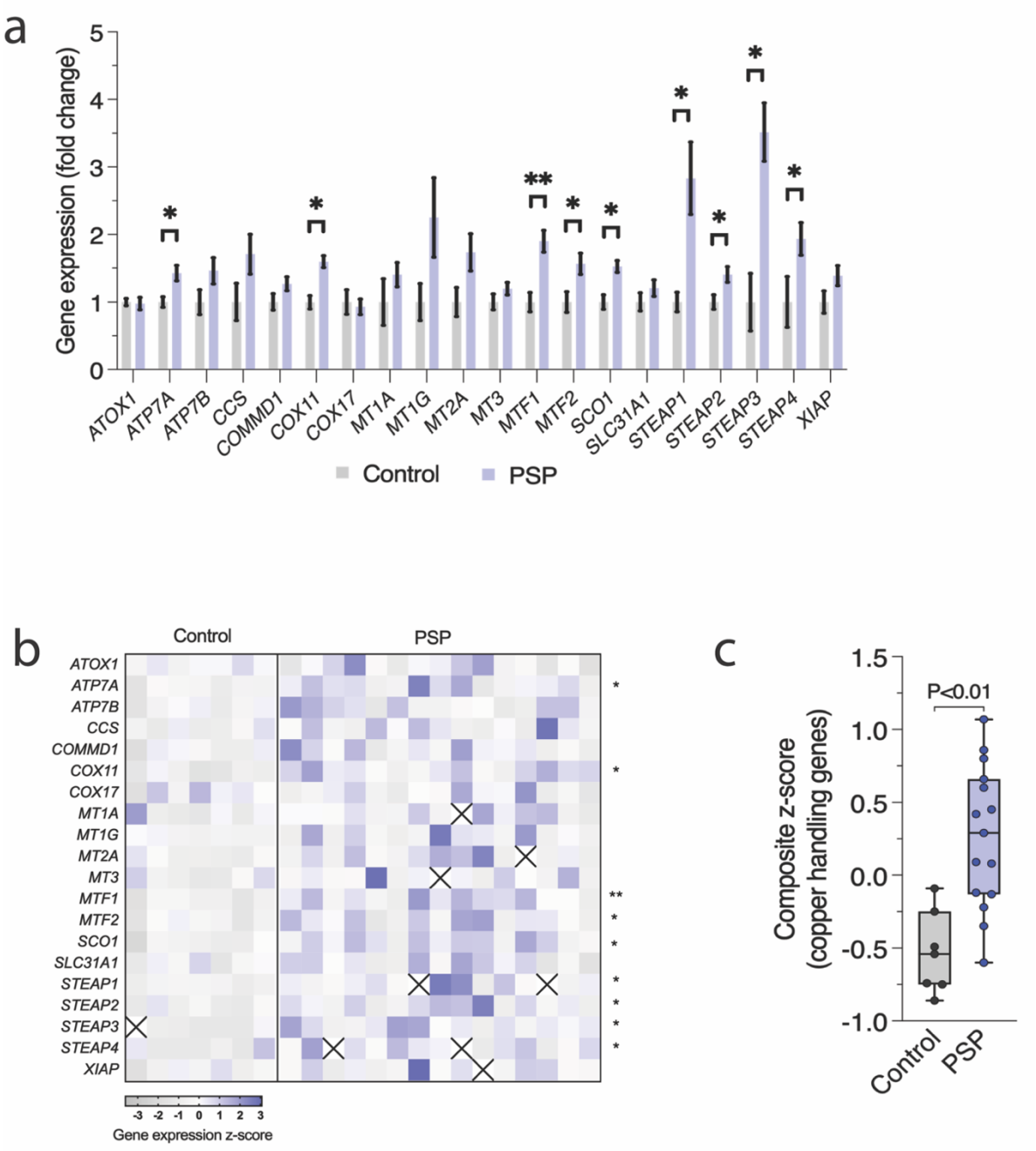

Figure 3.3. Molecular signature of copper handling genes in the substantia nigra of patients with PSP

Measurement of gene profiles using qPCR from tissue homogenates from the substantia nigra; **a**) relative fold change in copper-handling genes compared to control **b**) standardised z-score heatmap of copper handling genes, and **c**) composite z-scores of overall copper handling genes. Data expressed as mean ± SEM expression relative to control except for graphs **b** and **c** being expressed as z-scores. Multiple t-tests (two-sided) were used to test significance. Significance indicated ** P<0.01, * P<0.05 compared to control.

Table 3.3. Relationships between ICPMS copper levels and copper handling genes within the substantia nigra

Gene	Soluble copper concentration	Insoluble copper concentration
ATP7A	Pearson r = -0.3862	Pearson r = -0.3642
(N = 22)	P (two-tailed) = 0.0758	P (two-tailed) = 0.0956
COX11	Pearson r = -0.3938	Pearson r = -0.2933
(N = 22)	P (two-tailed) = 0.0697	P (two-tailed) = 0.1852
MTF1	Pearson r = -0.2258	Pearson r = -0.3639
(N = 22)	P (two-tailed) = 0.3123	P (two-tailed) = 0.096
MTF2	Pearson r = 0.005106	Pearson r = -0.2186
(N = 22)	P (two-tailed) = 0.982	P (two-tailed) = 0.3285
SCO1	Pearson r = -0.1084	Pearson r = -0.1274
(N = 22)	P (two-tailed) = 0.6311	P (two-tailed) = 0.5719
STEAP1	Spearman r = -0.3394	Spearman r = -0.522
(N = 20)	P (two-tailed) = 0.1433	P (two-tailed) = 0.0182 *****
STEAP2	Pearson r = -0.2048	Pearson r = -0.3626
(N = 22)	P (two-tailed) = 0.3607	P (two-tailed) = 0.0972
STEAP3	Pearson r = -0.5527	Pearson r = -0.576
(N = 21)	P (two-tailed) = 0.0094 ******	P (two-tailed) = 0.0063 ******
STEAP4	Pearson r = -0.3726	Pearson r = -0.2927
(N = 20)	P (two-tailed) = 0.1057	P (two-tailed) = 0.2105

Significance is indicated **P<0.01 and *P<0.05.

3.4.3 Alterations in cuproenzymes

The supply of copper to various cuproenzymes is regulated by many transporters and chaperones. Decreased levels of both cytosolic and membrane associated copper in PSP (**Figure 3.1a**) may have a profound effect on both the expression and specific activity of cuproenzymes in PSP. Therefore, we measured expression profiles of selected cuproenzymes, ceruloplasmin; *CP*, dopamine beta hydroxylase; *DβH*, hephaestin; *HEPH,* monoamine oxidase B; *MAOB*, myeloperoxidase; *MPO* and *SOD1* in the substantia nigra of PSP cases (**Figure 3.4**). The presented study showed an increase in mRNA levels in ferroxidases ceruloplasmin and hephaestin (**Figure 3.4a, b**) which both contain multiple copper ions that facilitates iron efflux [205, 280, 288, 303, 560] and genes *DβH*, *MAOB*, *MPO* and *SOD1* were unchanged. SOD1 protein expression (**Figure 3.4c**) and activity (**Figure3.4f**) showed no alterations in PSP. Commensurate with mRNA levels, protein levels of ceruloplasmin (**Figure 3.4d**) and hephaestin were elevated in PSP (**Figure 3.4e**) however no alteration in ferroxidase activity was observed (**Figure 3.4g**).

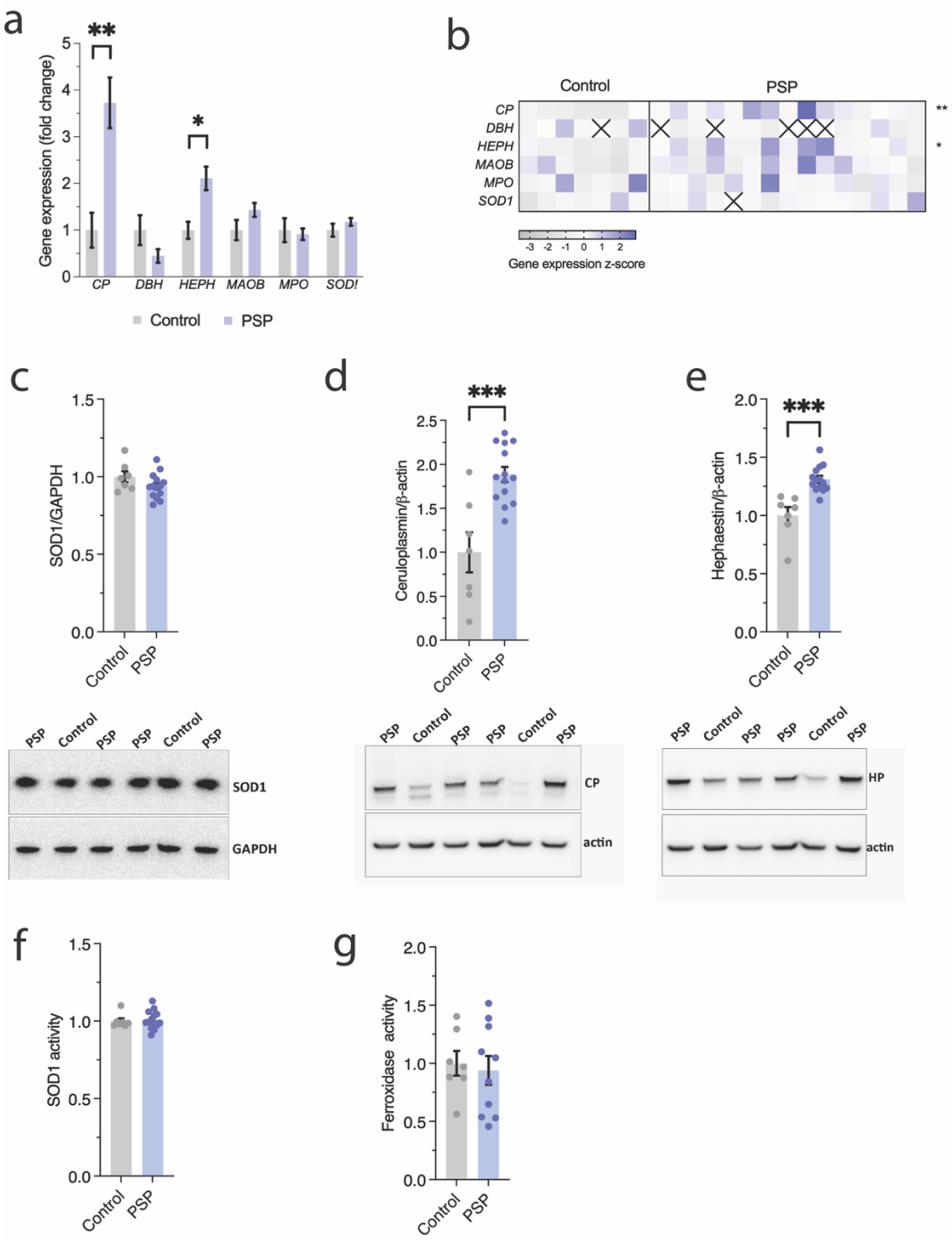

Figure 3.4. Gene, protein and activities levels of cuproenzymes in PSP

mRNA and protein levels of cuproenzymes (ceruloplasmin; *CP*, dopamine beta hydroxylase; *DBH*, hephaestin; *HEPH*, monoamine oxidase b; *MAOB*, myeloperoxidase; MPO and superoxide dismutase 1; SOD1) measured from tissue homogenates from the substantia nigra; **a**) relative mRNA fold change in cuproenzymes, **b**) standardised Z- score heatmap of cuproenzymes and protein levels of measured by western blot of cuproenzymes c) SOD1, **d**) ceruloplasmin, **e**) hephaestin, **f**) SOD1 specific activity and **g**) ferroxidase activity measured in the substantia nigra. Except for z-score heatmap, data are expressed as the mean ± SEM, t-tests (two-tailed) was used to test significance with non-significance (ns) and significance being indicated when *p<0.1, **p<0.01 and ***p<0.001.

3.5 Discussion

We report here that brain tissue from cases of PSP exhibit features indicative of copper dyshomeostasis. Not least of which, it was found that the copper content in the substantia nigra was significantly decreased when assessed using two complementary analytical techniques, with the *pars compacta* subregion showing more extensive copper loss (**Figures 3.1** and **3.2**). One of the greatest regions for neuronal cell loss is in the substantia nigra *pars compacta* and appears to be universal in all PSP cases [102]. In PSP, there was an overall copper deficiency seen in both subcellular compartments. Copper levels were decreased by 37% within the cytosolic fraction, where SOD1, an important antioxidant resides. The membrane associated fraction which would include plasma membranes, vesicles, organelles like the mitochondria also showed a 27.5% decreased in the copper levels associated with this fraction where important cuproenzymes like complex IV, ceruloplasmin and hephaestin function. We also observed alterations in the insoluble iron and zinc pool in PSP tissue (**Figure 3.1b, c**), which if left unregulated can cause a change in the redox status of the cell where free iron can induce metal-mediated toxic cascade leading to degeneration [14]. *In situ* assessment of iron and zinc using LA-ICPMS indicated unchanged concentrations of iron and zinc (**Figure 3.2b, c**) which appeared in contrast to results obtained from solution ICPMS analysis of the TBS-soluble and -insoluble fractions (**Figure 3.1b,c**). This result could be explained by a number of factors such as differences in sample preparation and processing and capacity for LA-ICPMS analysis to more specifically extract data from defined regions of interest. However, we anticipate that the much smaller number of samples per group used for LA-ICPMS (N = 3) may have played the larger role, with higher overall variation in the LA-ICPMS data noticeable.

Iron can also induce the aggregation of tau [561] where there is also putative binding sites for tau and iron to interact [562]. Iron is also found within NFTs bound to ferritin that is seen in PSP brain tissue [563]. Zinc on the other hand is redox inert however under low zinc levels, the activity of SOD1 is increased to protect against oxidative stress [564]. The binding of zinc to SOD1 ensures its conformational stability [553], but an excess of zinc has been reported to decrease its activity [565]. Zinc is known to be increased in the metallothionine transcription factors *MFT1* and *MFT2* [566], although there was no significant increase in metallothionines seen in PSP tissue.

Few studies have shown copper alterations in the PSP brain [21] and the substantia nigra is one of the areas that is most abundant in copper [168, 173, 174, 176, 375]. This study used copper handling genes as additional indicators of copper dyshomeostasis, and altered copper concentration is likely to be a result of dysfunctional copper handling. It was observed that there were several copper handling genes significantly altered (**Figure 3.3**) resulting in an overall shift in copper handling in PSP tissue (**Figure 3.3c**). Copper trafficking is a homeostatic process of delivering copper to various compartments and cuproenzymes, which is facilitated by chaperones and the ATPases. Of note, we saw an increased levels of *ATP7A*, which is known to be expressed predominately in choroid plexus, the cerebellum, and the substantia nigra [176]. The essential role of ATP7A is seen when it is defective in the neurodegenerative condition Menkes disease, animal models of Menkes disease and altered expression of its ortholog in drosophila leading to age-related motor decline [181, 186, 256, 567]. It is possible that the altered levels of *ATP7A* is a contributing factor to the loss of copper in PSP as seen in mice with altered expression in the *Atp7a* gene, copper levels are decreased in most tissues, including the brain [568]. ATP7A regulates copper by directing its removal from the trans Golgi network to the plasma membrane when intracellular copper levels are elevated [569]. Mutations that cause a dysfunction in ATP7A as seen in Menkes disease patients show a sensitivity to copper with accumulated copper seen in fibroblast cultures [570]. Overexpression of *ATP7A* in CHO cells shows copper resistance where intracellular copper levels remained very low even when being exposed to increasing copper concentration [569]. As Camarkaris *et al*. (1995) have demonstrated, increasing *ATP7A* mRNA levels by 3, 7 and 70-fold confers copper resistance resulting in the higher copper efflux of the 7 and 10-fold *ATP7A* variants [569]. The amount of extracellular copper influences ATP7A cellular localisation whereby high extracellular levels of copper induces its translocation to the plasma membrane [258]. Accordingly, copper levels within cells are decreased because ATP7A promotes copper efflux rather than copper insertion in copper-dependent enzymes [569]. In cell lines derived from mouse lung primary fibroblasts, the deleting of genes *Atp7a* and metallothionine 1 by Adeno-Cre virus caused lethality due to extreme copper insensitivity [571]. The levels of copper significantly increased when *ATP7A* (*ATP7A*$^{-}$) and *ATP7A*/metallothionine 1 (*ATP7A*$^{-}$/MT1^{-}) were deleted in a medium containing only 1.7 µM copper [571]. Introducing the copper chelator BCS into the media decreased the intracellular copper levels in these cells, however the copper levels were still more than the wildtype control cells [571]. The addition

of 0.25 µM of copper into the media was shown to cause a decreased in cellular viability in both the *ATP7A*$^{-}$ and the *ATP7A*$^{-}$/*MT1*$^{-}$ cells. Metallothionines are shown to regulate the availability of copper for ATP7A. This is shown in the cells with no metallothionine 1, there was a greater proportion of ATP7A found in cytoplasmic vesicles and the addition of copper chelator BCS shifting to perinuclear region with an increase in copper trafficking of cuproenzyme lysyl oxidase [571]. The ATP7 interactome, identified by quantitative mass spectrometry using co-isolated proteins with ATP7A, identified 541 proteins that interact with ATP7A in neuroblastoma cells, that were treated with BCS or with copper [506]. Comstra *et al.* (2017) using western blot showed that DβH being one of the strong interactors with ATP7A with or without the copper or BCS treatment [506] and using mass spectrometry, 134 proteins that co-purified with ATP7A were proteins were unaffected by copper chelator BCS or with copper chloride [506]. Bioinformatics using gene ontology algorithms found that ATP7A interactome is overrepresented in membrane trafficking and vesicular transport with enrichment in neuronal ontological pathways of growth cone, dendrite and synapse formation [506]. Phenotypes significantly associated with the ATP7A interactome were neurodegenerative diseases, and among these tauopathies were highlighted [506]. Severe degeneration in neurons, together with axonal disruption and loss of synapses, is profound in PSP tissue [572]. Since most of the functional studies of ATP7A have been investigated in enterocytes, there is little data on ATP7A and its functioning in neurons and glial cells [573, 574]. It is known that ATP7A is involved in synaptogenesis where ATP7A can shift locations readily from the neuronal cell body to axons during this process [575, 576]. Menkes disease mouse model using mottled brindled *Atp7a* mutation, the olfactory epithelial cells show disruption in synapse formation with sensory olfactory neurons as well as disturbance in transitioning from immature to mature using markers for axonal growth and synaptic connections [575]. The release of copper within the synapse is thought to occur through ATP7A, since the Menkes *Atp7a* mouse mutant shows little copper within synapses [577]. Copper is also found to modulate secretory vesicles and synaptic markers, synaptophysin and t-SNARE docking protein SNAP-25, when neuroendocrine PC-12 cells were treated with copper-complex Cu^{II}(gtsm) [578]. While it is still not clear as to why copper is also released at the synapse, it is suggested that copper could modulate neural transmission, protect from glutamate excitotoxicity and induce synaptic plasticity [579]. It may also be important to

highlight the importance of copper's role in controlling axonal growth and synaptogenesis through the mechanism of ATP7A.

Copper is supplied by ATP7A to DβH and MAOB, while ATP7B is believed to supply copper to ceruloplasmin and hephaestin at the trans Golgi network [287, 580]. We found no statistically significant change in ATP7B, but the magnitude of the change in ATP7B levels was similar to that of ATP7B (**Figure 3.3a**). Furthermore, we did find increased mRNA and protein levels of multi-copper ferroxidases ceruloplasmin and hephaestin. Multicopper ferroxidases are significantly affected by the decrease in availability of copper as iron accumulates within substantia nigra despite increased expression of both proteins as seen our PSP cohort (**Figure 3.4g**). The regulation of both ceruloplasmin and hephaestin is mediated by intracellular iron and copper levels. A diet deprived of copper given to rats and mice induces a decrease in GPI-linked ceruloplasmin protein levels in the liver and spleen with no changes to its mRNA expression, supporting that copper deficient ceruloplasmin is rapidly degraded in these tissues [581]. Intracellular iron levels are suggested to regulate hypoxia-inducible factor-1 [582], which is a transcription factor to over sixty different genes, including ceruloplasmin [583]. Hypoxia-inducible factor-1 expression increases in response to decreased iron levels via translocation to the nucleus for transcriptional regulation via its response element to upregulate ceruloplasmin. Copper also promotes hypoxia-inducible factor-1 transcriptional regulation through its response element to upregulate ceruloplasmin in response to decreased iron levels [582, 584]. Ceruloplasmin is an acute phase reactant, which is transiently upregulated by a variety of factors, including cytokines and ROS, but in diseases like sporadic ALS [196], in which ceruloplasmin levels are increased, removing excess iron from the central nervous system could serve as a compensatory mechanism to prevent iron-mediated toxicity. As in PD and ALS, iron accumulates potentially due to decreased ferroxidase activity of ceruloplasmin, as seen in our PSP cohort with an additional ferroxidase hephaestin, since copper supply to these cuproenzymes is presumably restricted by the overall decrease in tissue copper content. It has been shown that CNS tissue in mice deficient for both ceruloplasmin and hephaestin accumulates more iron than mice with either mutant alone [308]. For confirmation, it would be interesting to determine which cells are accumulating iron using more resolved based techniques capable of measuring metal concentrations in single cells due to the cell specificity of ceruloplasmin and hephaestin. Iron

accumulation is common in neurodegenerative conditions including PSP [21, 373, 379, 439, 440, 552, 585-588], and its increased levels can also overtly participate in oxidative stress [136, 589] inducing the aggregation of various proteins like tau, which lead to neuronal cell death and gliosis [590]. In the remaining cuproenzymes that we measured, we saw no difference in the mRNA levels, and no changes in the mRNA or the proteins levels in SOD1. Despite seeing misfolded SOD1 in the substantia nigra of sections from PSP cases detected by immunohistochemistry (Chapter 2), SOD1 mRNA levels, SOD1 protein levels, and its specific activity were all unchanged in PSP. Based on their density, SOD1 aggregates would be found in high concentrations in insoluble fractions rather than in cytosolic compartment which is where biochemical activity was measured. It is possible that that most of the copper-deficient SOD1 would be bound up in the insoluble fraction, presenting as misfolded SOD1 in aggregates.

SLC31A1 (CTR1) mRNA levels did not change in PSP, indicating a disconnect between copper levels and its importation. The uptake of copper performed by CTR1, one of the necessary mechanisms for transport of copper inside cells, including within the brain. CTR1 is transcriptionally regulated by Sp1 under copper depletion conditions [591] and CTR1 is degraded when copper levels are high [592]. If there is less intracellular copper, CTR1 expression would be increased to bring more copper inside the cell. We observed that there were no alterations in mRNA levels of *SLC31A1* which is seemingly different to what is seen in post-mortem PD tissue [175]. Notably, copper import can also be via other mechanisms. Monovalent copper can only be transported by CTR1 [240]. However, copper in its bivalent form is suggested to be transported within cells by DMT1 [593]. DMT1 is suggested to act as a compensatory mechanism to when CTR1 is deficient [594]. DMT1 levels are increased within the substantia nigra in PD patients [595] however, we saw no change in *DMT1* in PSP (see **Figure A1** in **Appendices**).

Tissue-specific expression patterns of *Steap* metalloreductases stimulate the uptake of copper and iron in cells [236]. According to our data, copper levels are negatively correlated with STEAP (STEAP1 and STEAP3) gene expression, indicating that the STEAP family are involved in copper absorption. *STEAP1-4* transcripts were all upregulated in the substantia nigra of PSP tissue suggesting that it is possible that the lack of copper drives the upregulation

of *Steap1-4* to potentially import more copper inside the cell with the assumption that the STEAP1-4 proteins work in conjunction with CTR1 [236]. *STEAP4* overexpression has been shown to promote copper uptake by tumor cells in inflammatory conditions, such as presence of cytokine interleukin-17 [596].

Mitochondrial dysfunction is a factor in the pathogenesis of PSP [597, 598] and a key component of mitochondrial activity is complex IV which requires copper for its function. Two mitochondrial chaperones COX11 and SCO1 deliver copper to form the assembly of complex IV in the inner membrane space [271]. We found that expression levels for both *COX11* and *SCO1* were significantly upregulated in PSP (**Figure 3.3a, b**). SCO1 and COX11 receive their copper from COX17 [599], which is shuttled from the cytoplasm into the inner membrane space where SCO1 and COX11 are anchored [600, 601]. Most mitochondrial chaperone studies are not performed in mammalian systems and have been studied using their orthologs found in yeast and plants [271, 602]. What is seen in overexpression of a homolog of *Cox11* in *Arabidopsis,* surprisingly showed to inhibit complex IV activity [603]. However, Cox11 functions to partially attenuate oxidative stress [604] and in this role it does not require copper for functionality [605]. This response is also seen similarly with Sco1 [606]. Therefore, the increase in *COX11* and *SCO1* levels in PSP tissue might be a response to oxidative stress levels being excessively produced in the mitochondria. Complex IV has also been shown to be downregulated in globus pallidus in PSP tissue compared to control tissue [598] and ATP levels are significantly decreased in the basal ganglion [607]. No specific measurement of complex IV activity has been reported in PSP brain. However, one study by Qaud *et al.* (2021) assessed complex IV activity in red blood cells from a heterogeneous pool of atypical PD samples which included some cases of PSP [608]. They reported decreased complex IV activity levels in atypical PD group. Measuring complex IV activity in brain samples is confounded by reliance on post-mortem tissue which compromises capacity to enrich for mitochondria which is a requirement for accurate assessment of mitochondrial enzyme activity. Overcoming this obstacle would likely provide important insight to the impact of altered copper availability in PSP.

The aim of this chapter was to determine whether there is evidence of copper dysregulation in the neurodegenerative condition PSP. Significant alterations in copper were detected,

together with changes involving genes associated with copper handling and cuproenzymes. Thus, copper deficiency in the degenerating substantia nigra may be crucial for pathological changes implicating SOD1 with PSP.

Chapter 4. Examining decreased copper bioavailability as a putative model for PSP

Chapter 4. Examining decreased copper bioavailability as a putative model for PSP

Results presented in Chapter 2 show that in PSP, SOD1 accumulates and is misfolded in regions with marked neurodegeneration and gliosis, indicating a proteinopathy in PSP that may be related to disrupted availability of copper required for physiological folding and maturation of this highly abundant cuproenzyme. In Chapter 3, we report that the PSP-affected brain is characterised by decreased copper concentrations in affected regions and altered expression of genes associated with copper handling. In addition, some evidence was provided to indicate a disconnect between copper-dependent ferroxidase activity and abundance of the ferroxidases ceruloplasmin and hephaestin. To explore a potential causal connection between copper and neuronal death in PSP we examined in this chapter a strain of mouse that is heterozygous deficient for the copper uptake transporter Slc31a1 (**Figure 1.8**). At present, mouse models for PSP are lacking. An objective in this Chapter, therefore, was to determine whether inducing decreased copper availability *in vivo* could model features of PSP.

4.1 Introduction

Early efforts into developing a mouse model for PSP relied on replicating tau pathology by the overexpression of human mutant tau due to the distinctive tau pathology evident in PSP. Numerous mouse lines based on tau have been established which display a broad range of pathological and phenotypical manifestations (**Table 4.1**) and findings derived from these mice require careful interpretation. The lack of animal models specifically for PSP is mainly a result of the disease complexity and significant overlap with other more common tauopathies such as AD and PD. Further confounding the development of specific animal models of PSP is the fact that PSP is primarily a sporadic disease with no known causal mutations [60].

Of the many tauopathies, the one with the closest resemblances to PSP clinicopathology is frontal-dementia with parkinsonism linked to chromosome 17 (FTDP-17)[609, 610], a familial disorder with an autosomal dominance pattern of inheritance with frequent mutations in tau (N279K, P301S and P301L). The discovery of several mutations in intronic and exonic regions in *MAPT* provided a link with tau and neurodegenerative disease. Several tau mouse lines

have been created by inserting these familial mutations into the genome, including the N279K, P301S and P301L mutations, that cause the microtubules to be destabilised and disassembled [611, 612] (**Table 4.1**). While these models mimic basic cellular alterations such as aggregation, cytoskeletal dysfunction, cell death and gliosis [613-615], there are several caveats as to the distribution of tau within specific regions and with cell types does not fully replicate what is seen in PSP. In addition, this raises concerns about whether *in vivo* transgenic models using tau overexpression induced by a variety of mutations/promoters are accurate representation PSP cytopathology. Potential development of non tau-based models for PSP is a relatively unexplored field.

Chapter 4. Examining decreased copper bioavailability as a putative model for PSP

Table 4.1. Summary of tau animal models

				Pathology		Behavioural phenotype	
Mouse line	**mutation**	**Promoter**	**isoform**	**Area affected**	**Cytopathology**	**Neurological**	**Refs**
Mapt$^{-/-}$	KO	N/A	N/A	N/A	None reported	Muscle weakness, hyperactivity in locomotor	[616], [617]
T44 (B6D2F1)	Wildtype	PrP	0N3R	Spinal cord, Pons, cortices, hippocampus, amygdala, entorhinal cortex	NFTs	Motor impairment (tail suspension)	[618], [619], [407]
8c (SWxB6D2F1)	Wildtype	PAC (Tau)	3R (0N, 1N, 2N) > 4R (0N, 1N, 2N)	Spinal cord, cortex, hippocampus, striatum,	NFTS	No motor abnormalities observed	[620], [621]
htau (SWxB6D2F1)	Wildtype	PAC (Tau), Mapt-/-	3R (0N, 1N, 2N) > 4R (0N, 1N, 2N)	Hippocampus, medial septum, entorhinal cortex, nucleus of the diagonal band, hypothalamus	NFTs	None reported	[621]
htau (B6D2F1)	Wildtype	Thy-1.2	2N4R	Hippocampus, olfactory tract, cerebral cortex, dentate gyrus, amygdala, brainstem, spinal cord, and nerve bundles of skeletal tissue	NFTs, neuropil threads, axonal spheroids	Hindlimb clasping	[622]
Htau40 (FVB/N)	Wildtype	Thy-1.2	2N4R	Cortex, hippocampus, thalamus, spinal cord, amygdala,	NFTS	Motor and sensorimotor impairments	[623]
GFAP/tau Tg B6C3/F1)	wildtype	GFAP	1N4R	Spinal cord, brainstem, thalamus, amygdala, caudate putamen, midbtain, medulla, cortices, midbrain	TA	Motor impairments (data not shown)	[624]
PrP-TA (B6D2F1)	G272V (Exon 9)	PrP	2N4R	Brain and spinal cord	NFTs, Oligodendrocytes	Not reported	[625]
VWL (C57BL/6J× CBA)	G272V/ P301L/ R406W	Thy-1.2	2N4R	Hippocampus and cortices	NFTs	Not reported	[626]
JNPL3 (C57BL/DBA 2/SW)	P301L (exon 10)	PrP	0N4R	Amygdala, pons, midbrain, hypothalamus, pre-optic nuclei, septal nuclei, spinal cord, brainstem and dentate nucleus	NFTs, filaments in neurons Axonal spheroids	Hindlimb Clasping, muscle weakness, hunched, dystonia	[613]
pR5 (B6D2F1)	P301L (exon 10)	Thy-1.2	2N4R	Hippocampus, cortices, brainstem and spinal cord	NFTs	Impaired spatial reference memory, accelerated extinction of condition taste aversion	[627], [628, 629]
Tg Tau 23027 (129SvEv × FVB/N)	P301L (exon 10)	PrP	2N4R	Hippocampus, cerebral cortex, amygdala, basal forebrain nucleus, locus coeruleus, Caudate putamen, accumbens nucleus and substantia nigra, Spinal cord	NFTs, glial tangles in astrocytes, oligodendrocytes	Impairment learning of taste aversion, impaired working memory and spatial learning	[614]
Tau-AR, P301L (FVB/N)	P301L (exon 10)	Thy-1.2	2N4R	Cerebral cortex brainstem, spinal cord	NTFs	Severe motor impairment, clasping	[630]
Tg4510 (FVB/N)	P301L (exon 10)	CaMKII	0N4R	Frontal cortex, hippocampus, spinal cord	NFTs	Decreased ambulation, motor impairment, hindlimb dysfunction, impaired spatial reference memory	[615]
2541 (C57BL/6J× CBA/ca)	P301S (exon 10)	Thy-1.2	0N4R	Spinal cord, hippocampus, cerebral cortex, amygdala, dentate nucleus, brainstem	NFTs	Paraparesis, muscle weakness	[631]
PS5, PS19 (B6C3H/F1)	P301S (exon 10)	PrP	1N4R	neocortex, amygdala, hippocampus, brainstem and spinal cord	NFTs	Clasping, limb weakness, paralysis	[632]
N279K (C57BL/6 × SJL)	N279K (exon 10)	PrP	0N4R	N/A	No pathology	Impaired spatial learning, hyperactivity, deficits in fear learning,	[633]
THY-Tau22 (C57BL6/CBA)	G272V, P301S (exon 10)	Thy-1.2	1N4R	Hippocampus, dentate gyrus, amygdala, spinal cord	NFTs, neurites	Impaired spatial and learning memory, increased anxiety, no motor impairments	[634]
Tg212, Tg214, Tg216 (B6SJL)	V337M (exon 11)	PDGF-beta	2N4R	Hippocampus, cerebral cortex	NFTs	Increased time in open arms, no deficits in spatial or learning memory	[635], [636]
Tg748, 502, 492,483 (B6SJL)	R406W (exon 13)	CaMKII	2N4R	Hippocampus, amygdala, and neocortex	NFTs	No impairments in sensorimotor/motor/anxiety, impairment in fear conditioning	[637]
RW tau B6C3/F1)	R406W (exon 13)	PrP	2N4R	Hippocampus	NFTs	Progressive motor weakness	[638]
TgTau R406W (FVB/N)	R406W(exon 13)	PrP	2N4R	Hippocampus, amygdala, neocortices	NFTs	Motor impairment, impairment in acquired memory	[639]

Promoters; prion protein (PrP), penicillin G acylase encoding gene (PAC), Thymus cell antigen (Thy-1), platelet-derived growth factor (PDGF), calmodulin-stimulated protein kinase II (CaMKII). Cytopathology; neurofibrillary tangles (NFTs), tufted astrocytes (

4.1.1 Animal models of copper deficiency as a putative model for PSP

Despite its similar symptoms to iron-deficient anaemia, dietary copper insufficiency is uncommon in humans. There have been many studies that show severe neurological effects associated with dietary copper depletion among ruminants with low copper levels in their forage, including ataxia, tremors, uncoordinated gait, and death [640, 641]. Further examination of the CNS of these animals reveals primary lesions on the spinal cord, low myelination, collapse of white matter, and necrosis within the brain [642-644]. Laboratory rodents have been used for further investigation of the biochemical and neurological effects of decreased dietary copper. Multiple organs are affected by copper deficiency, particularly the liver, cardiovascular system, and brain, and these can be partially reversed with copper supplementation [645]. A diet low in copper leads to inflammation, hypercholesterolemia, cardiac hypertrophy, and mitochondrial dysfunction in rodents [646]. In the brain, the impairment of mitochondria is observed, with decreased levels of complex IV activity due to low supply of copper [276]. The activities of several copper-containing enzymes are lower in the body including SOD1, ceruloplasmin, lysyl oxidase, and hephaestin [206, 227, 237], which can persist into adulthood if dietary copper is depleted from a young age [276]. Although some of these cuproenzymes (ceruloplasmin and hephaestin) regulate iron efflux from cells, iron levels are not always consistently elevated in these copper deficient models [647, 648]. In aged mice, dietary copper depletion showed significant alterations in copper levels in the parietal lobes together with decreased levels of metallothionines with no profound abnormal behaviour [647]. Conversely, in perinatal mice with severe copper depletion motor activity is impaired and ataxia occurs [648, 649]. After 6 weeks, catatonia and seizures become apparent [227]. It is suggested that factors that contribute to these manifestations include decreased ATP levels, altered neurotransmitter biosynthesis, decreased myelination, lesions, and necrosis in the brain [649-652].

In addition to these neuronal effects, copper depletion has been shown to trigger microglial and astrocytic activation in the thalamus and the cerebral cortex [653], revealing that copper plays a role in gliosis. Copper is known to be involved in immunity and copper deficiency in rodents suppresses natural killer cells and antibody titres and therefore these mice become

more susceptible to infections [654], similar to what is seen when humans present with copper deficiency [655].

A mouse model that shows significant decreased in total copper levels in the CNS involves partial abolition of the *Slc31a1* gene, causing a 50% decreased in the transcript of one of the body's main copper transporter, *Slc31a1* [239]. Similar, to mice expressing mutant *Atp7a* which develop severe signs of copper deficiency and die prematurely (Section 1.5.2), mice that are homozygous deficient for *Slc31a1* (*Slc31a1*$^{-/-}$) die *in utero*, demonstrating the necessary requirement for Ctr1 in development. By contrast, mice that heterozygous deficient for *Slc31a1* (*Slc31a1*$^{-/+}$) are phenotypically indistinguishable from wildtype littermates, with normal weight gain and no gross abnormalities up to 15 months of age [239]. Commensurate with this there is no loss of copper in the gut, kidney or liver [239, 277], demonstrating that these tissues are able to acquire physiological levels of copper despite decreased expression of the transporter. Alternatively, there may be a compensatory mechanism that pumps copper into peripheral organs when Ctr1 levels are decreased, such as Dmt1 which is reported to be inversely regulated to Ctr1 [594]. In contrast to these tissues, copper levels in the brain and spleen are decreased by approximately 50% in *Slc31a1*$^{+/-}$ mice [277]. Partial knockdown of *Slc31a1* decreases complex IV and SOD1 activities in the brain, demonstrating the importance of both functional alleles for copper homeostasis [277]. CTR1 expression is associated within degenerating substantia nigra of PD patients at post-mortem [175] and a rare *CTR1* homozygous variant c.284 G > A (p.Arg95His) found in twins with this causing extensive cortical and cerebellar atrophy and enlargement of the ventricles [656]. To date there is no published data on the effect of decreased copper levels on neuronal viability in the substantia nigra of *Slc31a1*$^{-/+}$ mice.

Chapter 4. Examining decreased copper bioavailability as a putative model for PSP

4.2 Hypothesis and Aim

We examined a strain of mice that is heterozygous deficient in the copper uptake transporter k*Slc31a1* (*Slc31a1*$^{+/-}$ mice) in which concentrations of copper in the CNS are suppressed. We hypothesised that decreased copper concentrations in the brain induces biochemical and histological changes that replicate those seen in PSP. Currently, there is no established *in vivo* model of PSP. Our aim, therefore, was to assess brain samples from *Slc31a1*$^{-/+}$ mice for indications of PSP-related copper changes and pathology.

The specific aims of this current study as per Section 1.8.1 are as follows:

> **Aim 6.** Examine the relationship between copper availability and neuronal survival in vivo by partially knocking out the gene for copper transporter (*Slc31a1*).

Chapter 4. Examining decreased copper bioavailability as a putative model for PSP

4.3 Methods

4.3.1 Mouse samples

All animal handling and procedures were approved by a University of Melbourne Small Laboratory Animal ethics committee and conducted in accordance with guidelines of the Australian National Health and Medical Research Council. Male and female mice heterozygous for a functional form of the copper uptake transporter *Slc31a1* (a.k.a. Ctr1) (Jackson Laboratory stock# #025649) and wild-type littermate controls mice were bred and housed in animal house facilities at the University of Melbourne under 12-hour light/dark cycle with access to food and water ad libitum. Genotype of *Slc31a1*$^{-/+}$ mice was determined by automated services provided by Transnetyx and utilising reported information for targeted disruption of the gene [277].

Mice were aged to 9-10 months of age before collection of tissue samples. Animals were anaesthetised with a cocktail of ketamine and xylazine (120 mg/kg and 16 mg/kg body weight respectively) then killed by transcardial perfusing with 20 mL of perfusate (see **Table A4** in **Appendices**). The brain was removed from the skull and left to chill on ice. Using a pre-chilled stainless steel brain matrix (1 mm coronal guides, Plastics One), the right hemisphere of the brain was micro-dissected to remove the substantia nigra which was weighed then fresh-frozen on dry ice and stored at -80°C. The left hemisphere was placed in 4% paraformaldehyde (Sigma-Aldrich) made in 0.1 M PBS overnight at 4°C. Paraformaldehyde-fixed brains were transferred the following day to a 30% sucrose solution (made in 0.1 M PBS, pH 7.4) and kept at 4°C and a second change of fresh 30% sucrose solution (made in 0.1 M PBS, pH 7.4) was done the following day and stored at 4°C until absorbed the sucrose solution to sink to the bottom of the tube (a week in solution) until sectioned.

4.3.2 Inductively Coupled Plasma-Mass Spectrometry

Pre-weighed, fresh-frozen substantia nigra samples from mice (section 4.3.1) were lyophilised overnight. Nitric acid (65% Suprapur, Merck) was then added to digest each sample for several hours at room temperature, then for a further 20 min at 90°C. An equal

volume of 30 µL of H_2O_2 (30% Aristar, BDH chemicals) was then added to break down lipids from the samples via incubation at room temperature for 30 min then at 70°C for 15 min. A final addition of 1% nitric acid was added to each sample. Multiple elemental measurements were made using a 7700 series ICPMS (Agilent) under routine operating conditions with a helium reaction gas cell. Certified multiple element calibration solutions at 0, 5, 10, 50, 100 and 500 parts per billion (ICPMS-CAL2-1, ICPMS-CAL-3 and ICPMS-CAL-4, Accustandard), together with an internal standard containing 200 ppb of Yttrium (Y89), were used. The concentrations for copper, iron and zinc were calculated as µg element per g wet weight tissue.

4.3.3 Gene expression

Gene expression was performed on the substantia nigra samples from *Slc31a1*$^{-/+}$ and wildtype mice. For complete methods please refer to Section 2.3.7 (Chapter 2) and the list of genes/probes of interest can be found in **Table A3**, in **Appendices**). Relative expression was calculated using the ΔΔct method when correcting to housekeeper gene *Gapdh*, with results presented as fold-change relative to controls (bar graphs) or as gene expression z-scores (heatmaps).

4.3.4 Immunohistochemistry on frozen mouse sections

Fixed mouse brains (see Section 4.3.1) were mounted in OCT before being sectioned using a cryostat (Lecia, D1950). At a temperature of -20°C, sections were cut at a thickness of 30 µm and collected on precoated gelatine slides (0.5% gelatine made in ddH_20). Sections were collected in series, sampling one of every three sections from anterior to posterior of the substantia nigra *pars compacta* and were frozen at -80°C. The first series was removed from -80°C and dried for 1 hour in a 37°C oven to remove excess water, then stained with 2% Neutral red solution (Nissl) for stereological analysis. The second series was immunostained for Sod1, Gfap and Iba-1. Sections were blocked using 3% donkey serum (D9663, Sigma-Aldrich) made in 3% Triton X-100 and TBS (pH 7.5) for 1 hour at room temperature then incubated in primary antibodies Sod1 (1:200; HPA001401, Sigma-Aldrich) and Gfap (1:500; Ab53554, Abcam) made in 0.1% donkey serum, 1% Triton X-100 and TBS (pH 7.5) overnight at 4°C. Sections were washed 3 times in TBS-T (pH 8.0) for 10 min each to remove excess

antibodies following incubation of secondaries conjugated with fluorophores donkey-anti goat Alexa488 (1:1000 A32814, Invitrogen) and donkey-anti rabbit Alexa594 (1:1000, Ab150064, Abcam) for 1 hour at room temperature. Sections were rinsed 3 times in TBS-T (pH 8.0). Sections were reblocked using 3% BSA blocking buffer for 30 min then incubated with Iba-1 conjugated Alexa647 (1:100; EPR16588, Ab225261, Abcam). Sections were washed in 0.1 M PBS (pH 7.4) 3 times for 10 min each following a counterstain with DAPI (300 nM in PBS, D1306, Life Technologies) for 2 min and a final rinse in 0.1 M PBS (pH 7.4). Sections were mounted in anti-fade aqueous mounting media fluroshield (F6182, Sigma-Aldrich) and sealed.

4.3.5 Stereological estimate of total neuronal cells within the substantia nigra pars compacta

Stereological assessment of substantia nigra *pars compacta* were performed using an optical fractionator probe which accounts for tissue shrinkage which occurs when processing thick mounted sections [657]. The average tissue thickness was measured prior to counting using three independent sections sampling three sites per section (total of 9 sites throughout the substantia nigra *pars compacta*). The substantia nigra *pars compacta* region was delineated (at 10X magnification) using a superimposed grid size of 140 x 140 µm and both neurons and glia were counted independently using a 45 x 45 µm unbiased counting frame (total area size of 2025 μm^2). Neurons and glia were counted at 63X (1.4 numerical aperture NA) oil objective according to Gundersen un-biased rules with an optical dissector height of 14 µm [657, 658]. Neurons, glia and endothelial cells in the substantia nigra *pars compacta* were distinguished from each other and also from surrounding regions of the ventral tegmental area based on several cellular characteristics including shape, size (16 - 20 µm cell body), clear nuclear membrane and prominent nucleolus (see **Figure 4.1**). The cell numbers in the substantia nigra *pars compacta* were estimated using Stereological software (Stereo investigator 11.0, MBF Bioscience) and viewed using Stereological microscope (DMBL, Lecia). Total neurons and glia were calculated using optical fractionator method with a Gundersen coefficient error of 0.10 (10%).

Chapter 4. Examining decreased copper bioavailability as a putative model for PSP

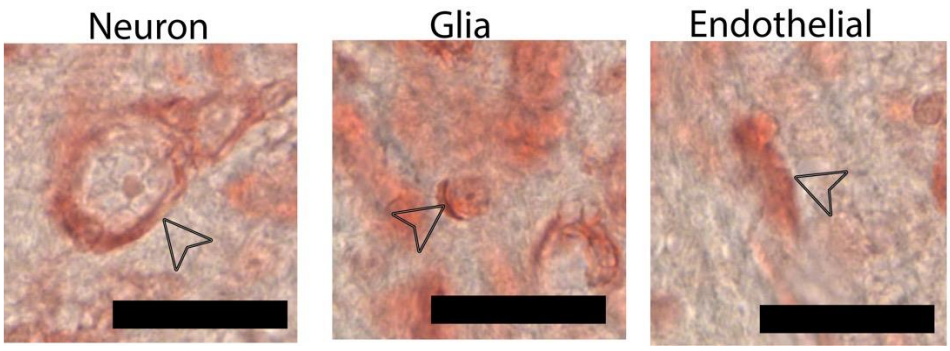

Figure 4.1. Morphological criteria for cellular discrimination of neurons, glia and endothelial cells in a mouse brain

Neurons, glia and endothelial cells from mouse brains were distinguished by their individual cellular characteristics (nuclei, size and shape) under 63X magnification, 2% neutral red (Nissl) staining. Neuron as indicated by black arrowhead in neuron panel, have a prominent nucleus and nucleolus with a spherical shape and size (16 - 20 µm). Glia, have a cellular morphology that is distinguished from neurons and endothelial cells by their size and shape and can be multinucleated. Glial cells are smaller in size of (10 µm) than neurons without processes as indicated in Glia panel with black arrowhead. Endothelial cells are elongated and parallel to vessels as indicated by black arrowhead in Endothelial cell panel. Black scale bar 25 µm.

4.3.6 Quantification of immunofluorescence images of the mouse substantia nigra

Two adjacent representative images were taken at 20X magnification per mouse for each genotype (WT N = 4, *Slc31a1*$^{-/+}$ N = 5) at the same section of the substantia nigra *pars compacta* and substantia nigra *pars reticulata* where the mammillary tract was present (mouse brain coordinates interaural; 0.72 mm, bregma; -3.08 mm [659]) (**Figure 4.2**). ImageJ software was used to measure area of the substantia nigra *pars compacta* and substantia nigra *pars reticulata* and photoshop (Adobe Photoshop) was used to merge each channel. Sod1 positive astrocytes (Gfap) and microglia (Iba-1) were counted in each image and were normalised to area (mm^2) and averaged across two independent images.

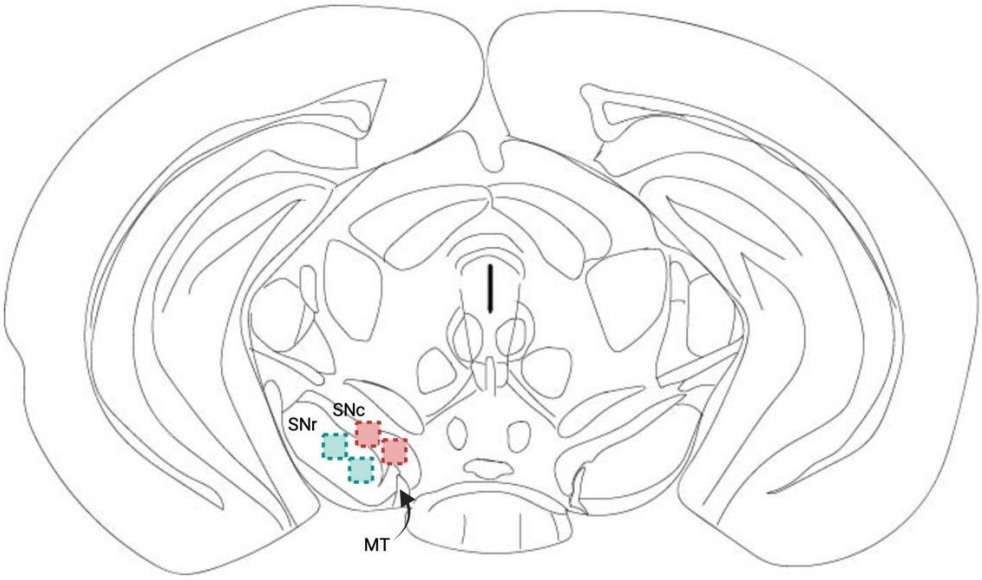

Figure 4.2. Schematic diagram illustrating sampling of two independent sites per substantia nigra region within a mouse brain for immunohistochemical quantification
Mouse brain sections obtained at one fixed point where the mammalian tract (MT) was most prevalent (coordinates, ML; 2.6 mm, AP; -3.1, DV; 1.6, figure 56, [660]) were sampled per genotype (WT N = 4, *Slc31a1*$^{-/+}$ N = 5) to quantify the presence of Sod1, Gfap and Iba-1 immunological staining within the substantia nigra *pars compacta* (SNc; red dotted squares) and substantia nigra *pars reticulata* (SNr; green dotted squares).

4.3.7 Statistical analysis

We assessed an animal model of altered copper availability to determine whether there is a similar molecular and histological signature that is seen in PSP. The data collected across a variety of assays was graphed in GraphPad Prism (version 10) and expressed as the mean ± SEM (unless stated otherwise). All statistical analyses were calculated using Graphpad Prism and statistical outliers were determined using ROUT method as previously described [559]. Significant differences in the mean scores between *Slc31a1*$^{-/+}$ and wildtype littermates (WT) were determined using t-tests (two tailed) with the assumptions of equal variance. F tests used to determine equal variances and in the instance of unequal variances, a Welsch's correction was used.

Chapter 4. Examining decreased copper bioavailability as a putative model for PSP

4.4 Results

4.4.1 Expression of copper handling genes in Slc31a1$^{-/+}$ mice

Our purpose in examining the brain was to ensure that substantia nigra (**Figure 4.3a**) copper levels were reduced as in PSP tissue (Chapter 3), given partial knockout of the primary cellular copper importer. Compared to wild-type littermate controls, *Slc31a1*$^{+/-}$ mice had 45% less copper in the substantia nigra (**Figure 4.3b**). By contrast, partial deletion of *Slc31a1* had no effect on iron (**Figure 4.3c**) or zinc (**Figure 4.3d**).

Gene expression analysis confirmed a 50% decreased in *Slc31a1* mRNA levels in the substantia nigra of *Slc31a1*$^{-/+}$ mice (**Figure 4.3e, f**). Commensurate with this, *Atox1* mRNA levels were elevated 27% and *Steap1* RNA levels elevated 145.3% in the *Slc31a1*$^{-/+}$ mice (**Figure 4.3e, f**). The increase in *Steap1* matched that observed in human cases of PSP (Chapter 3, **Figure 3.3a, b**). However, none of the other gene expression changes detected in the *Slc31a1*$^{-/+}$ mice, including *Atox1*, matched those detected in the human PSP cases (**Figure 4.3e, f**). In contrast to human cases of PSP, the composite gene expression profile measured in substantia nigra samples from *Slc31a1*$^{-/+}$ mice indicated no overall perturbation to the copper handling mechanisms (**Figure 4.3g**).

Chapter 4. Examining decreased copper bioavailability as a putative model for PSP

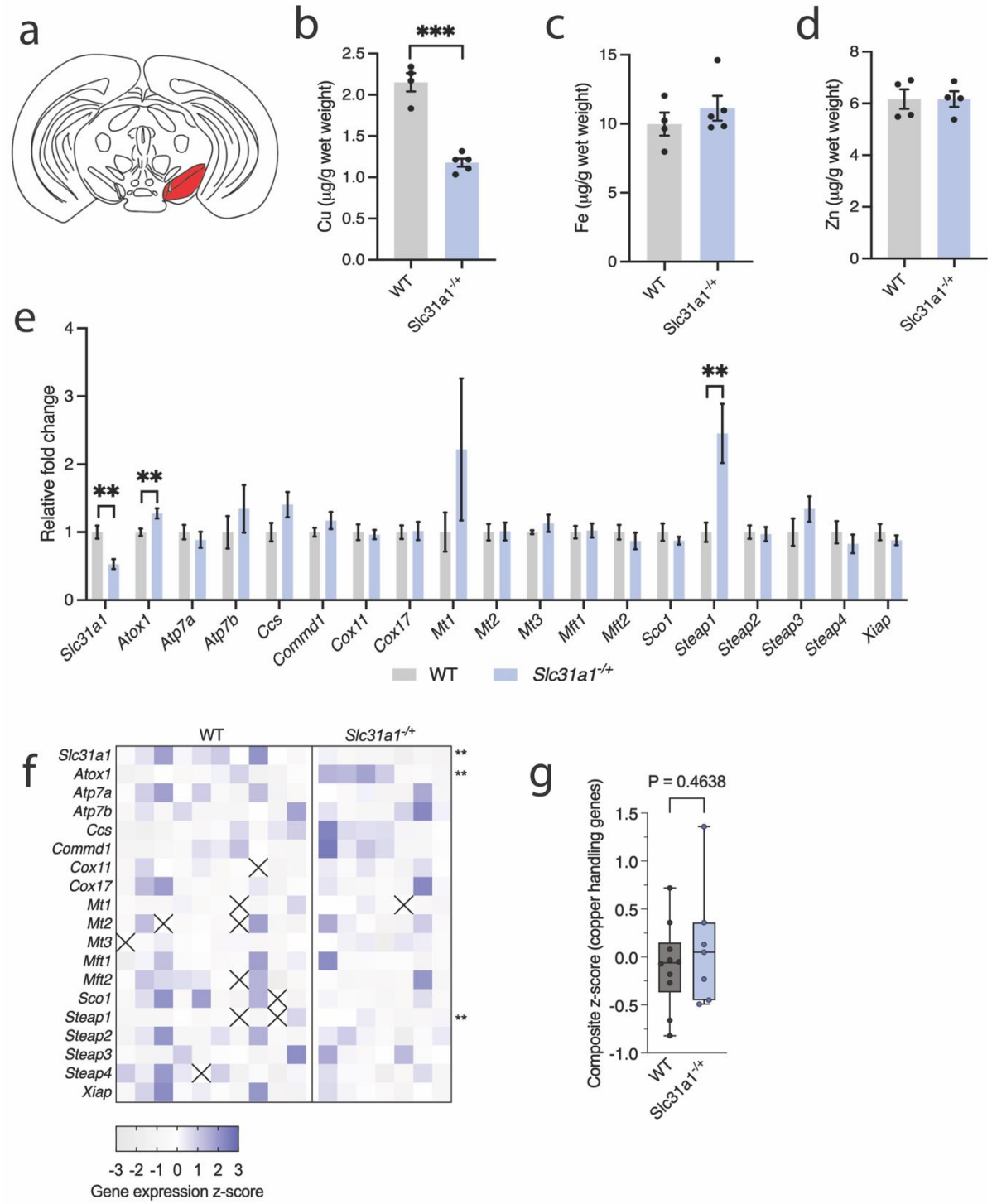

Figure 4.3. Copper and associated copper-handling gene expression in Scl31a1$^{-/+}$ mice
a) Substantia nigra (highlighted in red) was microdissected tissue from brain samples. Trace metal analysis of elements **b**) copper, **c**) iron **d**) zinc measured in the substantia nigra in WT and *Scl31a1*$^{-/+}$ mice (WT; N= 4, Slc31a1$^{-/+}$; N = 5); **e**) relative gene expression fold change in copper-handling genes (WT; N= 10, Slc31a1$^{-/+}$; N = 7), **f**) standardised z-score heatmap of cell copper-handling genes, **g**) composite z-scores of overall copper handling genes. Data in **b**-**e** are expressed as the mean ± SEM, with non-significance (ns) and significance being indicated when *p<0.1, **p<0.01 and ***p<0.001. Data in **f** and **g** are presented as composite z score by which the latter is a calculation each gene's z-score is averaged across cases or animals.

4.4.2 Cell specific marker expression in Slc31a1$^{-/+}$ mice

We investigated to see if copper deficiency influenced the expression of cell-specific genetic markers that were measured in the PSP cohort (**Figure 4.4**). Although there was a large variation in expression of neurofilament gene *Nefh*, no significant changes in expression in any neuronal, astrocytic or oligodendrocytes markers.

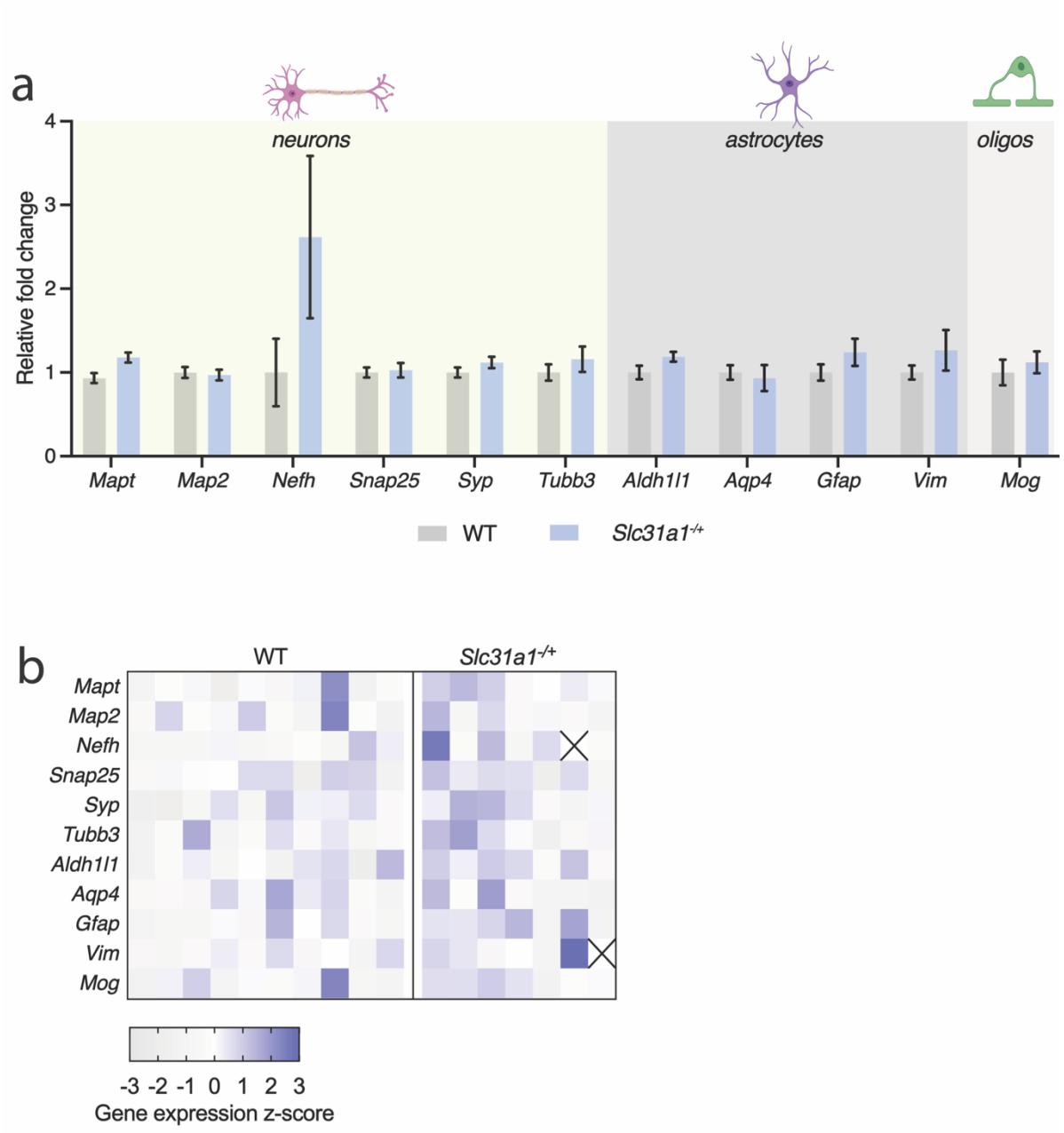

Figure 4.4. Molecular signature of cell specific genes markers in the substantia nigra of Scl31a1$^{-/+}$ mice

Measurement of gene expression profiles using qPCR from tissue homogenates from the substantia nigra; **a**) Relative gene expression fold change in cell specific markers in *Scl31a1*$^{-/+}$ mice (WT; N= 10, Slc31a1$^{-/+}$; N = 7), **b**) standardised Z- score heatmap of cell specific gene markers. Data in **a** are expressed as the mean ± SEM, with non-significance (ns) and significance being indicated when *p<0.1, **p<0.01 and ***p<0.001.

4.4.3 Immunohistochemical assessment of the substantia nigra in Slc31a1$^{-/+}$ mice

A histological approach was used to determine whether a lack of copper leads to neuronal loss, gliosis, or accumulation of Sod1 in the substantia nigra (**Figure 4.5**). Stereological analysis of total neurons and glial populations in the substantia nigra *pars compacta* region of *Slc31a1*$^{-/+}$ mice revealed that there was a 9.4% decrease in neurons in the substantia nigra *pars compacta* (**Figure 4.5a, h**) while no changes were detected in glial cell numbers (**Figure 4.5b, h**). Loss of copper and its availability within cells causes nascent SOD1 to misfold and form intracellular pathological aggregates and toxicity [497]. Due to the observation that SOD1 accumulates within the glial cells in PSP, we performed triple-labelled immunofluorescence to determine if Sod1 accumulates within the glial cells in *Slc31a1*$^{-/+}$ mice, given the decreased in copper availability in these transgenic animals (**Figures 4.5c, d, i** and **j**). There was no difference in the amount of accumulated Sod1 found within astrocytes and microglia in *Slc31a1*$^{-/+}$ mice compared to wildtype in the substantia nigra *pars compacta* and substantia nigra *pars reticulata* (**Figure 4.c**) and (**Figure 4.5d**) respectively.

Chapter 4. Examining decreased copper bioavailability as a putative model for PSP

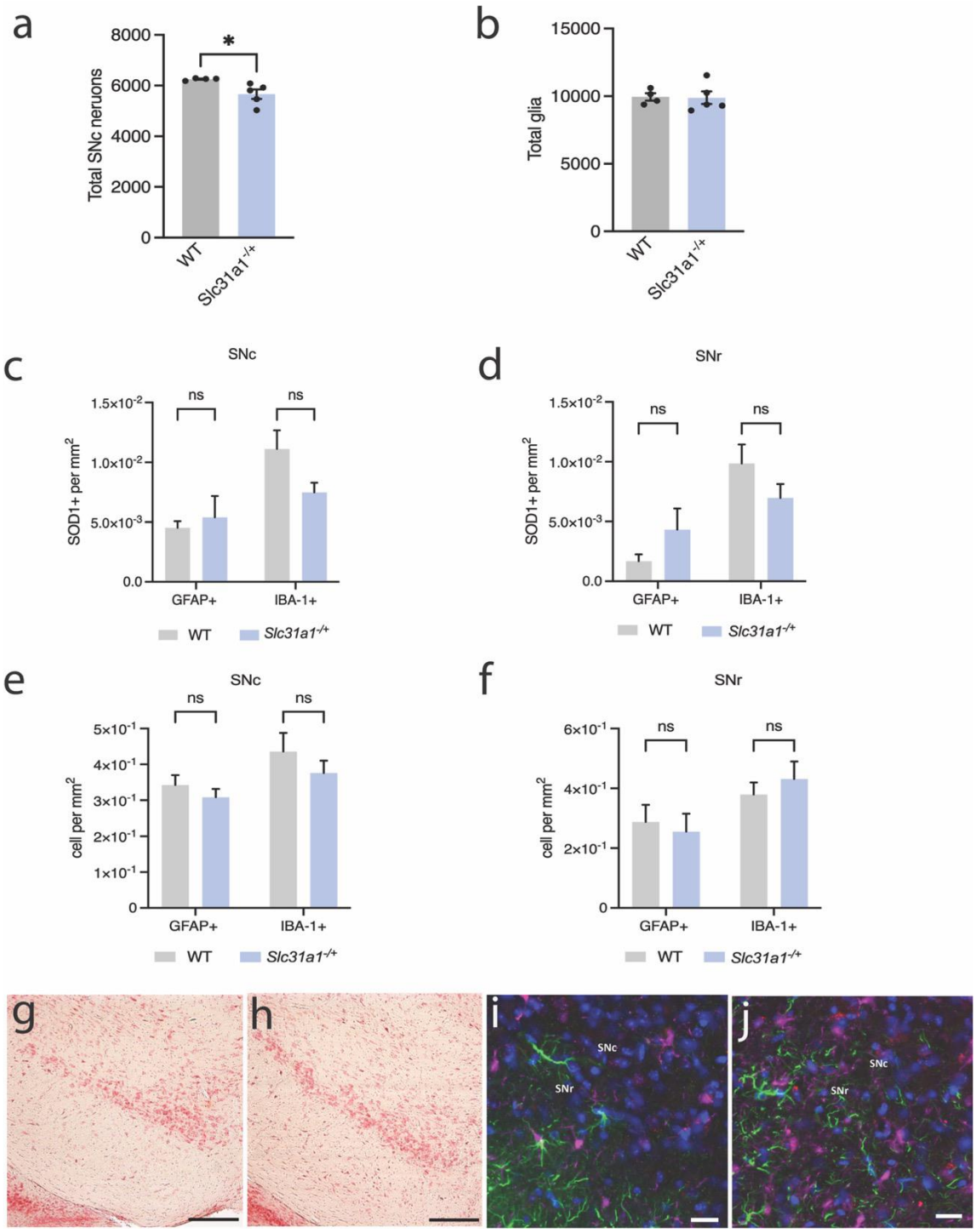

Figure 4.5. Histological analysis of the substantia nigra in Slc3a1$^{-/+}$ mice
Stereological evaluation of total number of **a**) neurons and **b**) glia cells within the substantia nigra *pars compacta* of 9 – 10-month-old *Scl31a1*$^{-/+}$ and littermate wildtype (WT) controls (WT; N = 4, Slc31a1$^{-/+}$; N = 5). Sod1 positive astrocytes (Gfap) and microglia (Iba-1) were counted in the **c**) substantia nigra *pars compacta* (SNc) and **d**) substantia nigra *pars reticulata* (SNr) with total numbers of Gfap and Iba-1 positive cells in the **e**) SNc and **f**) SNr. Picture micrographs of neutral red staining in **g**) wildtype and **h**) *Scl31a1*$^{-/+}$ mice. Triple-label staining of Sod1 (red), Gfap (green) and Iba-1 (purple) in substantia nigra of **i**) wildtype and **j**) *Scl31a1*$^{-/+}$. Scale bars 25 µm (black) and 20 µm (white). Data are expressed as the mean ± SEM, with non-significance (ns) and significance being indicated when *p<0.1 compared to wildtype.

4.5 Discussion

An animal model involving mice with partial deletion of the *Slc31a1* gene was used to explore how brain tissue copper levels might influence pathways that lead to the pathogenesis of PSP. From birth, the *Slc31a1*$^{-/+}$ heterozygosity is ubiquitous, yet the 50% loss of functional Slc31a1 affects copper levels in the brain more than other tissues [277, 661]. Levels of iron and zinc are unaffected (**Figure 4.3c, d**). Apart from the expected 50% decreased in *Scl31a1* transcript [240, 277], these mice surprisingly showed minimal alterations in copper handling genes (**Figure 4.3**). Intriguingly, iron accumulation was not observed in the substantia nigra of *Slc31a1*$^{-/+}$ mice (**Figure 4.3c**). As copper levels inversely decrease, iron accumulates in the brain of PSP patients [21, 439, 440]. No changes in iron levels have also been reported in earlier studies by Lee *at el*. (2001) in this strain [277]. It could be implied that the loss of 45% nigral copper seen in these mice could still be an adequate amount for the supply to ceruloplasmin activity for intracellular iron efflux. Dietary copper deficient mice have inconsistent reports of brain iron changes depending on copper deficient paradigms [451], this could be supportive of the theory that mice are able to survive on a small amount of copper. There is also a possibility that copper is preferentially supplied to ceruloplasmin for its activity at the expense of other cuproenzymes as a means for cellular protection and survival. For example, it has been shown that there was a 20% loss in Sod1 and complex IV activity as reported using whole brain homogenates from *Slc31a1*$^{-/+}$ mice aged 5-6 weeks. However, as detected by immunohistochemistry, Sod1 staining was no different in the *Slc31a1*$^{-/+}$ mice compared to wildtype with minimal staining observed in both the substantia nigra *pars compacta* and substantia nigra *pars reticulata*. We did not measure Sod1 gene/protein or activity levels. As a result, measuring both the mRNA and protein levels of cuproenzymes, as well as their specific activities, would be crucial for assessing the level of copper metalation status within each of these important copper-dependent processes.

Consistent with most copper-related genes assessed, we saw no significant changes in any cell-specific markers in substantia nigra tissue from *Slc31a1*$^{-/+}$ mice. Contrary to what was observed in PSP (**Figure 2.12**), we did not see evidence of gliosis based on the number of glia and the upregulation of astrocytic markers in the brains from *Slc31a1*$^{-/+}$ mice. Copper deficient rodents that have lost 80% of their copper levels in their third post-partum week

show prominent microglia activation observed in the thalamic and cortical layers in the brain [653]. Astrogliosis, using Gfap as an indicator was also seen later in the fifth week onwards within the cerebral cortex and hippocampus [653]. Microglial and astrocytic activation is also seen in a copper deficient brindled *Atp7a*^{mobr} mice with the deletion of 6bp in *Atp7a* genes.

Despite *Slc31a1*$^{-/+}$ mice having 45% less copper in the brain than wildtype littermates, they do not display overt signs of gross neurological or motor impairment. Commensurate with this, neuronal cell loss within the substantia nigra of *Slc31a1*$^{-/+}$ mice was moderate, at 9.4% decrease relative to wildtype littermate controls (**Figure 4.5a**). In humans, a rare homozygous mutation found in *SLC31A1* found in twins appearing normal at birth have severe neurodegeneration by 10 weeks of age [656]. At 8 months, there was a 40% decrease in copper in the CSF and by 9.5 months, these children display a lack of spontaneous movement [656]. Similarly, the mottled brindled *Atp7a*^{mobr} mice, display significant motor decline and grip strength when there is a 73-75% loss of copper in the brain and evidence of necrosis within pyramidal Purkinje and hippocampal neurons through the identification of pyknotic nuclei at 10 weeks of age [662]. Neurodegeneration and gliosis appear to occur most frequently in copper-deficient animal models that show severe copper depletion >75%. Thus, it appears possible that physiological function of copper-dependent processes within the mouse brain can be sustained despite a 45% loss of copper. Our LA-ICPMS assessment of human PSP-affected substantia nigra *pars compacta* indicated a loss of copper at ~67% (**Figure 3.2**). Alternatively, or perhaps additionally, the upregulation of *Atox1* detected in the substantia nigra of *Slc31a1*$^{-/+}$ mice may have provided some neuroprotection. ATOX1 has dual functions of a copper chaperone and also as an antioxidant which can be transcriptional upregulated by oxidative stressors [663]. *Atox1* is shown to protect from superoxide in yeast when Sod1 is deficient [664]. Furthermore, neurons derived from rats (NT2 cells) are protected from serum starvation and oxidative stressors H_2O_2 and MPTP when *Atox1* levels are increased [663, 665]. In a PD animal model that uses the neurotoxin MPTP, induction of Tat-ATOX1 was shown to protect dopaminergic neurons by the suppression of apoptosis [666]. Notably, *ATOX1* mRNA levels are unchanged in the substantia nigra from cases of PD [175] or PSP (**Figure 3.3**, Chapter 3). Therefore, it is possible that the up-regulation of *Atox1* detected in the *Slc31a1*$^{-/+}$ mice provided a mechanism for neuroprotection that does not occur in human cases of PD or PSP. From the evidence gathered, the *Slc31a1*$^{-/+}$ mice strain

had no biochemical, histological or pathology similarities to PSP other than decreased levels of copper in the substantia nigra and a marginal decrease in neuron numbers. A more extensive histological assessment would be required to determine whether the observed decrease in copper induced PSP-relevant SOD1 and/or tau pathology. If detected, the *Slc31a1*$^{-/+}$ mouse model would provide intriguing insight to the relationship between the protein pathology of PSP and neuronal function, such as the timeframes involved in progressing from protein pathology to neurodegeneration and the onset of neurological symptoms. Limitations on the use of animal models to mimic neurological diseases will be further discussed in detail Chapter 6 (Discussion).

The absence of many of these changes in the brains of *Slc31a1*$^{-/+}$ mice may indicate that decreased brain concentrations of copper per se do not cause PSP. Alternatively, results from the *Slc31a1*$^{-/+}$ mice may indicate that copper related changes are an early-stage phenomenon in PSP and that our assessment of the mice at the age of 9 - 10 months represented a pre-symptomatic stage of disease that is not captured by assessment of post-mortem human brain tissue.

Chapter 5. Proteomic analysis of human, PSP -affected substantia nigra

In Chapter 3, copper levels within the substantia nigra of a PSP brain were shown to be decreased. Further, gene expression analysis showed that the expression of genes involved in maintaining cellular copper homeostasis is disrupted in PSP and some cuproenzymes may not receive their required copper supply. This may be a factor relevant to results presented in Chapter 2 that show the cuproenzyme SOD1 accumulates in the PSP-affected substantia nigra in potential copper-deficient state. However, although optimal neuronal function is dependent upon an adequate supply of copper, it remains unclear how/if altered copper availability may lead to neuronal degeneration in PSP. To address this, here we conducted a proteomic analysis of human, PSP-affected substantia nigra tissue. The objective was to employ an unbiased proteomic analysis approach to explore molecular and cellular pathways affected in the PSP.

5.1 Introduction

Proteomics, like all other omics research, is a collective endeavour to characterise proteins by their functions and relationships inside cells. With the use of mass spectrometry together with integrated proteomics workflows, this powerful tool is used to profile proteins and peptides in biological samples and impute data to identify and quantify proteins. Mass spectrometry - based proteomics workflows have enabled detection of whole tissue or cell preparations from clinical samples with high sensitivity, fast acquisition, and high resolution [667].

When applied in the context of pathology, mass spectrometry based proteomics affords an unbiased approach that moves beyond hallmark proteinopathy to consider many molecular and cellular mechanisms that may contribute to the disease development. This is in direct contrast to historically standard biochemical approaches which are often low-scale and rely on traditional protein markers with limited quantitative capacity and low sensitivity. Illustrative of this, a study of the mouse brain proteome identified over 10,000 proteins that were differentially expressed across different regions of the brain and within different CNS cell types [668]. Additionally, this enables rapid development of the proteome brain atlas and

its analogues, such as the atlas brain maps and the connectome project, both vital tools for bioscientific research [669].

Over the last few years mass spectrometry based proteomics has identified thousands of different proteins in many diseases that may act as novel biomarkers for disease [670]. These biomarkers could be differentially upregulated in various stages of a disease and provide opportunity for novel diagnostic, prognostic, or therapeutic developments. Brain biopsy samples from patients who are living with neurodegenerative diseases are very rarely available and therefore most tissue is provided from post-mortem cases who had reached the terminal stage of disease.

5.1.1 Proteomics – Mass spectrometry

Over the last decade there has been a dramatic expansion in development of experimental 'omic' techniques, covering proteomics, transcriptomics, lipidomics and metabolomics. Liquid chromatography in tandem with mass spectrometry (LC-MS/MS) is utilised in proteomics to detect lowest abundance tryptic cleaved proteins. LC-MS/MS systems are designed to measure the mass to charge ratio (m/z) to determine the molecular weight of protein digestion products. After purification and separation using LC-MS, the molecules are transformed to gas-phase ions with the second involving separation of ion based on m/z under the influence of electro/magnetic mass analyser. Lastly, the ions that have been separated together with the amount of peptide with the m/z value are measured.

There are three approaches for protein identification using mass spectrometry: top-down, bottom-up and shotgun approaches. In the top-down approach, full length and undigested proteins are sent to mass spectrometry for analysis [671]. The technique represents the true form of proteins in biological samples, but identifying heavily modified proteins becomes problematic, and this technique still has many challenges that need to be addressed [672]. The bottom-up approach by contrast is when proteins are fragmented into peptides by enzymatic or chemical approaches. Similar to bottom-up proteomics, shotgun proteomics involves analysis of fragmented proteins followed by their identification and post-translational modifications by reference to sequence databases utilising data dependent engines [673]. In large-scale runs, data-dependent acquisition (DDA) is typically used, in which

ions are fragmented based on their intensity or abundance, whereas data independent acquisition (DIA) captures all of the fragmented ions within a m/z window range and can detect all analytes in the sample, regardless of their abundance or m/z value [673]. One problem is that before interpreting quantitative proteomics from DIA, DDA spectrum libraries need to be created and this comes at a cost of the sample and also the time and effort spent with fractioning the sample.

5.1.2 Bioinformatics in proteomics

Proteome analyses usually yield a long list of identified proteins and peptides, along with quantifications and probability scores. This makes interpreting each of these proteins/peptides a challenging task since each of those proteins is involved in a variety of pathways and mechanisms. Interpretation of proteomics datasets therefore requires a bioinformatic approach and central to this is large databases such as Uniprot and Ensembl that provide unique identifiers for each protein. Interpretation of differentially expressed proteins identified via proteomics requires that the unique protein identifier is associated with its gene ontology (GO) [674]. Each protein is assigned a GO term that consists of a hierarchically clustered group of functional terms related to molecular, biological and cellular functions. GO terms are constantly evolving as more data becomes available and the function of many gene/proteins in the human genome is still not completely understood. Researchers can perform enrichment analyses on a set of proteins using either algorithm-based software or web-based programs [674-676] which are up to date with GO annotations. The enrichment pathways analysis has a threshold of p value of 0.05 calculates a enrichment p value that is based on the probability of the number of proteins out of all total annotated of the GO term with the number closest to 0 being the most significant (https://geneontology.org/docs/go-enrichment-analysis/).

One highly valuable resource to facilitate bioinformatic interpretation of proteomics datasets is the Kyoto Encyclopedia of Genes and Genomes (KEGG), an integrated resource that consists of over 20 curated databases with pathway maps and graphical representations being a main component [677]. To infer the systemic functioning of a cell or organism, the proteins are matched against the KEGG pathway reference databases for pathway mapping. The KEGG resource has organised pathway maps for human diseases that include causative genes and

protein aggregates that have been identified across a wide range of diseases. Numerous diseases, particularly neurodegenerative disease, show significant overlap.

5.1.3 Proteomic analysis of neurodegenerative diseases

Molecular and cellular abnormalities have been found in neurodegenerative conditions like AD, with Hondius *et al.* (2016) discovering the first molecular changes in early detected AD cases [678]. With both western blotting and immunohistochemistry validation, this elegant study revealed that using cluster analysis of 40 hippocampal samples from cases with AD, 89 differentially expressed proteins were detected at the earliest stage of the disease out of the 3000 proteins detected at different stages of Braak AD [678]. According to their clustering analysis, astrocytic proteins were over-represented in the upregulated protein set during early Braak staging of AD, suggesting that astrocytes played a role in disease progression. Neuronal proteins were over-represented in the downregulated proteins, indicating cell death and loss of synapses [678]. In 2017, samples from the olfactory bulb from cases with early, intermediate, and late stages of AD showed that over 50% of proteins that were differentially expressed where localised at the synaptic terminals [679]. Network analysis revealed that dysregulation of the cytoskeleton, cell-to-cell junctions in the early stages, redox signalling imbalance in the intermediate stages and impairment of mRNA splicing and RNA stability were more evident in the late stages of AD [679]. It was found by Seyfriend *et al*. (2017) that the proteosomes of presymptomatic AD cases were different from those of AD, with increases in proteins associated with extracellular matrix and decreases in proteins related to synaptogenesis [680]. Synaptic markers were also a focus of other proteomic studies comparing AD to dementia with Lewy bodies and PD with dementia to healthy controls whereby 25 out 851 synaptic transmission-based proteins were significantly dysregulated in all of these dementias [681]. There are also synaptic proteome changes associated with ALS, where 500 associated synaptic proteins showed altered expression in ALS brain tissue and isolated synaptoneurosomes [682]. Other pathways that have been identified in ALS using mass spectrometry based techniques include upregulated proteins involved in transcription, cell cycle, lipoprotein remodelling and splicing of the neurofilaments [683].

Chapter 5. Proteomic analysis of human, PSP -affected substantia nigra

Proteomic profiling studies have also investigated protein changes in PD. Samples from the substantia nigra of PD cases show alterations in proteins associated with oxidative stress, cytoskeleton impairment and mitochondrial dysfunction [684]. In addition, a novel protein nebulette was founded to be overexpressed in the substantia nigra of PD cases which has a modulation effect on cell survival and cytoskeleton remodelling and could act as a biomarker for the disease [684]. Petyuk *et al*. (2021) used proteomic profiling of the substantia nigra to determine pathways associated with the formation of Lewy bodies using a label free LC-MS/MS approach. It was uncovered that the likely drivers of Lewy body formation were pathways involving the deregulation in synaptic function, actin nucleation/filament polymerisation process, poly(A) RNA binding, and H_2O_2 metabolic processes [685].

To date, there are only two reported proteomic analyses performed using PSP tissue. Jang *et al*. (2022) using isobaric tandem mass tag (TMT)-base mass spectrometry experiments with 15 healthy controls, 15 PD and 15 PSP GP samples showed that Parkinson's Disease KEGG pathway was the most enriched pathway, and a majority of these enriched proteins were involved in mitochondria and involved in oxidative phosphorylation [598]. In KEGG pathways, genes/proteins and molecular networks associated with diseases are represented as maps. Parkinson's disease KEGG pathway includes causative genes, protein aggregates, and molecular pathways that lead to neurodegeneration with overlap with other neurodegenerative diseases' molecular networks. In the more recent study by Radford *et al*. (2023), proteins that were in close proximity to tau-aggregates were examined using proximity ligation methods coupled with mass spectrometry in the motor cortices [686]. Of the 117 proteins in proximity to phosphorylated tau, multiple groups of proteins were identified as being associated with cytoskeletal dynamics, neurotransmission, and metabolic processes [686]. A typical brain tissue sample can contain many thousands of proteins depending on isoforms present and the number of post-translational modifications or splicing events that are present. To date, there has been no comprehensive analysis of the PSP substantia nigra proteome, a region that contains a large distribution of tau pathology and cellular death. Therefore, in this current chapter, we used largescale proteomics as a means to understand the underlying molecular and cellular pathways that could contribute to or cause the disease.

Chapter 5. Proteomic analysis of human, PSP -affected substantia nigra

5.2 Hypothesis and aim

Hypothesis: Post-mortem nigral tissue collected from human cases of PSP displays an abundance of differentially expressed proteins and that some of these will map to distinct enrichment pathways related to copper biology.

The specific aim for this current study as per Section 1.8.1 are as follows:

> **Aim 5.** Proteomic analysis to quantitate protein changes and pathways that are disrupted in PSP brain tissue.

Chapter 5. Proteomic analysis of human, PSP -affected substantia nigra

5.3 Methods

5.3.1 Fresh frozen post-mortem human samples

Fresh frozen substantia nigra tissue from cases of PSP and non-neurological controls was used for all proteomic analyses. Specific details of each case and the analyses for which they were used are included in **Appendices**, as **Table A1**. A summary of cases used for proteomic analyses is shown in **Table 5.1**. The substantia nigra tissue blocks encompassed both the substantia nigra pars compacta and substantia nigra pars reticulata and are collectively termed substantia nigra. These were prepared as a uniform sample as outlined in (**Figure 1.7**). A 10 mg sample from each case was used for proteomic analyses.

Table 5.1. Summary of PSP and control cases used for proteomic analyses

Group	N	Males	females	Age (years)	PMI	Disease duration (years)[#]
PSP	15	8	7	74.73 ± 1.263	22.53 ± 2.548**	5.526 ± 0.7887
Control	7	5	2	74.71 ± 3.183	40.57 ± 5.707	N/A

Control cases were pathologically confirmed free of neurological disease. [#]Period from diagnosis to death. PSP: Progressive supranuclear palsy; PMI: Post-mortem interval; n/a: not applicable; significance is indicated when *P<0.05 (two-tailed t-test)

5.3.2 Sample preparation for mass spectrometry

Frozen substantia nigra samples were removed from storage at -80°C then immediately solubilised in fresh 4% SDS lysis buffer made in Tris (pH 8.5). Samples were next boiled at 95°C and shaken on a thermomixer at 2000 RPM for 10 min then cooled on ice for 10 min. The process of boiling and cooling was repeated until visible solubilisation of the material for all cases was evident. Protein concentration of each sample was measured using the BCA Assay (Thermo Fisher Scientific). Aliquots containing 50 µg of protein were collected then reduction of disulphide bonds and carbamidomethylate residues was performed by the addition of a freshly prepared reduction/alkylation buffer (100 mM TCEP, 400 mM chloroacetamide and 1 M Tris, pH 8.5) at a ratio of 10 µL reduction/alkylation buffer per 1 µL sample. Samples were incubated with the reduction/alkylation buffer for 30 min at 45°C in the dark with shaking at 1500 RPM. Samples were then removed from the heat and allowed to cool at room temperature. The removal of detergents/chaotropic agents was perform with Single-pot solid-phase-enhanced sample preparation (SP3) as these chemicals are incompatible and interfere with LCMS/MS analysis [687]. SP3 clean-up was performed using SeraMag SP3 beads in a final volume of 50% ethanol solution (mass spectrometry grade) as described previously [687, 688]. Samples were mixed for 10 min at 1000 RPM on a thermomixer at room temperature. Following placement of samples on a magnetic rack, the supernatant was removed after the clearing of the suspension. The pellet was rinsed three times with 80% ethanol (mass spectrometry grade), spun in the magnetic rack, then the remaining 80% ethanol removed. Typsin/Lys C (Promega V5071 made in 100 mM Tris, pH 8.5) was added to the samples at a ratio of 1:100 (wt/wt) then the samples digested overnight at 37°C, with shaking. To obtain extremely clean peptide samples for the LC MS/MS, the SP3 cleanup with mixed mode-based chromatography resin styrene- divinylbenzene reverse phase sulfonate (SDB-RPS) Strata-X-C columns was used. For SDB-RPS clean-up, a 1.25 volume of Isopropranol (HPLC grade) was added to the digest and vortexed to ensure the contents were well mixed. Pre-wet SDB-RPS columns with acetonitrile were used following an addition of 10% TFA (Trifluoracetic acid in ddH_20). SDB-RPS columns were washed with 30% methanol in 1% TFA solution, then with 90% isopropanol in 1% TFA solution. Samples were loaded on to the SDB-RPS columns and washed with 90% isopropanol in 1% TFA solution,

then with 90% ethyl acetate in 1% TFA solution and lastly with 1% TFA solution. Samples were eluted off the SDB-RPS column with 5% ammonium hydroxide and 80% acetonitrile (mass spectrometry grade) and were dried down in a speed vac and stored at-20°C.

5.2.3 LC-MS/MS

Purified peptides from each sample prepared as described in Section 5.3.2 were resuspended in Buffer A1 (**Table A3** in **Appendices**) and separated using a two-columns; PepMap100 C_{18} 20 mm by 75 µm trap and a PepMap C18 500 mm by 75 µm analytical column (Thermo Fisher Scientific). Using Buffer A2 (**Table A3** in **Appendices**), samples were concentrated onto the trap column at 5 µL/min for 5 min, then infused into an Orbitrap Fusion Eclipse Mass Spectrometer (Thermo Fisher Scientific) at 300 nL/min via the analytical column using a Dionex Ultimate 3000 UPLC (Thermo Fisher Scientific). Analytical runs of 125 min were carried out by changing buffer composition from 2% of Buffer B (**Table A4,** found in **Appendices**) to 23% of Buffer B over 95 min, then from 23% of Buffer B to 40% of Buffer B over 10 min, then from 40% of Buffer B to 80% of Buffer B over 5 min. The composition was held at 80% Buffer B for 5 min and then dropped to 2% Buffer B over 2 min, before being held at 2% Buffer B for another 8 min. The Orbitrap Fusion Eclipse Mass Spectrometer (Thermo Fisher Scientific) was operated in data-independent mode (DIA), which allows high reproducibility and low variation in the quantification of thousands of proteins [689]. DIA interrogates >90% of trypsin cleaved peptides in selected m/z windows in one go [690]. The Orbitrap Eclipse Mass Spectrometer switched between 50 cycles of MS1 and MS2 scans, as it stepped through the whole mass range and cycled through the LC gradient. The MS1 scan operated at; 350-1100 m/z, maximal injection time of 50 ms with an Automated Gain Control; AGC set to 1 x 10^6 ions and a resolution of 120k and scans the entire mass range. The MS2 scan operated at; Normalised Collision Energy 30%, 30k resolution, AGC 1x10^6, 200-2000 m/z and a maximal injection time of 54 ms which all peptides in this mass range are fragmented and detected. A pooled gas-phase fractionation spectral library was created in Spectronaut Pulsar™ [690, 691] repeating measurements over each sample to get in-depth detail in m-to-z ranges [692]. This was performed by importing the acquired data from Max-Quant (version 2.0.2.0) into Spectronaut Pulsar™ (Biognosys). The separated peptides are identified by searching the protein FASTA database (UniPro). The library consists of the elution time together with its

ion fragment pattern of each identified protein [693]. DIA MS/MS quantification was reported as the sum of the integrated fragment ion peak areas.

5.3.4 Quantification and statistical analysis

As stated above, Max-Quant (version 2.0.2.0) together with Spectronaut Pulsar™ was used for identification and label-free quantification (LFQ) analysis [694], with Perseus (version 2.0.11) for data analysis [695]. Using Perseus, the table of data results were filtered for contaminants, proteins matching to the reverse database, then further filtered for sample groups (controls and PSP) with <50% valid values in in both groups (total control = 7; total PSP = 15). LQF intensities were transformed in Log_2 values and missing values were imputed with a normal distribution (downshift 1.8, width 0.3). After data filtering, principal component analysis was performed to identify protein intensities that had a batch effect after transformation (**Figure 5.1**). A two-sample t-test corrected for multiple testing was performed between control and PSP groups (Benjamini-Hochberg FDR 0.05, S0) and identified significantly differentiated proteins (P value of 0.05).

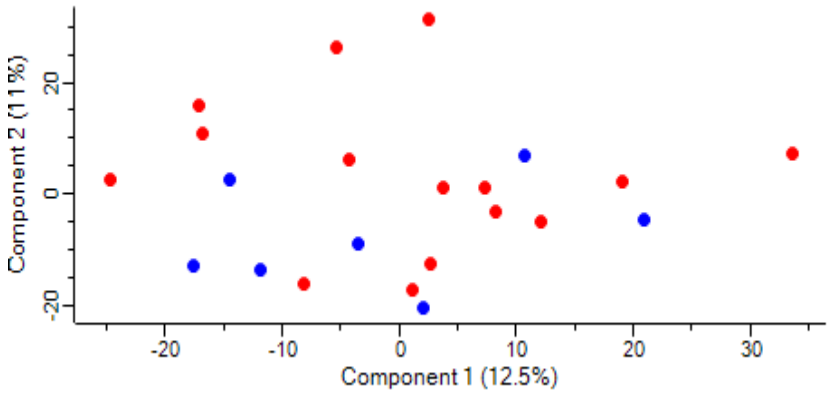

Figure 5.1. Principal component analysis (PCA) after data transformation
To visualise the effect of sample batch effects after data were transformed in Perseus, 22 substantia nigra samples were plotted on a 2D PCA plot (PSP= 15 in red dots; control = 7 in blue dots).

5.3.5 Gene enrichment pathway analysis

Kyoto Encyclopedia of Genes and Genomes (KEGG) was used to identify pathways potentially disrupted in PSP based on proteins that were significantly differentially expressed between PSP cases and controls. The web-based bioinformatic resource Shinygo (version 0.8) was used on the substantia nigra datasets comparing to the human reference dataset containing all GO annotations taxonomy for enrichment analysis [675]. The fold enrichment for each GO term is determined by comparing the percentage of substantia nigra proteome dataset in the pathways divided by the human proteome reference. The false discovery rate (FDR) is a measure of how likely the enrichment is by chance, and it is calculated from a hypergeometric distribution from a nominal P-value. A cell type-based classification of differentially expressed proteins was based on RNA cluster analysis using the Human Protein Atlas database); https://www.proteinatlas.org/humanproteome/brain/cell+types)

Chapter 5. Proteomic analysis of human, PSP -affected substantia nigra

5.4 Results

5.4.1 Statistical analysis of the proteome in PSP

From the original raw dataset of LFQ intensity values obtain from Maxquant, there were 7,900 proteins in 15 cases of PSP and 7 controls. However, LC-MS/MS can introduce exogenous contaminants and interferences from solvents, ion sources and polymers. MaxQuant can detect contaminants via the contaminants-FASTA database built into the software [696]. Therefore, false positives and common contaminants detected by MaxQuant were removed from the analysis. In addition, samples that had a missing intensity value of >50% per condition (i.e Control or PSP) were selected and missing values were imputed with normal distributed values were used for downstream analysis. This meant that after data filtering, 3,146 proteins were confidently identified. We checked the variability in the dataset by principal component analysis which forces the reduction of a number of variables in a large dataset whilst still retaining the largest possible variances to see if there are batch effects in samples that may skew the data (**Figure 5.1**). The principal component analysis revealed less data variability between controls and PSP.

Perseus performs a robust analysis from microarray data analysis (known as significance analysis of microarray) to determine proteins that have been significantly altered. By using permutations of repeated measurements, this principle estimates how many proteins/genes are identified by false discovery rates (FDRs, cut off value p = 0.05) and with the q- value estimations [697]. We identified 191 proteins that were differentially expressed in the substantia nigra in PSP tissue, with 106 being upregulated and 85 downregulated (see **Figure 5.2a**, see **Appendices Table A8**). The 10 proteins that were most upregulated (based on $-Log_2$ P) were MAOB, PLCD1, MSN, ESD, PGLS, HL1, PGAM2, PI16, TAGLN2, and ANXA1. The 10 proteins most downregulated were HSPA12A, PDHX, ATP1A3, EPDR1, OGDHL, COX6B1, COX5A, MAP6, TOM1L2 and OAT. MAPT (full length tau) was also one of 106 upregulated proteins in PSP (see **Figure 5.2a**, **Appendices Table A8**).

Cell specificity of the all the changed proteins was assessed using the human protein atlas (**Figure 5.2b** and **c**). This revealed that the largest proportion of differentially expressed

proteins (38%) could be found in all cell types (i.e., non-specific). Neuronal proteins accounted for 21% of all differentially expressed proteins and astrocytic proteins accounted for an additional 21% of all differentially expressed proteins (**Figure 5.2b**). But despite their equal representation in the overall pool of differentially expressed proteins, differentially expressed astrocytic proteins were mostly up-regulated in PSP whereas neuronal proteins were mostly down-regulated in PSP (**Figure 5.2c**). Although microglial proteins accounted for a relatively small proportion of differentially expressed proteins in PSP at 4.7%, all were upregulated in PSP (**Figure 5.2b** and **c**). One differentially expressed protein identified, the negatively charged glycoprotein alpha 2-hs glycoprotein (AHSG), is not attributed to the brain in the human protein atlas and classified as 'non-CNS'. In PSP, AHSG was in the top 14 most downregulated proteins in PSP (based on Log P) with a fold change of 1.8-fold in the substantia nigra (Log P 3.88, see **Appendices Table A8**). The reason for detection of this protein in human substantia nigra tissue is not clear.

Chapter 5. Proteomic analysis of human, PSP -affected substantia nigra

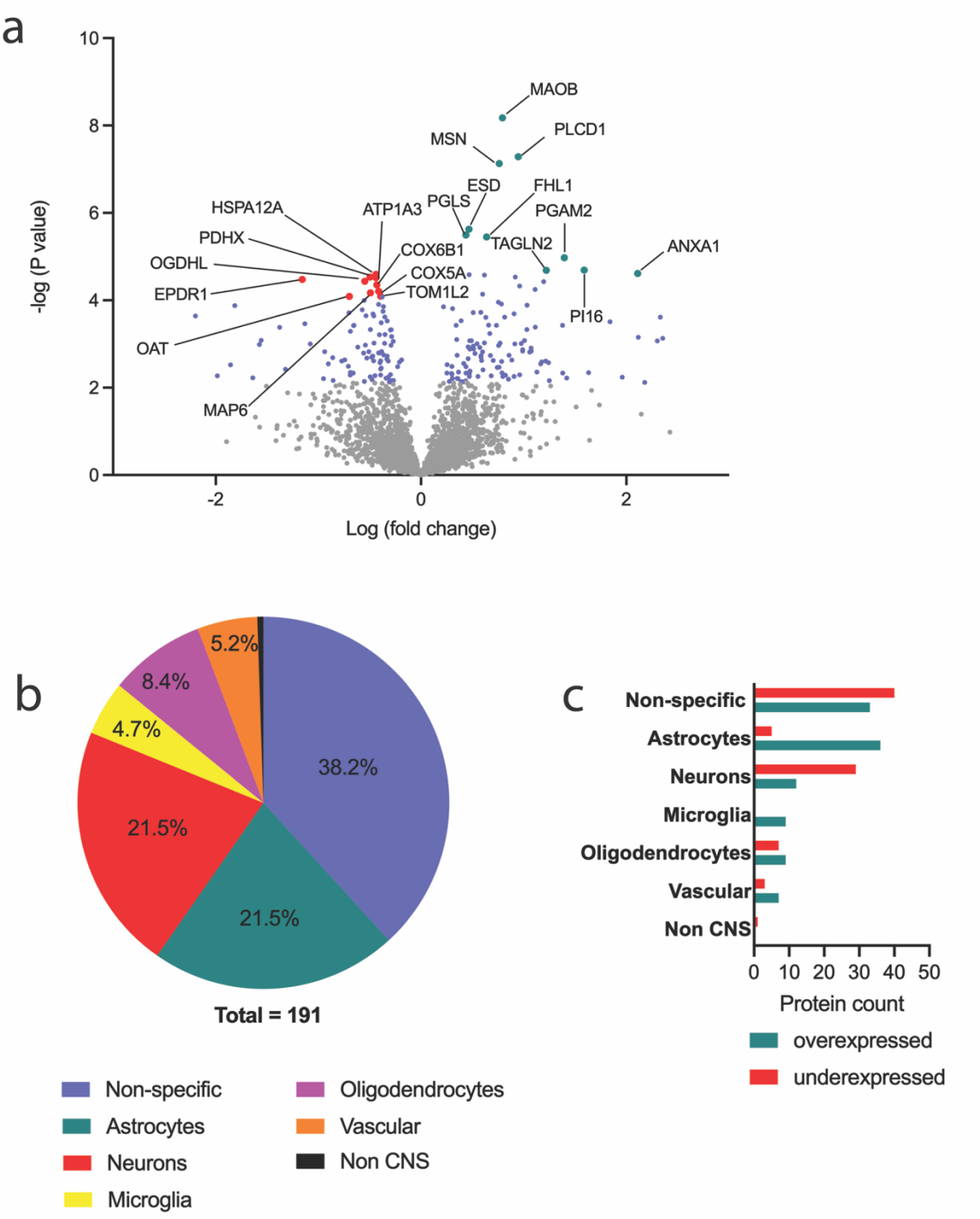

Figure 5.2. Differentially expressed proteins identified in PSP

Differentially expressed proteins in the substantia nigra from PSP cases (N =15) compared to non-neurological controls (Control; N= 7). 191 Proteins that were significantly differential expressed, were detected in the substantia nigra of the PSP brain. **a**) Volcano plot of proteins identified in the substantia nigra of PSP. The red highlighted proteins were the 10 most significantly downregulated, and the green highted proteins were the 10 most significantly upregulated, and the other 171 significantly differently expressed proteins highlighted in blue with the remaining ~2900 proteins shown in grey. **b**) Cellular clustering of differentially expressed proteins from the Human protein Atlas, non-specific (expression in all cells), astrocytes, neurons, oligodendrocytes, microglia, vascular cells and not detected in brain and **c**) protein expression counts in each cellular type.

5.4.2 Gene enrichment

Differentially expressed proteins were used for gene set enrichment analyses using the bioinformatics resource Shinygo (version 0.8) [675]. We assessed molecular, cellular and KEGG pathways. The most enriched molecular pathways were structural constituents of cytoskeleton, followed by phospholipid binding, oxidoreductase activity, lipid binding, transporter activity, actin binding, calcium ion binding, primary active transmembrane transporter activity, structural molecule activity and cell adhesion molecule binding (**Figure 5.3**, see **Table A9** in **Appendices**). The constituents of the cytoskeleton had 11 out of 114 enrichments sets with the astrocytic intermediate filaments VIM and GFAP significantly upregulated (**Tables A8** and **A9** in **Appendices**) and neuronal-based neurofilament internexin neuronal intermediate filament protein alpha (INA) significantly down (**Tables A8** and **A9** in **Appendices**). The phospholipid pathway was enriched with 16 proteins, two of which are high-density lipoproteins, the APOA1 and APOA2, both of which are downregulated in PSP (**Figure 5.3**, **Tables A8** and **A9** in **Appendices**). The 25 proteins enriched in oxidoreductase activity pathway included astrocytic-based aldehyde dehydrogenases (ALDH1L1 and ALD7A1), NADH dehydrogenase/Complex I (NDUFV1, NDUFA9, NDUFA5), pyruvate dehydrogenase (PDHA1, PDHB) and cytochrome c oxidase/Complex IV (COX6C, COX6B1, COX5B and COX5A). Additionally, the oxidoreductase pathway included the metalloenzymes selenium binding protein 1 (SELENBP1) and MAOB, both were significantly upregulated in PSP and the latter is a cuproenzyme (**Figure 5.3**, **Tables A8** and **A9** in **Appendices**).

Cellular component analysis revealed that numerous mitochondrial pathways were enriched for the differentially expressed proteins. These included mitochondria protein-containing complex, the inner mitochondrial member protein complex, the respiratory chain complex, the mitochondrial matrix, the mitochondrial respirasome, and the respirasome (**Figure 5.4**, and refer to **Table A10** in **Appendices**). Protein subunits of complex I (NDUFA5, NDUFA9, NDUFV1, NDUFS8), complex III (UQCRQ, UQCRC1, UQCRC2), complex IV (COX5B, COX6B1, COX6C and COX5A), and complex V (ATP5F1D, ATP51B, ATP5F1A) were the most enriched in PSP compared to controls (see **Table A8** and **A10** in **Appendices**). These subunits of the mitochondrial respiratory chain complexes were all significantly downregulated in PSP (**Figure 5.4** and refer to **Table A8** and **Table A10** in **Appendices**). In addition, numerous mitochondrial

matrix proteins were downregulated in PSP including TIMM8A, OAT, HSPA9, LRPPRC, NFS1, GFM1, TSFM, PDHX, PDHB, NDUFA9, OGDHL, GLS, PDHA1, ACO2, SUCLA2, ALDH7A1 (**Table A8** and **Table A10** in **Appendices**). Collectively, the cellular component analysis highlights mitochondria as one of the most affected cellular components in the PSP-affected substantia nigra (**Figure 5.4**).

Assessment of protein sets in the KEGG pathways revealed metabolic pathways, Parkinson's diseases, diabetic cardiomyopathy, Huntington's disease, oxidative phosphorylation, prion disease, non-alcoholic fatty liver disease, amyotrophic lateral sclerosis, cardiac muscle contraction, and chemical carcinogenesis-reactive oxygen species as the most enriched pathways for differentially expressed proteins in PSP (**Figure 5.5**, refer to **Table A11** in **Appendices**). Proteins associated with metabolic processes were the most abundant with respect to differential expression in PSP, with a total of 53 proteins changed in PSP, and these were almost evenly distributed between upregulated proteins (24) and down-regulated proteins (26). In contrast, the other enriched pathways detected in PSP were consistently characterised by protein down-regulation. An exception among these was MAOB which is a constituent of the metabolic and Parkinson's disease pathways and was upregulated in PSP (**Figure 5.6** and refer **Table A10** in **Appendices**). Consistent with the close association between pathological features of PD and PSP [54] and also the large involvement of mitochondrial features in PSP highlighted by the cellular component enrichment analysis (**Figure 5.4**), the KEGG pathway analyses highlighted the PD (**Figure 5.6)** oxidative phosphorylation (**Figure 5.7**) and chemical carcinogenesis (**Figure 5.8**) as high-level hits for KEGG enrichment in PSP.

Chapter 5. Proteomic analysis of human, PSP -affected substantia nigra

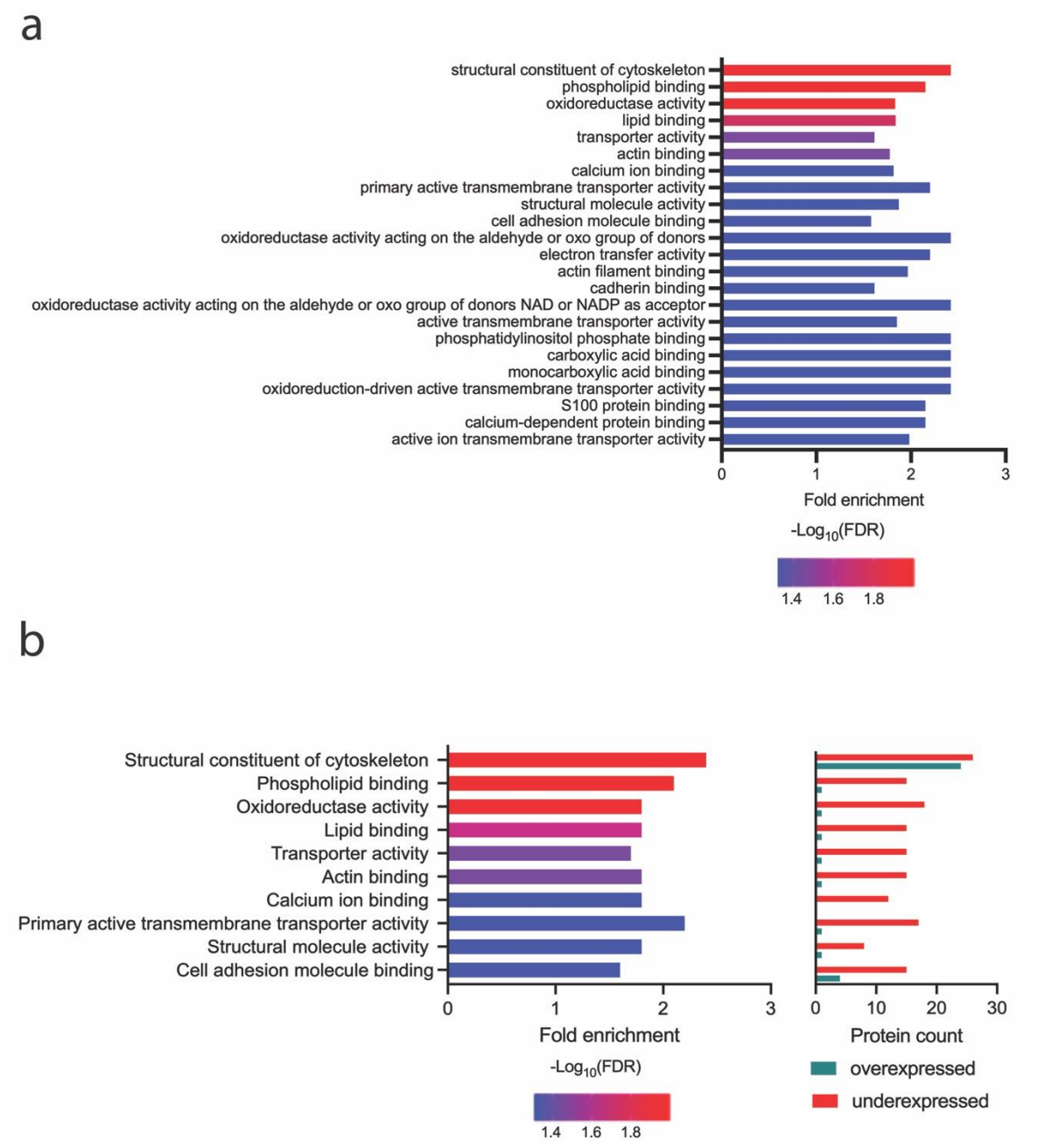

Figure 5.3. GO molecular component enrichment analysis
Gene ontology (GO) analysis of proteins within the nigra using all significant differentially expressed proteins. Enrichment molecular pathways ranked in the lowest FDR scale (-Log (FDR; false discovery rate) for (**a**) all pathways detected and the (**b**) top 10 pathways enriched together with the protein count showing the proteins upregulated (green) and down regulated (red) in each pathway.

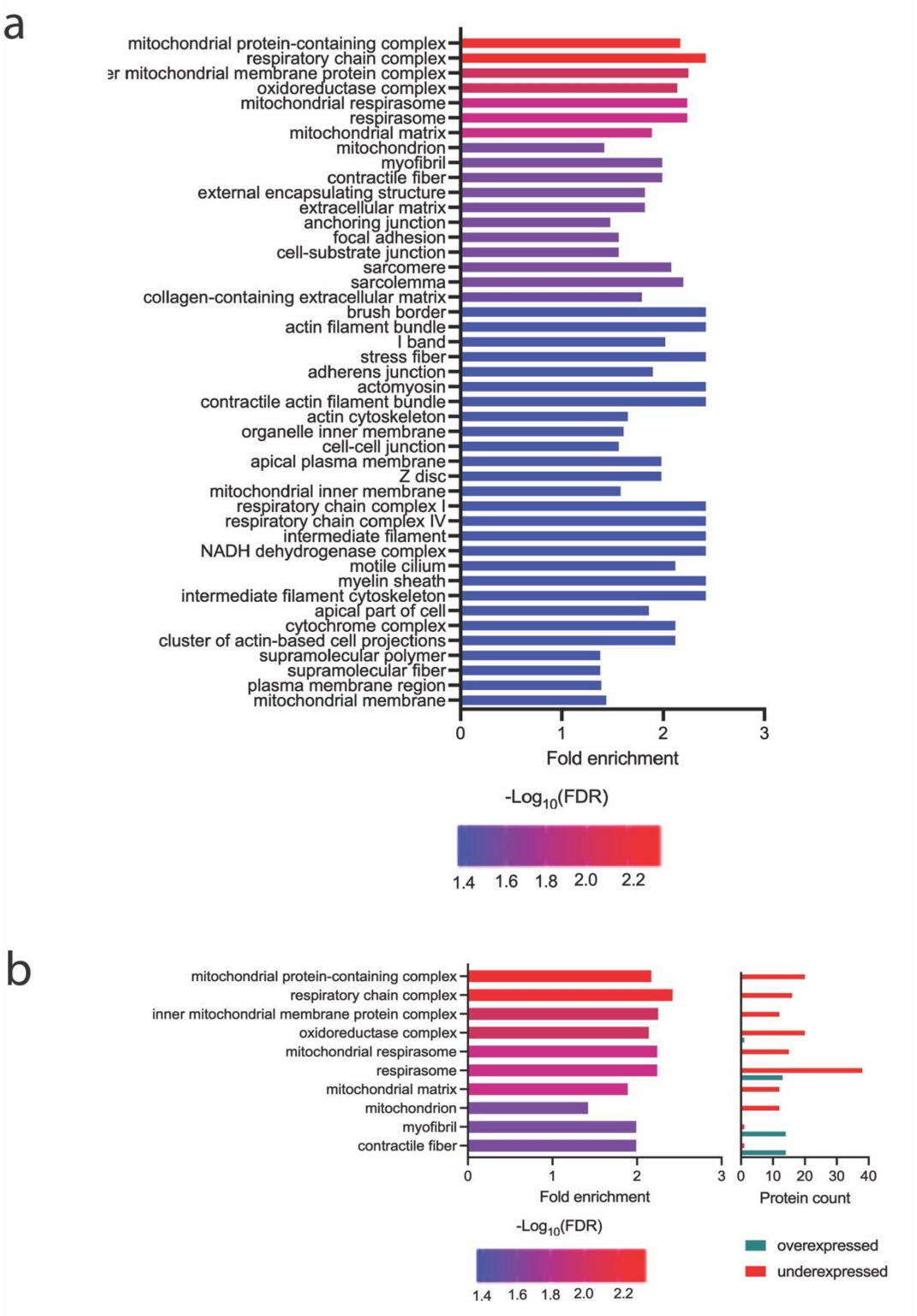

Figure 5.4. GO cellular component enrichment analysis

Gene ontology (GO) analysis of proteins within the nigra using all significant differentially expressed proteins. Enrichment cellular pathways ranked in the lowest FDR scale (-Log (FDR) (**a**) all pathways detected and the (**b**) top 10 pathways enriched together with the protein count showing the proteins upregulated (green) and down regulated (red) in each pathway.

Chapter 5. Proteomic analysis of human, PSP -affected substantia nigra

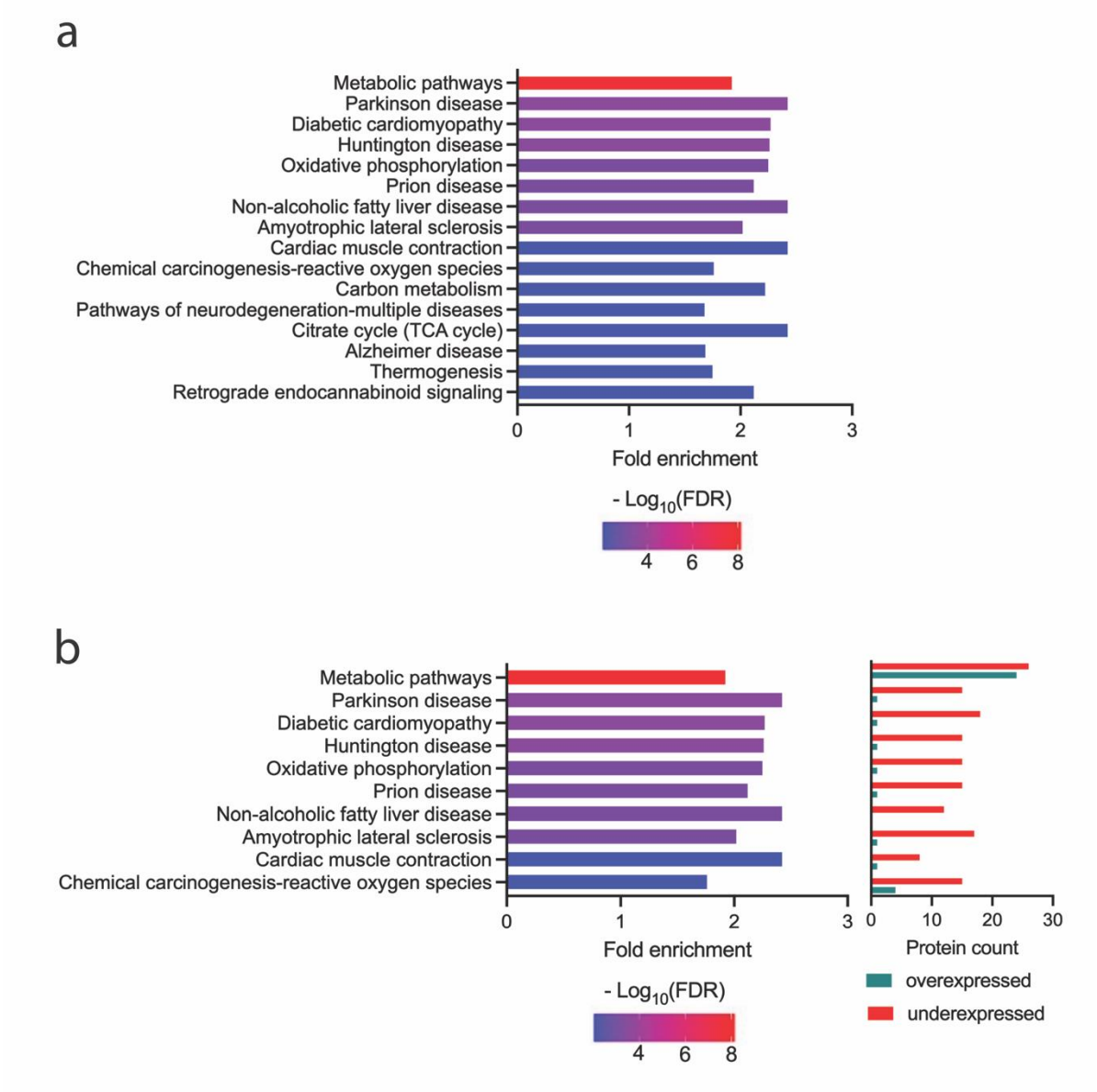

Figure 5.5. GO KEGG pathway enrichment analysis
Gene ontology (GO) analysis of proteins within the nigra using all significant differentially expressed proteins. Enrichment KEGG pathways ranked in the lowest FDR scale (-Log (FDR) (**a**) all pathways detected and the (**b**) top 10 pathways enriched together with the protein count showing the proteins upregulated (green) and down regulated (red) in each pathway.

Chapter 5. Proteomic analysis of human, PSP -affected substantia nigra

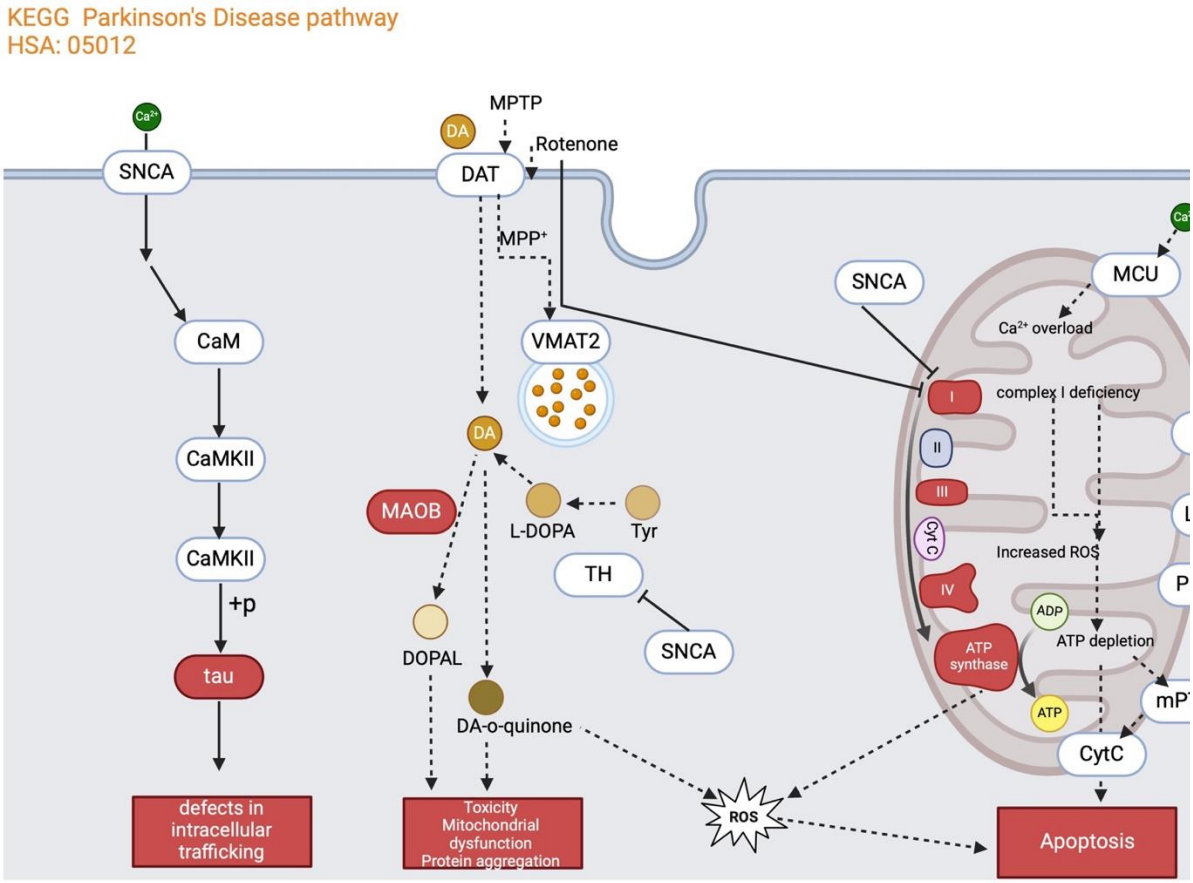

Figure 5.6. Parkinson's disease KEGG pathway identified by gene set enrichment analysis

The Parkinson's disease KEGG pathway was one of the top hits for KEGG enrichment with the differentially expressed proteins in PSP and the downstream effects highlighted in red (Tau, Monoamine oxidase B; MAOB, complex I;(I), complex III; (III), Complex IV; (IV) and complex V; ATP synthase) and DA refers to dopamine. Created in Biorender.

Chapter 5. Proteomic analysis of human, PSP -affected substantia nigra

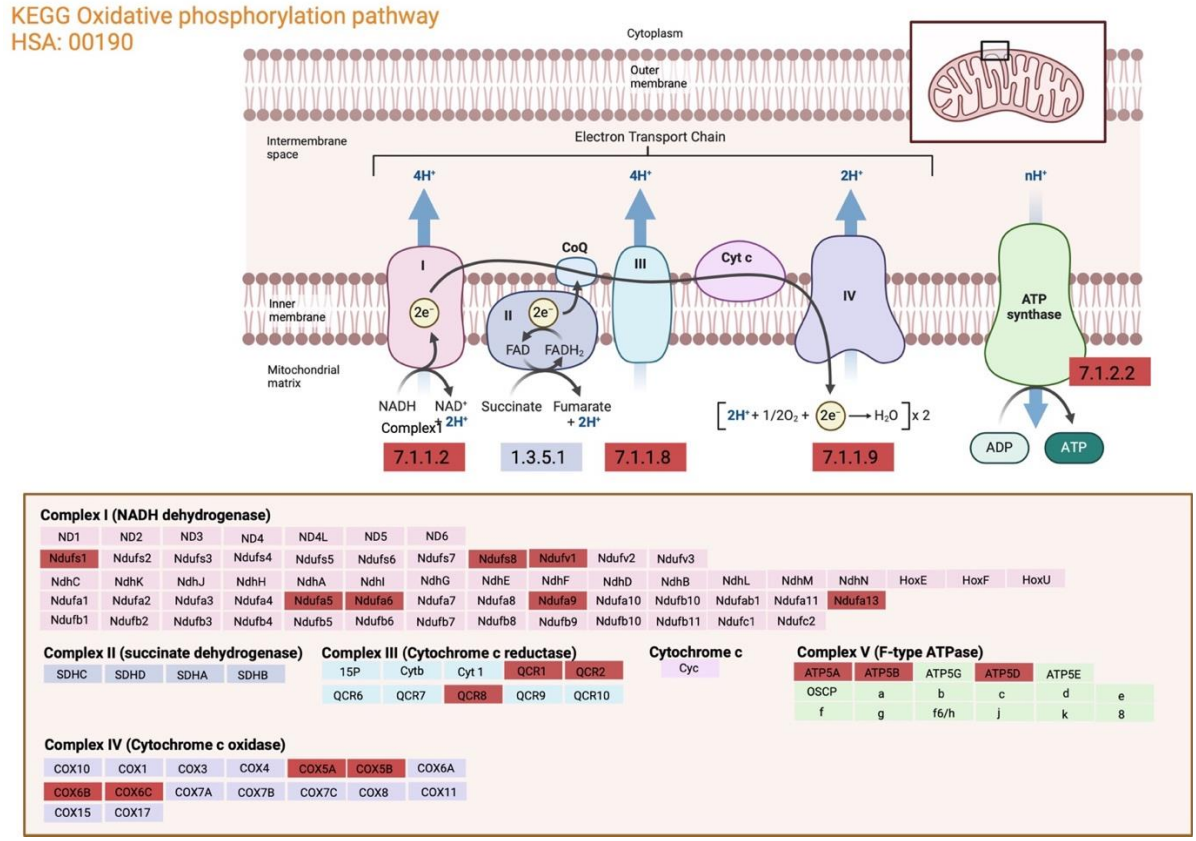

Figure 5.7. Oxidative phosphorylation KEGG pathway identified by gene set enrichment analysis

The oxidative phosphorylation pathway was one of the top hits for KEGG enrichment. The mitochondrial electron transport chain that is comprised of enzymatic complexes that sits within the inner membrane. Protons (H^+) are pumped through to the inner membrane space, with the proton gradient used to generate ATP (known as oxidative phosphorylation). Each of these complexes is made up of subunits (see boxes) within eukaryotes. The red highlighted subunits that make up each enzyme that are differential expressed in PSP (Complex I; NDUFS1, NDUFS8, NDUFV1, NDUFA5, NDUFA6, NDUFA9, NDUFA13; complex III; COR1, QCR2, QCR8, Complex IV; COX5A, COX5B, COX6B1, COX6C and complex V; ATP5F1A, ATP5F1B, ATP5F1C).

Chapter 5. Proteomic analysis of human, PSP -affected substantia nigra

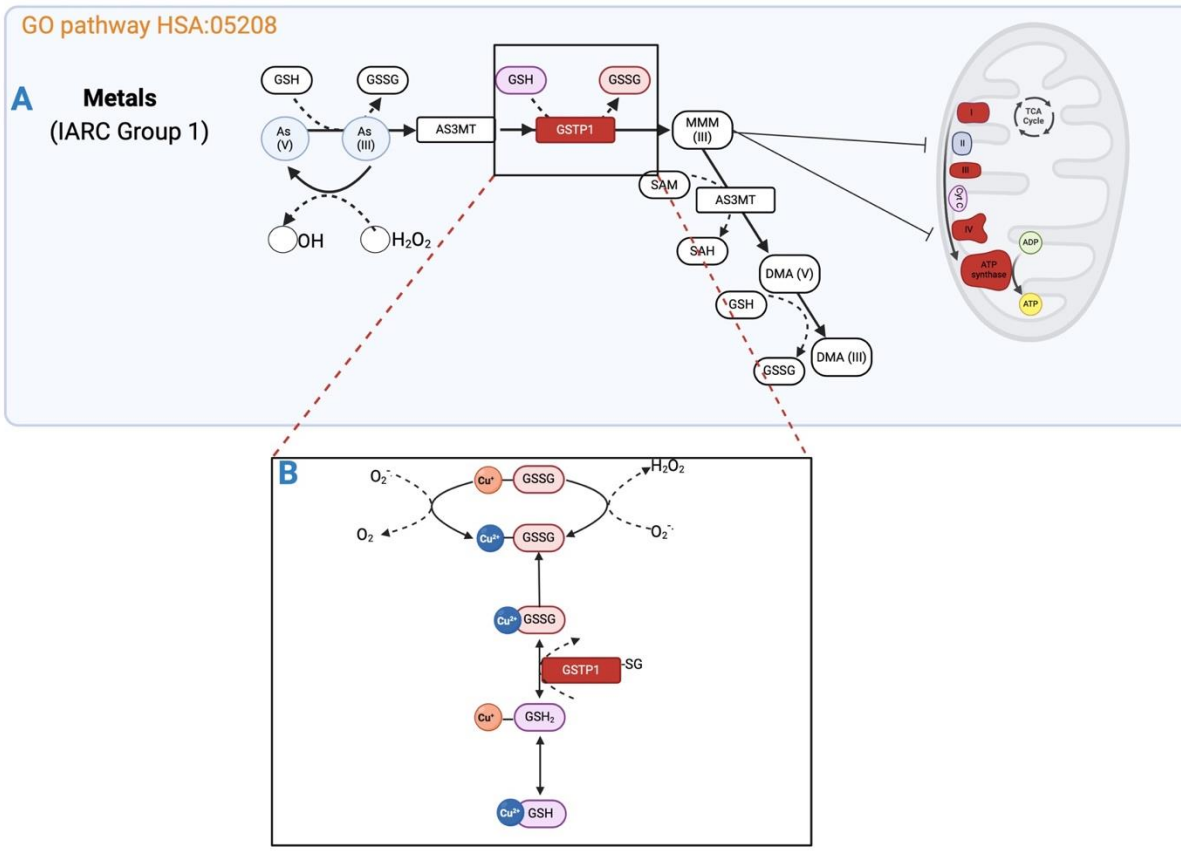

Figure 5.8. Chemical carcinogenesis KEGG pathway identified by gene set enrichment analysis

The chemical carcinogenesis pathway (**A**) was one of the top hits for KEGG enrichment with the differentially expressed protein in PSP highlighted in red (GSTP1; glutathione s-transferase Pi). Insert (**B)** represents copper-glutathione complexes reactions determine *in vitro* in the presence of oxygen and the reversible glutathionylation of sulfur (-SG) into cysteine residues of glutathione by GSTP1.

5.4 Discussion

Using human PSP substantia nigra tissue, we conducted an unbiased proteome analysis using a label-free method that detected over 3146 proteins after data clean up. We found 191 proteins that were significantly differentially expressed within the substantia nigra in PSP, with 106 being upregulated and 85 being downregulated. The upregulated proteins were tau (MAPT), which is consistent with PSP being a tauopathy and with the increased expression of *MAPT* that has been reported previously [698] and shown in Chapter 2.

Having identified a large set of differentially expressed proteins in PSP, we conducted a gene set enrichment analysis to help interpret our data and to extrapolate the pathways disrupted in PSP. Both cellular and molecular enrichment pathways were found to be related to mitochondria and respiratory complex energy production. We found a significant decrease in the proteins of complex I (NDUFA5, NDUFA9, NDUFV1, NDUFS8), complex III (UQCRQ, UQCRC1, UQCRC2), complex IV (COX5B, COX6B1, COX6C and COX5A), and complex V (ATP5F1A, ATP51FB and ATP5F1D) while there were no observed changes in complex II (succinate dehydrogenase). These proteins were also the top hits for the KEGG pathway analysis linking PD pathway to the other top enriched pathways (**Figure 5.5, Table A11** in **Appendices**). A key factor underlying the pathogenesis of PSP may be mitochondrial dysfunction due to dysregulation of electron transport chain (**Figure 5.7 Table A10** in **Appendices**). Dysregulation of the electron transport chain has also been identified as an underlying factor in a recent proteomic study using 15 PSP samples comparing to both healthy controls and PD [598] where similar proteins in the respirasome were also found to be decreased in the globus pallidus. The oxidoreductases within the mitochondrial inner membrane, complexes I to V are involved in election transfer, utilising nicotinamide adenine dinucleotide with hydrogen (NADH) as a substrate to initiate a series of redox reactions with oxygen as the terminal electron acceptor. Utilising NADH from the TCA cycle, complex I generates 2 electrons by binding to and oxidising NADH and transferring electrons between flavin mononucleotide, 7-iron-sulfur clusters and ubiquinone. The expression of proteins from the glycolysis and TCA cycles (ACO2, DLST, SUCL2, PDHA1, OGDM) were also seen to be decreased, which would lower the amount of NADH available to feed into the electron transport chain, ultimately decreasing the levels of ATP. The increase in nicotinamide

phosphoribosyltransferase (NAMPT) that was seen in PSP tissue maybe a compensatory mechanism to increase the NADH for this process [699]. In addition, complexes I, III, IV and V require the addition of copper, iron and magnesium to be functional, which means copper, iron and magnesium must be available to support maturation of nascent peptides [700]. The decreased availability of copper which has been shown in PSP tissue [21, 22] and also described in Chapter 3, could potentially have a profound effect on the functionality of copper in complex IV, with an inability to function as it a multi-copper complex that requires 3 copper ions [701]. The transcriptional regulation of all *COX* genes is influenced by the copper sensing transcription factor Sp1 [269, 702] and copper supplementation is shown to rescue complex IV assembly in yeast cells [703].

In addition, we saw a decrease in one of the iron-sulfur cluster assembly proteins cysteine desulfurase (NFS1) that plays a role as a binding platform in iron-sulfur cluster biosynthesis [704]. Disorders of the biosynthesis of iron-sulfur clusters result in increased levels of mitochondrial iron in the brain, heart and muscle together, with deficiency in the electron transport chain [705]. In humans, there is evidence of decreased complex IV transcripts in healthy individuals from 18 - 89 years of age, with a decline of up to 10% per decade in muscle cells [706]. The brain is particularly sensitive to aging and is rather a complex structure in stark contrast to other cells in the body especially when it comes to mitochondrial location. Neurons and glial cells have different energy demands that require the distribution of mitochondria to specific intracellular compartments, the soma, axons, dendrites and synapses [707, 708]. Synaptic mitochondria seem to be the most susceptible to aging related dysfunction. The nerve terminals require a significant level of mitochondria to sustain the ATP demands of synaptic transmission. An example of this is seen in high metabolic turnover region of the brain the substantia nigra *pars compacta*. The substantia nigra *pars compacta* has an estimated number of 2.4 million synapses, with 4.5 meters in axonal projections per dopaminergic neuron [709] and would demand a large quantity of energy for maintenance. Synapses and nodes of Ranvier are high energy regions of neurons where mitochondria are transported to support and supply ATP [710]. Mitochondrial dysfunction is a common molecular pathway disrupted in both PD and PSP [597]. In our PSP proteomic dataset, we observed a decrease in Complex I (NDUFS1, NDUFS8, NDUFV1, NDUFA5, NDUFA9) and Complex IV (COX5A, COX5B, COX6B1, COX6C). In PD, increased levels of NDUFB8 (complex I)

and COX1 (complex IV) were seen in mitochondria within axons of surviving dopaminergic neurons [710]. In addition, the surviving dopaminergic neurons have higher mitochondrial density per axon as well as enlarged presynaptic terminals in PD [710]. Therefore, this suggests that together with the expansion of pre-synaptic terminals, this acts as a compensatory mechanism to accommodate the increased number of mitochondria and to preserve mitochondria function as seen in PD. The overall effect of this would be to preserve the remaining neurons for motor function [710]. There is not an extensive study that have investigate mitochondrial dysfunction in PSP within the neurons or synapses in substantia nigra *pars reticulata*. However, what has been shown is that GABAergic neurons in the substantia nigra *pars reticulata* possess mitochondria with different metabolic characteristics, and that mitochondrial heterogeneity is also seen in cultured astrocytes [711]. Mitochondrial metabolism seems to also contribute to the energy supply to GABAergic neurons within the substantia *nigra pars reticulata* [712]. Cellular metabolism through glycolysis can influence the spontaneous firing of substantia nigra *pars reticulata* and when glucose levels are low or absent, mitochondrial fuels are capable of sustaining the firing of these subpopulation of cells [712]. In our PSP cohort, we saw alterations in metabolic processes with a decrease in protein expression in glycolysis pathway which could also put strain on the function of the remaining mitochondria.

Depletion of ATP intriguingly appears to have a downstream effect on intracellular tau being redistributed and inducing its aggregation [171]. Indications of mitochondrial dysfunction that have been assessed in diseased brains when decreased in expression/activity of mitochondrial respiration complexes I-V have been detected in AD, ALS, Huntington's disease and PD [4, 15, 710, 713-717]. Neurons also rely on mitochondria for buffering calcium which under damage can accumulate excessively within the matrix causing opening of channels (mitochondrial permeability transition pore opening) and compromising the electrochemical gradient. By increasing matrix permeability, ROS accumulates, causing membrane destruction and lipid peroxidation, which leads to cell death [718]. Previously reported in PSP, complex I, II, III, IV and V were significantly decreased together with ATP levels in cybrids [719]. Increased levels of lipid peroxidation have also been identified in PSP [201]. ATP is required for cellular functions in the brain including cell survival, cytoskeletal remodelling, plasticity, neurotransmitter biosynthesis, synaptic transmission and calcium homeostasis [720]. An

insufficiency in ATP impairs neuronal polarisation, preventing neurotransmitter release and preventing its reuptake.

In the gene enrichment PD pathway, we observed an increase in the substantia nigra the cuproenzyme MAOB, a primary amine oxidase involved in dopamine catabolism (see **Figure 5.6**). MAOB elevation has also been reported previously in many parkinsonian disorders including PSP [316, 686]. Expressed mostly in astrocytes, MAOB levels can be elevated in acute and chronic disease conditions [316]. MAOB is a major source of ROS whereby dopamine under oxidative deamination yields three products: ammonia which is utilized by mitochondria; H_2O_2; and the toxic metabolite 3, 4 dihydroxyphenylacetaldehyde (DOPAL) [721, 722] (see **Figure 5.6**). DOPAL is a known endogenous neurotoxic aldehyde that gets metabolised to 3,4-dihydroxyphenylacetic acid by ALDHs under normal conditions. Accumulation of DOPAL in neurons and glia is reported to initiate neurotoxic events [723]. Although, it is not clear why MAOB levels increase in neurodegenerative conditions, it is suggested that the increase is to regulate the levels of GABA. Yoon *et al.* (2014) demonstrated that astrocytic MAOB and aldehyde dehydrogenase 1A1 (ALDH1A1) both regulate GABA synthesis in various brain regions, including the substantia nigra [724]. Therefore, the increase in MAOB may reflect and compensate for the lack of GABA found in the substantia nigra of PSP cases. A novel finding of MAOB was shown to possibly interact with phosphorylated tau using mass spectrometry detection, which warrants further exploration [725].

In addition to the cuproenzymes MAOB and complex IV, another finding related to copper that was altered in PSP is involved in glutathione biosynthesis and its related enzymes. In PSP, glutathione is shown to be elevated in various regions of the brain including the substantia nigra [20, 111]. Consistent with this we observed an increase in expression of both the enzyme S-formylglutathione hydrolase (also known as Esterase D; ESD) and glutathione S-transferase Pi 1 (GSTP1). Esterase D is an enzyme involved in the hydrolytic cleavage of thioesters to produce formic acid and glutathione [726] (see **Figure 5.8**). Copper-treated macrophage cell lines had higher levels of esterase D [727], indicating copper increases glutathione biosynthesis. Esterase D has also been linked to an increased susceptibility to developing Wilson's disease with variants identified in families and copper toxicosis seen in

dogs [728, 729]. As part of the glutathione antioxidant and detoxification system, GSTP1 promotes glutathione coupling reactions by conjugation of sulfur atoms to glutathione (see **Figure 5.8**) [730]. GSTP1 is part of a superfamily of glutathione s-transferases that are involved in cellular protection against foreign chemicals and oxidative stress including lipid peroxidation marker 4-hydroxynonenal [731]. GSTP1 overexpression has been implicated in AD, ALS and polymorphisms have been shown to be linked to PD [732-735]. GSTP1 expression in the brain is found within endothelial cells of the BBB and within astrocytes [736]. It has been indicated that the exposure to pesticides or neurotoxic agents may increase the susceptibility to PD if harbouring a polymorphism in GSTP1 [735]. Under conditions of oxidative stress, GSPT1 increases gluthionylation of proteins as a defence mechanism that protects thiol proteins in metabolic, cytoskeletal remodelling, and apoptosis pathways from oxidation [737-739]. Glutathione S transferases can also conjugate dopamine quinones, produced from dopamine breakdown to glutathione to prevent its redox cycling as a defence mechanism against increased levels of dopamine [740]. GSTP1 expression and activity increased with exposure to copper in freshwater crabs and clams [741, 742] and copper is shown to bind between its reactive glutathione binding cysteine residues and cause glutathione S transferases overall inhibition [743]. Two putative Sp1 binding sites have also been identified in the proximal promotor in GSTP1 [744] and the loss of GSTP1 function due to its knockdown in human pancreatic ductal adenocarcinoma cells results in the increased ROS and the downregulation of Sp1 [745]. The inhibition of GSTP1 *in vitro* has been shown by various heavy metals, including copper, which either directly binds to GSTP1 or indirectly binds through glutathione [746]. Therefore, this may have implications by decreasing its activity as a secondary cellular defence against rising ROS [245]. The binding of copper to glutathione S transferases is likely to decrease the bioavailability of copper to prevent to its participation in redox reactions. Overexpression of GSTP1 may be protective in the attenuation of lipid peroxidation [747], however the binding of copper to glutathione S transferases may also cause the abolition of its activity [743]. Seen previously, glutathione complexed with copper also loses its ability to scavenge for ROS [245]. Although glutathione expression has been shown to increase in PSP brain tissue [20, 142], the activity of both glutathione and glutathione S transferases have not been fully characterised in PSP.

Chapter 5. Proteomic analysis of human, PSP -affected substantia nigra

There are many complex factors that require further examination to determine the underlying factors that may initiate or contribute to the pathogenesis of PSP. Our study is limited by the use of post-mortem tissue, which only captures end stages of the disease. Furthermore, of the cuproenzymes and copper handling proteins we found to be altered in Chapter 3, we did not observe any changes in ceruloplasmin, SCO1 and COX17 (just outside of significance) in our proteomic dataset. Hephaestin and ATP7A were beyond the limitation for detection which is further discussed in Chapter 6. SOD1 was readily detected in our proteomics analysis and the absence of a detectable change was consistent with our western blot results (**Figure 3.4c**).

When the PSP substantia nigra proteome was analysed for changes in expression within cell type, proteins expressed in all cells (non-specific) represented the largest proportion (38.2%), with most proteins involved in canonical metabolic pathways (**Figure 5.2b** and **c**). The protein expression profiles in neurons showed a downward trend, which is attributable to the degenerative processes involved in the death of these cells. In contrast, the protein levels expressed in microglia and astrocytes exhibit the highest upregulation, which is consistent with gliosis in PSP. In Chapter 2, we analysed cell-specific changes across neurons, astrocytes, microglia, and oligodendrocytes and observed similar trends as in our proteomic studies. Upregulation of astrocytic and microglial gliosis markers was consistent with our histological staining and our qPCR expression analyses. The upregulation of GFAP and VIM indicates astrocyte activation, and GFAP and VIM together enable intermediate filament assembly and extension in astrocytic processes. It is common to see reactive gliosis in PSP, which have altered expressions of GFAP and VIM near pathological lesioned sites [521] and are most prominent in areas with increased NFTs in PSP [748]. In spite of the suggestion that activated astrocytes serve as a protective response against penetrating CNS lesions [749], it is also recognised that astrogliosis is a major contributor to neuroinflammation and neuronal death in neurodegenerative diseases [750], whether through loss of function, gain of function, or a combination of both. Astrocytes play critical roles for in many cellular functions including regulating ions and neurotransmitters, regulating synapse function and energy delivery and the disruption of these functions during reactive process can cause disruptions to the BBB, increased neuroinflammation, neuronal dysfunction, and pathology [751]. It is well known now that astrocytes can store and utilise glycogen particularly in areas with higher density of

synapses [752]. During periods of high neuronal activity this stored glycogen can be broken down into lactate and utilised to sustain activity [752, 753]. Since we observed significant alterations in metabolic changes in PSP, the micro-environment could influence the metabolic profile of different types therefore it would be beneficial to investigate single-cell metabolic profiling to elucidate cell specific responses in PSP.

The toxic gain of function is shown in cell culture studies whereby healthy neurons incubated with astrocytes that express disease causative mutations cause toxicity to neighbouring neurons [754]. Furthermore, activated microglia can also convert resting astrocytes into reactive, toxic state by secretion of inflammatory cytokines [755]. It has been shown that reactive astrogliosis can damage neurons as seen in neurodegenerative diseases through inhibition of axonal regeneration, increased ROS production, exacerbation of inflammation, and disruption of the BBB. PSP is also associated with BBB disruption, and in a mouse model of disrupting the BBB, Gfap and Aqp4 are upregulated in astrocytes as a result [756]. APQ4 is found at the BBB to function as water exchanger transporter in astrocytes [757]. A significant increase in AQP4 levels was observed in PSP seen both in the proteomic dataset and in Chapter 2. There are also reports of overexpression of AQP4 in AD, PD, and ALS, and it has been shown to potentially be regulated by copper [758-761]. Blocking reactive astrogliosis has now been considered a therapeutic strategy with active discovery of molecules which could be involved in the mechanism of gliosis. Transplanting healthy mature astrocytes into mouse models of ALS has been shown to slow progression of ALS-like symptoms [762]. Our proteomic data indicates astrocyte-based markers might be feasible targets for treatment.

Constituents of the cytoskeleton were the top hit in the molecular pathways found to be disrupted in PSP (**Figure 5.3**). There are many components that makeup the cytoskeleton, including microtubules, neurofilaments and microfilaments, with additional adaptor proteins that modulate their interaction with cellular structures. It is well understood by various *in vitro* based studies that the hyperphosphorylation of tau causes the destabilisation microtubules [763]. Our proteomic data revealed a broader picture, with a variety of cytoskeletal proteins that control and remodel the cytoskeleton being significantly dysregulated in PSP. Cytoskeleton dysregulation is seen in many neurodegenerative conditions which lead to the aggregation of proteins, interference with antegrade and

retrograde trafficking of vesicles and organelles to axons and dendrites [764]. The dynamic remodelling of the cytoskeleton enables critical processes including neuronal migration, cellular adhesion, axonal regulation, dendritic spine formation and synaptogenesis. Human and animal neurodegenerative disease tissue proteomic studies have revealed that many cytoskeleton proteins are upregulated during pathogenesis [670, 765]. Proteins that bind and regulate actin promotes its polymerisation, stability and disassembly, in tauopathies, actin is significantly elevated in tissue and forms eosinophilic rod-like aggregates called Hirano bodies that are found in brain tissues from patients with AD [766]. We observed an overexpression of actin-associated proteins, such as spectrins (SPTAN1, SPTBN2), which are seen to be upregulated in PSP tissue and that they are associated with a variety of neurological diseases, including ALS and PD, and are found as a co-aggregate within Lewy body pathology [767]. Mutations in SPTBN2 lead to an autosomal recessively neurodegenerative disorder called Spinocerebellar ataxia type 5, with variants showing both a decrease in axonal outgrowth and a limited capacity to expand and stabilise dendritic arborisation [768, 769]. Spinocerebellar ataxia type 5 is characterised by similar clinical manifestation to PSP including uncontrollable eye movements, dystharia and progressive uncoordinated gait [770].

We also observed upregulation of various constituents of the cytoskeleton that associate with actin (MSN, EZR, PLEC, ADD3) where overexpression leads to stalling of axonal growth and fewer dendritic projections. Our dataset revealed significant alterations in intermediate filaments found in astrocytes, VIM, GFAP, and Synemin (SYNM) as well as neuronal filament internexin neuronal intermediate filament protein alpha (INA). Intermediates filaments are responsible for providing support to the cytoskeleton and are essential for the cell-to-cell and cell-to-extracellular matrix adhesion see review [771]. Neurofilaments on the other hand help expand the axonal calibre of myelin to support polarisation [772] and are integral to the function of synapses [773]. Alterations in neuronal-based intermediate filaments have also been reported in neurodegenerative conditions, with the knockout of INA in mice showing disrupted axonal transport [773]. Inappropriate interactions with the cytoskeleton and its binding partners can result in cell death [774].

In summary, we used proteomic analysis to examine proteins and pathways that may provide new insight to PSP. We found PSP could be characterised as a disease involving disrupted mitochondrial function, alterations in cytoskeletal dynamics, and oxidative stress. As

reported by the proteomics data, several copper-dependent enzymes and associated proteins involved in PSP pathways were significantly altered. As a result of our findings, copper appears to play an important role in the pathogenesis of PSP, as it may influence cardinal metabolic functions of the cell. Further investigation is needed to understand the role of these cuproenzymes and other significant altered proteins in PSP pathogenesis

Chapter 6. Discussion

The research presented herein involved examination of human post-mortem tissue and a mouse model of CNS copper deficiency to uncover a potential role for disrupted copper availability and associated SOD1 pathology in PSP. Initial analyses were hypothesis-driven and targeted specific aspects of copper biology. These analyses were guided by previously reported findings that implicate a role for disrupted copper availability in diverse neurodegenerative diseases, including PSP. Subsequent analyses involved proteomic analysis of PSP tissue. The objective here was two-fold: first, to determine whether features related to disrupted copper availability would be evident in PSP when using an un-biased analytical approach, and second, to gain broader insight to the molecular and cellular pathways that are affected in PSP. Overall, the results generated in this thesis indicate that copper deficiency can result from failure of homeostatic regulation, as seen in PSP, considering that copper is required by several important cellular pathways.

6.1 Astrocytic SOD1 pathology in PSP is associated with indications of disrupted copper availability

In post-mortem PSP tissue, immunohistochemical staining for SOD1 was performed on paraffin embedded sections from several neuroanatomical regions from the basal ganglion and cerebellum (Chapter 2). All regions examined except the non-pathological control region of the visual cortex contained accumulated levels of SOD1, including some positive SOD1 staining seen in the non-neurological controls (**Figure 2.6**). Anti-SOD1 antibodies will detect a wide variety of SOD1 variants, including both pathologically accumulated and physiological versions of SOD1. PSP patients, however, showed a more pronounced accumulation of SOD1 when compared to control cases. This accumulation of SOD1 detected in PSP cases was initially characterised as 'glial' pathology due to the morphological features that indicated its presence as non-neuronal (**Figure 2.6**). Subsequent co-localisation immunofluorescence microscopy indicated the accumulated SOD1 detected in PSP cases occurred within astrocytes due to its co-localisation with the astrocytic marker GFAP (**Figure 2.10**). Spherical inclusions like those found in PD [775] were also observed to have stained positively for SOD1 within the PSP-affected brain tissue (**Figure 2.7**). SOD1 positive Lewy like hyaline inclusions were

also located in astrocytes within the basal ganglion, with prominent elevation seen in the substantia nigra *pars reticulata* (**Figure 2.7**). The use of an antibody that only detects an epitope that is inaccessible within physiologically folded SOD1 indicated that the accumulation of SOD1 detected in astrocytes in PSP involved its accumulation in a misfolded state (**Figure 2.11**). SOD1 accumulation and misfolding is consistent with this highly abundant cytosolic cuproenzyme being unsatiated for its physiological requirement for copper [321, 328, 330]. Thus, we investigated whether copper availability might be facilitating the misfolding of SOD1 that was observed in PSP-affected regions of the human brain by directly measuring tissue copper concentrations. Assessment of copper in TBS-soluble and -insoluble fractions generated from tissue samples enriched for the substantia nigra revealed copper levels are broadly decreased in PSP-affected nigral tissue (**Figure 3.1**). *In situ* assessment of tissue copper levels using LA-ICPMS indicated copper is decreased across all subregions of the substantia nigra, albeit with the substantia nigra *pars compacta* producing the only statistically significant result (**Figure 3.2**). These changes in tissue copper levels were associated with altered expression of 9 out of the 20 genes analysed that are involved in cellular copper handling (**Figure 3.3**). We found a direct correlation between copper levels and STEAP metalloreductases expression (**Table 3.3**), where their activity stimulated copper uptake. Thus, the increase in expression seen in PSP (**Figure 3.3**) may be in response to increase bioavailability of copper. Several classes of oxidoreductases, especially those that involve metal ions, are also affected in PSP (**Figure 3.3**, **Figure 3.4**, **Figure 5.4** and **Table A10**). Moreover, the observed accumulation of the ferroxidases ceruloplasmin and hephaestin without any detectable increase in ferroxidase activity (**Figure 3.4**) further indicated a disconnect between the requirement for copper in PSP and its tissue availability.

There are several pathological abnormalities associated with PSP, including tau aggregation in cells of the CNS, neurodegeneration, and reactive gliosis in areas affected by the disease. The expression profile across neurons shows that neuronal based genes/proteins are generally downregulated (**Figures 2.12** and **5.2c**) indicating that neuronal functions are lost. Conversely as seen in the glial cells, astrocytes and microglia having upregulated gene/protein response highlighting the reactive activation in response to damage (**Figures 2.12** and **5.2c**). In the CNS, astrocytes have a prominent role in maintaining copper homeostasis with elevated levels of glutathione and metallothionines that can store copper are a much larger capacity

than other CNS cells [178, 179]. Copper administration to astrocytes leads to rapid copper accumulation *in vitro* with the release of copper from astrocytes being performed by ATP7A [776, 777]. ATP7A is a fast-acting ATPase that is highly expressed in astrocytes [776], which we observed significant alterations in levels in the substantia nigra in PSP (**Figure 3.3**). Astrocytes are most likely to be responsible for copper distribution to other CNS cells. In response to damage or pathological situations like the formation of protein aggregates like SOD1, the phenotypic change of astrocytes from quiescent to reactive can arise [521]. Consequently, dysfunctional astrocytes would affect both the uptake of neurotransmitters and the regulation of ionic transport such as copper delivery to neurons, microglia and oligodendrocytes. We found misfolded SOD1 in astrocytes, suggesting copper deficiency maybe occurring in astrocytes, an event that may be a precursor to PSP given that in aged healthy controls it was also observed, albeit at much lower levels. While further X-ray imaging of single cells is required to confirm copper deficiency within astrocytes, there are several questions as to how and why these astrocytes could become copper-deficient. Overexpression of ATP7A can lower levels of intracellular copper because its enhanced activity induces its mislocalisation at the plasma membrane to promote copper efflux, conferring resistance when extracellular copper levels are high [569, 778]. ATP7A is the rate limiting step in copper acquisition in astrocytes and it is regulated by copper and iron levels in the cell. The transcriptional regulation of ATP7A is mediated by copper sensor Sp1 binding to GC motif promotor region which is necessary for hypoxia inducible factor 2 alpha to induce its transcription [779, 780]. Sp1 is self-regulatory and like CTR1 is elevated under copper deficient conditions which is a beneficial mechanism to restore homeostasis and prevent large fluctuations efficiently and rapidly [591]. However, there is a copper homeostatic disconnect in PSP where there could be a breakdown in these responses which is evident when we did not see any change in CTR1 to counteract the lower copper levels in PSP tissue. A possible mechanism that could affect copper levels in astrocytes in PSP tissue is the upregulation of *APQ4*, as AQP4 is known to upregulate in many neurodegenerative conditions including AD, PD, and ALS [758-760]. The astrocytic water channel protein AQP4 could potentially be involved in the regulation of CNS copper levels as it has been recently shown *in vitro* studies [528]. In the substantia nigra of the PSP brain, we observed significantly elevated levels of AQP4, detected by both qPCR (**Figure 2.12**) and by proteomic analysis (**Table A8** in **Appendices**). Furthermore, we observed cellular morphology of astrocytes change, where

swelling of the cytoplasm was evident in a subset of astrocytes that co-express GFAP and accumulated SOD1 levels, referred to as Lewy like hyaline inclusions (**Figures 2.10n**). Increases in AQP4 cause changes in the influx of water (hyposmolality) in cells, where it induces swelling which is usually a rapid process as they turn back to normal size within minutes [781]. The swelling of astrocytes is suggested to be a protective mechanism whereby the astrocytes are using the osmotic gradient to potentially flush out toxins from the brain through the glymphatic systems to prevent further cytotoxicity [782]. However, it is also known that AQP4 permeability is affected by metals by which the inhibition of water permeability is shown only when there is copper found intracellularly [761]. AQP4 permeability as shown in CHO cells is modulated by monovalent copper as it has predicted copper binding site at C178 and C253 on the intracellular domain of the protein [528]. AQP4 upregulation is seen when mice are treated with the copper chelator cuprizone where swelling occurred after 5 weeks of a low dose of cuprizone with edema and swelling of the astrocytic end-feet around blood vessels within the neocortex in mice [783]. This suggests that AQP4 may have a role in copper importation. However, we do not fully understand why copper regulates AQP4 activity, and it is an intriguing insight given that PSP has low copper levels with copper potentially influencing its expression or migration. Additionally, since CNS copper is acquired through the dietary intake, and there is a lack of definitive reports on the peripheral levels of copper in PSP patients and there are conflicting reports on copper levels in both serum and CSF in neurodegenerative conditions [784-787].

Astrocytes being one of the most abundant cell types in the CNS however undergo functional changes in response to injury and disease. There has been plenty of evidence of toxicity of astrocytes in neurodegenerative conditions [754, 788, 789] with pathogenetic astrocytes seen to secrete toxic factors to induce non-cell autonomous cell death [754, 789]. The presence of pathological inclusions like SOD1 can both diminish neurotrophic/protective factors and increases pathological proteins and ROS [790, 791]. SOD1 proteinopathy within astrocytes has been described in both ALS and within human mutant variants of SOD1 expressed in mice [337, 339, 792, 793] where loss of motor neurons may be a consequence of glial dysfunction [792]. Cell culture studies have also found the effect of SOD1 pathology in astrocytes whereby mutant SOD1 expressing astrocytes co-cultured with primary motor neurons derived from mouse spinal cords were shown to kill primary motor neurons after 7 days of incubation [754].

In addition, it was found that when the culture medium collected from mutant SOD1 expressing astrocytes was transferred to primary motor neurons it caused a 60% loss of these neurons after 7 days [754]. Mutant SOD1 was also found to be in the media from primary cultured astrocytes from SOD1-ALS mutant mice where they can be excreted via exosomes and efficiently internalised by stable neuronal cell lines [794]. SOD1 is known to misfold under genetic aberration, copper deficiency or under high levels of oxidative stress [321, 497] and the blocking of residues that are involved in its conformational change is shown to decrease its misfolding, decrease gliosis and increase neuronal survival [795]. The presence of misfolded SOD1 is not only detected in ALS, but also in degenerating regions of PD and also now seen in PSP [35, 141, 321, 497].

It has been shown that misfolded SOD1 affects the density, morphology, and location of mitochondria, whereby it is enriched within mitochondria within axons before the onset of ALS symptoms in mice [796]. We observed a higher level of misfolded SOD1 in PSP and as it is known that misfolded SOD1 can repress mitochondrial function [797] this may be a possible explanation for the mitochondrial dysfunction results presented in Chapter 5 (**Figure 5.4**). In a similar tauopathy with clinical and pathological overlap to PSP, frontotemporal lobar dementia, SOD1 accumulated within astrocytes in the frontal cortex and co-localised with aberrant levels of lipid peroxidation markers [465]. Lipid peroxidation markers are found in diseased affected regions in PSP [10, 201] and these markers are known cause damage to various proteins and also mitochondrial membranes leading to its impairment [798]. Mutated human SOD1 expressed in mice, impairs the mitochondrial respirasome function, as isolated mitochondria from these transgenic animals showed decreased activity in complex I, II, III, and IV, as well as increased lipid peroxidation. [799]. Mitochondrial dysfunction has been reported in several studies in PSP [597] and additionally we also saw alterations in expression of various mitochondrial based proteins (**Figure 5.4** and **Table A10** in **Appendices**). Glucose utilisation measured by PET in several studies is seen to be much lower within frontal cortex and within basal ganglion structures in PSP [115, 800, 801]. Our proteomic assessment of PSP emphasised that the substantia nigra relies on a high energy source to function efficiently and decreased mitochondrial proteins involved in metabolic process of TCA cycle, glycolysis and the electron transport chain would have a profound effect on the entire functioning of many processes in cells. Defects in the electron transport chain have also been reported previously,

resulting in decreases of the respiratory complexes I, II, III, IV, and V [19, 597, 598, 802]. Mitochondria are one of major sources of ROS, contributing up to 80% of neuronal ROS production [803]. The generation of ATP from the electron transport chain results in the production of ROS, which is buffered by the presence of antioxidants, including SOD1 [803]. However, the alterations in various antioxidants are seen in PSP, and SOD1 accumulates and is misfolded and unavailable to participate in the breakdown of ROS. We also saw changes to other antioxidant defences, including proteins involved in glutathione biosynthesis and catalysis of conjugated ligands to glutathione (such as GSTP1 and ESD, **Figure 5.8** and **Tables A8** and **A11** in **Appendices**). Prior studies indicate that the abundance/activity/location of these proteins can be influenced by copper [745, 746]. This could result in continuous oxidative damage within cells, particularly within mitochondria, leading to disease susceptibility and death [804, 805]. Astrocytic oxidative stress that can occur from mitochondrial dysfunction and by the breakdown of dopamine. We observed both the mitochondrial dysfunction in the substantia nigra in PSP and an increase of astrocytic based MAOB in our proteomics analysis (**Figures 5.6, 5.7** and **Tables A8, A10** and **A11** in **Appendices**). We also assessed MAOB as part of our qPCR cuproenzyme suite and we observed no changes in mRNA levels (**Figure 3.4a, b**). MAOB has a long half-life of up to 40 days in humans [806, 807], which could explain the disconnect between the transcript and translation. Copper is known to facilitate the function of complex IV and also MAOB, an enzyme which breaks down dopamine [808]. The ROS generated by the inhibition of the mitochondrial respirasome as well as the breakdown of dopamine with the by-product of superoxide, a primary factor that contributes to the damage to neurons in PSP [809, 810].

6.2 Decreased CNS copper alone appears insufficient to cause PSP

The balance between too much and too little copper in the intracellular environment is delicate, so precise regulation is crucial to cellular homeostasis. Abnormal levels of copper through the genetic mutation, environment and aging can lead to many diseases including neurodegenerative disease. In PSP, we saw depletion in copper levels within the substantia nigra (**Figures 3.1** and **3.2**). Therefore, using a genetic animal model of CNS copper deficiency, we investigated whether copper deficiency alone within the CNS could induce pathological or phenotypic changes that are seen in PSP. Using a partial knockout of *Slc31a1* gene (encoding

the copper transporter CTR1) within mice, had a substantial decrease in CNS copper (45%) by adulthood (**Figure 4.3b**). This in turn was shown to cause a small but significant decreased in neurons within substantia nigra *pars compacta* (**Figure 4.5a**). No other pathologies of gliosis or Sod1 accumulation were evident, despite a decrease in brain copper levels (**Figures 4.4** and **4.5b, c, d, e, f**). These results indicate that mice are less susceptible to changes in copper within a certain threshold, or that a compensatory mechanism may be at play when copper levels are scarce. The absence of changes to *Slc31a1* mRNA in human PSP-affected brain tissue highlights that *Slc31a1*$^{-/+}$ mice do not have construct validity for PSP and that exploring the role of other copper handling mechanisms such as ATP7A may be more beneficial in modelling PSP. Copper alone in this animal model was not sufficient to induce pathological changes like increased gliosis and SOD1 accumulation in astrocytes that is seen in PSP. It has been documented that human SOD1 misfolds when copper levels are low [321]. Thus, the propensity for endogenous mouse Sod1 to aggregate may be an additional or alternate consideration of significance. Prior cell culture and *in vivo* studies have demonstrated that human SOD1 has a higher propensity to form aggregates than endogenous mouse Sod11 [811, 812]. Although mouse Sod1 has 84% amino acid homology with human SOD1, the 16% non-homology, includes a change in amino acid of serine at position 111 in the mouse Sod1 sequence that is highly conserved amongst mammals [813]. In humans however, this position encodes a cysteine residue which is a critical residue for its aggregation [758]. Combined with copper and zinc insertion, cysteine at position 111 forms an intermolecular disulfide bond and stabilises the enzyme [758]. If left exposed, when copper is not co-ordinating into its 3 histidine residues (H45, H48, H120) [814] the cysteine 111 residue is susceptible to self-aggregate and to be targeted for aberrant oxidation [815]. This could explain why endogenous mouse Sod1 did not aggregate in the *Slc31a1*$^{+/-}$ mouse tissue. Other proteins related to neurodegenerative disease pathology also exhibit this phenomenon, such as mouse α-synuclein which does not aggregate despite being exposed to conditions that would usually promote it aggregation of the human protein [816, 817].

Other critical observations that are also see in PSP are that in addition to copper deficiency, PSP is associated with an increase gliosis and in iron levels [21, 439, 440], which may account for the exacerbation in pathology and neurodegeneration seen in PSP. Copper depletion showed no effect on inducing gliosis in the *Slc31a1*$^{+/-}$ mice (**Figures 4.4** and **4.5**). It is

understood that free copper can induce gliosis as seen in the copper overload condition of Wilson's disease [477]. Copper deficiency in a model of traumatic brain injury in mice caused a small number of neurons to die without affecting astrogliosis, unlike zinc deficiency, which caused a lower level of astrogliosis 2 days after brain injury [818]. In addition, these copper deficient mice had higher levels of oxidative stress with lipid peroxidation marker malondialdehyde and decreased Sod1 levels which could account for the small loss of neurons indicated by increase in TUNNEL staining 2 days post lesion [818]. Thus, similarly in our study, the small loss of neurons could be afforded by both a decrease in Sod1 levels and/or other cuproenzymes like complex IV. The lack of a reactive gliosis response could also be an additional factor that can contribute to the detriment of neurons. *Slc31a1*$^{+/-}$mouse brains do not accumulate Sod1 as shown by immunohistochemical staining or show misfolded Sod1 pathology, which may also influence gliosis induction. This could highlight the importance and the contribution of the gliosis response and its potential loss or gain for function in that leads to neuronal cell loss seen in neurodegenerative conditions.

It is known that iron plays a role in neurodegenerative diseases like PSP as it is most certainly observed in elevation as detected by MRI and also at post-mortem [21, 373, 439, 586]. Iron can induce the aggregation of tau, where it can bind strongly to histidine residues that are found within the microtubule domain [819]. Furthermore, ferritin is also shown to colocalise with tau pathology in the PSP brain [563]. No increase in iron was detected in the substantia nigra of the *Scl31a1*$^{-/+}$ mice at 9-10 months of age (**Figure 4.3c**). In cells, excessive iron accumulation that is not complexed to iron binding proteins can cause oxidative stress due to its overt involvement in Fenton redox chemistry, which can cause damage to antioxidants like glutathione, induce gliosis and exacerbates oxidative stress [820-822]. Studies in cell culture have shown that acute overload treatment of iron to rat cortical astrocytes that were initially activated by microglial cytokines (IL-6β and TNFα), provide protection against iron-mediated oxidative stress. [820, 823]. In the iron overload condition, the transition from resting to reactive astrocytes preserved mitochondrial activity and increased glutathione levels [820]. Therefore, the increase in iron may be protective mechanism to prevent damage inflicted by glia.

It is known that excess and unregulated iron can cause toxicity to cells. Due to the lack of excess iron in the substantia nigra of *Slc31a1*$^{-/+}$ mice, neuronal cell death may not have been enhanced. Iron mediated cell death that differs from apoptosis, necrosis, etc. is now recognised as a unique form of regulated cell death, known as ferroptosis [824]. Ferroptosis is caused by alterations within the intracellular environment which lead to oxidative alterations (lipid peroxidation) that is also controlled by changes in glutathione, glutathione peroxidase 4, and iron [824, 825]. Ferroptosis mainly affects the mitochondria and therefore could be a main driver in neuronal cell death in many neurodegenerative diseases including PSP [825]. There are several key morphological changes in PSP tissue, including increases in iron and lipid peroxidation, as well as alterations in mitochondria and antioxidant defences, so further investigation into ferroptosis regulatory pathway is needed. However, there is question as to whether copper is essential for ferroptosis as both copper deficiency and iron accumulation may have synergistic role together in neurodegenerative disease. It is not well understood as to which precedes the other or if they are a trigger or a consequence of pathological processes.

6.3 Additional factors in PSP

Proteomic analysis of the substantia nigra from cases diagnosed with PSP was performed in order to investigate dysfunctional molecular and cellular pathways using an unbiased approach. Parsing of differential expressed proteins into annotated GO pathways using gene enrichment analysis showed abnormalities in many additional pathways including cytoskeletal dynamics and phospholipid binding. Two very critical biological processes that aid the structural and functional development of the substantia nigra are cytoskeletal organisation and phospholipid binding. Phospholipids are essential component for many lipids bilayers and are important for signalling and for the structural integrity of intracellular and cell surface proteins [826]. As phospholipids are found at the plasma membranes and in vesicles, they make up 75% of the total cellular lipid content [827]. In experimental models of phospholipid deficiency, embryonic lethality is observed [828]. Alterations in all three major classes of phospholipids (phosphatidylinositol, phosphatidylethanolamine, and phosphatidylcholine) have been shown in AD cases where levels are decreased, or their metabolism altered [829, 830]. A large metabolic study using 156 PSP samples only recently

showed that PSP exhibited similar perturbed levels of lipids to AD highlighting that the lipidome is also dysregulated in PSP [725]. Myelin, which is comprised of cholesterol, phospholipids, and glycolipids, is compromised in PSP where severe loss of white matter is seen in cerebellum, and there was significant decrease in apolipoproteins A1 and A2 that facilitate the entry of cholesterol needed for membrane envelopment, synaptic transmission, and myelin sheath formation. This is seen in cerebrovascular disorders like **a**therosclerosis where the decreased in APOA1 and APOA4 causes cholesterol to accumulate within the blood [831, 832].

Neuronal and glial cytoskeletal pathology is evident in PSP, where the microtubule binding protein tau is seen to be dissociated from the microtubules and found as insoluble aggregates within neurons and glia [48, 53, 87]. Cytoskeletal remodelling has also been found to be a factor that is disrupted in PSP as shown in another proteomic analysis of close proximity proteins to tau aggregates from a small subset of PSP [686]. In this study 117 proteins that were differentially expressed were identified and >80% had been previously associated with tau, with 10 of these proteins associated with cellular assembly and actin binding [686]. It was observed in our proteosome dataset that cell specific changes to cytoskeleton where it is known that axons, synapses, and dendrites distinguish the neuronal from the non-neuronal cytoskeleton, and changes associated with the cytoskeleton (neurofilaments) in neurons were downregulated in PSP as shown in our gene expression (**Figure 2.12**) and within proteomic data (**Table A8** in **Appendices**). Conversely to neuronal cytoskeletal profile in PSP, the intermediate neurofilaments found within astrocytes and most associated with altered morphology in gliosis were upregulated (**Table A8** and **A9** in **Appendices**). Only recently tau is known to possibly interact with the astrocytic intermediate filament GFAP [686]. Cytoskeleton remodelling helps to maintain the cell's integrity and in neurons it is required to be flexible particularly during axonal regeneration during development [833]. However during apoptosis the cell is undergoing contraction [834] and the cytoskeleton must undergo reorganisation and the dismantling and disorganisation during this phase [835].

In PSP, the complex nature of not only multiple pathologies but also cellular pathways makes it a multifaceted disorder. In light of this complexity, there is no one single pathway that could lead to a breakthrough in treatment. A multi-based therapeutic approach might therefore be

necessary that targets a variety of pathways and homeostatic processes involved in the disease.

6.4 Study limitations and future directions

Analysis of human post-mortem tissue offers excellent opportunity to investigate abnormalities that may represent significant events in the development of neurodegenerative diseases such as PSP. It is important to note however, that the availability of tissues from biorepositories is often limited by several factors. Not least of which is the number of PSP cases and controls available for study. PSP is a relatively rare neurodegenerative disease, with an incidence of 180 cases per year in Australia, and not all of these cases necessarily donate tissue for research purposes. Additionally, whilst control cases might be expected to be more numerous, this is generally not the case, as the motivations for tissue donation that apply to people with a neurodegenerative disease do not necessarily apply to those who do not. As a consequence, some considerations that would be met in an ideal study (such as larger numbers of cases that are perfectly matched for sex, age and post-mortem interval) are not necessarily feasible. In the present study this affected several key aspects. First was that not all analyses could be performed on all tissue samples acquired, and this restricted capacity to make meaningful correlations across all parameters measured. Second, SOD1 proteinopathy was assessed in paraffin embedded tissue by using immunohistochemistry coupled with quantitative stereology. In addition to providing case versus control outcomes, quantitative stereology of human tissue also enables identification of cell specific changes. However, stereology requires systematic unbiased sampling throughout the entire neuroanatomical region of interest to get an accurate number of cell populations. We had access to only one paraffin section per case and not all of these were located at the same brain coordinate. Thus, without sampling throughout the whole neuroanatomical region, completeness of the stereology is restricted.

The number of samples in our non-neurological control group is quite small due to tissue availability in biobank repositories with the ideal of having larger or equal number of samples. The data normalisation process in our proteomics dataset involved a 50% per group cut off is quite a conversative approach and particularly when there is a low number of non-

neurological control samples mean that this lower abundance proteins were most likely excluded from our analysis. In other experiments, such as LA-ICPMS, a small number of cases (N=3 per group) were available, and due to the lack of tissue availability, significant differences in iron and zinc values could not be determined. Therefore, this would require higher level resourcing of the tissue banks necessary for increased recruitment of tissue donors.

An additional limitation associated with this study is that although some results indicated the significance of cell-specific changes in PSP (e.g., the apparent accumulation of SOD1 in astrocytes), the methodologies we applied to detect levels of copper in the PSP-affected brain tissue could not provide cell-specific information. The use of homogenisation in a TBS-based buffer provided some opportunity to investigate potential changes in the biochemical partitioning of copper in PSP (**Figure 3.1**), and our LA-ICPMS methodology enabled examination of copper within specific subregions of the substantia nigra (**Figure 3.2**), but neither provided cell-specific information. LA-ICPMS technology has advanced to the point where detection of endogenous elements is feasible at the level of cellular resolution [836]. The additional use of antibodies tagged with lanthanides or gold-nanoparticles, can facilitate identification of cell-specificity [837, 838]. In addition, the use of µPIXE could also be an important complementary analytical tool to both address whether the SOD1 aggregates that are found within PSP tissue are appropriately metalated and quantify the amount of copper and zinc that is bound to SOD1 [839].

Proteomics analysis was used to determine both the abundances of proteins and the enriched pathways that these differentially expressed proteins are involved in. Since there are differences between the results of standard biochemical analyses (i.e. western blotting versus proteomics), there are several explanations for these disparities which indicate technical limitations and strengths in each of these proteomic approaches. Firstly, there is no universal sample preparation to extract the proteins/peptides from the post-mortem tissues and it is developed in-house depending on user and equipment and these are also not standardised across various assays. The extraction method that was used in biochemical assays (western blot) as well as in the proteomic study is considered a 'hard extraction' given the method deviated significantly from physiologically conditions (e.g., it involved boiling, a pH of 8.5 and

homogenisation). Such extraction methods can give rise to proteins or peptides being lost and/or having minimal biological activity [840]. Potentially because of this, it was revealed that some of the copper handling proteins/chaperones like ATP7A and ATP7B and the cuproenzyme hephaestin were beyond detection limits in our proteomic study. The discrepancy in results and the lack of change in ceruloplasmin and hephaestin could be attributed to different protein preparations and different physiological conditions between western blotting and protein purification, which may be related to the sample processing stage [558].

There are caveats using human post-mortem tissue which can affect the outcome of our proteomic analysis which include sample heterogeneity (gender differences, patient's history, drug treatments), quality (longer periods in frozen storage, repeated freeze-thaw) and by PMI. With a longer interval between the collection of the brain specimen, this might explain the lack of neurotransmitter receptors like $GABA_{A1}$ and some synaptic vesicle proteins detected within the samples. While it is hard to control for the PMI of samples given the lack of tissue availability that is seen in most biobanks, it would be prudent not to control for this if this experiment was to be repeated in the future.

The future directions of research based on our current findings would be to assess other basal ganglion regions in PSP cases that showed pathological changes including the globus pallidus and subthalamic nucleus. Globus pallidus and subthalamic nucleus are both regions (other than the substantia nigra) that contain severe levels of tau pathology including oligodendrocyte pathology [50]. Therefore, it would be beneficial to determine if the copper deficiency also extends to other regions to get a rounded understanding of pathological changes that associate with SOD1 and copper deficiency in PSP. Given that we observed SOD1 accumulation and Lewy like hyaline inclusions in aged control tissue, it would be valuable to assess the changes in other younger age groups to determine when copper deficiency and SOD1 pathology might begin. There is no study that looked at this currently and associate copper changes that might occurred in aging tissue. Furthermore, to get a better understanding of both the metal status and the cell specific metabolic changes that are observed in PSP, additional experiments to address include 1) single cell proteomics/RNAseq and 2) single cell LACIPMS imaging. Newer technologies now make proteomic measures

within single cell types that can give insights into cellular processes and states and can capture post-translation modifications at the transcriptome level. Due to the limited resolution of LA-ICPMS, we were only able to detect cell specific changes within various CNS cell types. To detect metal concentrations within CNS cells, cell specific markers along with secondary antibodies labelled with gold/AU or lanthanide particles that tag different cell types thus can quantify metal levels may be a better option as mentioned previously. In an extension to the copper deficiency that is seen in PSP, it would also be favourable to use XFM or µPIXE imaging as reported by Genoud *et al*. (2020) to quantify the metal state of SOD1 within SOD1 pathology in PSP brain as a confirmation of the metal status of SOD1 [395]. To complete our set of cuproenzyme analysis in both PSP and in copper deficient *Slc31a1*$^{-/+}$ mice, a focus on protein expression of cuproenzymes (DβH, myeloperoxidase, lysyl oxidase) and specific activities of ceruloplasmin, hephaestin, dopamine beta hydroxylase, myeloperoxidase, lysyl oxidase might give us a better understanding of the extent of copper deficiency on a range of cuproenzymes.

6.5 Concluding remarks

The overall findings of this work show that brain tissue from cases of PSP displays evidence for disrupted availability of copper. This indicates that as per other neurodegenerative diseases, altered copper availability may play a significant role in PSP. It remains to be determined whether altered copper availability may be involved as a primary trigger or part of a secondary event. Our assessment of *Slc31a1*$^{-/+}$ mice was intended to provide some insight on this topic, but results from these mice were inconclusive.

Initial assessments conducted for this study involved histological assessment of SOD1 in human, PSP-affected brain tissue. Our data demonstrated an accumulation of SOD1 in PSP, and that this accumulation occurred within astrocytes. Whether this represents a potential mechanism of non-cell autonomous neuronal death in PSP of perhaps just an indicator of disrupted copper availability in the brain remains unclear. Analogous outstanding issues remain for other neurodegenerative diseases such as AD where the pathogenic significance of amyloid plaques remains intensely debated.

Chapter 6. Discussion

One result that appeared clear from our analyses and supported independently reported findings is that copper levels are decreased in the PSP-affected brain. The mechanism as to what causes this loss of copper from the PSP-affected substantia nigra, and to where it is re-distributed is still not known.

References

1. Finkel, T. and N.J. Holbrook, *Oxidants, oxidative stress and the biology of ageing.* Nature, 2000. **408**(6809): p. 239-47.
2. Zhao, Y. and B. Zhao, *Oxidative stress and the pathogenesis of Alzheimer's disease.* Oxid Med Cell Longev, 2013. **2013**: p. 316523.
3. Zhang, J., et al., *Parkinson's disease is associated with oxidative damage to cytoplasmic DNA and RNA in substantia nigra neurons.* Am J Pathol, 1999. **154**(5): p. 1423-9.
4. Wang, X., et al., *Oxidative stress and mitochondrial dysfunction in Alzheimer's disease.* Biochim Biophys Acta, 2014. **1842**(8): p. 1240-7.
5. Nielsen, F., et al., *Plasma malondialdehyde as biomarker for oxidative stress: reference interval and effects of life-style factors.* Clin Chem, 1997. **43**(7): p. 1209-14.
6. Niedzielska, E., et al., *Oxidative Stress in Neurodegenerative Diseases.* Mol Neurobiol, 2016. **53**(6): p. 4094-4125.
7. Migliore, L. and F. Coppede, *Environmental-induced oxidative stress in neurodegenerative disorders and aging.* Mutat Res, 2009. **674**(1-2): p. 73-84.
8. Martinez, A., et al., *Glycolitic enzymes are targets of oxidation in aged human frontal cortex and oxidative damage of these proteins is increased in progressive supranuclear palsy.* J Neural Transm (Vienna), 2008a. **115**(1): p. 59-66.
9. Aoyama, K., K. Matsubara, and S. Kobayashi, *Aging and oxidative stress in progressive supranuclear palsy.* Eur J Neurol, 2006. **13**(1): p. 89-92.
10. Albers, D.S., et al., *Evidence for oxidative stress in the subthalamic nucleus in progressive supranuclear palsy.* J Neurochem, 1999. **73**(2): p. 881-4.
11. Liu, Q., et al., *Alzheimer-specific epitopes of tau represent lipid peroxidation-induced conformations.* Free Radic Biol Med, 2005. **38**(6): p. 746-54.
12. Dexter, D.T., et al., *Increased levels of lipid hydroperoxides in the parkinsonian substantia nigra: an HPLC and ESR study.* Mov Disord, 1994. **9**(1): p. 92-7.
13. Dexter, D.T., et al., *Basal lipid peroxidation in substantia nigra is increased in Parkinson's disease.* J Neurochem, 1989. **52**(2): p. 381-9.
14. Barnham, K.J., C.L. Masters, and A.I. Bush, *Neurodegenerative diseases and oxidative stress.* Nature Reviews Drug Discovery, 2004. **3**(3): p. 205-214.
15. Obrador, E., et al., *Oxidative Stress, Neuroinflammation and Mitochondria in the Pathophysiology of Amyotrophic Lateral Sclerosis.* Antioxidants (Basel), 2020. **9**(9).
16. Tabner, B.J., et al., *Protein aggregation, metals and oxidative stress in neurodegenerative diseases.* Biochem Soc Trans, 2005. **33**(Pt 5): p. 1082-6.
17. Surmeier, D.J., J.A. Obeso, and G.M. Halliday, *Selective neuronal vulnerability in Parkinson disease.* Nat Rev Neurosci, 2017. **18**(2): p. 101-113.
18. Cheng, X., et al., *Variability of mitochondrial energy balance across brain regions.* J Neurochem, 2021. **157**(4): p. 1234-1243.

References

19. Albers, D.S., et al., *Further evidence for mitochondrial dysfunction in progressive supranuclear palsy.* Exp Neurol, 2001. **168**(1): p. 196-8.

20. Cantuti-Castelvetri, I., et al., *Expression and activity of antioxidants in the brain in progressive supranuclear palsy.* Brain Res, 2002. **930**(1-2): p. 170-81.

21. Dexter, D.T., et al., *Alterations in the levels of iron, ferritin and other trace metals in Parkinson's disease and other neurodegenerative diseases affecting the basal ganglia.* Brain, 1991. **114 (Pt 4)**: p. 1953-75.

22. Loeffler, D.A., et al., *Increased regional brain concentrations of ceruloplasmin in neurodegenerative disorders.* Brain Res, 1996. **738**(2): p. 265-74.

23. McCord, J.M. and I. Fridovich, *Superoxide dismutase. An enzymic function for erythrocuprein (hemocuprein).* J Biol Chem, 1969. **244**(22): p. 6049-55.

24. Glasauer, A., et al., *Targeting SOD1 reduces experimental non-small-cell lung cancer.* J Clin Invest, 2014. **124**(1): p. 117-28.

25. Bhaskaran, S., et al., *Neuron-specific deletion of CuZnSOD leads to an advanced sarcopenic phenotype in older mice.* Aging Cell, 2020. **19**(10): p. e13225.

26. Saccon, R.A., et al., *Is SOD1 loss of function involved in amyotrophic lateral sclerosis?* Brain, 2013. **136**(8): p. 2342-2358.

27. Rosen, D.R., et al., *Mutations in Cu/Zn superoxide dismutase gene are associated with familial amyotrophic lateral sclerosis.* Nature, 1993. **362**(6415): p. 59-62.

28. Bunton-Stasyshyn, R.K., et al., *SOD1 Function and Its Implications for Amyotrophic Lateral Sclerosis Pathology: New and Renascent Themes.* Neuroscientist, 2015. **21**(5): p. 519-29.

29. Forsberg, K., et al., *Novel antibodies reveal inclusions containing non-native SOD1 in sporadic ALS patients.* PLoS One, 2010. **5**(7): p. e11552.

30. Guareschi, S., et al., *An over-oxidized form of superoxide dismutase found in sporadic amyotrophic lateral sclerosis with bulbar onset shares a toxic mechanism with mutant SOD1.* Proc Natl Acad Sci U S A, 2012. **109**(13): p. 5074-9.

31. Hilton, J.B., et al., *The accumulation of enzymatically inactive cuproenzymes is a CNS-specific phenomenon of the SOD1(G37R) mouse model of ALS and can be restored by overexpressing the human copper transporter hCTR1.* Exp Neurol, 2018. **307**: p. 118-128.

32. Hilton, J.B., et al., *Cu(II)(atsm) improves the neurological phenotype and survival of SOD1(G93A) mice and selectively increases enzymatically active SOD1 in the spinal cord.* Sci Rep, 2017. **7**: p. 42292.

33. Huai, J. and Z. Zhang, *Structural Properties and Interaction Partners of Familial ALS-Associated SOD1 Mutants.* Front Neurol, 2019. **10**: p. 527.

34. Karch, C.M., et al., *Role of mutant SOD1 disulfide oxidation and aggregation in the pathogenesis of familial ALS.* Proc Natl Acad Sci U S A, 2009. **106**(19): p. 7774-9.

35. Pare, B., et al., *Misfolded SOD1 pathology in sporadic Amyotrophic Lateral Sclerosis.* Sci Rep, 2018. **8**(1): p. 14223.

References

36. Trist, B.G., et al., *Altered SOD1 maturation and post-translational modification in amyotrophic lateral sclerosis spinal cord.* Brain, 2022. **145**(9): p. 3108-3130.

37. Wilcox, K.C., et al., *Modifications of superoxide dismutase (SOD1) in human erythrocytes: a possible role in amyotrophic lateral sclerosis.* J Biol Chem, 2009. **284**(20): p. 13940-13947.

38. Yamagishi, S., et al., *An in vitro model for Lewy body-like hyaline inclusion/astrocytic hyaline inclusion: induction by ER stress with an ALS-linked SOD1 mutation.* PLoS One, 2007. **2**(10): p. e1030.

39. Alster, P., et al., *Progressive Supranuclear Palsy-Parkinsonism Predominant (PSP-P)-A Clinical Challenge at the Boundaries of PSP and Parkinson's Disease (PD).* Front Neurol, 2020. **11**: p. 180.

40. Richardson, J.C., J. Steele, and J. Olszewski, *Supranuclear Ophthalmoplegia, Pseudobulbar Palsy, Nuchal Dystonia and Dementia. A Clinical Report on Eight Cases of "Heterogenous System Degeneration".* Trans Am Neurol Assoc, 1963. **88**: p. 25-9.

41. Swallow, D.M.A., C.S. Zheng, and C.E. Counsell, *Systematic Review of Prevalence Studies of Progressive Supranuclear Palsy and Corticobasal Syndrome.* Mov Disord Clin Pract, 2022. **9**(5): p. 604-613.

42. Alquezar, C., et al., *Heavy metals contaminating the environment of a progressive supranuclear palsy cluster induce tau accumulation and cell death in cultured neurons.* Sci Rep, 2020. **10**(1): p. 569.

43. Litvan, I., et al., *Environmental and occupational risk factors for progressive supranuclear palsy: Case-control study.* Mov Disord, 2016. **31**(5): p. 644-52.

44. Golbe, L.I., et al., *Prevalence and natural history of progressive supranuclear palsy.* Neurology, 1988. **38**(7): p. 1031-4.

45. Yamada, T., P.L. McGeer, and E.G. McGeer, *Appearance of paired nucleated, Tau-positive glia in patients with progressive supranuclear palsy brain tissue.* Neurosci Lett, 1992. **135**(1): p. 99-102.

46. Yamada, T., et al., *Further observations on Tau-positive glia in the brains with progressive supranuclear palsy.* Acta Neuropathol, 1993. **85**(3): p. 308-15.

47. Williams, D.R., et al., *Pathological tau burden and distribution distinguishes progressive supranuclear palsy-parkinsonism from Richardson's syndrome.* Brain, 2007. **130**(Pt 6): p. 1566-76.

48. Sergeant, N., A. Wattez, and A. Delacourte, *Neurofibrillary degeneration in progressive supranuclear palsy and corticobasal degeneration: tau pathologies with exclusively "exon 10" isoforms.* J Neurochem, 1999. **72**(3): p. 1243-9.

49. Santpere, G. and I. Ferrer, *Delineation of early changes in cases with progressive supranuclear palsy-like pathology. Astrocytes in striatum are primary targets of tau phosphorylation and GFAP oxidation.* Brain Pathol, 2009. **19**(2): p. 177-87.

50. Kovacs, G.G., et al., *Distribution patterns of tau pathology in progressive supranuclear palsy.* Acta Neuropathol, 2020. **140**(2): p. 99-119.

51. Kovacs, G.G., *Invited review: Neuropathology of tauopathies: principles and practice.* Neuropathol Appl Neurobiol, 2015. **41**(1): p. 3-23.

References

52. Jellinger, K.A., *Different tau pathology pattern in two clinical phenotypes of progressive supranuclear palsy.* Neurodegener Dis, 2008. **5**(6): p. 339-46.

53. Arai, T., et al., *Identification of amino-terminally cleaved tau fragments that distinguish progressive supranuclear palsy from corticobasal degeneration.* Ann Neurol, 2004. **55**(1): p. 72-9.

54. Williams, D.R., et al., *Characteristics of two distinct clinical phenotypes in pathologically proven progressive supranuclear palsy: Richardson's syndrome and PSP-parkinsonism.* Brain, 2005. **128**(Pt 6): p. 1247-58.

55. Litvan, I., et al., *Clinical research criteria for the diagnosis of progressive supranuclear palsy (Steele-Richardson-Olszewski syndrome): report of the NINDS-SPSP international workshop.* Neurology, 1996. **47**(1): p. 1-9.

56. Respondek, G., et al., *The phenotypic spectrum of progressive supranuclear palsy: a retrospective multicenter study of 100 definite cases.* Mov Disord, 2014. **29**(14): p. 1758-66.

57. Donker Kaat, L., et al., *Familial aggregation of parkinsonism in progressive supranuclear palsy.* Neurology, 2009. **73**(2): p. 98-105.

58. Fujioka, S., et al., *Three sib-pairs of autopsy-confirmed progressive supranuclear palsy.* Parkinsonism Relat Disord, 2015. **21**(2): p. 101-5.

59. Tetrud, J.W., et al., *Autopsy-proven progressive supranuclear palsy in two siblings.* Neurology, 1996. **46**(4): p. 931-934.

60. Fujioka, S., et al., *Similarities between familial and sporadic autopsy-proven progressive supranuclear palsy.* Neurology, 2013. **80**(22): p. 2076-8.

61. Ogaki, K., et al., *Analyses of the MAPT, PGRN, and C9orf72 mutations in Japanese patients with FTLD, PSP, and CBS.* Parkinsonism Relat Disord, 2013. **19**(1): p. 15-20.

62. Ross, O.A., et al., *Lrrk2 R1441 substitution and progressive supranuclear palsy.* Neuropathol Appl Neurobiol, 2006. **32**(1): p. 23-5.

63. Coughlin, D.G. and I. Litvan, *Progressive supranuclear palsy: Advances in diagnosis and management.* Parkinsonism Relat Disord, 2020. **73**: p. 105-116.

64. Höglinger, G.U., et al., *Identification of common variants influencing risk of the tauopathy progressive supranuclear palsy.* Nat Genet, 2011. **43**(7): p. 699-705.

65. Sanchez-Contreras, M., et al., *Study of LRRK2 variation in tauopathy: Progressive supranuclear palsy and corticobasal degeneration.* Mov Disord, 2017. **32**(1): p. 115-123.

66. Lee, W.S., et al., *Syntaxins 6 and 8 facilitate tau into secretory pathways.* Biochem J, 2021. **478**(7): p. 1471-1484.

67. Stutzbach, L.D., et al., *The unfolded protein response is activated in disease-affected brain regions in progressive supranuclear palsy and Alzheimer's disease.* Acta Neuropathol Commun, 2013. **1**: p. 31.

68. Caparros-Lefebvre, D., et al., *A geographical cluster of progressive supranuclear palsy in northern France.* Neurology, 2015. **85**(15): p. 1293-300.

References

69. Lannuzel, A., M. Ruberg, and P.P. Michel, *Atypical parkinsonism in the Caribbean island of Guadeloupe: etiological role of the mitochondrial complex I inhibitor annonacin.* Mov Disord, 2008. **23**(15): p. 2122-8.

70. Lannuzel, A., et al., *Atypical parkinsonism in Guadeloupe: a common risk factor for two closely related phenotypes?* Brain, 2007. **130**(Pt 3): p. 816-27.

71. Caparros-Lefebvre, D. and A. Elbaz, *Possible relation of atypical parkinsonism in the French West Indies with consumption of tropical plants: a case-control study. Caribbean Parkinsonism Study Group.* Lancet, 1999. **354**(9175): p. 281-6.

72. Angibaud, G., C. Gaultier, and O. Rascol, *Atypical parkinsonism and Annonaceae consumption in New Caledonia.* Mov Disord, 2004. **19**(5): p. 603-4.

73. Champy, P., et al., *Annonacin, a lipophilic inhibitor of mitochondrial complex I, induces nigral and striatal neurodegeneration in rats: possible relevance for atypical parkinsonism in Guadeloupe.* J Neurochem, 2004. **88**(1): p. 63-9.

74. Lannuzel, A., et al., *The mitochondrial complex I inhibitor annonacin is toxic to mesencephalic dopaminergic neurons by impairment of energy metabolism.* Neuroscience, 2003. **121**(2): p. 287-96.

75. Quílez, A.M., et al., *Potential therapeutic applications of the genus Annona: Local and traditional uses and pharmacology.* J Ethnopharmacol, 2018. **225**: p. 244-270.

76. Coyle-Gilchrist, I.T., et al., *Prevalence, characteristics, and survival of frontotemporal lobar degeneration syndromes.* Neurology, 2016. **86**(18): p. 1736-43.

77. Ling, H., *Clinical Approach to Progressive Supranuclear Palsy.* J Mov Disord, 2016. **9**(1): p. 3-13.

78. Williams, D.R. and A.J. Lees, *Progressive supranuclear palsy: clinicopathological concepts and diagnostic challenges.* Lancet Neurol, 2009. **8**(3): p. 270-9.

79. Steele, J.C., J.C. Richardson, and J. Olszewski, *Progressive Supranuclear Palsy. A Heterogeneous Degeneration Involving the Brain Stem, Basal Ganglia and Cerebellum with Vertical Gaze and Pseudobulbar Palsy, Nuchal Dystonia and Dementia.* Arch Neurol, 1964. **10**: p. 333-59.

80. Litvan, I., *Cognitive disturbances in progressive supranuclear palsy.* J Neural Transm Suppl, 1994. **42**: p. 69-78.

81. Litvan, I., et al., *Accuracy of clinical criteria for the diagnosis of progressive supranuclear palsy (Steele-Richardson-Olszewski syndrome).* Neurology, 1996. **46**(4): p. 922-30.

82. Maher, E.R. and A.J. Lees, *The clinical features and natural history of the Steele-Richardson-Olszewski syndrome (progressive supranuclear palsy).* Neurology, 1986. **36**(7): p. 1005-8.

83. Srulijes, K., et al., *In vivo comparison of Richardson's syndrome and progressive supranuclear palsy-parkinsonism.* J Neural Transm (Vienna), 2011. **118**(8): p. 1191-7.

84. Charcot, J., *Leçons du Mardi: Policlinique de la Salpêtrière, 1887–1888.* Bureaux du Progrès Médical, Paris: Lesson of June, 1888. **12**: p. 1888.

References

85. Batla, A., R. Nehru, and T. Vijay, *Vertical wrinkling of the forehead or Procerus sign in Progressive Supranuclear Palsy.* J Neurol Sci, 2010. **298**(1-2): p. 148-9.

86. Dickson, D.W., *Neuropathologic differentiation of progressive supranuclear palsy and corticobasal degeneration.* J Neurol, 1999. **246 Suppl 2**: p. II6-15.

87. Wray, S., et al., *Direct analysis of tau from PSP brain identifies new phosphorylation sites and a major fragment of N-terminally cleaved tau containing four microtubule-binding repeats.* J Neurochem, 2008. **105**(6): p. 2343-52.

88. Roy, S., et al., *Electron microscopic study of neurofibrillary tangles in Steele-Richardson-Olszewski syndrome.* Acta Neuropathol, 1974. **29**(2): p. 175-9.

89. Kahlson, M.A. and K.J. Colodner, *Glial Tau Pathology in Tauopathies: Functional Consequences.* J Exp Neurosci, 2015. **9**(Suppl 2): p. 43-50.

90. Arima, K., *Ultrastructural characteristics of tau filaments in tauopathies: immuno-electron microscopic demonstration of tau filaments in tauopathies.* Neuropathology, 2006. **26**(5): p. 475-83.

91. Nishimura, M., et al., *Glial fibrillary tangles with straight tubules in the brains of patients with progressive supranuclear palsy.* Neurosci Lett, 1992. **143**(1-2): p. 35-8.

92. Iwasaki, Y., et al., *Distribution of tuft-shaped astrocytes in the cerebral cortex in progressive supranuclear palsy.* Acta Neuropathol, 2004. **108**(5): p. 399-405.

93. Ikeda, K., *Glial fibrillary tangles and argyrophilic threads: Classification and disease specificity.* Neuropathology, 1996. **16**: p. 71-77.

94. Shibuya, K., et al., *Perivascular orientation of astrocytic plaques and tuft-shaped astrocytes.* Brain Res, 2011. **1404**: p. 50-4.

95. Ferrer, I., et al., *Aging-related tau astrogliopathy (ARTAG): not only tau phosphorylation in astrocytes.* Brain Pathol, 2018. **28**(6): p. 965-985.

96. Ikeda, K., et al., *Thorn-shaped astrocytes: possibly secondarily induced tau-positive glial fibrillary tangles.* Acta Neuropathol, 1995. **90**(6): p. 620-5.

97. Yamada, T. and P.L. McGeer, *Oligodendroglial microtubular masses: an abnormality observed in some human neurodegenerative diseases.* Neurosci Lett, 1990. **120**(2): p. 163-6.

98. Arima, K., et al., *Ultrastructural characterization of the tau-immunoreactive tubules in the oligodendroglial perikarya and their inner loop processes in progressive supranuclear palsy.* Acta Neuropathol, 1997. **93**(6): p. 558-66.

99. Yoshida, M., *Astrocytic inclusions in progressive supranuclear palsy and corticobasal degeneration.* Neuropathology, 2014. **34**(6): p. 555-70.

100. Oyanagi, K., et al., *Substantia nigra in progressive supranuclear palsy, corticobasal degeneration, and parkinsonism-dementia complex of Guam: specific pathological features.* J Neuropathol Exp Neurol, 2001. **60**(4): p. 393-402.

101. Hardman, C.D., et al., *Progressive supranuclear palsy affects both the substantia nigra pars compacta and reticulata.* Exp Neurol, 1997. **144**(1): p. 183-92.

102. Halliday, G.M., et al., *A role for the substantia nigra pars reticulata in the gaze palsy of progressive supranuclear palsy.* Brain, 2000. **123 (Pt 4)**: p. 724-32.

References

103. Hauw, J.J., et al., *Preliminary NINDS neuropathologic criteria for Steele-Richardson-Olszewski syndrome (progressive supranuclear palsy).* Neurology, 1994. **44**(11): p. 2015-9.

104. Zhang, L., et al., *Progressive supranuclear palsy: Neuropathology of patients with a short disease duration due to unexpected death.* Neuropathology, 2021. **41**(3): p. 174-182.

105. Rajput, A. and A.H. Rajput, *Progressive supranuclear palsy: clinical features, pathophysiology and management.* Drugs Aging, 2001. **18**(12): p. 913-25.

106. Kish, S.J., et al., *Progressive supranuclear palsy: relationship between extrapyramidal disturbances, dementia, and brain neurotransmitter markers.* Ann Neurol, 1985. **18**(5): p. 530-6.

107. Pascual, J., et al., *Dopamine D1 and D2 receptors in progressive supranuclear palsy: an autoradiographic study.* Ann Neurol, 1992. **32**(5): p. 703-7.

108. Ruberg, M., et al., *Dopaminergic and cholinergic lesions in progressive supranuclear palsy.* Ann Neurol, 1985. **18**(5): p. 523-9.

109. Landwehrmeyer, B. and J.M. Palacios, *Alterations of neurotransmitter receptors and neurotransmitter transporters in progressive supranuclear palsy.* J Neural Transm Suppl, 1994. **42**: p. 229-46.

110. Lantos, P.L., *The neuropathology of progressive supranuclear palsy.* Journal of Neural Transmission. Supplementa,, 1994. **42**.

111. Perry, T.L., S. Hansen, and K. Jones, *Brain amino acids and glutathione in progressive supranuclear palsy.* Neurology, 1988. **38**(6): p. 943-6.

112. Desai Bradaric, B., et al., *Evidence for angiogenesis in Parkinson's disease, incidental Lewy body disease, and progressive supranuclear palsy.* J Neural Transm (Vienna), 2012. **119**(1): p. 59-71.

113. Gerhard, A., et al., *In vivo imaging of microglial activation with [11C](R)-PK11195 PET in progressive supranuclear palsy.* Mov Disord, 2006. **21**(1): p. 89-93.

114. Ishizawa, K. and D.W. Dickson, *Microglial activation parallels system degeneration in progressive supranuclear palsy and corticobasal degeneration.* J Neuropathol Exp Neurol, 2001. **60**(6): p. 647-57.

115. Foster, N.L., et al., *Progressive subcortical gliosis and progressive supranuclear palsy can have similar clinical and PET abnormalities.* J Neurol Neurosurg Psychiatry, 1992. **55**(8): p. 707-13.

116. Rivest, S., *Regulation of innate immune responses in the brain.* Nat Rev Immunol, 2009. **9**(6): p. 429-39.

117. Tong, J., et al., *Low levels of astroglial markers in Parkinson's disease: relationship to α-synuclein accumulation.* Neurobiol Dis, 2015. **82**: p. 243-253.

118. Fernández-Botrán, R., et al., *Cytokine expression and microglial activation in progressive supranuclear palsy.* Parkinsonism Relat Disord, 2011. **17**(9): p. 683-8.

119. Hagemeier, J., J.J. Geurts, and R. Zivadinov, *Brain iron accumulation in aging and neurodegenerative disorders.* Expert Rev Neurother, 2012. **12**(12): p. 1467-80.

References

120. Halliday, G.M. and C.H. Stevens, *Glia: initiators and progressors of pathology in Parkinson's disease.* Mov Disord, 2011. **26**(1): p. 6-17.

121. Dickson, D.W., R. Rademakers, and M.L. Hutton, *Progressive supranuclear palsy: pathology and genetics.* Brain Pathol, 2007. **17**(1): p. 74-82.

122. Whitwell, J.L., et al., *Clinical correlates of white matter tract degeneration in progressive supranuclear palsy.* Arch Neurol, 2011. **68**(6): p. 753-60.

123. Ishizawa, K., et al., *A qualitative and quantitative study of grumose degeneration in progressive supranuclear palsy.* J Neuropathol Exp Neurol, 2000. **59**(6): p. 513-24.

124. Meyer-Franke, A., et al., *Characterization of the signaling interactions that promote the survival and growth of developing retinal ganglion cells in culture.* Neuron, 1995. **15**(4): p. 805-19.

125. Wang, L.M., et al., *Bioimaging of copper alterations in the aging mouse brain by autoradiography, laser ablation inductively coupled plasma mass spectrometry and immunohistochemistry.* Metallomics, 2010. **2**(5): p. 348-53.

126. Ashraf, A., et al., *Regional Distributions of Iron, Copper and Zinc and Their Relationships With Glia in a Normal Aging Mouse Model.* Front Aging Neurosci, 2019. **11**: p. 351.

127. Pushkar, Y., et al., *Aging results in copper accumulations in glial fibrillary acidic protein-positive cells in the subventricular zone.* Aging Cell, 2013. **12**(5): p. 823-32.

128. Camandola, S. and M.P. Mattson, *Brain metabolism in health, aging, and neurodegeneration.* EMBO J, 2017. **36**(11): p. 1474-1492.

129. Ijomone, O.M., et al., *The aging brain: impact of heavy metal neurotoxicity.* Crit Rev Toxicol, 2020. **50**(9): p. 801-814.

130. White, A.R., K.M. Kanninen, and P.J. Crouch, *Editorial: Metals and neurodegeneration: restoring the balance.* Front Aging Neurosci, 2015. **7**: p. 127.

131. Mezzaroba, L., et al., *The role of zinc, copper, manganese and iron in neurodegenerative diseases.* Neurotoxicology, 2019. **74**: p. 230-241.

132. Pham, A.N. and T.D. Waite, *Cu(II)-catalyzed oxidation of dopamine in aqueous solutions: mechanism and kinetics.* J Inorg Biochem, 2014. **137**: p. 74-84.

133. Spencer, W.A., et al., *Oxidatively generated DNA damage after Cu(II) catalysis of dopamine and related catecholamine neurotransmitters and neurotoxins: Role of reactive oxygen species.* Free Radic Biol Med, 2011. **50**(1): p. 139-47.

134. Zucca, F.A., et al., *Interactions of iron, dopamine and neuromelanin pathways in brain aging and Parkinson's disease.* Prog Neurobiol, 2017. **155**: p. 96-119.

135. Hare, D.J.L., P.; Ayton, S.; Roberts, B. R.; Grimm, R.; George, J. L.; Bishop, D. P.; Beavis, A. D.; Donovan, S. J.; McColl, G.; Volitakis, I.; Masters, C. L.; Adlard, P. A.; Cherny, R. A.; Bush, A. I.; Finkelstein, D.I.; Doble, P. A., *An iron–dopamine index predicts risk of parkinsonian neurodegeneration in the substantia nigra pars compacta.* Chemical Science, 2014. **5**(6): p. 2160-2169.

136. Halliwell, B. and J.M. Gutteridge, *Biologically relevant metal ion-dependent hydroxyl radical generation. An update.* FEBS Lett, 1992. **307**(1): p. 108-12.

References

137. Rae, T.D., et al., *Undetectable intracellular free copper: the requirement of a copper chaperone for superoxide dismutase.* Science, 1999. **284**(5415): p. 805-8.

138. Jung, Y.S., et al., *Effect of pH on Fenton and Fenton-like oxidation.* Environ Technol, 2009. **30**(2): p. 183-90.

139. Alam, Z.I., et al., *A generalised increase in protein carbonyls in the brain in Parkinson's but not incidental Lewy body disease.* J Neurochem, 1997. **69**(3): p. 1326-9.

140. Floor, E. and M.G. Wetzel, *Increased protein oxidation in human substantia nigra pars compacta in comparison with basal ganglia and prefrontal cortex measured with an improved dinitrophenylhydrazine assay.* J Neurochem, 1998. **70**(1): p. 268-75.

141. Trist, B.G., et al., *Amyotrophic lateral sclerosis-like superoxide dismutase 1 proteinopathy is associated with neuronal loss in Parkinson's disease brain.* Acta Neuropathol, 2017. **134**(1): p. 113-127.

142. Sian, J., et al., *Alterations in glutathione levels in Parkinson's disease and other neurodegenerative disorders affecting basal ganglia.* Ann Neurol, 1994. **36**(3): p. 348-55.

143. Su, B., et al., *Chronic oxidative stress causes increased tau phosphorylation in M17 neuroblastoma cells.* Neurosci Lett, 2010. **468**(3): p. 267-71.

144. Perez, M., et al., *Phosphorylated, but not native, tau protein assembles following reaction with the lipid peroxidation product, 4-hydroxy-2-nonenal.* FEBS Lett, 2000. **486**(3): p. 270-4.

145. Feng, Y., et al., *Cleavage of GSK-3beta by calpain counteracts the inhibitory effect of Ser9 phosphorylation on GSK-3beta activity induced by H(2)O(2).* J Neurochem, 2013. **126**(2): p. 234-42.

146. Hoover, B.R., et al., *Tau mislocalization to dendritic spines mediates synaptic dysfunction independently of neurodegeneration.* Neuron, 2010. **68**(6): p. 1067-81.

147. Sayre, L.M., et al., *In situ oxidative catalysis by neurofibrillary tangles and senile plaques in Alzheimer's disease: a central role for bound transition metals.* J Neurochem, 2000. **74**(1): p. 270-9.

148. Kitazawa, M., D. Cheng, and F.M. Laferla, *Chronic copper exposure exacerbates both amyloid and tau pathology and selectively dysregulates cdk5 in a mouse model of AD.* J Neurochem, 2009. **108**(6): p. 1550-60.

149. Bacchella, C., et al., *Binding and Reactivity of Copper to R1 and R3 Fragments of tau Protein.* Inorg Chem, 2020. **59**(1): p. 274-286.

150. Schneider, A., et al., *Phosphorylation that detaches tau protein from microtubules (Ser262, Ser214) also protects it against aggregation into Alzheimer paired helical filaments.* Biochemistry, 1999. **38**(12): p. 3549-58.

151. Crouch, P.J., et al., *Increasing Cu bioavailability inhibits Abeta oligomers and tau phosphorylation.* Proc Natl Acad Sci U S A, 2009. **106**(2): p. 381-6.

References

152. Guo, J., et al., *Copper Promotes Tumorigenesis by Activating the PDK1-AKT Oncogenic Pathway in a Copper Transporter 1 Dependent Manner.* Adv Sci (Weinh), 2021. **8**(18): p. e2004303.

153. Hermida, M.A., J. Dinesh Kumar, and N.R. Leslie, *GSK3 and its interactions with the PI3K/AKT/mTOR signalling network.* Adv Biol Regul, 2017. **65**: p. 5-15.

154. Beurel, E., S.F. Grieco, and R.S. Jope, *Glycogen synthase kinase-3 (GSK3): regulation, actions, and diseases.* Pharmacol Ther, 2015. **148**: p. 114-31.

155. Hickey, J.L., et al., *Copper(II) complexes of hybrid hydroxyquinoline-thiosemicarbazone ligands: GSK3beta inhibition due to intracellular delivery of copper.* Dalton Trans, 2011. **40**(6): p. 1338-47.

156. Crouch, P.J., et al., *The Alzheimer's therapeutic PBT2 promotes amyloid-β degradation and GSK3 phosphorylation via a metal chaperone activity.* J Neurochem, 2011. **119**(1): p. 220-30.

157. Sedjahtera, A., et al., *Targeting metals rescues the phenotype in an animal model of tauopathy.* Metallomics, 2018. **10**(9): p. 1339-1347.

158. Ferrer, I., M. Barrachina, and B. Puig, *Glycogen synthase kinase-3 is associated with neuronal and glial hyperphosphorylated tau deposits in Alzheimer's disease, Pick's disease, progressive supranuclear palsy and corticobasal degeneration.* Acta Neuropathol, 2002. **104**(6): p. 583-91.

159. Holmberg, C.G. and C.B. Laurell, *Investigations in serum copper; nature of serum copper and its relation to the iron-binding protein in human serum.* Acta Chem Scand, 1947. **1**(10): p. 944-50.

160. Stepien, K.B., et al., *Catecholamine melanins. Structural changes induced by copper ions.* Biochim Biophys Acta, 1989. **997**(1-2): p. 49-54.

161. Fridovich, I., *Superoxide dismutases.* Adv Enzymol Relat Areas Mol Biol, 1974. **41**(0): p. 35-97.

162. Buse, G., et al., *Evidence for a copper-coordinated histidine-tyrosine cross-link in the active site of cytochrome oxidase.* Protein Sci, 1999. **8**(5): p. 985-90.

163. Hevel, J.M., S.A. Mills, and J.P. Klinman, *Mutation of a strictly conserved, active-site residue alters substrate specificity and cofactor biogenesis in a copper amine oxidase.* Biochemistry, 1999. **38**(12): p. 3683-93.

164. Konecny, R., et al., *CuZn Superoxide Dismutase Geometry Optimization, Energetics, and Redox Potential Calculations by Density Functional and Electrostatic Methods.* Inorg Chem, 1999. **38**(5): p. 940-950.

165. Zimmerman, A.W., et al., *Hypomyelination in copper-deficient rats. Prenatal and postnatal copper replacement.* Arch Neurol, 1976. **33**(2): p. 111-9.

166. Abudu, N., M.Y. Banjaw, and T. Ljones, *Kinetic studies on the activation of dopamine beta-monooxygenase by copper and vanadium ions.* Eur J Biochem, 1998. **257**(3): p. 622-9.

167. Blades, B., et al., *Copper and lipid metabolism: A reciprocal relationship.* Biochim Biophys Acta Gen Subj, 2021. **1865**(11): p. 129979.

References

168. Ramos, P., et al., *Anatomical region differences and age-related changes in copper, zinc, and manganese levels in the human brain.* Biol Trace Elem Res, 2014. **161**(2): p. 190-201.

169. Tarohda, T., M. Yamamoto, and R. Amamo, *Regional distribution of manganese, iron, copper, and zinc in the rat brain during development.* Anal Bioanal Chem, 2004. **380**(2): p. 240-6.

170. Palm, R., G. Wahlstrom, and G. Hallmans, *Age related changes in weight and the concentrations of zinc and copper in the brain of the adult rat.* Lab Anim, 1990. **24**(3): p. 240-5.

171. Escobar-Khondiker, M., et al., *Annonacin, a natural mitochondrial complex I inhibitor, causes tau pathology in cultured neurons.* J Neurosci, 2007. **27**(29): p. 7827-37.

172. Fu, S., W. Jiang, and W. Zheng, *Age-dependent increase of brain copper levels and expressions of copper regulatory proteins in the subventricular zone and choroid plexus.* Front Mol Neurosci, 2015. **8**: p. 22.

173. Krebs, N., et al., *Assessment of trace elements in human brain using inductively coupled plasma mass spectrometry.* J Trace Elem Med Biol, 2014. **28**(1): p. 1-7.

174. Popescu, B.F., et al., *Iron, copper, and zinc distribution of the cerebellum.* Cerebellum, 2009. **8**(2): p. 74-9.

175. Davies, K.M., et al., *Copper pathology in vulnerable brain regions in Parkinson's disease.* Neurobiol Aging, 2014. **35**(4): p. 858-66.

176. Davies, K.M., et al., *Localization of copper and copper transporters in the human brain.* Metallomics, 2013. **5**(1): p. 43-51.

177. Tiffany-Castiglion, E. and Y. Qian, *Astroglia as metal depots: molecular mechanisms for metal accumulation, storage and release.* Neurotoxicology, 2001. **22**(5): p. 577-92.

178. Dringen, R., I.F. Scheiber, and J.F. Mercer, *Copper metabolism of astrocytes.* Front Aging Neurosci, 2013. **5**: p. 9.

179. Bulcke, F., K. Thiel, and R. Dringen, *Uptake and toxicity of copper oxide nanoparticles in cultured primary brain astrocytes.* Nanotoxicology, 2014. **8**(7): p. 775-85.

180. Lorincz, M.T., *Neurologic Wilson's disease.* Ann N Y Acad Sci, 2010. **1184**: p. 173-87.

181. Kaler, S.G., et al., *Neonatal diagnosis and treatment of Menkes disease.* N Engl J Med, 2008. **358**(6): p. 605-14.

182. Machado, A., et al., *Neurological manifestations in Wilson's disease: Report of 119 cases.* Mov Disord, 2006. **21**(12): p. 2192-6.

183. Menkes, J.H., et al., *A sex-linked recessive disorder with retardation of growth, peculiar hair, and focal cerebral and cerebellar degeneration.* Pediatrics, 1962. **29**: p. 764-79.

184. Moon, N., et al., *Clinical Manifestations of Copper Deficiency: A Case Report and Review of the Literature.* Nutr Clin Pract, 2020.

185. Kaler, S.G., *Inborn errors of copper metabolism.* Handb Clin Neurol, 2013. **113**: p. 1745-54.

References

186. Lenartowicz, M., et al., *Mottled Mice and Non-Mammalian Models of Menkes Disease.* Front Mol Neurosci, 2015. **8**: p. 72.

187. Cecchi, C. and P. Avner, *Genomic organization of the mottled gene, the mouse homologue of the human Menkes disease gene.* Genomics, 1996. **37**(1): p. 96-104.

188. Fraser, A.S., T. Nay, and H.N. Turner, *Growth of the mouse coat. II. Effect of sex and pregnancy.* Aust J Biol Sci, 1953. **6**(4): p. 645-56.

189. Kim, B.E. and M.J. Petris, *Phenotypic diversity of Menkes disease in mottled mice is associated with defects in localisation and trafficking of the ATP7A protein.* J Med Genet, 2007. **44**(10): p. 641-6.

190. Grimes, A., et al., *Molecular basis of the brindled mouse mutant (Mo(br)): a murine model of Menkes disease.* Hum Mol Genet, 1997. **6**(7): p. 1037-42.

191. Harris, D., et al., *Bone marrow from blotchy mice is dispensable to regulate blood copper and aortic pathologies but required for inflammatory mediator production in LDLR-deficient mice during chronic angiotensin II infusion.* Ann Vasc Surg, 2015. **29**(2): p. 328-40.

192. Yoshimura, N., et al., *Histochemical localization of copper in various organs of brindled mice after copper therapy.* Pathol Int, 1995. **45**(1): p. 10-8.

193. Yajima, K. and K. Suzuki, *Neuronal Degeneration in the Brain of the Brindled Mouse—A Light Microscope Study.* Journal of Neuropathology & Experimental Neurology, 1979. **38**(1): p. 35-46.

194. Yoshimura, N., et al., *Neuronal Degeneration in the Brain of Brindled Mice: Combined Histochemical and Biochemical Studies on Cytochrome Oxidase and Superoxide Dismutase Activities.* Neuropathology, 1994. **14**(2): p. 81-89.

195. Lenartowicz, M., et al., *Prenatal treatment of mosaic mice (Atp7a mo-ms) mouse model for Menkes disease, with copper combined by dimethyldithiocarbamate (DMDTC).* PLoS One, 2012. **7**(7): p. e40400.

196. Hilton, J.B., et al., *Disrupted copper availability in sporadic ALS: Implications for CuII(atsm) as a treatment option.* bioRxiv, 2020.

197. James, S.A., et al., *Elevated labile Cu is associated with oxidative pathology in Alzheimer disease.* Free Radic Biol Med, 2012. **52**(2): p. 298-302.

198. Lovell, M.A., et al., *Copper, iron and zinc in Alzheimer's disease senile plaques.* J Neurol Sci, 1998. **158**(1): p. 47-52.

199. Uitti, R.J., et al., *Regional metal concentrations in Parkinson's disease, other chronic neurological diseases, and control brains.* Can J Neurol Sci, 1989. **16**(3): p. 310-4.

200. Exley, C., *Aluminium and iron, but neither copper nor zinc, are key to the precipitation of beta-sheets of Abeta_{42} in senile plaque cores in Alzheimer's disease.* J Alzheimers Dis, 2006. **10**(2-3): p. 173-7.

201. Odetti, P., et al., *Lipoperoxidation is selectively involved in progressive supranuclear palsy.* J Neuropathol Exp Neurol, 2000. **59**(5): p. 393-7.

References

202. Schonhaut, D.R., et al., *(18) F-flortaucipir tau positron emission tomography distinguishes established progressive supranuclear palsy from controls and Parkinson disease: A multicenter study.* Ann Neurol, 2017. **82**(4): p. 622-634.

203. Aquino, D., et al., *Age-related iron deposition in the basal ganglia: quantitative analysis in healthy subjects.* Radiology, 2009. **252**(1): p. 165-72.

204. Malpetti, M., et al., *Neuroinflammation predicts disease progression in progressive supranuclear palsy.* J Neurol Neurosurg Psychiatry, 2021. **92**(7): p. 769-775.

205. Messerschmidt, A. and R. Huber, *The blue oxidases, ascorbate oxidase, laccase and ceruloplasmin. Modelling and structural relationships.* Eur J Biochem, 1990. **187**(2): p. 341-52.

206. Chen, Z., et al., *Multi-copper ferroxidase deficiency leads to iron accumulation and oxidative damage in astrocytes and oligodendrocytes.* Sci Rep, 2019. **9**(1): p. 9437.

207. Osaki, S. and D.A. Johnson, *Mobilization of liver iron by ferroxidase (ceruloplasmin).* J Biol Chem, 1969. **244**(20): p. 5757-8.

208. Ayton, S., et al., *Ceruloplasmin dysfunction and therapeutic potential for Parkinson disease.* Ann Neurol, 2013. **73**(4): p. 554-9.

209. Loeffler, D.A., A.A. Sima, and P.A. LeWitt, *Ceruloplasmin immunoreactivity in neurodegenerative disorders.* Free Radic Res, 2001. **35**(2): p. 111-8.

210. Scott, K.C.T., . J.R. , *Compartmental model of copper metabolism in adult men.* The Journal of Nutritional Biochemistry, 1994. **5**(7): p. 342-350.

211. Linder, M.C. and M. Hazegh-Azam, *Copper biochemistry and molecular biology.* Am J Clin Nutr, 1996. **63**(5): p. 797S-811S.

212. Wapnir, R.A., *Copper absorption and bioavailability.* Am J Clin Nutr, 1998. **67**(5 Suppl): p. 1054S-1060S.

213. Fransson, G.B. and B. Lonnerdal, *Distribution of trace elements and minerals in human and cow's milk.* Pediatr Res, 1983. **17**(11): p. 912-5.

214. Lonnerdal, B., *Trace element absorption in infants as a foundation to setting upper limits for trace elements in infant formulas.* J Nutr, 1989. **119**(12 Suppl): p. 1839-44; discussion 1845.

215. Casey, C.E., M.C. Neville, and K.M. Hambidge, *Studies in human lactation: secretion of zinc, copper, and manganese in human milk.* Am J Clin Nutr, 1989. **49**(5): p. 773-85.

216. Khaghani, S., et al., *Zinc and copper concentrations in human milk and infant formulas.* Iran J Pediatr, 2010. **20**(1): p. 53-7.

217. Mertz, W., *Mineral elements: new perspectives.* J Am Diet Assoc, 1980. **77**(3): p. 258-63.

218. Chubaka, C.E., et al., *Lead, Zinc, Copper, and Cadmium Content of Water from South Australian Rainwater Tanks.* Int J Environ Res Public Health, 2018. **15**(7).

219. Gletsu-Miller, N., et al., *Incidence and prevalence of copper deficiency following roux-en-y gastric bypass surgery.* Int J Obes (Lond), 2012. **36**(3): p. 328-35.

References

220. Halfdanarson, T.R., et al., *Copper deficiency in celiac disease.* J Clin Gastroenterol, 2009. **43**(2): p. 162-4.

221. Weigand, E., *Absorption of trace elements: zinc.* Int J Vitam Nutr Res Suppl, 1983. **25**: p. 67-81.

222. Raghupathy, L. and V.N. Sharma, *Zinc and copper concentrations in the hair of workers from zinc based industries in India.* Sci Total Environ, 1985. **41**(1): p. 73-8.

223. Lanska, D.J. and B. Remler, *Myelopathy among zinc-smelter workers in Upper Silesia during the late 19th century.* Neurology, 2014. **82**(13): p. 1175-9.

224. Nations, S.P., et al., *Denture cream: an unusual source of excess zinc, leading to hypocupremia and neurologic disease.* Neurology, 2008. **71**(9): p. 639-43.

225. Penland, J.G. and J.R. Prohaska, *Abnormal motor function persists following recovery from perinatal copper deficiency in rats.* J Nutr, 2004. **134**(8): p. 1984-8.

226. Prohaska, J.R. and R.G. Hoffman, *Auditory startle response is diminished in rats after recovery from perinatal copper deficiency.* J Nutr, 1996. **126**(3): p. 618-27.

227. Prohaska, J.R., et al., *Effect of dietary copper deficiency on the distribution of dopamine and norepinephrine in mice and rats.* J Nutr Biochem, 1990. **1**(3): p. 149-54.

228. Liu, N., et al., *Transcuprein is a macroglobulin regulated by copper and iron availability.* J Nutr Biochem, 2007. **18**(9): p. 597-608.

229. Allen, K.G. and L.M. Klevay, *Copper: an antioxidant nutrient for cardiovascular health.* Curr Opin Lipidol, 1994. **5**(1): p. 22-8.

230. Sharonov, B.P. and N. Govorova, *[Oxidation of ceruloplasmin by hypochlorite. The loss of blue color and preservation of oxidase activity].* Biokhimiia, 1990. **55**(6): p. 1145-8.

231. Monnot, A.D., et al., *Regulation of brain copper homeostasis by the brain barrier systems: effects of Fe-overload and Fe-deficiency.* Toxicol Appl Pharmacol, 2011. **256**(3): p. 249-57.

232. Dringen, R., I. Scheiber, and F. Bulcke, *Copper metabolism of astrocytes.* Springerplus, 2015. **4**(Suppl 1): p. L3.

233. Burdo, J.R., et al., *Distribution of divalent metal transporter 1 and metal transport protein 1 in the normal and Belgrade rat.* J Neurosci Res, 2001. **66**(6): p. 1198-207.

234. Codazzi, F., et al., *Iron entry in neurons and astrocytes: a link with synaptic activity.* Front Mol Neurosci, 2015. **8**: p. 18.

235. Scheiber, I.F. and R. Dringen, *Astrocyte functions in the copper homeostasis of the brain.* Neurochem Int, 2013. **62**(5): p. 556-65.

236. Ohgami, R.S., et al., *The Steap proteins are metalloreductases.* Blood, 2006. **108**(4): p. 1388-94.

237. Gybina, A.A. and J.R. Prohaska, *Variable response of selected cuproproteins in rat choroid plexus and cerebellum following perinatal copper deficiency.* Genes Nutr, 2006. **1**(1): p. 51-9.

References

238. Zheng, W. and A.D. Monnot, *Regulation of brain iron and copper homeostasis by brain barrier systems: implication in neurodegenerative diseases.* Pharmacol Ther, 2012. **133**(2): p. 177-88.

239. Kuo, Y.M., et al., *The copper transporter CTR1 provides an essential function in mammalian embryonic development.* Proc Natl Acad Sci U S A, 2001. **98**(12): p. 6836-41.

240. Lee, J., et al., *Biochemical characterization of the human copper transporter Ctr1.* J Biol Chem, 2002. **277**(6): p. 4380-7.

241. Ogra, Y., M. Aoyama, and K.T. Suzuki, *Protective role of metallothionein against copper depletion.* Arch Biochem Biophys, 2006. **451**(2): p. 112-8.

242. Suzuki, K.T., et al., *Roles of metallothionein in copper homeostasis: responses to Cu-deficient diets in mice.* J Inorg Biochem, 2002. **88**(2): p. 173-82.

243. Maryon, E.B., et al., *Rate and regulation of copper transport by human copper transporter 1 (hCTR1).* J Biol Chem, 2013. **288**(25): p. 18035-46.

244. Lafleur, M.V., et al., *The ambivalent role of glutathione in the protection of DNA against singlet oxygen.* Free Radic Res, 1994. **21**(1): p. 9-17.

245. Jimenez, I. and H. Speisky, *Effects of copper ions on the free radical-scavenging properties of reduced gluthathione: implications of a complex formation.* J Trace Elem Med Biol, 2000. **14**(3): p. 161-7.

246. Dodani, S.C., et al., *A targetable fluorescent sensor reveals that copper-deficient SCO1 and SCO2 patient cells prioritize mitochondrial copper homeostasis.* J Am Chem Soc, 2011. **133**(22): p. 8606-16.

247. Rothstein, J.D., et al., *The copper chaperone CCS is abundant in neurons and astrocytes in human and rodent brain.* J Neurochem, 1999. **72**(1): p. 422-9.

248. Torres, A.S., et al., *Copper stabilizes a heterodimer of the yCCS metallochaperone and its target superoxide dismutase.* J Biol Chem, 2001. **276**(42): p. 38410-6.

249. Wong, P.C., et al., *Copper chaperone for superoxide dismutase is essential to activate mammalian Cu/Zn superoxide dismutase.* Proc Natl Acad Sci U S A, 2000. **97**(6): p. 2886-91.

250. Beckman, J.S., et al., *CCS knockout mice establish an alternative source of copper for SOD in ALS.* Free Radic Biol Med, 2002. **33**(10): p. 1433-5.

251. Hatori, Y. and S. Lutsenko, *The Role of Copper Chaperone Atox1 in Coupling Redox Homeostasis to Intracellular Copper Distribution.* Antioxidants (Basel), 2016. **5**(3).

252. Setty, S.R., et al., *Cell-specific ATP7A transport sustains copper-dependent tyrosinase activity in melanosomes.* Nature, 2008. **454**(7208): p. 1142-6.

253. Kosonen, T., et al., *Incorporation of copper into lysyl oxidase.* Biochem J, 1997. **327 (Pt 1)**: p. 283-9.

254. Terada, K., et al., *Restoration of holoceruloplasmin synthesis in LEC rat after infusion of recombinant adenovirus bearing WND cDNA.* J Biol Chem, 1998. **273**(3): p. 1815-20.

References

255. Steveson, T.C., et al., *Menkes protein contributes to the function of peptidylglycine alpha-amidating monooxygenase.* Endocrinology, 2003. **144**(1): p. 188-200.

256. Niciu, M.J., et al., *Altered ATP7A expression and other compensatory responses in a murine model of Menkes disease.* Neurobiol Dis, 2007. **27**(3): p. 278-91.

257. Kodama, H., et al., *Genetic expression of Menkes disease in cultured astrocytes of the macular mouse.* J Inherit Metab Dis, 1991. **14**(6): p. 896-901.

258. Petris, M.J., et al., *Ligand-regulated transport of the Menkes copper P-type ATPase efflux pump from the Golgi apparatus to the plasma membrane: a novel mechanism of regulated trafficking.* Embo j, 1996. **15**(22): p. 6084-95.

259. Vonk, W.I., et al., *Liver-specific Commd1 knockout mice are susceptible to hepatic copper accumulation.* PLoS One, 2011. **6**(12): p. e29183.

260. Forman, O.P., et al., *Characterization of the COMMD1 (MURR1) mutation causing copper toxicosis in Bedlington terriers.* Anim Genet, 2005. **36**(6): p. 497-501.

261. Klomp, A.E., et al., *The ubiquitously expressed MURR1 protein is absent in canine copper toxicosis.* J Hepatol, 2003. **39**(5): p. 703-9.

262. Narindrasorasak, S., et al., *Characterization and copper binding properties of human COMMD1 (MURR1).* Biochemistry, 2007. **46**(11): p. 3116-28.

263. Tao, T.Y., et al., *The copper toxicosis gene product Murr1 directly interacts with the Wilson disease protein.* J Biol Chem, 2003. **278**(43): p. 41593-6.

264. Miyayama, T., et al., *Roles of COMM-domain-containing 1 in stability and recruitment of the copper-transporting ATPase in a mouse hepatoma cell line.* Biochem J, 2010. **429**(1): p. 53-61.

265. de Bie, P., et al., *Distinct Wilson's disease mutations in ATP7B are associated with enhanced binding to COMMD1 and reduced stability of ATP7B.* Gastroenterology, 2007. **133**(4): p. 1316-26.

266. Vonk, W.I., et al., *The Copper Metabolism MURR1 domain protein 1 (COMMD1) modulates the aggregation of misfolded protein species in a client-specific manner.* PLoS One, 2014. **9**(4): p. e92408.

267. Wen, M.H., et al., *Crossroads between membrane trafficking machinery and copper homeostasis in the nerve system.* Open Biol, 2021. **11**(12): p. 210128.

268. Bucher, P., *Weight matrix descriptions of four eukaryotic RNA polymerase II promoter elements derived from 502 unrelated promoter sequences.* J Mol Biol, 1990. **212**(4): p. 563-78.

269. Song, I.S., et al., *Transcription factor Sp1 plays an important role in the regulation of copper homeostasis in mammalian cells.* Mol Pharmacol, 2008. **74**(3): p. 705-13.

270. Yuan, S., et al., *Copper-finger protein of Sp1: the molecular basis of copper sensing.* Metallomics, 2017. **9**(8): p. 1169-1175.

271. Khalimonchuk, O., K. Ostermann, and G. Rödel, *Evidence for the association of yeast mitochondrial ribosomes with Cox11p, a protein required for the Cu(B) site formation of cytochrome c oxidase.* Curr Genet, 2005. **47**(4): p. 223-33.

References

272. Arnesano, F., et al., *Ortholog search of proteins involved in copper delivery to cytochrome C oxidase and functional analysis of paralogs and gene neighbors by genomic context.* J Proteome Res, 2005. **4**(1): p. 63-70.

273. Rigby, K., et al., *Mapping the functional interaction of Sco1 and Cox2 in cytochrome oxidase biogenesis.* J Biol Chem, 2008. **283**(22): p. 15015-22.

274. Zeng, H., J.T. Saari, and W.T. Johnson, *Copper deficiency decreases complex IV but not complex I, II, III, or V in the mitochondrial respiratory chain in rat heart.* J Nutr, 2007. **137**(1): p. 14-8.

275. Leary, S.C., et al., *The human cytochrome c oxidase assembly factors SCO1 and SCO2 have regulatory roles in the maintenance of cellular copper homeostasis.* Cell Metab, 2007. **5**(1): p. 9-20.

276. Prohaska, J.R. and W.R. Bailey, *Persistent regional changes in brain copper, cuproenzymes and catecholamines following perinatal copper deficiency in mice.* J Nutr, 1993. **123**(7): p. 1226-34.

277. Lee, J., J.R. Prohaska, and D.J. Thiele, *Essential role for mammalian copper transporter Ctr1 in copper homeostasis and embryonic development.* Proc Natl Acad Sci U S A, 2001. **98**(12): p. 6842-7.

278. Foti, S.C., et al., *Cerebral mitochondrial electron transport chain dysfunction in multiple system atrophy and Parkinson's disease.* Sci Rep, 2019. **9**(1): p. 6559.

279. Bosetti, F., et al., *Cytochrome c oxidase and mitochondrial F1F0-ATPase (ATP synthase) activities in platelets and brain from patients with Alzheimer's disease.* Neurobiol Aging, 2002. **23**(3): p. 371-6.

280. Patel, B.N. and S. David, *A novel glycosylphosphatidylinositol-anchored form of ceruloplasmin is expressed by mammalian astrocytes.* J Biol Chem, 1997. **272**(32): p. 20185-90.

281. Linder, M.C., *Apoceruloplasmin: Abundance, Detection, Formation, and Metabolism.* Biomedicines, 2021. **9**(3).

282. Musci, G., F. Polticelli, and M.C. Bonaccorsi di Patti, *Ceruloplasmin-ferroportin system of iron traffic in vertebrates.* World J Biol Chem, 2014. **5**(2): p. 204-15.

283. Chang, Y.Z., et al., *Effects of development and iron status on ceruloplasmin expression in rat brain.* J Cell Physiol, 2005. **204**(2): p. 623-31.

284. Tapryal, N., et al., *Reactive oxygen species regulate ceruloplasmin by a novel mRNA decay mechanism involving its 3'-untranslated region: implications in neurodegenerative diseases.* J Biol Chem, 2009. **284**(3): p. 1873-83.

285. Conley, L., T.L. Geurs, and L.A. Levin, *Transcriptional regulation of ceruloplasmin by an IL-6 response element pathway.* Brain Res Mol Brain Res, 2005. **139**(2): p. 235-41.

286. Hellman, N.E., et al., *Mechanisms of copper incorporation into human ceruloplasmin.* J Biol Chem, 2002. **277**(48): p. 46632-8.

287. Pierson, H., et al., *The Function of ATPase Copper Transporter ATP7B in Intestine.* Gastroenterology, 2018. **154**(1): p. 168-180.e5.

References

288. Patel, B.N., et al., *Ceruloplasmin regulates iron levels in the CNS and prevents free radical injury.* J Neurosci, 2002. **22**(15): p. 6578-86.

289. Hartmann, H.A. and M.A. Evenson, *Deficiency of copper can cause neuronal degeneration.* Med Hypotheses, 1992. **38**(1): p. 75-85.

290. Snaedal, J., et al., *Copper, ceruloplasmin and superoxide dismutase in patients with Alzheimer's disease . a case-control study.* Dement Geriatr Cogn Disord, 1998. **9**(5): p. 239-42.

291. Brewer, G.J., et al., *Copper and ceruloplasmin abnormalities in Alzheimer's disease.* Am J Alzheimers Dis Other Demen, 2010. **25**(6): p. 490-7.

292. Zanardi, A., et al., *Ceruloplasmin replacement therapy ameliorates neurological symptoms in a preclinical model of aceruloplasminemia.* EMBO Mol Med, 2018. **10**(1): p. 91-106.

293. Ernsberger, U., et al., *The expression of dopamine beta-hydroxylase, tyrosine hydroxylase, and Phox2 transcription factors in sympathetic neurons: evidence for common regulation during noradrenergic induction and diverging regulation later in development.* Mech Dev, 2000. **92**(2): p. 169-77.

294. Gavrilovic, L., et al., *Effect of immobilization stress on gene expression of catecholamine biosynthetic enzymes in heart auricles of socially isolated rats.* Braz J Med Biol Res, 2009. **42**(12): p. 1185-90.

295. Bergman, J., et al., *The Human Adrenal Gland Proteome Defined by Transcriptomics and Antibody-Based Profiling.* Endocrinology, 2017. **158**(2): p. 239-251.

296. Rahman, M.K., et al., *Dopamine-beta-Hydroxylase (DBH), Its Cofactors and Other Biochemical Parameters in the Serum of Neurological Patients in Bangladesh.* Int J Biomed Sci, 2009. **5**(4): p. 395-401.

297. Schmidt, K., et al., *ATP7A and ATP7B copper transporters have distinct functions in the regulation of neuronal dopamine-β-hydroxylase.* J Biol Chem, 2018. **293**(52): p. 20085-20098.

298. Hong, S.J., et al., *Transcription factor GATA-3 regulates the transcriptional activity of dopamine beta-hydroxylase by interacting with Sp1 and AP4.* Neurochem Res, 2008. **33**(9): p. 1821-31.

299. Prohaska, J.R. and B. Brokate, *Copper deficiency alters rat dopamine beta-monooxygenase mRNA and activity.* J Nutr, 1999. **129**(12): p. 2147-53.

300. Kaler, S.G. and C.S. Holmes, *Catecholamine metabolites affected by the copper-dependent enzyme dopamine-beta-hydroxylase provide sensitive biomarkers for early diagnosis of menkes disease and viral-mediated ATP7A gene therapy.* Adv Pharmacol, 2013. **68**: p. 223-33.

301. Vulpe, C.D., et al., *Hephaestin, a ceruloplasmin homologue implicated in intestinal iron transport, is defective in the sla mouse.* Nat Genet, 1999. **21**(2): p. 195-9.

302. Syed, B.A., et al., *Analysis of the human hephaestin gene and protein: comparative modelling of the N-terminus ecto-domain based upon ceruloplasmin.* Protein Eng, 2002. **15**(3): p. 205-14.

References

303. Jiang, R., et al., *Hephaestin and ceruloplasmin play distinct but interrelated roles in iron homeostasis in mouse brain.* J Nutr, 2015. **145**(5): p. 1003-9.

304. Zoller, H., et al., *Duodenal cytochrome b and hephaestin expression in patients with iron deficiency and hemochromatosis.* Gastroenterology, 2003. **125**(3): p. 746-54.

305. Han, O. and M. Wessling-Resnick, *Copper repletion enhances apical iron uptake and transepithelial iron transport by Caco-2 cells.* Am J Physiol Gastrointest Liver Physiol, 2002. **282**(3): p. G527-33.

306. Chen, H., et al., *Decreased hephaestin activity in the intestine of copper-deficient mice causes systemic iron deficiency.* J Nutr, 2006. **136**(5): p. 1236-41.

307. Zheng, J., et al., *Multi-Copper Ferroxidase-Deficient Mice Have Increased Brain Iron Concentrations and Learning and Memory Deficits.* J Nutr, 2018. **148**(4): p. 643-649.

308. Zhao, L., et al., *Cp/Heph mutant mice have iron-induced neurodegeneration diminished by deferiprone.* J Neurochem, 2015. **135**(5): p. 958-74.

309. Schulz, K., et al., *Iron efflux from oligodendrocytes is differentially regulated in gray and white matter.* J Neurosci, 2011. **31**(37): p. 13301-11.

310. Levitt, P., J.E. Pintar, and X.O. Breakefield, *Immunocytochemical demonstration of monoamine oxidase B in brain astrocytes and serotonergic neurons.* Proc Natl Acad Sci U S A, 1982. **79**(20): p. 6385-9.

311. Jo, S., et al., *GABA from reactive astrocytes impairs memory in mouse models of Alzheimer's disease.* Nat Med, 2014. **20**(8): p. 886-96.

312. Engberg, G., T. Elebring, and H. Nissbrandt, *Deprenyl (selegiline), a selective MAO-B inhibitor with active metabolites; effects on locomotor activity, dopaminergic neurotransmission and firing rate of nigral dopamine neurons.* J Pharmacol Exp Ther, 1991. **259**(2): p. 841-7.

313. Nara, S., B. Gomes, and K.T. Yasunobu, *Amine oxidase. VII. Beef liver mitochondrial monoamine oxidase, a copper-containing protein.* J Biol Chem, 1966. **241**(12): p. 2774-80.

314. Hunt, D.M., *Catecholamine biosynthesis and the activity of a number of copper-dependent enzymes in the copper deficient mottled mouse mutants.* Comp Biochem Physiol C Comp Pharmacol, 1977. **57**(1): p. 79-83.

315. Shih, J.C. and K. Chen, *Regulation of MAO-A and MAO-B gene expression.* Curr Med Chem, 2004. **11**(15): p. 1995-2005.

316. Tong, J., et al., *Brain monoamine oxidase B and A in human parkinsonian dopamine deficiency disorders.* Brain, 2017. **140**(9): p. 2460-2474.

317. Chang, L.Y., et al., *Molecular immunocytochemistry of the CuZn superoxide dismutase in rat hepatocytes.* J Cell Biol, 1988. **107**(6 Pt 1): p. 2169-79.

318. Crapo, J.D., et al., *Copper,zinc superoxide dismutase is primarily a cytosolic protein in human cells.* Proc Natl Acad Sci U S A, 1992. **89**(21): p. 10405-9.

319. Keller, G.A., et al., *Cu,Zn superoxide dismutase is a peroxisomal enzyme in human fibroblasts and hepatoma cells.* Proc Natl Acad Sci U S A, 1991. **88**(16): p. 7381-5.

320. Sturtz, L.A., et al., *A fraction of yeast Cu,Zn-superoxide dismutase and its metallochaperone, CCS, localize to the intermembrane space of mitochondria. A physiological role for SOD1 in guarding against mitochondrial oxidative damage.* J Biol Chem, 2001. **276**(41): p. 38084-9.

321. Furukawa, Y., *Redox environment is an intracellular factor to operate distinct pathways for aggregation of Cu,Zn-superoxide dismutase in amyotrophic lateral sclerosis.* Front Cell Neurosci, 2013. **7**: p. 240.

322. Arnesano, F., et al., *The unusually stable quaternary structure of human Cu,Zn-superoxide dismutase 1 is controlled by both metal occupancy and disulfide status.* J Biol Chem, 2004. **279**(46): p. 47998-8003.

323. Banci, L., et al., *Backbone dynamics of human Cu,Zn superoxide dismutase and of its monomeric F50E/G51E/E133Q mutant: the influence of dimerization on mobility and function.* Biochemistry, 2000. **39**(31): p. 9108-18.

324. Bonaccorsi di Patti, M.C., et al., *Analysis of Cu,ZnSOD conformational stability by differential scanning calorimetry.* Methods Enzymol, 2002. **349**: p. 49-61.

325. Roe, J.A., et al., *Differential scanning calorimetry of Cu,Zn-superoxide dismutase, the apoprotein, and its zinc-substituted derivatives.* Biochemistry, 1988. **27**(3): p. 950-8.

326. Furukawa, Y., A.S. Torres, and T.V. O'Halloran, *Oxygen-induced maturation of SOD1: a key role for disulfide formation by the copper chaperone CCS.* EMBO J, 2004. **23**(14): p. 2872-81.

327. Culotta, V.C., et al., *The copper chaperone for superoxide dismutase.* J Biol Chem, 1997. **272**(38): p. 23469-72.

328. Kabuta, T., Y. Suzuki, and K. Wada, *Degradation of amyotrophic lateral sclerosis-linked mutant Cu,Zn-superoxide dismutase proteins by macroautophagy and the proteasome.* J Biol Chem, 2006. **281**(41): p. 30524-33.

329. Furukawa, Y., et al., *Complete loss of post-translational modifications triggers fibrillar aggregation of SOD1 in the familial form of amyotrophic lateral sclerosis.* J Biol Chem, 2008. **283**(35): p. 24167-76.

330. Wang, J., et al., *Copper-binding-site-null SOD1 causes ALS in transgenic mice: aggregates of non-native SOD1 delineate a common feature.* Hum Mol Genet, 2003. **12**(21): p. 2753-64.

331. Trist, B.G., et al., *Superoxide Dismutase 1 in Health and Disease: How a Frontline Antioxidant Becomes Neurotoxic.* Angew Chem Int Ed Engl, 2021. **60**(17): p. 9215-9246.

332. Forsberg, K., et al., *Glial nuclear aggregates of superoxide dismutase-1 are regularly present in patients with amyotrophic lateral sclerosis.* Acta Neuropathol, 2011. **121**(5): p. 623-34.

333. Kato, S., *Amyotrophic lateral sclerosis models and human neuropathology: similarities and differences.* Acta Neuropathol, 2008. **115**(1): p. 97-114.

334. Hollander, J., et al., *Superoxide dismutase gene expression in skeletal muscle: fiber-specific effect of age.* Mech Ageing Dev, 2000. **116**(1): p. 33-45.

References

335. Roberts, B.R., et al., *Oral treatment with Cu(II)(atsm) increases mutant SOD1 in vivo but protects motor neurons and improves the phenotype of a transgenic mouse model of amyotrophic lateral sclerosis.* J Neurosci, 2014. **34**(23): p. 8021-31.

336. Williams, J.R., et al., *Copper delivery to the CNS by CuATSM effectively treats motor neuron disease in SODG93A mice co-expressing the Copper-Chaperone-for-SOD.* Neurobiology of disease, 2016. **89**: p. 1-9.

337. Kato, T., et al., *Lewy body-like hyaline inclusions in sporadic motor neuron disease are ubiquitinated.* Acta Neuropathol, 1989. **77**(4): p. 391-6.

338. Kato, S., et al., *Copper chaperone for superoxide dismutase co-aggregates with superoxide dismutase 1 (SOD1) in neuronal Lewy body-like hyaline inclusions: an immunohistochemical study on familial amyotrophic lateral sclerosis with SOD1 gene mutation.* Acta Neuropathol, 2001. **102**(3): p. 233-8.

339. Shibata, N., et al., *Immunohistochemical study on superoxide dismutases in spinal cords from autopsied patients with amyotrophic lateral sclerosis.* Dev Neurosci, 1996. **18**(5-6): p. 492-8.

340. Nishiyama, K., et al., *Cu/Zn superoxide dismutase-like immunoreactivity is present in Lewy bodies from Parkinson disease: a light and electron microscopic immunocytochemical study.* Acta Neuropathol, 1995. **89**(6): p. 471-4.

341. Trist, B.G., et al., *Accumulation of dysfunctional SOD1 protein in Parkinson's disease is not associated with mutations in the SOD1 gene.* Acta Neuropathol, 2018. **135**(1): p. 155-156.

342. Kato, S., et al., *Pathological characterization of astrocytic hyaline inclusions in familial amyotrophic lateral sclerosis.* Am J Pathol, 1997. **151**(2): p. 611-20.

343. Chou, S.M., H.S. Wang, and K. Komai, *Colocalization of NOS and SOD1 in neurofilament accumulation within motor neurons of amyotrophic lateral sclerosis: an immunohistochemical study.* J Chem Neuroanat, 1996. **10**(3-4): p. 249-58.

344. Okamoto, Y., et al., *Colocalization of 14-3-3 proteins with SOD1 in Lewy body-like hyaline inclusions in familial amyotrophic lateral sclerosis cases and the animal model.* PLoS One, 2011. **6**(5): p. e20427.

345. Templeton, D.M., *Biomedical aspects of trace element speciation.* Fresenius' journal of analytical chemistry, 1999. **363**: p. 505-511.

346. Walsh, A., *The application of atomic absorption spectra to chemical analysis.* Spectrochimica Acta, 1955. **7**: p. 108-117.

347. Robinson, J.W., *Atomic Absorption Spectroscopy.* Analytical Chemistry, 1960. **32**(8): p. 17A-29A.

348. Garcia-Serres, R., et al., *Contribution of Mössbauer spectroscopy to the investigation of Fe/S biogenesis.* J Biol Inorg Chem, 2018. **23**(4): p. 635-644.

349. Debrunner, P.G. and H. Frauenfelder, *Introduction to the Mössbauer effect.* An Introduction to Mössbauer Spectroscopy, 1971: p. 1-22.

350. Gütlich, P., E. Bill, and A. Trautwein, *Mössbauer spectroscopy and transition metal chemistry fundamentals and application*. 2011, Berlin ;: Springer.

References

351. Maddock, A.G., *Mossbauer spectroscopy: principles and applications*. 1997: Elsevier.

352. Hare, D.J., M. Gerlach, and P. Riederer, *Considerations for measuring iron in post-mortem tissue of Parkinson's disease patients.* Journal of neural transmission, 2012. **119**: p. 1515-1521.

353. Porcaro, F., et al., *Advances in element speciation analysis of biomedical samples using synchrotron-based techniques.* TrAC Trends in Analytical Chemistry, 2018. **104**: p. 22-41.

354. Hackett, M.J., et al., *"A spectroscopic picture paints 1000 words" mapping iron speciation in brain tissue with "full spectrum per pixel" X-ray absorption near-edge structure spectroscopy.* Clinical Spectroscopy, 2021. **3**: p. 100017.

355. Ide-Ektessabi, A. and M. Rabionet, *The role of trace metallic elements in neurodegenerative disorders: quantitative analysis using XRF and XANES spectroscopy.* Anal Sci, 2005. **21**(7): p. 885-92.

356. Ortega, R., G. Devès, and A. Carmona, *Bio-metals imaging and speciation in cells using proton and synchrotron radiation X-ray microspectroscopy.* J R Soc Interface, 2009. **6 Suppl 5**(Suppl 5): p. S649-58.

357. Kabatas, S., et al., *Boron-Containing Probes for Non-optical High-Resolution Imaging of Biological Samples.* Angew Chem Int Ed Engl, 2019. **58**(11): p. 3438-3443.

358. Vreja, I.C., et al., *Secondary-ion mass spectrometry of genetically encoded targets.* Angew Chem Int Ed Engl, 2015. **54**(19): p. 5784-8.

359. Nuñez, J., et al., *NanoSIMS for biological applications: Current practices and analyses.* Biointerphases, 2017. **13**(3): p. 03b301.

360. Quintana, C., et al., *Morphological and chemical studies of pathological human and mice brain at the subcellular level: correlation between light, electron, and nanosims microscopies.* Microsc Res Tech, 2007. **70**(4): p. 281-95.

361. Li, Q., et al., *Research progress of nano-scale secondary ion mass spectrometry (NanoSIMS) in soil science: Evolution, applications, and challenges.* Science of The Total Environment, 2023. **905**: p. 167257.

362. Wilschefski, S.C. and M.R. Baxter, *Inductively Coupled Plasma Mass Spectrometry: Introduction to Analytical Aspects.* Clin Biochem Rev, 2019. **40**(3): p. 115-133.

363. Houk, R.S., et al., *Inductively coupled argon plasma as an ion source for mass spectrometric determination of trace elements.* Analytical Chemistry, 1980. **52**(14): p. 2283-2289.

364. Nuttall, K.L., W.H. Gordon, and K.O. Ash, *Inductively coupled plasma mass spectrometry for trace element analysis in the clinical laboratory.* Ann Clin Lab Sci, 1995. **25**(3): p. 264-71.

365. Clases, D. and R. Gonzalez de Vega, *Facets of ICP-MS and their potential in the medical sciences-Part 1: fundamentals, stand-alone and hyphenated techniques.* Anal Bioanal Chem, 2022. **414**(25): p. 7337-7361.

366. Genoud, S., et al., *Subcellular compartmentalisation of copper, iron, manganese, and zinc in the Parkinson's disease brain.* Metallomics, 2017. **9**(10): p. 1447-1455.

References

367. Rembach, A., et al., *Decreased Copper in Alzheimer's Disease Brain Is Predominantly in the Soluble Extractable Fraction.* International Journal of Alzheimer's Disease, 2013. **2013**: p. 623241.

368. Jacobs, R.W., et al., *A reexamination of aluminum in Alzheimer's disease: analysis by energy dispersive X-ray microprobe and flameless atomic absorption spectrophotometry.* Can J Neurol Sci, 1989. **16**(4 Suppl): p. 498-503.

369. Yasui, M., et al., *Magnesium and calcium contents in CNS tissues of amyotrophic lateral sclerosis patients from the Kii peninsula, Japan.* Eur Neurol, 1992. **32**(2): p. 95-8.

370. Kurlander, H.M. and B.M. Patten, *Metals in spinal cord tissue of patients dying of motor neuron disease.* Ann Neurol, 1979. **6**(1): p. 21-4.

371. Corrigan, F.M., G.P. Reynolds, and N.I. Ward, *Hippocampal tin, aluminum and zinc in Alzheimer's disease.* Biometals, 1993. **6**(3): p. 149-54.

372. Rembach, A., et al., *Decreased copper in Alzheimer's disease brain is predominantly in the soluble extractable fraction.* Int J Alzheimers Dis, 2013. **2013**: p. 623241.

373. Lee, H., et al., *Iron accumulation in the oculomotor nerve of the progressive supranuclear palsy brain.* Sci Rep, 2021. **11**(1): p. 2950.

374. Hutchinson, R.W., et al., *Imaging and spatial distribution of beta-amyloid peptide and metal ions in Alzheimer's plaques by laser ablation-inductively coupled plasma-mass spectrometry.* Anal Biochem, 2005. **346**(2): p. 225-33.

375. Becker, J.S., et al., *Imaging of copper, zinc, and other elements in thin section of human brain samples (hippocampus) by laser ablation inductively coupled plasma mass spectrometry.* Anal Chem, 2005. **77**(10): p. 3208-16.

376. Cruz-Alonso, M., et al., *Laser ablation ICP-MS for simultaneous quantitative imaging of iron and ferroportin in hippocampus of human brain tissues with Alzheimer's disease.* Talanta, 2019. **197**: p. 413-421.

377. Ren, M., et al., *Iron concentrations and distributions in the parkinsonian substantia nigra of aged and young primate models.* Nuclear Instruments and Methods in Physics Research Section B: Beam Interactions with Materials and Atoms, 2001. **181**(1-4): p. 522-528.

378. Gardner, B., et al., *Metal concentrations and distributions in the human olfactory bulb in Parkinson's disease.* Sci Rep, 2017. **7**(1): p. 10454.

379. Dexter, D.T., et al., *Increased nigral iron content in postmortem parkinsonian brain.* Lancet, 1987. **2**(8569): p. 1219-20.

380. Galazka-Friedman, J., et al., *The role of iron in neurodegeneration--Mossbauer spectroscopy, electron microscopy, enzyme-linked immunosorbent assay and neuroimaging studies.* J Phys Condens Matter, 2012. **24**(24): p. 244106.

381. Gerlach, M., et al., *Mössbauer spectroscopic studies of purified human neuromelanin isolated from the substantia nigra.* J Neurochem, 1995. **65**(2): p. 923-6.

382. Gałazka-Friedman, J., et al., *Iron in parkinsonian and control substantia nigra--a Mössbauer spectroscopy study.* Mov Disord, 1996. **11**(1): p. 8-16.

383. Quintana, C., et al., *Study of the localization of iron, ferritin, and hemosiderin in Alzheimer's disease hippocampus by analytical microscopy at the subcellular level.* Journal of structural biology, 2006. **153**(1): p. 42-54.

384. Wu, B. and J.S. Becker, *Imaging of elements and molecules in biological tissues and cells in the low-micrometer and nanometer range.* International Journal of Mass Spectrometry, 2011. **307**(1): p. 112-122.

385. Miller, L.M., et al., *Synchrotron-based infrared and X-ray imaging shows focalized accumulation of Cu and Zn co-localized with beta-amyloid deposits in Alzheimer's disease.* J Struct Biol, 2006. **155**(1): p. 30-7.

386. Rajendran, R., et al., *A novel approach to the identification and quantitative elemental analysis of amyloid deposits--insights into the pathology of Alzheimer's disease.* Biochem Biophys Res Commun, 2009. **382**(1): p. 91-5.

387. Danscher, G., et al., *Increased amount of zinc in the hippocampus and amygdala of Alzheimer's diseased brains: a proton-induced X-ray emission spectroscopic analysis of cryostat sections from autopsy material.* J Neurosci Methods, 1997. **76**(1): p. 53-9.

388. Yoshida, S., *Therapeutic Strategies and Metal-Induced Oxidative Stress: Application of Synchrotron Radiation Microbeam to Amyotrophic Lateral Sclerosis in the Kii Peninsula of Japan.* Front Neurol, 2022. **13**: p. 884439.

389. Ide-Ektessabi, A., S. Fujisawa, and S. Yoshida, *Chemical state imaging of iron in nerve cells from a patient with Parkinsonism-dementia complex.* Journal of applied physics, 2002. **91**(3): p. 1613-1617.

390. Chwiej, J., et al., *Investigations of differences in iron oxidation state inside single neurons from substantia nigra of Parkinson's disease and control patients using the micro-XANES technique.* J Biol Inorg Chem, 2007. **12**(2): p. 204-11.

391. Yoshida, S., A. Ektessabi, and S. Fujisawa, *XANES spectroscopy of a single neuron from a patient with Parkinson's disease.* J Synchrotron Radiat, 2001. **8**(Pt 2): p. 998-1000.

392. Tomik, B., et al., *Implementation of X-ray fluorescence microscopy for investigation of elemental abnormalities in amyotrophic lateral sclerosis.* Neurochem Res, 2006. **31**(3): p. 321-31.

393. Szczerbowska-Boruchowska, M., et al., *Topographic and quantitative microanalysis of human central nervous system tissue using synchrotron radiation.* X-Ray Spectrometry: An International Journal, 2004. **33**(1): p. 3-11.

394. Popescu, B.F., et al., *Mapping metals in Parkinson's and normal brain using rapid-scanning x-ray fluorescence.* Phys Med Biol, 2009. **54**(3): p. 651-63.

395. Genoud, S., et al., *Simultaneous structural and elemental nano-imaging of human brain tissue.* Chem Sci, 2020. **11**(33): p. 8919-8927.

396. Lobinski, R., C. Moulin, and R. Ortega, *Imaging and speciation of trace elements in biological environment.* Biochimie, 2006. **88**(11): p. 1591-604.

397. Bourassa, M.W. and L.M. Miller, *Metal imaging in neurodegenerative diseases.* Metallomics, 2012. **4**(8): p. 721-38.

398. Nuebling, G., et al., *PROSPERA: a randomized, controlled trial evaluating rasagiline in progressive supranuclear palsy.* J Neurol, 2016. **263**(8): p. 1565-74.

399. Stamelou, M. and G. Hoglinger, *A Review of Treatment Options for Progressive Supranuclear Palsy.* CNS Drugs, 2016. **30**(7): p. 629-36.

400. Apetauerova, D., et al., *CoQ10 in progressive supranuclear palsy: A randomized, placebo-controlled, double-blind trial.* Neurol Neuroimmunol Neuroinflamm, 2016. **3**(5): p. e266.

401. Bensimon, G., et al., *Riluzole treatment, survival and diagnostic criteria in Parkinson plus disorders: the NNIPPS study.* Brain, 2009. **132**(Pt 1): p. 156-71.

402. Boxer, A.L., et al., *Davunetide in patients with progressive supranuclear palsy: a randomised, double-blind, placebo-controlled phase 2/3 trial.* Lancet Neurol, 2014. **13**(7): p. 676-85.

403. Tolosa, E., et al., *A phase 2 trial of the GSK-3 inhibitor tideglusib in progressive supranuclear palsy.* Mov Disord, 2014. **29**(4): p. 470-8.

404. NCT01056965, *Davunetide (AL-108) in Predicted Tauopathies - Pilot Study*.

405. NCT01110720, *Study to Evaluate the Safety and Efficacy of Davunetide for the Treatment of Progressive Supranuclear Palsy*.

406. NCT01049399, *Safety, Tolerability, and Efficacy of Two Different Oral Doses of NP031112 Versus Placebo in the Treatment of Patients With Mild-to-Moderate Progressive Supranuclear Palsy (Tauros*.

407. Zhang, B., et al., *Microtubule-binding drugs offset tau sequestration by stabilizing microtubules and reversing fast axonal transport deficits in a tauopathy model.* Proc Natl Acad Sci U S A, 2005. **102**(1): p. 227-31.

408. Tsai, R.M., et al., *Reactions to Multiple Ascending Doses of the Microtubule Stabilizer TPI-287 in Patients With Alzheimer Disease, Progressive Supranuclear Palsy, and Corticobasal Syndrome: A Randomized Clinical Trial.* JAMA Neurol, 2020. **77**(2): p. 215-224.

409. Zhang, B., et al., *The microtubule-stabilizing agent, epothilone D, reduces axonal dysfunction, neurotoxicity, cognitive deficits, and Alzheimer-like pathology in an interventional study with aged tau transgenic mice.* J Neurosci, 2012. **32**(11): p. 3601-11.

410. NCT03174886, *A 24-month Phase 1 Pilot Study of AADvac1 in Patients With Non Fluent Primary Progressive Aphasia (AIDA)*.

411. Kontsekova, E., et al., *First-in-man tau vaccine targeting structural determinants essential for pathological tau-tau interaction reduces tau oligomerisation and neurofibrillary degeneration in an Alzheimer's disease model.* Alzheimers Res Ther, 2014. **6**(4): p. 44.

412. Novak, P., et al., *FUNDAMANT: an interventional 72-week phase 1 follow-up study of AADvac1, an active immunotherapy against tau protein pathology in Alzheimer's disease.* Alzheimer's Research & Therapy, 2018. **10**(1): p. 108.

References

413. Novak, P., et al., *ADAMANT: a placebo-controlled randomized phase 2 study of AADvac1, an active immunotherapy against pathological tau in Alzheimer's disease.* Nature Aging, 2021. **1**(6): p. 521-534.

414. NCT02579252, *24 Months Safety and Efficacy Study of AADvac1 in Patients With Mild Alzheimer's Disease (ADAMANT)*.

415. Qureshi, I.A., et al., *A randomized, single ascending dose study of intravenous BIIB092 in healthy participants.* Alzheimers Dement (N Y), 2018. **4**: p. 746-755.

416. Boxer, A.L., et al., *Safety of the tau-directed monoclonal antibody BIIB092 in progressive supranuclear palsy: a randomised, placebo-controlled, multiple ascending dose phase 1b trial.* Lancet Neurol, 2019. **18**(6): p. 549-558.

417. NCT02460094, *Multiple Ascending Dose Study of Intravenously Administered BMS-986168 (BIIB092) in Patients With Progressive Supranuclear Palsy (CN002-003)*.

418. NCT03068468, *Study of BIIB092 in Participants With Progressive Supranuclear Palsy (PASSPORT)*.

419. Barnham, K.J. and A.I. Bush, *Biological metals and metal-targeting compounds in major neurodegenerative diseases.* Chem Soc Rev, 2014. **43**(19): p. 6727-49.

420. Gaeta, A. and R.C. Hider, *The crucial role of metal ions in neurodegeneration: the basis for a promising therapeutic strategy.* Br J Pharmacol, 2005. **146**(8): p. 1041-59.

421. Zhang, Y.Y., et al., *Restoration of metal homeostasis: a potential strategy against neurodegenerative diseases.* Ageing Res Rev, 2023. **87**: p. 101931.

422. NCT03204929, *A Phase 1 Dose Escalation Study of Cu(II)ATSM Administered Orally to Patients With Early Idiopathic Parkinson's Disease*.

423. NCT04082832, *A Multicenter, Randomized, Double-Blind, Placebo-Controlled Phase 2 Study of Cu(II)ATSM in Patients With Amyotrophic Lateral Sclerosis/Motor Neuron Disease*.

424. NCT00471211, *Study Evaluating the Safety, Tolerability and Efficacy of PBT2 in Patients With Early Alzheimer's Disease.*

425. NCT03293069, *Conservative Iron Chelation as a Disease-modifying Strategy in Amyotrophic Lateral Sclerosis (FAIR-ALS II).*

426. NCT02655315, *Conservative Iron Chelation as a Disease-modifying Strategy in Parkinson's Disease (FAIRPARKII).*

427. Donnelly, P.S., et al., *An impaired mitochondrial electron transport chain increases retention of the hypoxia imaging agent diacetylbis(4-methylthiosemicarbazonato)copperII.* Proc Natl Acad Sci U S A, 2012. **109**(1): p. 47-52.

428. McKenzie-Nickson, S., et al., *Modulating Protein Phosphatase 2A Rescues Disease Phenotype in Neurodegenerative Tauopathies.* ACS Chem Neurosci, 2018. **9**(11): p. 2731-2740.

429. Hung, L.W., et al., *The hypoxia imaging agent CuII(atsm) is neuroprotective and improves motor and cognitive functions in multiple animal models of Parkinson's disease.* J Exp Med, 2012. **209**(4): p. 837-54.

References

430. Soon, C.P.W., et al., *Diacetylbis(N(4)-methylthiosemicarbazonato) copper(II) (CuII(atsm)) protects against peroxynitrite-induced nitrosative damage and prolongs survival in amyotrophic lateral sclerosis mouse model.* J Biol Chem, 2011. **286**(51): p. 44035-44044.

431. Ikawa, M., et al., *Evaluation of striatal oxidative stress in patients with Parkinson's disease using [62Cu]ATSM PET.* Nucl Med Biol, 2011. **38**(7): p. 945-51.

432. Ikawa, M., et al., *Increased oxidative stress is related to disease severity in the ALS motor cortex: A PET study.* Neurology, 2015. **84**(20): p. 2033-9.

433. Okazawa, H., et al., *Cerebral Oxidative Stress in Early Alzheimer's Disease Evaluated by (64)Cu-ATSM PET/MRI: A Preliminary Study.* Antioxidants (Basel), 2022. **11**(5).

434. Holland, J.P., J.S. Lewis, and F. Dehdashti, *Assessing tumor hypoxia by positron emission tomography with Cu-ATSM.* Q J Nucl Med Mol Imaging, 2009. **53**(2): p. 193-200.

435. Yoshii, Y., et al., *Radiolabeled Cu-ATSM as a novel indicator of overreduced intracellular state due to mitochondrial dysfunction: studies with mitochondrial DNA-less ρ0 cells and cybrids carrying MELAS mitochondrial DNA mutation.* Nucl Med Biol, 2012. **39**(2): p. 177-85.

436. Collins, S., et al., *The Effects of Copper and Copper Blocking Agents on Gill Mitochondrial O(2) Utilization of Crassostrea virginica.* In Vivo (Brooklyn), 2010. **32**(1): p. 14-19.

437. Collin, F., *Chemical Basis of Reactive Oxygen Species Reactivity and Involvement in Neurodegenerative Diseases.* Int J Mol Sci, 2019. **20**(10).

438. Yamada, K., *[Glucose metabolism in the basal ganglia].* Brain Nerve, 2009. **61**(4): p. 381-8.

439. Lee, J.H., et al., *Quantitative assessment of subcortical atrophy and iron content in progressive supranuclear palsy and parkinsonian variant of multiple system atrophy.* J Neurol, 2013. **260**(8): p. 2094-101.

440. Lee, J.H. and M.S. Lee, *Brain Iron Accumulation in Atypical Parkinsonian Syndromes: in vivo MRI Evidences for Distinctive Patterns.* Front Neurol, 2019. **10**: p. 74.

441. Deng, H.X., et al., *Amyotrophic lateral sclerosis and structural defects in Cu,Zn superoxide dismutase.* Science, 1993. **261**(5124): p. 1047-51.

442. Saccon, R.A., et al., *Is SOD1 loss of function involved in amyotrophic lateral sclerosis?* Brain, 2013. **136**(Pt 8): p. 2342-58.

443. Robinson, J.L., et al., *Neurodegenerative disease concomitant proteinopathies are prevalent, age-related and APOE4-associated.* Brain, 2018. **141**(7): p. 2181-2193.

444. Giannakopoulos, P., et al., *Tangle and neuron numbers, but not amyloid load, predict cognitive status in Alzheimer's disease.* Neurology, 2003. **60**(9): p. 1495-500.

445. Bejanin, A., et al., *Tau pathology and neurodegeneration contribute to cognitive impairment in Alzheimer's disease.* Brain, 2017. **140**(12): p. 3286-3300.

446. Liu, C.H., et al., *Melanin bleaching with dilute hydrogen peroxide: a simple and rapid method.* Appl Immunohistochem Mol Morphol, 2013. **21**(3): p. 275-9.

References

447. Bokulić, E., et al., *The Stereological Analysis and Spatial Distribution of Neurons in the Human Subthalamic Nucleus.* Front Neuroanat, 2021. **15**: p. 749390.

448. García-Cabezas, M., et al., *Distinction of Neurons, Glia and Endothelial Cells in the Cerebral Cortex: An Algorithm Based on Cytological Features.* Front Neuroanat, 2016. **10**: p. 107.

449. Atlasi, R.S., et al., *Investigation of Anti-SOD1 Antibodies Yields New Structural Insight into SOD1 Misfolding and Surprising Behavior of the Antibodies Themselves.* ACS Chem Biol, 2018. **13**(9): p. 2794-2807.

450. Rakhit, R., et al., *An immunological epitope selective for pathological monomer-misfolded SOD1 in ALS.* Nat Med, 2007. **13**(6): p. 754-9.

451. Abarikwu, S.O., A.B. Pant, and E.O. Farombi, *4-Hydroxynonenal induces mitochondrial-mediated apoptosis and oxidative stress in SH-SY5Y human neuronal cells.* Basic Clin Pharmacol Toxicol, 2012. **110**(5): p. 441-8.

452. Adams, N.E., et al., *GABAergic cortical network physiology in frontotemporal lobar degeneration.* Brain, 2021. **144**(7): p. 2135-2145.

453. Levy, R., et al., *Alterations of GABAergic neurons in the basal ganglia of patients with progressive supranuclear palsy: an in situ hybridization study of GAD67 messenger RNA.* Neurology, 1995. **45**(1): p. 127-34.

454. Saadoun, S., et al., *Involvement of aquaporin-4 in astroglial cell migration and glial scar formation.* J Cell Sci, 2005. **118**(Pt 24): p. 5691-8.

455. Li, L., et al., *Proinflammatory role of aquaporin-4 in autoimmune neuroinflammation.* Faseb j, 2011. **25**(5): p. 1556-66.

456. Goto, S., et al., *Development of a highly sensitive immunohistochemical method to detect neurochemical molecules in formalin-fixed and paraffin-embedded tissues from autopsied human brains.* Front Neuroanat, 2015. **9**: p. 22.

457. Rimm, D.L., *What brown cannot do for you.* Nat Biotechnol, 2006. **24**(8): p. 914-6.

458. Camp, R.L., G.G. Chung, and D.L. Rimm, *Automated subcellular localization and quantification of protein expression in tissue microarrays.* Nat Med, 2002. **8**(11): p. 1323-7.

459. Eng, L.F., R.S. Ghirnikar, and Y.L. Lee, *Glial fibrillary acidic protein: GFAP-thirty-one years (1969-2000).* Neurochem Res, 2000. **25**(9-10): p. 1439-51.

460. Petrovic, N., A. Comi, and M.J. Ettinger, *Identification of an apo-superoxide dismutase (Cu,Zn) pool in human lymphoblasts.* J Biol Chem, 1996. **271**(45): p. 28331-4.

461. Schmitz, C. and P.R. Hof, *Design-based stereology in neuroscience.* Neuroscience, 2005. **130**(4): p. 813-31.

462. von Bartheld, C., *Counting particles in tissue sections: choices of methods and importance of calibration to minimize biases.* Histol Histopathol, 2002. **17**(2): p. 639-48.

463. Litvan, I., et al., *Validity and reliability of the preliminary NINDS neuropathologic criteria for progressive supranuclear palsy and related disorders.* J Neuropathol Exp Neurol, 1996. **55**(1): p. 97-105.

464. Ling, H., et al., *Characteristics of progressive supranuclear palsy presenting with corticobasal syndrome: a cortical variant.* Neuropathol Appl Neurobiol, 2014. **40**(2): p. 149-63.

465. Martínez, A., et al., *Type-dependent oxidative damage in frontotemporal lobar degeneration: cortical astrocytes are targets of oxidative damage.* J Neuropathol Exp Neurol, 2008b. **67**(12): p. 1122-36.

466. Yamanaka, K., et al., *Astrocytes as determinants of disease progression in inherited amyotrophic lateral sclerosis.* Nat Neurosci, 2008. **11**(3): p. 251-3.

467. Yates, D., *Neurodegenerative disease: Factoring in astrocytes.* Nat Rev Neurosci, 2015. **16**(2): p. 67.

468. Kim, J.H., et al., *Astroglia contribute to the pathogenesis of spinocerebellar ataxia Type 1 (SCA1) in a biphasic, stage-of-disease specific manner.* Glia, 2018. **66**(9): p. 1972-1987.

469. Izco, M., et al., *Glial activation precedes alpha-synuclein pathology in a mouse model of Parkinson's disease.* Neurosci Res, 2021. **170**: p. 330-340.

470. Wilson, J.X., *Antioxidant defense of the brain: a role for astrocytes.* Can J Physiol Pharmacol, 1997. **75**(10-11): p. 1149-63.

471. Dringen, R., *Metabolism and functions of glutathione in brain.* Prog Neurobiol, 2000. **62**(6): p. 649-71.

472. Hirano, A., L.T. Kurland, and G.P. Sayre, *Familial Amyotrophic Lateral Sclerosis: A Subgroup Characterized by Posterior and Spinocerebellar Tract Involvement and Hyaline Inclusions in the Anterior Horn Cells.* Archives of Neurology, 1967. **16**(3): p. 232-243.

473. Kato, S., et al., *New consensus research on neuropathological aspects of familial amyotrophic lateral sclerosis with superoxide dismutase 1 (SOD1) gene mutations: inclusions containing SOD1 in neurons and astrocytes.* Amyotroph Lateral Scler Other Motor Neuron Disord, 2000. **1**(3): p. 163-84.

474. Murayama, S., et al., *Immunocytochemical and ultrastructural study of Lewy body-like hyaline inclusions in familial amyotrophic lateral sclerosis.* Acta Neuropathol, 1989. **78**(2): p. 143-52.

475. Shibata, N., et al., *Cu/Zn superoxide dismutase-like immunoreactivity in Lewy body-like inclusions of sporadic amyotrophic lateral sclerosis.* Neurosci Lett, 1994. **179**(1-2): p. 149-52.

476. Goldman, J.E., *Alzheimer Type I Astrocytes: Still Mysterious Cells.* J Neuropathol Exp Neurol, 2022. **81**(8): p. 588-595.

477. Ma, K.C., et al., *Glial fibrillary acidic protein immunohistochemical study of Alzheimer I & II astrogliosis in Wilson's disease.* Acta Neurol Scand, 1988. **78**(4): p. 290-6.

478. Kruer, M.C., *The neuropathology of neurodegeneration with brain iron accumulation.* Int Rev Neurobiol, 2013. **110**: p. 165-94.

References

479. Castejón, O.J., *Morphological astrocytic changes in complicated human brain trauma. A light and electron microscopic study.* Brain Inj, 1998. **12**(5): p. 409-27; discussion 407.

480. Zagzag, D., et al., *Demyelinating disease versus tumor in surgical neuropathology. Clues to a correct pathological diagnosis.* Am J Surg Pathol, 1993. **17**(6): p. 537-45.

481. Bertrand, E., et al., *Neuropathological analysis of pathological forms of astroglia in Wilson's disease.* Folia Neuropathol, 2001. **39**(2): p. 73-9.

482. Mancuso, M., et al., *Hereditary ferritinopathy: a novel mutation, its cellular pathology, and pathogenetic insights.* J Neuropathol Exp Neurol, 2005. **64**(4): p. 280-94.

483. Bondi, H., et al., *Heterogenous response to aging of astrocytes in murine Substantia Nigra pars compacta and pars reticulata.* Neurobiol Aging, 2023. **123**: p. 23-34.

484. Bandyopadhyay, B., et al., *Tau aggregation and toxicity in a cell culture model of tauopathy.* J Biol Chem, 2007. **282**(22): p. 16454-64.

485. Cowan, C.M. and A. Mudher, *Are tau aggregates toxic or protective in tauopathies?* Front Neurol, 2013. **4**: p. 114.

486. Fatouros, C., et al., *Inhibition of tau aggregation in a novel Caenorhabditis elegans model of tauopathy mitigates proteotoxicity.* Hum Mol Genet, 2012. **21**(16): p. 3587-603.

487. Wang, X., et al., *Copper binding regulates intracellular alpha-synuclein localisation, aggregation and toxicity.* J Neurochem, 2010. **113**(3): p. 704-14.

488. Van Den Bosch, L. and W. Robberecht, *Crosstalk between astrocytes and motor neurons: what is the message?* Exp Neurol, 2008. **211**(1): p. 1-6.

489. Bandmann, O., et al., *Sequence of the superoxide dismutase 1 (SOD 1) gene in familial Parkinson's disease.* J Neurol Neurosurg Psychiatry, 1995. **59**(1): p. 90-1.

490. Petrov, D., X. Daura, and B. Zagrovic, *Effect of Oxidative Damage on the Stability and Dimerization of Superoxide Dismutase 1.* Biophys J, 2016. **110**(7): p. 1499-1509.

491. Bosco, D.A., et al., *Wild-type and mutant SOD1 share an aberrant conformation and a common pathogenic pathway in ALS.* Nat Neurosci, 2010. **13**(11): p. 1396-403.

492. Schmitt, N.D. and J.N. Agar, *Parsing disease-relevant protein modifications from epiphenomena: perspective on the structural basis of SOD1-mediated ALS.* J Mass Spectrom, 2017. **52**(7): p. 480-491.

493. Kaneko, K., et al., *Astrocytic deformity and globular structures are characteristic of the brains of patients with aceruloplasminemia.* J Neuropathol Exp Neurol, 2002. **61**(12): p. 1069-77.

494. Rakhit, R., et al., *Oxidation-induced misfolding and aggregation of superoxide dismutase and its implications for amyotrophic lateral sclerosis.* J Biol Chem, 2002. **277**(49): p. 47551-6.

495. Tainer, J.A., et al., *Determination and analysis of the 2 A-structure of copper, zinc superoxide dismutase.* J Mol Biol, 1982. **160**(2): p. 181-217.

References

496. Bourassa, M.W., et al., *Metal-deficient aggregates and diminished copper found in cells expressing SOD1 mutations that cause ALS.* Front Aging Neurosci, 2014. **6**: p. 110.

497. Tokuda, E., et al., *A copper-deficient form of mutant Cu/Zn-superoxide dismutase as an early pathological species in amyotrophic lateral sclerosis.* Biochim Biophys Acta Mol Basis Dis, 2018. **1864**(6 Pt A): p. 2119-2130.

498. Michael, G.J., et al., *Up-regulation of metallothionein gene expression in parkinsonian astrocytes.* Neurogenetics, 2011. **12**(4): p. 295-305.

499. Zambenedetti, P., R. Giordano, and P. Zatta, *Metallothioneins are highly expressed in astrocytes and microcapillaries in Alzheimer's disease.* J Chem Neuroanat, 1998. **15**(1): p. 21-6.

500. West, A.K., et al., *Metallothionein in the central nervous system: Roles in protection, regeneration and cognition.* Neurotoxicology, 2008. **29**(3): p. 489-503.

501. Tokuda, E., et al., *Overexpression of metallothionein-I, a copper-regulating protein, attenuates intracellular copper dyshomeostasis and extends lifespan in a mouse model of amyotrophic lateral sclerosis caused by mutant superoxide dismutase-1.* Hum Mol Genet, 2014. **23**(5): p. 1271-85.

502. Gunn, A., B. Roberts, and A. White, *Neuromethods–Metals in the Brain: Measurement and Imaging.* 2017.

503. Kfoury, N., et al., *Trans-cellular propagation of Tau aggregation by fibrillar species.* J Biol Chem, 2012. **287**(23): p. 19440-51.

504. Duan, W., et al., *Novel Insights into NeuN: from Neuronal Marker to Splicing Regulator.* Mol Neurobiol, 2016. **53**(3): p. 1637-1647.

505. Gu, J., et al., *Rbfox3/NeuN Regulates Alternative Splicing of Tau Exon 10.* J Alzheimers Dis, 2018. **66**(4): p. 1695-1704.

506. Comstra, H.S., et al., *The interactome of the copper transporter ATP7A belongs to a network of neurodevelopmental and neurodegeneration factors.* Elife, 2017. **6**.

507. Fujiwara, H., et al., *Inhibition of microtubule assembly competent tubulin synthesis leads to accumulation of phosphorylated tau in neuronal cell bodies.* Biochem Biophys Res Commun, 2020. **521**(3): p. 779-785.

508. Walker, K.L., et al., *Loss of neurofilaments alters axonal growth dynamics.* J Neurosci, 2001. **21**(24): p. 9655-66.

509. Rebelo, A.P., et al., *Cryptic Amyloidogenic Elements in the 3' UTRs of Neurofilament Genes Trigger Axonal Neuropathy.* Am J Hum Genet, 2016. **98**(4): p. 597-614.

510. Ishii, T., S. Haga, and S. Tokutake, *Presence of neurofilament protein in Alzheimer's neurofibrillary tangles (ANT). An immunofluorescent study.* Acta Neuropathol, 1979. **48**(2): p. 105-12.

511. Perry, G., et al., *Filaments of Pick's bodies contain altered cytoskeletal elements.* Am J Pathol, 1987. **127**(3): p. 559-68.

References

512. Brettschneider, J., et al., *Neurofilament heavy-chain NfH(SMI35) in cerebrospinal fluid supports the differential diagnosis of Parkinsonian syndromes.* Mov Disord, 2006. **21**(12): p. 2224-7.

513. Gaiottino, J., et al., *Increased neurofilament light chain blood levels in neurodegenerative neurological diseases.* PLoS One, 2013. **8**(9): p. e75091.

514. Bian, X., et al., *Whole-Genome Linkage Analysis with Whole-Exome Sequencing Identifies a Novel Frameshift Variant in NEFH in a Chinese Family with Charcot-Marie-Tooth 2: A Novel Variant in NEFH for Charcot-Marie-Tooth 2.* Neurodegener Dis, 2018. **18**(2-3): p. 74-83.

515. González-Hernández, T. and M. Rodríguez, *Compartmental organization and chemical profile of dopaminergic and GABAergic neurons in the substantia nigra of the rat.* J Comp Neurol, 2000. **421**(1): p. 107-35.

516. Hikosaka, O., *GABAergic output of the basal ganglia.* Prog Brain Res, 2007. **160**: p. 209-26.

517. Yasui, Y., et al., *Non-dopaminergic neurons in the substantia nigra project to the reticular formation around the trigeminal motor nucleus in the rat.* Brain Res, 1992. **585**(1-2): p. 361-6.

518. Liang, H., G. Paxinos, and C. Watson, *Projections from the brain to the spinal cord in the mouse.* Brain Struct Funct, 2011. **215**(3-4): p. 159-86.

519. Takakusaki, K., et al., *Basal ganglia efferents to the brainstem centers controlling postural muscle tone and locomotion: a new concept for understanding motor disorders in basal ganglia dysfunction.* Neuroscience, 2003. **119**(1): p. 293-308.

520. Sofroniew, M.V. and H.V. Vinters, *Astrocytes: biology and pathology.* Acta Neuropathol, 2010. **119**(1): p. 7-35.

521. Ben Haim, L., et al., *Elusive roles for reactive astrocytes in neurodegenerative diseases.* Front Cell Neurosci, 2015. **9**: p. 278.

522. Song, Y.J., et al., *Degeneration in different parkinsonian syndromes relates to astrocyte type and astrocyte protein expression.* J Neuropathol Exp Neurol, 2009. **68**(10): p. 1073-83.

523. Wilhelmsson, U., et al., *Redefining the concept of reactive astrocytes as cells that remain within their unique domains upon reaction to injury.* Proc Natl Acad Sci U S A, 2006. **103**(46): p. 17513-8.

524. Cahoy, J.D., et al., *A transcriptome database for astrocytes, neurons, and oligodendrocytes: a new resource for understanding brain development and function.* J Neurosci, 2008. **28**(1): p. 264-78.

525. Yang, Y., et al., *Molecular comparison of GLT1+ and ALDH1L1+ astrocytes in vivo in astroglial reporter mice.* Glia, 2011. **59**(2): p. 200-7.

526. Anderson, M.A., et al., *Astrocyte scar formation aids central nervous system axon regeneration.* Nature, 2016. **532**(7598): p. 195-200.

527. Nagelhus, E.A. and O.P. Ottersen, *Physiological roles of aquaporin-4 in brain.* Physiol Rev, 2013. **93**(4): p. 1543-62.

References

528. Vandebroek, A. and M. Yasui, *Cu(1+), but not Cu(2+) is capable of inhibition of AQP4 permeability in an in vitro CHO cell based model.* Biochem Biophys Rep, 2021. **28**: p. 101132.

529. Lan, Y.L., et al., *The Potential Roles of Aquaporin 4 in Alzheimer's Disease.* Mol Neurobiol, 2016. **53**(8): p. 5300-9.

530. Warth, A., M. Mittelbronn, and H. Wolburg, *Redistribution of the water channel protein aquaporin-4 and the K+ channel protein Kir4.1 differs in low- and high-grade human brain tumors.* Acta Neuropathol, 2005. **109**(4): p. 418-26.

531. Papadopoulos, M.C. and A.S. Verkman, *Aquaporin-4 and brain edema.* Pediatr Nephrol, 2007. **22**(6): p. 778-84.

532. Igarashi, H., et al., *Water influx into cerebrospinal fluid is significantly reduced in senile plaque bearing transgenic mice, supporting beta-amyloid clearance hypothesis of Alzheimer's disease.* Neurol Res, 2014. **36**(12): p. 1094-8.

533. Watanabe-Matsumoto, S., et al., *Dissociation of blood-brain barrier disruption and disease manifestation in an aquaporin-4-deficient mouse model of amyotrophic lateral sclerosis.* Neurosci Res, 2018. **133**: p. 48-57.

534. Hoshi, A., et al., *Expression of Aquaporin 1 and Aquaporin 4 in the Temporal Neocortex of Patients with Parkinson's Disease.* Brain Pathol, 2017. **27**(2): p. 160-168.

535. Thenral, S.T. and A.J. Vanisree, *Peripheral assessment of the genes AQP4, PBP and TH in patients with Parkinson's disease.* Neurochem Res, 2012. **37**(3): p. 512-5.

536. Zeppenfeld, D.M., et al., *Association of Perivascular Localization of Aquaporin-4 With Cognition and Alzheimer Disease in Aging Brains.* JAMA Neurol, 2017. **74**(1): p. 91-99.

537. Hoshi, A., et al., *Characteristics of aquaporin expression surrounding senile plaques and cerebral amyloid angiopathy in Alzheimer disease.* J Neuropathol Exp Neurol, 2012. **71**(8): p. 750-9.

538. Ximenes-da-Silva, A., *Metal Ion Toxins and Brain Aquaporin-4 Expression: An Overview.* Front Neurosci, 2016. **10**: p. 233.

539. Saijo, K. and C.K. Glass, *Microglial cell origin and phenotypes in health and disease.* Nat Rev Immunol, 2011. **11**(11): p. 775-87.

540. Alster, P., et al., *Microglial Activation and Inflammation as a Factor in the Pathogenesis of Progressive Supranuclear Palsy (PSP).* Front Neurosci, 2020. **14**: p. 893.

541. Ito, D., et al., *Microglia-specific localisation of a novel calcium binding protein, Iba1.* Brain Res Mol Brain Res, 1998. **57**(1): p. 1-9.

542. Schwabenland, M., et al., *Analyzing microglial phenotypes across neuropathologies: a practical guide.* Acta Neuropathol, 2021. **142**(6): p. 923-936.

543. Chidambaram, H., R. Das, and S. Chinnathambi, *Interaction of Tau with the chemokine receptor, CX3CR1 and its effect on microglial activation, migration and proliferation.* Cell Biosci, 2020. **10**: p. 109.

References

544. Gautier, E.L., et al., *Gene-expression profiles and transcriptional regulatory pathways that underlie the identity and diversity of mouse tissue macrophages.* Nat Immunol, 2012. **13**(11): p. 1118-28.

545. Bennett, M.L., et al., *New tools for studying microglia in the mouse and human CNS.* Proc Natl Acad Sci U S A, 2016. **113**(12): p. E1738-46.

546. Bonham, L.W., et al., *CXCR4 involvement in neurodegenerative diseases.* Transl Psychiatry, 2018. **8**(1): p. 73.

547. Arab, T., et al., *Surface phenotyping and quantitative proteomics reveal differentially enriched proteins of brain-derived extracellular vesicles in Parkinson's disease.* bioRxiv, 2022: p. 2022.10.17.512628.

548. Barko, K., et al., *Brain region- and sex-specific transcriptional profiles of microglia.* Front Psychiatry, 2022. **13**: p. 945548.

549. Chiu, I.M., et al., *A neurodegeneration-specific gene-expression signature of acutely isolated microglia from an amyotrophic lateral sclerosis mouse model.* Cell Rep, 2013. **4**(2): p. 385-401.

550. Madsen, E. and J.D. Gitlin, *Copper and iron disorders of the brain.* Annu Rev Neurosci, 2007. **30**: p. 317-37.

551. Williams, D.R., *Tauopathies: classification and clinical update on neurodegenerative diseases associated with microtubule-associated protein tau.* Intern Med J, 2006. **36**(10): p. 652-60.

552. Schrag, M., et al., *Iron, zinc and copper in the Alzheimer's disease brain: a quantitative meta-analysis. Some insight on the influence of citation bias on scientific opinion.* Prog Neurobiol, 2011. **94**(3): p. 296-306.

553. Nedd, S., et al., *Cu,Zn-superoxide dismutase without Zn is folded but catalytically inactive.* J Mol Biol, 2014. **426**(24): p. 4112-4124.

554. Hilton, J.B.W., et al., *Evidence for decreased copper associated with demyelination in the corpus callosum of cuprizone treated mice.* Metallomics, 2024.

555. Hare, D.J., et al., *Three-dimensional elemental bio-imaging of Fe, Zn, Cu, Mn and P in a 6-hydroxydopamine lesioned mouse brain.* Metallomics, 2010. **2**(11): p. 745-53.

556. Lear, J., et al., *High-resolution elemental bioimaging of Ca, Mn, Fe, Co, Cu, and Zn employing LA-ICP-MS and hydrogen reaction gas.* Anal Chem, 2012. **84**(15): p. 6707-14.

557. Shen, E.H., C.C. Overly, and A.R. Jones, *The Allen Human Brain Atlas: comprehensive gene expression mapping of the human brain.* Trends Neurosci, 2012. **35**(12): p. 711-4.

558. Wong, B.X., et al., *A comparison of ceruloplasmin to biological polyanions in promoting the oxidation of Fe(2+) under physiologically relevant conditions.* Biochim Biophys Acta, 2014. **1840**(12): p. 3299-310.

559. Motulsky, H.J. and R.E. Brown, *Detecting outliers when fitting data with nonlinear regression - a new method based on robust nonlinear regression and the false discovery rate.* BMC Bioinformatics, 2006. **7**: p. 123.

References

560. Harris, Z.L., et al., *Targeted gene disruption reveals an essential role for ceruloplasmin in cellular iron efflux.* Proc Natl Acad Sci U S A, 1999. **96**(19): p. 10812-7.

561. Yamamoto, A., et al., *Iron (III) induces aggregation of hyperphosphorylated tau and its reduction to iron (II) reverses the aggregation: implications in the formation of neurofibrillary tangles of Alzheimer's disease.* J Neurochem, 2002. **82**(5): p. 1137-47.

562. Ahmadi, S., et al., *Electrochemical studies of tau protein-iron interactions—Potential implications for Alzheimer's Disease.* Electrochimica Acta, 2017. **236**: p. 384-393.

563. Perez, M., et al., *Ferritin is associated with the aberrant tau filaments present in progressive supranuclear palsy.* Am J Pathol, 1998. **152**(6): p. 1531-9.

564. Oteiza, P.I., et al., *Zinc deficiency induces oxidative stress and AP-1 activation in 3T3 cells.* Free Radical Biology and Medicine, 2000. **28**(7): p. 1091-1099.

565. Reeves, P.G., K.L. Rossow, and D.J. Bobilya, *Zinc-induced metallothionein and copper metabolism in intestinal mucosa, liver, and kidney of rats.* Nutrition Research, 1993. **13**(12): p. 1419-1431.

566. Grzywacz, A., et al., *Metal responsive transcription factor 1 (MTF-1) regulates zinc dependent cellular processes at the molecular level.* Acta Biochim Pol, 2015. **62**(3): p. 491-8.

567. Bakkar, N., et al., *The M1311V variant of ATP7A is associated with impaired trafficking and copper homeostasis in models of motor neuron disease.* Neurobiol Dis, 2021. **149**: p. 105228.

568. Ke, B.X., et al., *Alteration of copper physiology in mice overexpressing the human Menkes protein ATP7A.* Am J Physiol Regul Integr Comp Physiol, 2006. **290**(5): p. R1460-7.

569. Camakaris, J., et al., *Gene amplification of the Menkes (MNK; ATP7A) P-type ATPase gene of CHO cells is associated with copper resistance and enhanced copper efflux.* Hum Mol Genet, 1995. **4**(11): p. 2117-23.

570. Goka, T.J., et al., *Menkes disease: a biochemical abnormality in cultured human fibroblasts.* Proc Natl Acad Sci U S A, 1976. **73**(2): p. 604-6.

571. Gudekar, N., et al., *Metallothioneins regulate ATP7A trafficking and control cell viability during copper deficiency and excess.* Sci Rep, 2020. **10**(1): p. 7856.

572. Adams, N.E., et al., *Neurophysiological consequences of synapse loss in progressive supranuclear palsy.* Brain, 2023. **146**(6): p. 2584-2594.

573. La Fontaine, S. and J.F. Mercer, *Trafficking of the copper-ATPases, ATP7A and ATP7B: role in copper homeostasis.* Archives of biochemistry and biophysics, 2007. **463**(2): p. 149-167.

574. Nyasae, L., et al., *Dynamics of endogenous ATP7A (Menkes protein) in intestinal epithelial cells: copper-dependent redistribution between two intracellular sites.* American Journal of Physiology-Gastrointestinal and Liver Physiology, 2007. **292**(4): p. G1181-G1194.

575. El Meskini, R., et al., *ATP7A (Menkes protein) functions in axonal targeting and synaptogenesis.* Mol Cell Neurosci, 2007. **34**(3): p. 409-21.

References

576. El Meskini, R., et al., *The developmentally regulated expression of Menkes protein ATP7A suggests a role in axon extension and synaptogenesis.* Dev Neurosci, 2005. **27**(5): p. 333-48.

577. Schlief, M.L. and J.D. Gitlin, *Copper homeostasis in the CNS: a novel link between the NMDA receptor and copper homeostasis in the hippocampus.* Mol Neurobiol, 2006. **33**(2): p. 81-90.

578. Duncan, C., et al., *Copper modulates the large dense core vesicle secretory pathway in PC12 cells.* Metallomics, 2013. **5**(6): p. 700-14.

579. Gaier, E.D., B.A. Eipper, and R.E. Mains, *Copper signaling in the mammalian nervous system: synaptic effects.* J Neurosci Res, 2013. **91**(1): p. 2-19.

580. Huster, D., et al., *Consequences of copper accumulation in the livers of the Atp7b-/- (Wilson disease gene) knockout mice.* Am J Pathol, 2006. **168**(2): p. 423-34.

581. Mostad, E.J. and J.R. Prohaska, *Glycosylphosphatidylinositol-linked ceruloplasmin is expressed in multiple rodent organs and is lower following dietary copper deficiency.* Exp Biol Med (Maywood), 2011. **236**(3): p. 298-308.

582. Mukhopadhyay, C.K., B. Mazumder, and P.L. Fox, *Role of hypoxia-inducible factor-1 in transcriptional activation of ceruloplasmin by iron deficiency.* J Biol Chem, 2000. **275**(28): p. 21048-54.

583. Semenza, G.L., *Regulation of mammalian O2 homeostasis by hypoxia-inducible factor 1.* Annu Rev Cell Dev Biol, 1999. **15**: p. 551-78.

584. Martin, F., et al., *Copper-dependent activation of hypoxia-inducible factor (HIF)-1: implications for ceruloplasmin regulation.* Blood, 2005. **105**(12): p. 4613-9.

585. Boelmans, K., et al., *Brain iron deposition fingerprints in Parkinson's disease and progressive supranuclear palsy.* Mov Disord, 2012. **27**(3): p. 421-7.

586. Lee, S.H., et al., *Brain regional iron contents in progressive supranuclear palsy.* Parkinsonism Relat Disord, 2017. **45**: p. 28-32.

587. Smith, M.A., et al., *Iron accumulation in Alzheimer disease is a source of redox-generated free radicals.* Proc Natl Acad Sci U S A, 1997. **94**(18): p. 9866-8.

588. Urrutia, P.J., D.A. Borquez, and M.T. Nunez, *Inflaming the Brain with Iron.* Antioxidants (Basel), 2021. **10**(1).

589. Halliwell, B., *Free radicals, antioxidants, and human disease: curiosity, cause, or consequence?* Lancet, 1994. **344**(8924): p. 721-4.

590. Wessling-Resnick, M., *Iron homeostasis and the inflammatory response.* Annu Rev Nutr, 2010. **30**: p. 105-22.

591. Liang, Z.D., et al., *Specificity protein 1 (sp1) oscillation is involved in copper homeostasis maintenance by regulating human high-affinity copper transporter 1 expression.* Mol Pharmacol, 2012. **81**(3): p. 455-64.

592. Petris, M.J., et al., *Copper-stimulated endocytosis and degradation of the human copper transporter, hCtr1.* J Biol Chem, 2003. **278**(11): p. 9639-46.

593. Arredondo, M., et al., *DMT1, a physiologically relevant apical Cu1+ transporter of intestinal cells.* Am J Physiol Cell Physiol, 2003. **284**(6): p. C1525-30.

References

594. Lin, C., et al., *Copper uptake by DMT1: a compensatory mechanism for CTR1 deficiency in human umbilical vein endothelial cells.* Metallomics, 2015. **7**(8): p. 1285-9.

595. Salazar, J., et al., *Divalent metal transporter 1 (DMT1) contributes to neurodegeneration in animal models of Parkinson's disease.* Proc Natl Acad Sci U S A, 2008. **105**(47): p. 18578-83.

596. Liao, Y., et al., *Inflammation mobilizes copper metabolism to promote colon tumorigenesis via an IL-17-STEAP4-XIAP axis.* Nat Commun, 2020. **11**(1): p. 900.

597. Albers, D.S. and M.F. Beal, *Mitochondrial dysfunction in progressive supranuclear palsy.* Neurochem Int, 2002. **40**(6): p. 559-64.

598. Jang, Y., et al., *Mass spectrometry-based proteomics analysis of human globus pallidus from progressive supranuclear palsy patients discovers multiple disease pathways.* Clin Transl Med, 2022. **12**(11): p. e1076.

599. Horng, Y.C., et al., *Specific copper transfer from the Cox17 metallochaperone to both Sco1 and Cox11 in the assembly of yeast cytochrome C oxidase.* J Biol Chem, 2004. **279**(34): p. 35334-40.

600. Carr, H.S., et al., *Functional analysis of the domains in Cox11.* J Biol Chem, 2005. **280**(24): p. 22664-9.

601. Rentzsch, A., et al., *Mitochondrial copper metabolism in yeast: mutational analysis of Sco1p involved in the biogenesis of cytochrome c oxidase.* Curr Genet, 1999. **35**(2): p. 103-8.

602. Beers, J., D.M. Glerum, and A. Tzagoloff, *Purification, characterization, and localization of yeast Cox17p, a mitochondrial copper shuttle.* J Biol Chem, 1997. **272**(52): p. 33191-6.

603. Radin, I., et al., *The Arabidopsis COX11 Homolog is Essential for Cytochrome c Oxidase Activity.* Front Plant Sci, 2015. **6**: p. 1091.

604. Radin, I., et al., *The mitochondrial copper chaperone COX11 has an additional role in cellular redox homeostasis.* PLoS One, 2021. **16**(12): p. e0261465.

605. Khalimonchuk, O., A. Bird, and D.R. Winge, *Evidence for a pro-oxidant intermediate in the assembly of cytochrome oxidase.* J Biol Chem, 2007. **282**(24): p. 17442-9.

606. Ekim Kocabey, A., G. Rödel, and U. Gey, *The antioxidant function of Sco proteins depends on a critical surface-exposed residue.* Biochim Biophys Acta Gen Subj, 2021. **1865**(2): p. 129781.

607. Stamelou, M., et al., *In vivo evidence for cerebral depletion in high-energy phosphates in progressive supranuclear palsy.* J Cereb Blood Flow Metab, 2009. **29**(4): p. 861-70.

608. Qadri, R., et al., *Alteration of Mitochondrial Function in Oxidative Stress in Parkinsonian Neurodegeneration: A Cross-Sectional Study.* Ann Indian Acad Neurol, 2021. **24**(4): p. 506-512.

609. Espay, A.J. and I. Litvan, *Parkinsonism and frontotemporal dementia: the clinical overlap.* J Mol Neurosci, 2011. **45**(3): p. 343-9.

References

610. Murray, B., T. Lynch, and M. Farrell, *Clinicopathological features of the tauopathies.* Biochem Soc Trans, 2005. **33**(Pt 4): p. 595-9.

611. Stöhr, J., et al., *A 31-residue peptide induces aggregation of tau's microtubule-binding region in cells.* Nat Chem, 2017. **9**(9): p. 874-881.

612. Hasegawa, M., M.J. Smith, and M. Goedert, *Tau proteins with FTDP-17 mutations have a reduced ability to promote microtubule assembly.* FEBS Lett, 1998. **437**(3): p. 207-10.

613. Lewis, J., et al., *Neurofibrillary tangles, amyotrophy and progressive motor disturbance in mice expressing mutant (P301L) tau protein.* Nat Genet, 2000. **25**(4): p. 402-5.

614. Murakami, T., et al., *Cortical neuronal and glial pathology in TgTauP301L transgenic mice: neuronal degeneration, memory disturbance, and phenotypic variation.* Am J Pathol, 2006. **169**(4): p. 1365-75.

615. Ramsden, M., et al., *Age-dependent neurofibrillary tangle formation, neuron loss, and memory impairment in a mouse model of human tauopathy (P301L).* J Neurosci, 2005. **25**(46): p. 10637-47.

616. Ikegami, S., A. Harada, and N. Hirokawa, *Muscle weakness, hyperactivity, and impairment in fear conditioning in tau-deficient mice.* Neurosci Lett, 2000. **279**(3): p. 129-32.

617. Harada, A., et al., *Altered microtubule organization in small-calibre axons of mice lacking tau protein.* Nature, 1994. **369**(6480): p. 488-91.

618. Ishihara, T., et al., *Age-dependent emergence and progression of a tauopathy in transgenic mice overexpressing the shortest human tau isoform.* Neuron, 1999. **24**(3): p. 751-62.

619. Ishihara, T., et al., *Age-dependent induction of congophilic neurofibrillary tau inclusions in tau transgenic mice.* Am J Pathol, 2001. **158**(2): p. 555-62.

620. Duff, K., et al., *Characterization of pathology in transgenic mice over-expressing human genomic and cDNA tau transgenes.* Neurobiol Dis, 2000. **7**(2): p. 87-98.

621. Andorfer, C., et al., *Hyperphosphorylation and aggregation of tau in mice expressing normal human tau isoforms.* J Neurochem, 2003. **86**(3): p. 582-90.

622. Probst, A., et al., *Axonopathy and amyotrophy in mice transgenic for human four-repeat tau protein.* Acta Neuropathol, 2000. **99**(5): p. 469-81.

623. Spittaels, K., et al., *Prominent axonopathy in the brain and spinal cord of transgenic mice overexpressing four-repeat human tau protein.* Am J Pathol, 1999. **155**(6): p. 2153-65.

624. Forman, M.S., et al., *Transgenic mouse model of tau pathology in astrocytes leading to nervous system degeneration.* J Neurosci, 2005. **25**(14): p. 3539-50.

625. Götz, J., et al., *Oligodendroglial tau filament formation in transgenic mice expressing G272V tau.* Eur J Neurosci, 2001b. **13**(11): p. 2131-40.

References

626. Lim, F., et al., *FTDP-17 mutations in tau transgenic mice provoke lysosomal abnormalities and Tau filaments in forebrain.* Mol Cell Neurosci, 2001. **18**(6): p. 702-14.

627. Götz, J., et al., *Tau filament formation in transgenic mice expressing P301L tau.* J Biol Chem, 2001a. **276**(1): p. 529-34.

628. Pennanen, L., et al., *Accelerated extinction of conditioned taste aversion in P301L tau transgenic mice.* Neurobiol Dis, 2004. **15**(3): p. 500-9.

629. Pennanen, L., et al., *Impaired spatial reference memory and increased exploratory behavior in P301L tau transgenic mice.* Genes Brain Behav, 2006. **5**(5): p. 369-79.

630. Terwel, D., et al., *Changed conformation of mutant Tau-P301L underlies the moribund tauopathy, absent in progressive, nonlethal axonopathy of Tau-4R/2N transgenic mice.* J Biol Chem, 2005. **280**(5): p. 3963-73.

631. Allen, B., et al., *Abundant tau filaments and nonapoptotic neurodegeneration in transgenic mice expressing human P301S tau protein.* J Neurosci, 2002. **22**(21): p. 9340-51.

632. Yoshiyama, Y., et al., *Synapse loss and microglial activation precede tangles in a P301S tauopathy mouse model.* Neuron, 2007. **53**(3): p. 337-51.

633. Taniguchi, T., et al., *Transgenic mice expressing mutant (N279K) human tau show mutation dependent cognitive deficits without neurofibrillary tangle formation.* FEBS Lett, 2005. **579**(25): p. 5704-12.

634. Schindowski, K., et al., *Alzheimer's disease-like tau neuropathology leads to memory deficits and loss of functional synapses in a novel mutated tau transgenic mouse without any motor deficits.* Am J Pathol, 2006. **169**(2): p. 599-616.

635. Tanemura, K., et al., *Formation of filamentous tau aggregations in transgenic mice expressing V337M human tau.* Neurobiol Dis, 2001. **8**(6): p. 1036-45.

636. Tanemura, K., et al., *Neurodegeneration with tau accumulation in a transgenic mouse expressing V337M human tau.* J Neurosci, 2002. **22**(1): p. 133-41.

637. Tatebayashi, Y., et al., *Tau filament formation and associative memory deficit in aged mice expressing mutant (R406W) human tau.* Proc Natl Acad Sci U S A, 2002. **99**(21): p. 13896-901.

638. Zhang, B., et al., *Retarded axonal transport of R406W mutant tau in transgenic mice with a neurodegenerative tauopathy.* J Neurosci, 2004. **24**(19): p. 4657-67.

639. Ikeda, M., et al., *Accumulation of filamentous tau in the cerebral cortex of human tau R406W transgenic mice.* Am J Pathol, 2005. **166**(2): p. 521-31.

640. Sanders, D.E. and A. Koestner, *Bovine neonatal ataxia associated with hypocupremia in pregnant cows.* J Am Vet Med Assoc, 1980. **176**(8): p. 728-30.

641. Suttle, N.F. and A.C. Field, *Effect of intake of copper, molybdenum and sulphate on copper metabolism in sheep. IV. Production of congenital and delayed swayback.* J Comp Pathol, 1969. **79**(4): p. 453-64.

642. Divers, T.J., *Acquired spinal cord and peripheral nerve disease.* Vet Clin North Am Food Anim Pract, 2004. **20**(2): p. 231-42, v-vi.

References

643. Suttle, N.F., *Copper imbalances in ruminants and humans: unexpected common ground.* Adv Nutr, 2012. **3**(5): p. 666-74.

644. Wouda, W., G.H. Borst, and E. Gruys, *Delayed swayback in goat kids, a study of 23 cases.* Vet Q, 1986. **8**(1): p. 45-56.

645. Li, H., et al., *Dietary Cholesterol Supplements Disturb Copper Homeostasis in Multiple Organs in Rabbits: Aorta Copper Concentrations Negatively Correlate with the Severity of Atherosclerotic Lesions.* Biol Trace Elem Res, 2022. **200**(1): p. 164-171.

646. Allen, K.G. and L.M. Klevay, *Cholesterolemia and cardiovascular abnormalities in rats caused by copper deficiency.* Atherosclerosis, 1978. **29**(1): p. 81-93.

647. Bolognin, S., et al., *Effects of a copper-deficient diet on the biochemistry, neural morphology and behavior of aged mice.* PLoS One, 2012. **7**(10): p. e47063.

648. Pyatskowit, J.W. and J.R. Prohaska, *Copper deficient rats and mice both develop anemia but only rats have lower plasma and brain iron levels.* Comp Biochem Physiol C Toxicol Pharmacol, 2008a. **147**(3): p. 316-23.

649. Lyons, J.A. and J.R. Prohaska, *Perinatal copper deficiency alters rat cerebellar purkinje cell size and distribution.* Cerebellum, 2010. **9**(1): p. 136-44.

650. Carlton, W.W. and W.A. Kelly, *Neural lesions in the offspring of female rats fed a copper-deficient diet.* J Nutr, 1969. **97**(1): p. 42-52.

651. Dipaolo, R.V., J.N. Kanfer, and P.M. Newberne, *Copper deficiency and the central nervous system. Myelination in the rat: morphological and biochemical studies.* J Neuropathol Exp Neurol, 1974. **33**(2): p. 226-36.

652. Prohaska, J.R. and T.L. Smith, *Effect of dietary or genetic copper deficiency on brain catecholamines, trace metals and enzymes in mice and rats.* J Nutr, 1982. **112**(9): p. 1706-17.

653. Zucconi, G.G., et al., *Copper deficiency elicits glial and neuronal response typical of neurodegenerative disorders.* Neuropathol Appl Neurobiol, 2007. **33**(2): p. 212-25.

654. Koller, L.D., et al., *Immune dysfunction in rats fed a diet deficient in copper.* Am J Clin Nutr, 1987. **45**(5): p. 997-1006.

655. Bhat, J.N. and P. Maertens, *Low function of natural killer cells in treated classic Menkes disease.* Turk J Pediatr, 2020. **62**(3): p. 498-500.

656. Batzios, S., et al., *Newly identified disorder of copper metabolism caused by variants in CTR1, a high-affinity copper transporter.* Hum Mol Genet, 2022. **31**(24): p. 4121-4130.

657. Finkelstein, D.I., et al., *The novel compound PBT434 prevents iron mediated neurodegeneration and alpha-synuclein toxicity in multiple models of Parkinson's disease.* Acta Neuropathol Commun, 2017. **5**(1): p. 53.

658. Finkelstein, D.I., et al., *Axonal sprouting following lesions of the rat substantia nigra.* Neuroscience, 2000. **97**(1): p. 99-112.

659. Paxinos, G., Franklin, K.B.J, *The Mouse Brain in Stereotaxic Coordinates. 2nd Edition*. 2001: Academic Press, San Diego.

References

660. Paxinos, G.F., KBJ., *The Mouse Brain in Stereotaxic Coordinates*. Second Edition ed. 2001: Academic Press, San Diego, 2001.

661. Kuo, Y.M., et al., *Copper transport protein (Ctr1) levels in mice are tissue specific and dependent on copper status.* J Nutr, 2006. **136**(1): p. 21-6.

662. Guthrie, L.M., et al., *Elesclomol alleviates Menkes pathology and mortality by escorting Cu to cuproenzymes in mice.* Science, 2020. **368**(6491): p. 620-625.

663. Liu, Y.Y., et al., *Hydrogen sulfide protects SH-SY5Y neuronal cells against d-galactose induced cell injury by suppression of advanced glycation end products formation and oxidative stress.* Neurochem Int, 2013. **62**(5): p. 603-9.

664. Lin, S.J. and V.C. Culotta, *The ATX1 gene of Saccharomyces cerevisiae encodes a small metal homeostasis factor that protects cells against reactive oxygen toxicity.* Proc Natl Acad Sci U S A, 1995. **92**(9): p. 3784-8.

665. Kelner, G.S., et al., *The copper transport protein Atox1 promotes neuronal survival.* J Biol Chem, 2000. **275**(1): p. 580-4.

666. Eum, W.S., et al., *Neuroprotective effects of Tat-ATOX1 protein against MPP(+)-induced SH-SY5Y cell deaths and in MPTP-induced mouse model of Parkinson's disease.* Biochimie, 2019. **156**: p. 158-168.

667. Hosp, F. and M. Mann, *A Primer on Concepts and Applications of Proteomics in Neuroscience.* Neuron, 2017. **96**(3): p. 558-571.

668. Sharma, K., et al., *Cell type- and brain region-resolved mouse brain proteome.* Nat Neurosci, 2015. **18**(12): p. 1819-31.

669. Pontén, F., et al., *The Human Protein Atlas as a proteomic resource for biomarker discovery.* J Intern Med, 2011. **270**(5): p. 428-46.

670. Raghunathan, R., K. Turajane, and L.C. Wong, *Biomarkers in Neurodegenerative Diseases: Proteomics Spotlight on ALS and Parkinson's Disease.* Int J Mol Sci, 2022. **23**(16).

671. Kelleher, N.L., *Peer Reviewed: Top-Down Proteomics.* Analytical Chemistry, 2004. **76**(11): p. 196 A-203 A.

672. Melby, J.A., et al., *Novel Strategies to Address the Challenges in Top-Down Proteomics.* J Am Soc Mass Spectrom, 2021. **32**(6): p. 1278-1294.

673. Vidova, V. and Z. Spacil, *A review on mass spectrometry-based quantitative proteomics: Targeted and data independent acquisition.* Anal Chim Acta, 2017. **964**: p. 7-23.

674. Malik, R., et al., *From proteome lists to biological impact--tools and strategies for the analysis of large MS data sets.* Proteomics, 2010. **10**(6): p. 1270-83.

675. Ge, S.X., D. Jung, and R. Yao, *ShinyGO: a graphical gene-set enrichment tool for animals and plants.* Bioinformatics, 2020. **36**(8): p. 2628-2629.

676. Jiao, X., et al., *DAVID-WS: a stateful web service to facilitate gene/protein list analysis.* Bioinformatics, 2012. **28**(13): p. 1805-6.

677. Kanehisa, M., et al., *KEGG for linking genomes to life and the environment.* Nucleic Acids Res, 2008. **36**(Database issue): p. D480-4.

References

678. Hondius, D.C., et al., *Proteomics analysis identifies new markers associated with capillary cerebral amyloid angiopathy in Alzheimer's disease.* Acta Neuropathol Commun, 2018. **6**(1): p. 46.

679. Lachén-Montes, M., et al., *Olfactory bulb neuroproteomics reveals a chronological perturbation of survival routes and a disruption of prohibitin complex during Alzheimer's disease progression.* Sci Rep, 2017. **7**(1): p. 9115.

680. Seyfried, N.T., et al., *A Multi-network Approach Identifies Protein-Specific Co-expression in Asymptomatic and Symptomatic Alzheimer's Disease.* Cell Syst, 2017. **4**(1): p. 60-72.e4.

681. Bereczki, E., et al., *Synaptic markers of cognitive decline in neurodegenerative diseases: a proteomic approach.* Brain, 2018. **141**(2): p. 582-595.

682. Laszlo, Z.I., et al., *Synaptic proteomics reveal distinct molecular signatures of cognitive change and C9ORF72 repeat expansion in the human ALS cortex.* Acta Neuropathol Commun, 2022. **10**(1): p. 156.

683. Oeckl, P., et al., *Proteomics in cerebrospinal fluid and spinal cord suggests UCHL1, MAP2 and GPNMB as biomarkers and underpins importance of transcriptional pathways in amyotrophic lateral sclerosis.* Acta Neuropathol, 2020. **139**(1): p. 119-134.

684. Licker, V., et al., *Proteomic analysis of human substantia nigra identifies novel candidates involved in Parkinson's disease pathogenesis.* Proteomics, 2014. **14**(6): p. 784-94.

685. Petyuk, V.A., et al., *Proteomic Profiling of the Substantia Nigra to Identify Determinants of Lewy Body Pathology and Dopaminergic Neuronal Loss.* J Proteome Res, 2021. **20**(5): p. 2266-2282.

686. Radford, R.A.W., et al., *Identification of phosphorylated tau protein interactors in progressive supranuclear palsy (PSP) reveals networks involved in protein degradation, stress response, cytoskeletal dynamics, metabolic processes, and neurotransmission.* J Neurochem, 2023. **165**(4): p. 563-586.

687. Hughes, C.S., et al., *Single-pot, solid-phase-enhanced sample preparation for proteomics experiments.* Nat Protoc, 2019. **14**(1): p. 68-85.

688. Hughes, C.S., et al., *Ultrasensitive proteome analysis using paramagnetic bead technology.* Mol Syst Biol, 2014. **10**(10): p. 757.

689. Collins, B.C., et al., *Multi-laboratory assessment of reproducibility, qualitative and quantitative performance of SWATH-mass spectrometry.* Nat Commun, 2017. **8**(1): p. 291.

690. Koopmans, F., et al., *Comparative Analyses of Data Independent Acquisition Mass Spectrometric Approaches: DIA, WiSIM-DIA, and Untargeted DIA.* Proteomics, 2018. **18**(1).

691. Pino, L.K., et al., *Acquiring and Analyzing Data Independent Acquisition Proteomics Experiments without Spectrum Libraries.* Mol Cell Proteomics, 2020. **19**(7): p. 1088-1103.

References

692. Fröhlich, K., et al., *Benchmarking of analysis strategies for data-independent acquisition proteomics using a large-scale dataset comprising inter-patient heterogeneity.* Nat Commun, 2022. **13**(1): p. 2622.

693. Li, K.W., et al., *Recent Developments in Data Independent Acquisition (DIA) Mass Spectrometry: Application of Quantitative Analysis of the Brain Proteome.* Front Mol Neurosci, 2020. **13**: p. 564446.

694. Cox, J. and M. Mann, *MaxQuant enables high peptide identification rates, individualized p.p.b.-range mass accuracies and proteome-wide protein quantification.* Nat Biotechnol, 2008. **26**(12): p. 1367-72.

695. Tyanova, S., et al., *The Perseus computational platform for comprehensive analysis of (prote)omics data.* Nat Methods, 2016. **13**(9): p. 731-40.

696. Keller, B.O., et al., *Interferences and contaminants encountered in modern mass spectrometry.* Anal Chim Acta, 2008. **627**(1): p. 71-81.

697. Tusher, V.G., R. Tibshirani, and G. Chu, *Significance analysis of microarrays applied to the ionizing radiation response.* Proc Natl Acad Sci U S A, 2001. **98**(9): p. 5116-21.

698. Forrest, S.L., et al., *Cell-specific MAPT gene expression is preserved in neuronal and glial tau cytopathologies in progressive supranuclear palsy.* Acta Neuropathol, 2023. **146**(3): p. 395-414.

699. Liu, L.Y., et al., *Nicotinamide phosphoribosyltransferase may be involved in age-related brain diseases.* PLoS One, 2012. **7**(10): p. e44933.

700. Atkinson, A. and D.R. Winge, *Metal acquisition and availability in the mitochondria.* Chem Rev, 2009. **109**(10): p. 4708-21.

701. Horn, D. and A. Barrientos, *Mitochondrial copper metabolism and delivery to cytochrome c oxidase.* IUBMB Life, 2008. **60**(7): p. 421-9.

702. Dhar, S.S., K. Johar, and M.T. Wong-Riley, *Bigenomic transcriptional regulation of all thirteen cytochrome c oxidase subunit genes by specificity protein 1.* Open Biol, 2013. **3**(3): p. 120176.

703. Ghosh, A., et al., *Copper supplementation restores cytochrome c oxidase assembly defect in a mitochondrial disease model of COA6 deficiency.* Hum Mol Genet, 2014. **23**(13): p. 3596-606.

704. Biederbick, A., et al., *Role of human mitochondrial Nfs1 in cytosolic iron-sulfur protein biogenesis and iron regulation.* Mol Cell Biol, 2006. **26**(15): p. 5675-87.

705. Rouault, T.A. and W.H. Tong, *Iron-sulfur cluster biogenesis and human disease.* Trends Genet, 2008. **24**(8): p. 398-407.

706. Short, K.R., et al., *Decline in skeletal muscle mitochondrial function with aging in humans.* Proc Natl Acad Sci U S A, 2005. **102**(15): p. 5618-23.

707. Hollenbeck, P.J. and W.M. Saxton, *The axonal transport of mitochondria.* J Cell Sci, 2005. **118**(Pt 23): p. 5411-9.

708. MacAskill, A.F. and J.T. Kittler, *Control of mitochondrial transport and localization in neurons.* Trends Cell Biol, 2010. **20**(2): p. 102-12.

References

709. Bolam, J.P. and E.K. Pissadaki, *Living on the edge with too many mouths to feed: why dopamine neurons die.* Mov Disord, 2012. **27**(12): p. 1478-83.

710. Reeve, A.K., et al., *Mitochondrial dysfunction within the synapses of substantia nigra neurons in Parkinson's disease.* NPJ Parkinsons Dis, 2018. **4**: p. 9.

711. Sonnewald, U., L. Hertz, and A. Schousboe, *Mitochondrial heterogeneity in the brain at the cellular level.* J Cereb Blood Flow Metab, 1998. **18**(3): p. 231-7.

712. Lutas, A., L. Birnbaumer, and G. Yellen, *Metabolism regulates the spontaneous firing of substantia nigra pars reticulata neurons via KATP and nonselective cation channels.* J Neurosci, 2014. **34**(49): p. 16336-47.

713. Gu, M., et al., *Mitochondrial DNA transmission of the mitochondrial defect in Parkinson's disease.* Ann Neurol, 1998. **44**(2): p. 177-86.

714. Mann, V.M., et al., *Complex I, iron, and ferritin in Parkinson's disease substantia nigra.* Ann Neurol, 1994. **36**(6): p. 876-81.

715. Arenas, J., et al., *Complex I defect in muscle from patients with Huntington's disease.* Ann Neurol, 1998. **43**(3): p. 397-400.

716. Tabrizi, S.J. and A.H. Schapira, *Secondary abnormalities of mitochondrial DNA associated with neurodegeneration.* Biochem Soc Symp, 1999. **66**: p. 99-110.

717. Wiedemann, F.R., et al., *Mitochondrial DNA and respiratory chain function in spinal cords of ALS patients.* J Neurochem, 2002. **80**(4): p. 616-25.

718. Mylonas, C. and D. Kouretas, *Lipid peroxidation and tissue damage.* In Vivo, 1999. **13**(3): p. 295-309.

719. Chirichigno, J.W., et al., *Stress-induced mitochondrial depolarization and oxidative damage in PSP cybrids.* Brain Res, 2002. **951**(1): p. 31-5.

720. Mattson, M.P., M. Gleichmann, and A. Cheng, *Mitochondria in neuroplasticity and neurological disorders.* Neuron, 2008. **60**(5): p. 748-66.

721. Pizzinat, N., et al., *Reactive oxygen species production by monoamine oxidases in intact cells.* Naunyn Schmiedebergs Arch Pharmacol, 1999. **359**(5): p. 428-31.

722. Meiser, J., D. Weindl, and K. Hiller, *Complexity of dopamine metabolism.* Cell Commun Signal, 2013. **11**(1): p. 34.

723. Burke, W.J., et al., *3,4-Dihydroxyphenylacetaldehyde is the toxic dopamine metabolite in vivo: implications for Parkinson's disease pathogenesis.* Brain Res, 2003. **989**(2): p. 205-13.

724. Yoon, B.E., et al., *Glial GABA, synthesized by monoamine oxidase B, mediates tonic inhibition.* J Physiol, 2014. **592**(22): p. 4951-68.

725. Batra, R., et al., *Comparative brain metabolomics reveals shared and distinct metabolic alterations in Alzheimer's disease and progressive supranuclear palsy.* medRxiv, 2023.

726. Uotila, L. and M. Koivusalo, *Expression of formaldehyde dehydrogenase and S-formylglutathione hydrolase activities in different rat tissues.* Adv Exp Med Biol, 1997. **414**: p. 365-71.

727. Triboulet, S., et al., *Molecular responses of mouse macrophages to copper and copper oxide nanoparticles inferred from proteomic analyses.* Mol Cell Proteomics, 2013. **12**(11): p. 3108-22.

728. Yuzbasiyan-Gurkan, V., et al., *Linkage studies of the esterase D and retinoblastoma genes to canine copper toxicosis: a model for Wilson disease.* Genomics, 1993. **15**(1): p. 86-90.

729. Chuang, L.M., et al., *Esterase D and retinoblastoma gene loci are tightly linked to Wilson's disease in Chinese pedigrees from Taiwan.* Hum Genet, 1991. **87**(4): p. 465-8.

730. Habig, W.H. and W.B. Jakoby, *Glutathione S-transferases (rat and human).* Methods Enzymol, 1981. **77**: p. 218-31.

731. Board, P.G., et al., *Zeta, a novel class of glutathione transferases in a range of species from plants to humans.* Biochem J, 1997. **328 (Pt 3)**(Pt 3): p. 929-35.

732. Smeyne, M., et al., *GSTpi expression mediates dopaminergic neuron sensitivity in experimental parkinsonism.* Proc Natl Acad Sci U S A, 2007. **104**(6): p. 1977-82.

733. Spalletta, G., et al., *Glutathione S-transferase P1 and T1 gene polymorphisms predict longitudinal course and age at onset of Alzheimer disease.* Am J Geriatr Psychiatry, 2007. **15**(10): p. 879-87.

734. Gajewska, B., et al., *GSTP1 Polymorphisms and their Association with Glutathione Transferase and Peroxidase Activities in Patients with Motor Neuron Disease.* CNS Neurol Disord Drug Targets, 2015. **14**(10): p. 1328-33.

735. Menegon, A., et al., *Parkinson's disease, pesticides, and glutathione transferase polymorphisms.* Lancet, 1998. **352**(9137): p. 1344-6.

736. Shang, W., et al., *Expressions of glutathione S-transferase alpha, mu, and pi in brains of medically intractable epileptic patients.* BMC Neurosci, 2008. **9**: p. 67.

737. Wang, J., et al., *Reversible glutathionylation regulates actin polymerization in A431 cells.* J Biol Chem, 2001. **276**(51): p. 47763-6.

738. Fratelli, M., et al., *Identification of proteins undergoing glutathionylation in oxidatively stressed hepatocytes and hepatoma cells.* Proteomics, 2003. **3**(7): p. 1154-61.

739. Velu, C.S., et al., *Human p53 is inhibited by glutathionylation of cysteines present in the proximal DNA-binding domain during oxidative stress.* Biochemistry, 2007. **46**(26): p. 7765-80.

740. Dagnino-Subiabre, A., et al., *Glutathione transferase M2-2 catalyzes conjugation of dopamine and dopa o-quinones.* Biochem Biophys Res Commun, 2000. **274**(1): p. 32-6.

741. Martín-Díaz, M.L., et al., *Field validation of a battery of biomarkers to assess sediment quality in Spanish ports.* Environ Pollut, 2008. **151**(3): p. 631-40.

742. Bigot, A., et al., *Early defense responses in the freshwater bivalve Corbicula fluminea exposed to copper and cadmium: Transcriptional and histochemical studies.* Environ Toxicol, 2011. **26**(6): p. 623-32.

743. Letelier, M.E., et al., *Inhibition of cytosolic glutathione S-transferase activity from rat liver by copper.* Chem Biol Interact, 2006. **164**(1-2): p. 39-48.

744. Moffat, G.J., A.W. McLaren, and C.R. Wolf, *Sp1-mediated transcriptional activation of the human Pi class glutathione S-transferase promoter.* J Biol Chem, 1996. **271**(2): p. 1054-60.

745. Singh, R.R., et al., *Glutathione S-Transferase pi-1 Knockdown Reduces Pancreatic Ductal Adenocarcinoma Growth by Activating Oxidative Stress Response Pathways.* Cancers (Basel), 2020. **12**(6).

746. Dierickx, P.J., *In vitro inhibition of the soluble glutathione S-transferases from rat liver by heavy metals.* Enzyme, 1982. **27**(1): p. 25-32.

747. Singhal, S.S., et al., *Antioxidant role of glutathione S-transferases: 4-Hydroxynonenal, a key molecule in stress-mediated signaling.* Toxicol Appl Pharmacol, 2015. **289**(3): p. 361-70.

748. Togo, T. and D.W. Dickson, *Tau accumulation in astrocytes in progressive supranuclear palsy is a degenerative rather than a reactive process.* Acta Neuropathol, 2002. **104**(4): p. 398-402.

749. Penfield, W. and P. del Rio Hortega, *Cerebral cicatrix: the reaction of neuroglia and microglia to brain wounds.* Bull. Johns Hopkins Hosp., 1927. **41**(Nov.): p. 278.

750. Jiwaji, Z. and G.E. Hardingham, *Good, bad, and neglectful: Astrocyte changes in neurodegenerative disease.* Free Radic Biol Med, 2022. **182**: p. 93-99.

751. Fuller, S., M. Steele, and G. Münch, *Activated astroglia during chronic inflammation in Alzheimer's disease--do they neglect their neurosupportive roles?* Mutat Res, 2010. **690**(1-2): p. 40-9.

752. Phelps, C.H., *Barbiturate-induced glycogen accumulation in brain. An electron microscopic study.* Brain Res, 1972. **39**(1): p. 225-34.

753. Pellerin, L. and P.J. Magistretti, *Glutamate uptake into astrocytes stimulates aerobic glycolysis: a mechanism coupling neuronal activity to glucose utilization.* Proc Natl Acad Sci U S A, 1994. **91**(22): p. 10625-9.

754. Nagai, M., et al., *Astrocytes expressing ALS-linked mutated SOD1 release factors selectively toxic to motor neurons.* Nat Neurosci, 2007. **10**(5): p. 615-22.

755. Liddelow, S.A., et al., *Neurotoxic reactive astrocytes are induced by activated microglia.* Nature, 2017. **541**(7638): p. 481-487.

756. Stavale, L.M., et al., *Temporal relationship between aquaporin-4 and glial fibrillary acidic protein in cerebellum of neonate and adult rats administered a BBB disrupting spider venom.* Toxicon, 2013. **66**: p. 37-46.

757. Bonomini, F. and R. Rezzani, *Aquaporin and blood brain barrier.* Curr Neuropharmacol, 2010. **8**(2): p. 92-6.

758. Cozzolino, M., et al., *Cysteine 111 affects aggregation and cytotoxicity of mutant Cu,Zn-superoxide dismutase associated with familial amyotrophic lateral sclerosis.* J Biol Chem, 2008. **283**(2): p. 866-74.

References

759. Tamtaji, O.R., et al., *Aquaporin 4: A key player in Parkinson's disease.* J Cell Physiol, 2019. **234**(12): p. 21471-21478.

760. Mader, S. and L. Brimberg, *Aquaporin-4 Water Channel in the Brain and Its Implication for Health and Disease.* Cells, 2019. **8**(2).

761. Yukutake, Y. and M. Yasui, *Regulation of water permeability through aquaporin-4.* Neuroscience, 2010. **168**(4): p. 885-91.

762. Lepore, A.C., et al., *Focal transplantation-based astrocyte replacement is neuroprotective in a model of motor neuron disease.* Nat Neurosci, 2008. **11**(11): p. 1294-301.

763. Alavi Naini, S.M. and N. Soussi-Yanicostas, *Tau Hyperphosphorylation and Oxidative Stress, a Critical Vicious Circle in Neurodegenerative Tauopathies?* Oxid Med Cell Longev, 2015. **2015**: p. 151979.

764. Kevenaar, J.T. and C.C. Hoogenraad, *The axonal cytoskeleton: from organization to function.* Front Mol Neurosci, 2015. **8**: p. 44.

765. Vega, I.E., et al., *Ezrin Expression is Increased During Disease Progression in a Tauopathy Mouse Model and Alzheimer's Disease.* Curr Alzheimer Res, 2018. **15**(12): p. 1086-1095.

766. Minamide, L.S., et al., *Neurodegenerative stimuli induce persistent ADF/cofilin-actin rods that disrupt distal neurite function.* Nat Cell Biol, 2000. **2**(9): p. 628-36.

767. Peuralinna, T., et al., *Genome-wide association study of neocortical Lewy-related pathology.* Ann Clin Transl Neurol, 2015. **2**(9): p. 920-31.

768. Avery, A.W., D.D. Thomas, and T.S. Hays, *β-III-spectrin spinocerebellar ataxia type 5 mutation reveals a dominant cytoskeletal mechanism that underlies dendritic arborization.* Proc Natl Acad Sci U S A, 2017. **114**(44): p. E9376-e9385.

769. Hammarlund, M., W.S. Davis, and E.M. Jorgensen, *Mutations in beta-spectrin disrupt axon outgrowth and sarcomere structure.* J Cell Biol, 2000. **149**(4): p. 931-42.

770. Sullivan, R., et al., *Spinocerebellar ataxia: an update.* J Neurol, 2019. **266**(2): p. 533-544.

771. Fletcher, D.A. and R.D. Mullins, *Cell mechanics and the cytoskeleton.* Nature, 2010. **463**(7280): p. 485-92.

772. Freymuth, P.S. and H.L. Fitzsimons, *The ERM protein Moesin is essential for neuronal morphogenesis and long-term memory in Drosophila.* Mol Brain, 2017. **10**(1): p. 41.

773. Yuan, A., et al., *Neurofilament subunits are integral components of synapses and modulate neurotransmission and behavior in vivo.* Mol Psychiatry, 2015. **20**(8): p. 986-94.

774. Jellinger, K.A., *Cell death mechanisms in neurodegeneration.* J Cell Mol Med, 2001. **5**(1): p. 1-17.

775. Forno, L.S., *Neuropathology of Parkinson's disease.* J Neuropathol Exp Neurol, 1996. **55**(3): p. 259-72.

References

776. Barnes, N., et al., *The copper-transporting ATPases, menkes and wilson disease proteins, have distinct roles in adult and developing cerebellum.* J Biol Chem, 2005. **280**(10): p. 9640-5.

777. Scheiber, I.F., J.F. Mercer, and R. Dringen, *Copper accumulation by cultured astrocytes.* Neurochem Int, 2010. **56**(3): p. 451-60.

778. La Fontaine, S., et al., *Intracellular Localization and Loss of Copper Responsiveness of Mnk, the Murine Homologue of the Menkes Protein, in Cells from Blotchy (Moblo) and Brindled (Mobr) Mouse Mutants.* Human Molecular Genetics, 1999. **8**(6): p. 1069-1075.

779. Xie, L. and J.F. Collins, *Transcriptional regulation of the Menkes copper ATPase (Atp7a) gene by hypoxia-inducible factor (HIF2{alpha}) in intestinal epithelial cells.* Am J Physiol Cell Physiol, 2011. **300**(6): p. C1298-305.

780. Xie, L. and J.F. Collins, *Transcription factors Sp1 and Hif2α mediate induction of the copper-transporting ATPase (Atp7a) gene in intestinal epithelial cells during hypoxia.* J Biol Chem, 2013. **288**(33): p. 23943-52.

781. Scemes, E. and D.C. Spray, *Increased intercellular communication in mouse astrocytes exposed to hyposmotic shocks.* Glia, 1998. **24**(1): p. 74-84.

782. Hao, C., et al., *Aquaporin-4 knockout enhances astrocyte toxicity induced by 1-methyl-4-phenylpyridinium ion and lipopolysaccharide via increasing the expression of cytochrome P4502E1.* Toxicol Lett, 2010. **198**(2): p. 225-31.

783. Fallier-Becker, P., I. Bonzheim, and F. Pfeiffer, *Cuprizone feeding induces swollen astrocyte endfeet.* Pflugers Arch, 2022. **474**(12): p. 1275-1283.

784. Tokuda, E., et al., *Wild-type Cu/Zn-superoxide dismutase is misfolded in cerebrospinal fluid of sporadic amyotrophic lateral sclerosis.* Mol Neurodegener, 2019. **14**(1): p. 42.

785. Squitti, R., et al., *Copper Imbalance in Alzheimer's Disease: Meta-Analysis of Serum, Plasma, and Brain Specimens, and Replication Study Evaluating ATP7B Gene Variants.* Biomolecules, 2021. **11**(7).

786. Zeng, Z., et al., *Dietary Copper Intake and Risk of Parkinson's Disease: a Cross-sectional Study.* Biol Trace Elem Res, 2024. **202**(3): p. 955-964.

787. Zhao, H.W., et al., *Assessing plasma levels of selenium, copper, iron and zinc in patients of Parkinson's disease.* PLoS One, 2013. **8**(12): p. e83060.

788. Fritz, E., et al., *Mutant SOD1-expressing astrocytes release toxic factors that trigger motoneuron death by inducing hyperexcitability.* J Neurophysiol, 2013. **109**(11): p. 2803-14.

789. Ramírez-Jarquín, U.N., et al., *Chronic infusion of SOD1(G93A) astrocyte-secreted factors induces spinal motoneuron degeneration and neuromuscular dysfunction in healthy rats.* J Cell Physiol, 2017. **232**(10): p. 2610-2615.

790. Staats, K.A. and L. Van Den Bosch, *Astrocytes in amyotrophic lateral sclerosis: direct effects on motor neuron survival.* J Biol Phys, 2009. **35**(4): p. 337-46.

791. Benkler, C., et al., *Aggregated SOD1 causes selective death of cultured human motor neurons.* Sci Rep, 2018. **8**(1): p. 16393.

References

792. Bruijn, L.I., et al., *ALS-linked SOD1 mutant G85R mediates damage to astrocytes and promotes rapidly progressive disease with SOD1-containing inclusions.* Neuron, 1997. **18**(2): p. 327-38.

793. Sasaki, S., et al., *Sporadic motor neuron disease with Lewy body-like hyaline inclusions.* Acta Neuropathol, 1989. **78**(5): p. 555-60.

794. Basso, M., et al., *Mutant copper-zinc superoxide dismutase (SOD1) induces protein secretion pathway alterations and exosome release in astrocytes: implications for disease spreading and motor neuron pathology in amyotrophic lateral sclerosis.* J Biol Chem, 2013. **288**(22): p. 15699-711.

795. Bakavayev, S., et al., *Blocking an epitope of misfolded SOD1 ameliorates disease phenotype in a model of amyotrophic lateral sclerosis.* Brain, 2023. **146**(11): p. 4594-4607.

796. Vande Velde, C., et al., *Misfolded SOD1 associated with motor neuron mitochondria alters mitochondrial shape and distribution prior to clinical onset.* PLoS One, 2011. **6**(7): p. e22031.

797. Reddi, A.R. and V.C. Culotta, *SOD1 integrates signals from oxygen and glucose to repress respiration.* Cell, 2013. **152**(1-2): p. 224-35.

798. Xiao, M., et al., *Pathophysiology of mitochondrial lipid oxidation: Role of 4-hydroxynonenal (4-HNE) and other bioactive lipids in mitochondria.* Free Radic Biol Med, 2017. **111**: p. 316-327.

799. Mattiazzi, M., et al., *Mutated human SOD1 causes dysfunction of oxidative phosphorylation in mitochondria of transgenic mice.* J Biol Chem, 2002. **277**(33): p. 29626-33.

800. Schröter, N., et al., *Nigral glucose metabolism as a diagnostic marker of neurodegenerative parkinsonian syndromes.* NPJ Parkinsons Dis, 2022. **8**(1): p. 123.

801. Nagahama, Y., et al., *Cerebral glucose metabolism in corticobasal degeneration: comparison with progressive supranuclear palsy and normal controls.* Mov Disord, 1997. **12**(5): p. 691-6.

802. Swerdlow, R.H., et al., *Mitochondrial dysfunction in cybrid lines expressing mitochondrial genes from patients with progressive supranuclear palsy.* J Neurochem, 2000. **75**(4): p. 1681-4.

803. Grossman, L.I., et al., *Molecular evolution of aerobic energy metabolism in primates.* Mol Phylogenet Evol, 2001. **18**(1): p. 26-36.

804. Harman, D., *Aging: a theory based on free radical and radiation chemistry.* J Gerontol, 1956. **11**(3): p. 298-300.

805. Harman, D., *Free radicals in aging.* Mol Cell Biochem, 1988. **84**(2): p. 155-61.

806. Kuhar, M.J., *On the use of protein turnover and half-lives.* Neuropsychopharmacology, 2009. **34**(5): p. 1172-3.

807. Kuhar, M.J. and A.R. Joyce, *Slow onset of CNS drugs: can changes in protein concentration account for the delay?* Trends Pharmacol Sci, 2001. **22**(9): p. 450-6.

References

808. Cohen, G., *The pathobiology of Parkinson's disease: biochemical aspects of dopamine neuron senescence.* J Neural Transm Suppl, 1983. **19**: p. 89-103.

809. Jacobson, J. and M.R. Duchen, *Mitochondrial oxidative stress and cell death in astrocytes--requirement for stored Ca2+ and sustained opening of the permeability transition pore.* J Cell Sci, 2002. **115**(Pt 6): p. 1175-88.

810. Kushnareva, Y., A.N. Murphy, and A. Andreyev, *Complex I-mediated reactive oxygen species generation: modulation by cytochrome c and NAD(P)+ oxidation-reduction state.* Biochem J, 2002. **368**(Pt 2): p. 545-53.

811. Prudencio, M., et al., *Modulation of mutant superoxide dismutase 1 aggregation by co-expression of wild-type enzyme.* J Neurochem, 2009. **108**(4): p. 1009-18.

812. Karch, C.M. and D.R. Borchelt, *Aggregation modulating elements in mutant human superoxide dismutase 1.* Arch Biochem Biophys, 2010. **503**(2): p. 175-82.

813. Wang, J., G. Xu, and D.R. Borchelt, *Mapping superoxide dismutase 1 domains of non-native interaction: roles of intra- and intermolecular disulfide bonding in aggregation.* J Neurochem, 2006. **96**(5): p. 1277-88.

814. Boyd, S.D., et al., *Copper Sources for Sod1 Activation.* Antioxidants (Basel), 2020. **9**(6).

815. Fujiwara, N., et al., *Oxidative modification to cysteine sulfonic acid of Cys111 in human copper-zinc superoxide dismutase.* J Biol Chem, 2007. **282**(49): p. 35933-44.

816. Fares, M.B., et al., *Induction of de novo α-synuclein fibrillization in a neuronal model for Parkinson's disease.* Proc Natl Acad Sci U S A, 2016. **113**(7): p. E912-21.

817. Landeck, N., et al., *Two C-terminal sequence variations determine differential neurotoxicity between human and mouse α-synuclein.* Mol Neurodegener, 2020. **15**(1): p. 49.

818. Penkowa, M., et al., *Zinc or copper deficiency-induced impaired inflammatory response to brain trauma may be caused by the concomitant metallothionein changes.* J Neurotrauma, 2001. **18**(4): p. 447-63.

819. Luna-Viramontes, N.I., et al., *PHF-Core Tau as the Potential Initiating Event for Tau Pathology in Alzheimer's Disease.* Front Cell Neurosci, 2020. **14**: p. 247.

820. Macco, R., et al., *Astrocytes acquire resistance to iron-dependent oxidative stress upon proinflammatory activation.* J Neuroinflammation, 2013. **10**: p. 130.

821. Mills, E., et al., *Mechanisms of brain iron transport: insight into neurodegeneration and CNS disorders.* Future Med Chem, 2010. **2**(1): p. 51-64.

822. Vilhardt, F., et al., *Microglia antioxidant systems and redox signalling.* Br J Pharmacol, 2017. **174**(12): p. 1719-1732.

823. Röhl, C., et al., *Activated microglia modulate astroglial enzymes involved in oxidative and inflammatory stress and increase the resistance of astrocytes to oxidative stress in vitro.* Glia, 2008. **56**(10): p. 1114-26.

824. Dixon, S.J., et al., *Ferroptosis: an iron-dependent form of nonapoptotic cell death.* Cell, 2012. **149**(5): p. 1060-72.

References

825. Xie, Y., et al., *Ferroptosis: process and function.* Cell Death Differ, 2016. **23**(3): p. 369-79.

826. Sunshine, H. and M.L. Iruela-Arispe, *Membrane lipids and cell signaling.* Curr Opin Lipidol, 2017. **28**(5): p. 408-413.

827. Drin, G., *Topological regulation of lipid balance in cells.* Annu Rev Biochem, 2014. **83**: p. 51-77.

828. Steenbergen, R., et al., *Disruption of the phosphatidylserine decarboxylase gene in mice causes embryonic lethality and mitochondrial defects.* J Biol Chem, 2005. **280**(48): p. 40032-40.

829. Prasad, M.R., et al., *Regional membrane phospholipid alterations in Alzheimer's disease.* Neurochem Res, 1998. **23**(1): p. 81-8.

830. González-Domínguez, R., T. García-Barrera, and J.L. Gómez-Ariza, *Combination of metabolomic and phospholipid-profiling approaches for the study of Alzheimer's disease.* J Proteomics, 2014. **104**: p. 37-47.

831. Smith, J.D., *Apolipoprotein A-I and its mimetics for the treatment of atherosclerosis.* Curr Opin Investig Drugs, 2010. **11**(9): p. 989-96.

832. Duong, M.T., et al., *Cholesterol, Atherosclerosis, and APOE in Vascular Contributions to Cognitive Impairment and Dementia (VCID): Potential Mechanisms and Therapy.* Front Aging Neurosci, 2021. **13**: p. 647990.

833. Heng, J.I., A. Chariot, and L. Nguyen, *Molecular layers underlying cytoskeletal remodelling during cortical development.* Trends Neurosci, 2010. **33**(1): p. 38-47.

834. Povea-Cabello, S., et al., *Dynamic Reorganization of the Cytoskeleton during Apoptosis: The Two Coffins Hypothesis.* Int J Mol Sci, 2017. **18**(11).

835. Moss, D.K. and J.D. Lane, *Microtubules: forgotten players in the apoptotic execution phase.* Trends Cell Biol, 2006. **16**(7): p. 330-8.

836. da Silva, A.B.S. and M.A.Z. Arruda, *Single-cell ICP-MS to address the role of trace elements at a cellular level.* J Trace Elem Med Biol, 2023. **75**: p. 127086.

837. Paul, B., et al., *Correction: Visualising mouse neuroanatomy and function by metal distribution using laser ablation-inductively coupled plasma-mass spectrometry imaging.* Chem Sci, 2016. **7**(10): p. 6576.

838. Asai, S. and A. Limbeck, *LA-ICP-MS of rare earth elements concentrated in cation-exchange resin particles for origin attribution of uranium ore concentrate.* Talanta, 2015. **135**: p. 41-9.

839. Roudeau, S., et al., *Native Separation and Metallation Analysis of SOD1 Protein from the Human Central Nervous System: a Methodological Workflow.* Anal Chem, 2021. **93**(32): p. 11108-11115.

840. Visser, N.F., H. Lingeman, and H. Irth, *Sample preparation for peptides and proteins in biological matrices prior to liquid chromatography and capillary zone electrophoresis.* Anal Bioanal Chem, 2005. **382**(3): p. 535-58.

Appendices

Table A1. Study demographic data for human tissue samples

Study ID	Age	Gender	Diagnosis	Disease duration (yrs)	PMI (hrs)	Cause of death	Histology	Solution ICPMS	LAICPMS	Western blot/activity
PSP-RS 01	77	Female	PSP-RS	1	9	Cardiorespiratory failure	X			
PSP-RS 02	70	Female	PSP-RS	3	37	Cachexia, swallow dyspraxia		X		X
PSP-RS 03	76	Female	PSP-RS	6	3	Cardiorespiratory failure	X	X		X
PSP-RS 04	81	Male	PSP-RS	9	8	Pneumonia	X	X		X
PSP-RS 05	78	Female	PSP-RS	5	18	Cardiorespiratory failure	X			
PSP-RS 06	78	Male	PSP-RS	14	31	Cardiovascular failure	X	X		X
PSP-RS 07	80	Male	PSP-RS	6	18	Cardiorespiratory failure		X		X
PSP-RS 08	70	Female	PSP-RS	5	32	Cardiorespiratory failure		X		X
PSP-RS 09	79	Male	PSP-RS	9	26	Respiratory failure	X	X		X
PSP-RS 10	86	Female	PSP-RS	1	69	Cardiorespiratory failure	X			
PSP-RS 11	74	Female	PSP-RS	5	27	Aspiration pneumonia		X		X
PSP-RS 12	68	Female	PSP-RS	2	13	Cardiorespiratory failure	X	X		X
PSP-RS 13	71	Male	PSP-RS	7	58	cardiorespiratory failure	X			
PSP-RS 14	80	Female	PSP-RS	3	14	Acute kidney injury		X		X
PSP-RS 15	76	Male	PSP-RS	2	30	cardiorespiratory failure	X	X		X
PSP-RS 16	72	Female	PSP-RS	4	33	Cardiorespiratory failure		X		X
PSP-RS 17	67	Male	PSP-RS	5	19	Cardiorespiratory failure		X		X
PSP-RS 18	70	Male	PSP-RS	11	22	Cardiorespiratory failure		X		X
PSP-RS 19	80	Male	PSP-RS	7	25	Multi organ failure		X		X
PSP-RS 20	63	Male	PSP-RS	6	38	Corticobasal degeneration			X	
PSP-RS 21	69	Female	PSP-RS	15	38.5	Coroners case - Unascertained			X	
PSP-RS 22	68	Male	PSP-RS	6	61	Aspiration pneumonia			X	
PSP-RS 23	76	Male	PSP-RS	5	50.5	Aspiration pneumonia			X	
PSP-P 01	69	Male	PSP-P	10	23	Cardiorespiratory failure	X			
PSP-P 02	88	Male	PSP-P	18	38	Cardiorespiratory failure	X			
PSP-P 03	75	Female	PSP-P	9	13	Cardiorespiratory failure	X			
NNC 01	68	Male	control	n/a	11	End stage renal failureheart disease	X			
NNC 02	85	Female	control	n/a	23	Pneumonia	X			
NNC 03	79	Male	control	n/a	8	Probable pulmonary embolism	X			
NNC 04	89	Male	control	n/a	24	Sepsis	X			
NNC 05	90	Female	control	n/a	58	Cardiovascular failure	X			
NNC 06	88	Female	control	n/a	31	Congestive cardiac failure	X			
NNC 07	84	Male	control	n/a	22	Cardiovascular failure	X	X		X
NNC 08	84	Male	control	n/a	36	Severe pulmonary hypertension	X	X		X
NNC 09	80	Female	control	n/a	29	Cardiac failure	X	X		X
NNC 10	64	Male	Control	n/a	68	Ischaemic Heart Disease		X	X	X
NNC 11	66	Female	Control	n/a	43	Metastatic leiomyosarcoma		X	X	X
NNC 12	69	Male	Control	n/a	36	Coronary artery disease		X	X	X
NNC 13	76	Male	Control	n/a	50	AMI		X	X	X

Control cases were pathologically confirmed free of neurological disease. [#]Period from diagnosis to death. PSP: Progressive supranuclear palsy; PMI: Post-mortem interval; n/a: not applicable

Appendices

Table A2. List of antibodies used for immunohistochemistry and western blotting

Protein target	Antibody	Assay	Host	Reactivity	Immunogen
Ionised calcium binding adaptor molecule 1 (IBA1)	Abcam (ab225261)	IHC	Rabbit	Human, mouse, rat	Unspecified
Glial Fibrillary Acidic protein (GFAP)	Abcam (Ab53554)	IHC	Goat	Human, mouse, rat	GFAP aa 400 to the C-terminus (C terminal)
SOD1 (accumulated)	Sigma HPA001401	IHC	Rabbit	Human, mouse, rat	Superoxide dismutase 1 recombindant protein epitope signature tag (PrEST)
SOD1-EDI (exposed dimer interface)	Stressmarq (SPC-206)	IHC	Rabbit	Human, mouse, rat, pig	C-terminal region of SOD1, exposed dimer interface (EDI)
Ceruloplasmin	Dako/Agilent (Q0121)	Western blot	Rabbit	Human	
Hephaestin	Abcam (ab95137)	Western blotting	Rabbit	Human	residues 400 - 500 of Human hephaestin
Beta-actin	Cell signalling (4970)	Western blotting	Rabbit	Human, mouse, rat, pig, monkey, bovine	N-terminus of human β-actin protein
GAPDH	Cell signalling (2118)	Western blotting	Rabbit	Human, mouse, rat, pig, monkey, bovine	residues surrounding Lys260 of human GAPDH protein
Human SOD1	Abcam (ab79390)	Western blotting	Rabbit	Human	Unspecified

Appendices

Table A3. List of Taqman human and mouse probes used in gene expression experiments

	Gene	Species	Taq #	Protein
Astrocyte marker	Aldh1l	Human	Hs01003842_m1	aldehyde dehydrogenase 1 family member L1
Astrocyte marker	Aqp4	Human	Hs00242342_m1	aquaporin 4
Copper handling	Atox	Human	Hs00187841_m1	Antioxidant 1 Copper Chaperone
Copper handling	Atp7a	Human	Hs00163707_m1	ATPase Copper Transporting Alpha
Copper handling	Atp7b	Human	Hs01075310_m1	ATPase Copper Transporting Beta
Copper handling	Ccs	Human	Hs00192851_m1	Copper chaperone for SOD
Neuronal marker	Chat	Human	Hs00758143_m1	Choline O-acetyltransferase
Copper handling	Commd1	Human	Hs00415059_m1	Copper Metabolism Domain Containing 1
Copper handling	Cox11	Human	Hs00362087_m1	Cytochrome C Oxidase Copper Chaperone COX11
Copper handling	Cox17	Human	Hs01053235_g1	Cytochrome C Oxidase Copper Chaperone COX17
Cuproenzyme	Cp	Human	Hs00236810_m1	Ceruloplasmin (ferroxidase)
Microglial marker	Cplx1	Human	Hs00362510_m1	Complexin 1
Microglial marker	Cplx2	Human	Hs00932617_m1	Complexin 2
Microglial marker	Cx3cr1	Human	Hs01922583_s1	C-X3-C motif chemokine receptor 1
Cuproenzyme	Dbh	Human	Hs01089840_m1	Dopamine beta-hydroxylase
Neuronal marker	Ddc	Human	Hs01105048_m1	Dopa decarboxylase
Neuronal marker	Gabra1	Human	Hs00971228_m1	Gamma-aminobutyric acid type A receptor alpha1 subunit
Housekeeper	Gapdh	Human	Hs02758991_g1	Glyceraldehyde-3-Phosphate dehydrogenase
Astrocyte marker	Gfap	Human	Hs00909233_m1	Glial fibrillary acidic protein
Cuproenzyme	Heph	Human	Hs00953259_m1	Hephaestin
Cuproenzyme	Maob	Human	Hs01106246_m1	Glial Fibrillary Acidic Protein
Neuronal marker	Map2	Human	Hs00258900_m1	Microtubule associated protein 2
Neuronal marker	Mapt	Human	Hs00902194_m1	Microtubule Associated Protein Tau
Oligo marker	Mbp	Human	Hs00921945_m1	Myelin basic protein
Oligo marker	Mog	Human	Hs01555268_m1	Myelin oligodendrocyte glycoprotein
Copper handling	Mt1a	Human	Hs00831826_s1	Metallothionein 1A
Copper handling	Mt1b	Human	Hs04401199_s1	Metallothionein 1G
Copper handling	Mt2a	Human	Hs02379661_g1	Metallothionein 2A
Copper handling	Mt3	Human	Hs00359394_g1	Metallothionein 3
Copper handling	Mtf1	Human	Hs00232306_m1	Metal Regulatory Transcription Factor 1
Copper handling	Mtf2	Human	Hs00980938_m1	Metal Regulatory Transcription Factor 2
Neuronal marker	Nefh	Human	Hs00606024_m1	Neurofilament heavy polypeptide
Neuronal marker	Rbfox	Human	Hs01370654_m1	RNA binding protein, fox-1 homolog 3
Copper handling	Sco1	Human	Hs01552201_m1	Myelin-Oligodendrocyte Glycoprotein
Copper handling	Slc31a1	Human	Hs00977266_g1	Solute carrier family 31 member 1
Cuproenzyme	Sod1	Human	Hs00533490_m1	Superoxide dismutase 1, soluble
Copper handling	Steap1	Human	Hs00185180_m1	Six transmembrane epithelial antigen of the prostate 1

Appendices

Copper handling	Steap2	Human	Hs00401292_m1	Six transmembrane epithelial antigen of the prostate 2
Copper handling	Steap3	Human	Hs00217292_m1	Six transmembrane epithelial antigen of the Prostate 3
Copper handling	Steap4	Human	Hs01026584_m1	Six transmembrane epithelial antigen of the prostate 4
Neuronal marker	Snap25	Human	Hs00938957_m1	Synaptosome associated protein 25
Neuronal marker	Th	Human	Hs00165941_m1	Tyrosine hydroxylase
Microglial marker	Tmem119	Human	Hs01938722_u1	Transmembrane protein 119
Neuronal marker	Tubb3	Human	Hs00801390_s1	Tubulin beta 3 class III
Copper handling	Xiap	Human	Hs00745222_s1	X-linked inhibitor of apoptosis
Astrocyte marker	Aldh1l1	Mouse	Mm03048957_m1	Aldehyde Dehydrogenase 1 Family Member L1
Copper handling	Atox1	Mouse	Mm00839626_m1	Antioxidant 1 Copper Chaperone
Copper handling	Atp7a	Mouse	Mm00437663_m1	ATPase Copper Transporting Alpha
Copper handling	Atp7b	Mouse	Mm00599675_m1	ATPase Copper Transporting Beta
Copper handling	Ccs	Mouse	Mm00444148_m1	Copper chaperone for SOD
Copper handling	Commd1	Mouse	Mm01239669_m1	Copper Metabolism Domain Containing 1
Copper handling	Cox11	Mouse	Mm01615963_g1	Cytochrome C Oxidase Copper Chaperone COX11
Copper handling	Cox17	Mouse	Mm01346225_m1	Cytochrome C Oxidase Copper Chaperone COX17
Housekeeper	Gapdh	Mouse	Mm99999915_g1	Glyceraldehyde-3-Phosphate Dehydrogenase
Astrocyte marker	Gfap	Mouse	Mm01253033_m1	Glial Fibrillary Acidic Protein
Neuronal marker	Mapt	Mouse	Mm00521988_m1	Microtubule Associated Protein Tau
Oligo marker	Mog	Mouse	Mm01279062_m1	Myelin-Oligodendrocyte Glycoprotein
Copper handling	Mt1	Mouse	Mm00496660_g1	metallothionein 1
Copper handling	Mt2	Mouse	Mm00809556_s1	metallothionein 2
Copper handling	Mt3	Mouse	Mm00496661_g1	metallothionein 3
Copper handling	Mtf1	Mouse	Mm00485274_m1	Metal Regulatory Transcription Factor 1
Copper handling	Mtf2	Mouse	Mm00489151_m1	Metal Response Element Binding Transcription Factor 2
Copper handling	Nefh	Mouse	Mm01191455_m1	Neurofilament Heavy Chain
Copper handling	Sco1	Mouse	Mm01329074_m1	Synthesis Of Cytochrome C Oxidase 1
Copper handling	Slc31a1 (Ctr1)	Mouse	Mm00558247_m1	Copper transport related protein 1 (copper import)
Copper handling	Steap1	Mouse	Mm00459097_m1	STEAP Family Member 1
Copper handling	Steap2	Mouse	Mm01320129_m1	STEAP Family Member 2
Copper handling	Steap3	Mouse	Mm01287243_m1	STEAP Family Member 3
Copper handling	Steap4	Mouse	Mm00475405_m1	STEAP Family Member 4
Neuronal marker	Syp	Mouse	Mm00436850_m1	Synaptophysin
Copper handling	Xiap	Mouse	Mm00776505_m1	X-Linked Inhibitor Of Apoptosis

Appendices

Table A4. Buffer and reagent preparation

Homogenisation buffer (Chapter 3, Section 3.2.2)	Homogenisation buffer consisted of 50mM Tris, 150mM NaCl, (pH 7.4) Containing cOmplete, EDTA-free protease inhibitor (Roche, Sigma-Aldrich), phosphatase inhibitors II (500 µL, Sigma-Aldrich) and DNAse I (500 µL prepared in 20mM HEPES/glycerol).
Perfusing buffer (Section 4.3.1)	Perfusate buffer was 0.1M PBS (pH 7.4) containing anti-coagulant heparin (20U/mL, Sigma-Aldrich), cOmplete, EDTA-free protease (Roche, Sigma-Aldrich) and phosphatase inhibitor (Sigma-Aldrich) cocktail II dissolved in 0.1M PBS (pH 7.4).
LCMS/MS Buffer A1 Section 5.2.3)	2% acetonitrile, 0.01% trifluoroacetic acid
LCMS/MS Buffer A2 (Section 5.2.3)	0.1% formic acid, 2% DMSO
LCMS/MS Buffer B (Section 5.2.3)	0.1% formic acid, 77.9% acetonitrile, 2% DMSO

Appendices

Table A5. Metal concentration in the substantia nigra within PSP detected by bulk ICPMS

	Copper µg g^{-1}		Iron µg g^{-1}		Zinc µg g^{-1}	
	Soluble	**Insoluble**	**Soluble**	**Insoluble**	**Soluble**	**Insoluble**
PSP	3.56 ± 0.29** (N = 15)	1.40 ± 0.08** (N = 15)	87.75 ± 9.44 (N = 15)	135.6 ± 17.71 (N = 15)*	4.73 ± 0.26 (N = 15)	7.21 ± 0.45 (N = 15)*
Control	5.65 ± 0.56 (N = 7)	1.93 ± 0.09 (N = 7)	56.82 ± 10.62 (N = 7)	75.81 ± 14.23 (N = 7)	3.84 ± 0.31 (N = 7)	5.66 ± 0.48 (N = 7)

Values represented as mean ± SEM, N. Two tailed t-test comparing metal concentration in control versus PSP in each within each fraction. Significance is noted when ** P<0.01 and * P<0.05.

Table A6. Metal concentration within PSP brain regions detected by LA-ICPMS

	Copper µg g^{-1}			Iron µg g^{-1}			Zinc µg g^{-1}		
	SNc	**SNr**	**CPn**	**SNc**	**SNr**	**CPn**	**SNc**	**SNr**	**CPn**
PSP	30.97 ± 1.90 (N = 3)	31.3 ± 1.41 (N = 3)	20.47 ± 3.01 (N = 3)	617.067 ± 143.88 N = 3)	585.67 ± 80.52 N = 3)	542.23 ± 89.97 N = 3)	47.13 ± 3.23 (N = 3)	52.6 ± 2.80 (N = 3)	39.77± 1.18 (N = 3)*
Control	95.47 ± 11.43 (N = 3)	88.67 ± 29.50 (N = 3)	63.00 ± 34.57 (N = 3)	656.07 ± 230.79 (N = 3)	727.43 ± 298.59 (N = 3)	336.87 ± 137.03 (N = 3)	65.00 ± 7.6 (N = 2)	70.05 ± 6.05 (N = 2)	49.55 ± 1.35 (N = 2)

SNc; substantia nigra *pars compacta*, SNr; substantia nigra *pars reticulata*; and cerebral peduncle (CPn). Values represented as mean ± SEM, N. Multiple t-tests (two sided) comparing the metal concentrations between PSP and control within each region. Significance is noted when ** P<0.01 and * P<0.05.

Table A7. Metal concentration within substantia nigra of Slc31a1$^{-/+}$ mice detected by ICPMS

	Copper µg g^{-1}	Iron µg g^{-1}	Zinc µg g^{-1}
Slc31a1$^{-/+}$	1.18 ± 0.05*** (N = 5)	11.14 ± 0.90 (N = 5)	6.17 ± 0.30 (N = 4)
Wildtype	2.15 ± 0.11 (N = 4)	9.98 ± 0.84 (N = 4)	6.17 ± 0.38 (N = 4)

Values represented as mean ± SEM, N. Two tailed t-test comparing metal concentration in substantia nigra within wildtype versus Slc31a1$^{-/+}$ mice. Significance is noted when *** P<0.001.

Appendices

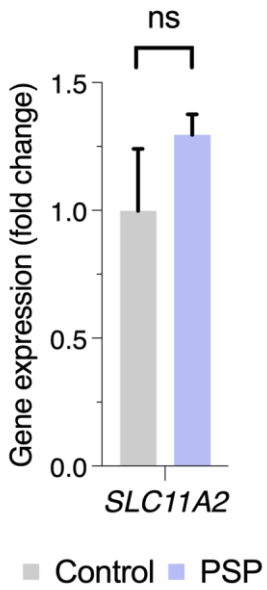

Figure A1. The mRNA levels of *SLC11A2* in PSP relative to control

Measurement of divalent metal transporter 1 (*DMT1*; *SLC11A2*) levels using qPCR from tissue homogenates within the substantia nigra from PSP cases. Data expressed as mean ± SEM expression relative to control. T-test (two tailed) was used to test significance.

Appendices

Table A8. The differentially expressed protein in the substantia nigra of PSP

Upregulated			Downregulated		
Protein	**Fold change**	**-Log P**	**Protein**	**Fold change**	**-Log P**
Monoamine oxidase B (MAOB)	0.79	8.17	Heat shock protein family A (Hsp70) member 12A (HSPA12A)	-0.44	4.59
1-phosphatidylinositol 4,5-bisphosphate phosphodiesterase delta-1 (PLCD1)	0.95	7.29	Pyruvate dehydrogenase complex component X (PDHX)	-0.5	4.53
Moesin (MSN)	0.76	7.13	Sodium/potassium-transporting ATPase subunit alpha-3 (ATP1A3)	-0.44	4.52
Esterase D (ESD)	0.47	5.63	Mammalian ependymin-related protein 1 (EPDR1/UCC1)	-1.16	4.48
6-phosphogluconolactonase (PGLS)	0.44	5.5	Oxoglutarate dehydrogenase L (OGDHL)	-0.55	4.44
Four and a half LIM domains protein 1 (FHL1)	0.64	5.45	Cytochrome c oxidase subunit 6B1 (COX6B1)	-0.43	4.35
Phosphoglycerate mutase 2 (PGAM2)	1.4	4.97	Cytochrome c oxidase subunit 5A (COX5A)	-0.41	4.21
Transgelin-2 (TAGLN2)	1.22	4.69	Microtubule associated protein 6 (MAP6)	-0.49	4.17
Peptidase inhibitor 16 (PI16)	1.59	4.69	Ornithine aminotransferase (OAT)	-0.7	4.09
Annexin (ANXA1)	2.11	4.61	Target of myb1 like 2 membrane trafficking protein (TOM1L2)	-0.39	4.09
Mitogen-activated protein kinase;Mitogen-activated protein kinase 1 (MAPK1)	0.47	4.59	ATP synthase subunit beta (ATP5F1B)	-0.38	4.08
Sorcin (SRI)	0.62	4.58	Spectrin beta (SPTBN2)	-0.55	4
Ezrin (EZR)	0.92	4.53	Sodium-Potassium ATPase Subunit Beta 1 (ATP1B1)	-0.41	3.91
CD44 antigen (CD44)	1.2	4.43	Alpha 2-HS Glycoprotein (AHSG)	-1.81	3.88
Lymphocyte Cytosolic Protein 1 (LCP1)	0.96	4.33	Erythrocyte membrane protein band 4.1 like 3 (EPB41L3)	-0.37	3.85
Glial fibrillary acidic protein (GFAP)	1.11	4.25	Eukaryotic translation elongation factor 1 gamma (EEF1G)	-0.57	3.78
Leucine aminopeptidase 3 (LAP3)	0.6	4.14	ATP synthase subunit delta (ATP5F1D)	-0.37	3.75
Diazepam Binding Inhibitor (Acyl-CoA-binding protein) (DBI)	0.75	3.96	Solute carrier family 25 member 10 (SLC25A10)	-0.7	3.71
Histamine N-methyltransferase (HNMT)	0.78	3.92	DnaJ heat shock protein family (Hsp40) member C6 (DNAJC6)	-0.47	3.69
Capping actin Protein, Gelsolin Like (CAPG)	1.03	3.89	NFS1 cysteine desulfurase (NFS1)	-0.54	3.65
Neural cell adhesion molecule 1 (NCAM1)	0.22	3.85	Apolipoprotein A2 (APOA2)	-2.2	3.64
Phosphatidylethanolamine-binding protein 1 (PEBP1)	0.31	3.81	Cytochrome c oxidase subunit 6C (COX6C)	-0.46	3.64
RAB2 (RAB21)	0.58	3.73	Microtubule associated protein 1A (MAP1A)	-0.35	3.62
Aldehyde dehydrogenase 7 family member A1 (ALDH7A1)	0.51	3.72	Pyruvate dehydrogenase E1 subunit beta (PDHB)	-0.33	3.53
Neuroblast differentiation-associated protein AHNAK (AHNAK)	0.91	3.69	Pyruvate dehydrogenase E1 subunit alpha 1 (PDHA1)	-0.39	3.49
Synemin (SYNM)	2.33	3.62	G elongation factor mitochondrial 1 (GFM1)	-1.13	3.46
Adducin 3 (ADD3)	0.63	3.61	Leucine rich pentatricopeptide repeat containing (LRPPRC)	-0.65	3.43

Appendices

PDZ and LIM domain 5 (PDLIM5)	0.82	3.61	Eukaryotic translation elongation factor 1 alpha 2(EEF1A2)	-0.66	3.42
Aldehyde dehydrogenase 9 family member A1 (ALDH9A1)	0.39	3.53	SRA Stem-Loop Interacting RNA Binding Protein (SLIRP)	-1.38	3.38
Heat shock protein beta-6 (HSPB6)	1.84	3.51	NADH:ubiquinone oxidoreductase core subunit V1 (NDUFV1)	-0.49	3.33
Leukotriene A4 hydrolase (LTA4H)	0.34	3.43	Dihydrolipoamide S-succinyltransferase (DLST)	-0.29	3.33
Selenium binding protein 1 (SELENBP1)	0.66	3.43	Tyrosyl-tRNA synthetase 1 (YARS1)	-0.3	3.32
Gamma-butyrobetaine hydroxylase 1 (BBOX1)	0.73	3.43	Synuclein gamma (SNCG)	-0.69	3.29
Ras-related protein (RAB4A)	1.38	3.43	Oxoglutarate dehydrogenase (OGDH)	-0.35	3.22
Aquaporin-4 (AQP4)	1.11	3.38	Acyl-CoA thioesterase 7(ACOT7)	-0.41	3.21
Heat shock protein beta-1 (HSPB1)	1.03	3.33	VAMP associated protein B and C (VAPB)	-0.29	3.17
Argininosuccinate synthase 1 (ASS1)	0.67	3.24	Apolipoprotein A1 (APOA1)	-1.56	3.09
Calcyphosin (CAPS)	2.12	3.15	Annexin A6 (ANXA6)	-0.27	3.06
Modulator of VRAC current 1 (MLC1)	2.35	3.13	Ts translation elongation factor (TSFM)	-0.46	3.02
Microtubule associate protein Tau (MAPT)	0.35	3.1	Heat shock protein family A (Hsp70) member 9 (HSPA9)	-0.35	3.02
Calpain 2 (CAPN2)	0.48	3.08	1,4-alpha-glucan branching enzyme 1 (GBE1)	-1.08	3
Tropomyosin 3 (TPM3)	0.49	3.08	Neurocan core protein (NCAN)	-1.57	2.99
Galectin 3 (LGALS3)	1.01	3.08	Kinesin family member 21A (KIF21A)	-0.54	2.98
Filamin C (FLNC)	2.3	3.07	Aconitase 2 (ACO2)	-0.29	2.97
Abhydrolase domain containing 14B (ABHD14B)	0.62	3.03	Internexin neuronal intermediate filament protein alpha (INA)	-0.62	2.93
Guanosine monophosphate reductase (GMPR)	0.77	3.02	NADH:ubiquinone oxidoreductase subunit A6 (NDUFA6)	-0.51	2.83
Catenin delta 2 (CTNND2)	0.55	3.01	Amphiphysin (AMPH)	-0.38	2.83
Nicotinamide phosphoribosyltransferase (NAMPT)	0.98	3.01	Sialic acid acetylesterase (SIAE)	-0.94	2.82
Secreted protein acidic and cysteine rich (SPARC)	0.91	3	Ubiquinol-cytochrome c reductase core protein 1 (UQCRC1)	-0.41	2.8
Filamin A (FLNA)	0.76	2.97	Synuclein beta (SNCB)	-0.56	2.79
Adenylate kinase 1 (AK1)	0.51	2.95	Cytochrome c oxidase subunit 5B (COX5B)	-0.41	2.79
Glycogenin 1 (GYG1)	0.46	2.94	Eukaryotic translation initiation factor 5 (EIF5)	-0.36	2.75
Phosphoserine aminotransferase 1 (PSAT1)	0.57	2.92	Contactin 2 (CNTN2)	-0.47	2.73
Annexin A2 (ANXA2)	1.07	2.91	Succinate-CoA ligase ADP-forming subunit beta (SUCLA2)	-0.33	2.73
Aldo-keto reductase family 7 member A2 (AKR7A2)	0.51	2.89	NADH:ubiquinone oxidoreductase core subunit S8 (NDUFS8)	-0.48	2.71
Glutathione S-transferase pi 1 (GSTP1)	0.48	2.88	NADH:ubiquinone oxidoreductase subunit A13 (NDUFA13)	-0.48	2.7
Hepatic and glial cell adhesion molecule (HEPACAM)	0.99	2.87	Complexin 1 (CPLX1)	-0.86	2.69
p calcium binding protein A11 (S100A11)	0.99	2.84	Glutaminase (GLS)	-0.53	2.68
Fumarylacetoacetate hydrolase (FAH)	1.07	2.84	Reticulon 4 (RTN4)	-0.33	2.66
Fatty acid binding protein 5 (FABP5)	0.6	2.82	Transferrin (TF)	-0.74	2.64

Appendices

Copine 3 (CPNE3)	1.06	2.81
FERM domain containing kindlin 2 (FERMT2)	0.53	2.78
Myosin heavy chain 9 (MYH9)	0.35	2.74
Plectin (PLEC)	0.68	2.74
LIM zinc finger domain containing 1 (LIMS1)	0.86	2.74
PBX homeobox interacting protein 1 (PBXIP1)	0.58	2.73
Aldehyde dehydrogenase 1 family member L1 (ALDH1L1)	0.58	2.7
Peroxiredoxin 1 (PRDX1)	0.46	2.66
Glycogen phosphorylase L (PYGL)	0.89	2.63
Phospholipase C delta 3 (PLCD3)	0.59	2.62
IQ motif containing GTPase activating protein 1 (IQGAP1)	0.7	2.62
Protein S100-A6 (S100A6)	1.21	2.61
Epoxide hydrolase 4 (EPHX4)	0.79	2.6
Vimentin (VIM)	1.18	2.59
Potassium channel tetramerization domain containing 12 (KCTD12)	1.24	2.57
Ciliary rootlet coiled-coil, rootletin (CROCC)	0.42	2.55
Serpin family b member 1 (SERPINB1)	1.17	2.55
Catenin beta 1 (CTNNB1)	0.25	2.53
Dimethylarginine dimethylaminohydrolase 1 (DDAH1)	0.3	2.48
cysteine and glycine rich protein 1 (CSRP1)	0.44	2.48
GH3 domain containing (GHDC)	0.74	2.47
RAS related (RRAS)	0.76	2.47
Annexin A4 (ANXA4)	0.6	2.41
Phospholysine phosphohistidine inorganic pyrophosphate phosphatase (LHPP)	0.48	2.38
Ro60, Y RNA binding protein (TROVE2)	0.37	2.36
Phytanoyl-CoA dioxygenase domain containing 1 (PHYHD1)	1.13	2.36
Kelch repeat and BTB domain containing 11 (KBTBD11)	0.44	2.34
Glia maturation factor beta (GMFB)	0.79	2.34
Sequestosome-1 (SQSTM1)	1.38	2.34
Serpin family A member 3 (SERPINA3)	1.63	2.34
Heat shock protein 90 alpha family class A member 1 (HSP90AA1)	-0.19	2.64
Ubiquinol-cytochrome c reductase core protein 2 (UQCRC2)	-0.39	2.62
prolyl isomerase 3 (FKBP3)	-0.46	2.61
Heat shock protein 90 alpha family class B member 1 (HSP90AB1)	-0.32	2.61
Complexin 2 (CPLX2)	-0.77	2.61
Fumarylacetoacetate hydrolase domain containing 1 (FAHD1)	-0.21	2.59
NADH:ubiquinone oxidoreductase core subunit S1 (NDUFS1)	-0.4	2.57
Solute carrier family 12 member 5 (SLC12A5)	-0.9	2.54
Solute carrier family 25 member 10 (SLC25A10)	-1.85	2.52
Translocase of inner mitochondrial membrane 8A (TIMM8A)	-0.71	2.49
Synaptojanin 1 (SYNJ1)	-0.23	2.48
Heat shock protein family A (Hsp70) member 4 (HSPA4)	-0.39	2.45
Glutamyl-prolyl-tRNA synthetase 1 (EPRS)	-0.39	2.43
ELAV like RNA binding protein 4 (ELAVL4)	-1.32	2.42
Solute carrier family 1 member 2 (SLC2A1)	-0.69	2.35
Nicotinate phosphoribosyltransferase (NARPT)	-0.66	2.34
ATP synthase F1 subunit alpha (ATP5F1A)	-0.3	2.3
NADH:ubiquinone oxidoreductase complex assembly factor 4 (NDUFAF4)	-0.69	2.29
Ubiquinol-cytochrome c reductase complex III subunit VII (UQCRQ)	-0.39	2.29
Mono-ADP ribosylhydrolase 1 (MACROD1)	-1.98	2.27
NADH:ubiquinone oxidoreductase subunit A5 (NDUFS4)	-0.45	2.27
NADH:ubiquinone oxidoreductase subunit A9 (NDUFA9)	-0.49	2.25
Parvalbumin (PVALB)	-1.64	2.23
Phenylalanyl-tRNA synthetase subunit alpha (FARSA)	-0.95	2.21
LIM domain kinase 1 (LIMK1)	-0.48	2.18
Phenylalanyl-tRNA synthetase subunit beta (FARSB)	-0.86	2.17

Appendices

Protein kinase C alpha (PRKCA)	0.3	2.33
Serpin family B member 6 (SERPINB6)	0.47	2.33
Profilin 1 (PFN1)	0.3	2.31
Aldo-keto reductase family 1 member C3 (AKR1C3)	0.82	2.29
Solute carrier family 4 member 3 (SLC4A3)	0.96	2.29
NAC alpha domain containing (NACAD)	0.68	2.27
Syntrophin alpha 1 (SNTA1)	0.47	2.26
Glutathione S-transferase mu 2 (GSTM2)	0.56	2.26
BAG cochaperone 3 (BAG3)	0.8	2.26
Small ubiquitin like modifier 2 (SUMO2)	0.91	2.26
S100 calcium binding protein A9 (S100A9)	1.96	2.24
Ectonucleoside triphosphate diphosphohydrolase 2 (ENTPD2)	1.42	2.22
Ferritin light chain (FTL)	0.85	2.19
Transglutaminase 2 (TGM2)	1.25	2.16
Spectrin alpha chain (SPTAN1)	2.18	2.12

Appendices

Table A9. GO Molecular pathways enrichment in the substantia nigra of PSP cases using differentially expressed proteins

Pathways	Fold Enrichment	Protein count	total pathway proteins	%	Proteins	enrichment false discovery rate
GO:0005200 structural constituent of cytoskeleton	2.4	11	114	9.6%	VIM GFAP INA PLEC SYNM CROCC ADD3 SPTBN2 EPB41L3 MSN SPTAN1	1.2E-09
GO:0005543 phospholipid binding	2.1	16	488	3.3%	CAPG AMPH CPNE3 APOA1 ANXA1 APOA2 ANXA2 ANXA6 FERMT2 PFN1 IQGAP1 PLCD1 ANXA4 SPTBN2 TOM1L2 PEBP1	4.6E-05
GO:0016491 oxidoreductase activity	1.8	25	820	3.0%	AKR7A2 MAOB OGDH NDUFS8 BBOX1 PDHA1 ALDH1L1 PDHB AKR1C3 OGDHL GSTP1 PDHX PRDX1 GMPR ALDH7A1 PHYHD1 GSTM2 SELENBP1 NDUFV1 NDUFA9 COX6B1 NDUFA5 UQCRC1 COX5B COX5A	4.6E-05
GO:0008289 lipid binding	1.8	22	841	2.6%	CAPG AMPH CPNE3 APOA1 ANXA1 APOA2 FABP5 ANXA2 ANXA6 FERMT2 PFN1 IQGAP1 PLCD1 ANXA4 PEBP1 DBI SPTBN2 TOM1L2 GSTP1 GSTM2 ATP1A3 S100A9	1.6E-04
GO:0005215 transporter activity	1.7	26	1346	1.9%	SLC2A1 AQP4 ATP1A3 SLC1A2 ATP5F1B SLC4A3 SLC12A5 ATP5F1A ANXA2 SLC25A10 ANXA6 ATP5F1D APOA1 APOA2 NDUFS8 ATP1B1 NDUFV1 CPLX1 S100A6 FABP5 COX6B1 NDUFA5 NDUFA9 UQCRC1 COX5B COX5A	3.0E-04
GO:0003779 actin binding	1.8	22	476	4.6%	CAPG EZR PFN1 LCP1 IQGAP1 TPM3 MSN ADD3 PDLIM5 MAP1A SPTBN2 ANXA6 SPTAN1 MYH9 FLNA CROCC FERMT2 EPB41L3 SNTA1 FLNC PLEC GMFB	6.2E-04
GO:0005509 calcium ion binding	1.8	20	775	2.6%	SPARC ANXA1 S100A11 S100A9 ANXA2 ANXA4 ANXA6 S100A6 SNCB SRI IQGAP1 TGM2 CAPG CAPS NCAN LCP1 CAPN2 PLCD1 SPTAN1 SLC1A2	7.8E-04
GO:0015399 primary active transmembrane transporter activity	2.2	11	215	5.1%	ATP1A3 NDUFS8 ATP5F1B ATP1B1 NDUFV1 COX6B1 NDUFA5 NDUFA9 UQCRC1 COX5B COX5A	8.9E-04
GO:0005198 structural molecule activity	1.8	17	908	1.9%	VIM GFAP INA CSRP1 SPTBN2 PLEC SYNM HSPB6 CROCC EPB41L3 SNTA1 ADD3 AHNAK MAP1A SPARC MSN SPTAN1	9.1E-03
GO:0050839 cell adhesion molecule binding	1.6	30	594	5.1%	CAPG EZR HSP90AB1 MYH9 EIF5 PFN1 RTN4 PRDX1 VAPB AHNAK ANXA1 IQGAP1 BAG3 TAGLN2 PDLIM5 S100A11 CTNNB1 SPTBN2 PLEC ANXA2 FLNA SPTAN1 EEF1G FERMT2 MSN CTNND2 CNTN2 GFAP LCP1 PRKCA	9.2E-03

Appendices

Table A10. Cellular pathways enrichment in the substantia nigra of PSP cases using differentially expressed proteins

Pathways	Fold Enrichment	Gene count	Total Pathway Genes	%	Proteins	enrichment false discovery rate
GO:0098798 mitochondrial protein-containing complex	2.2	20	339	5.9%	HSPA9 ATP5F1D NDUFS8 ATP5F1B NDUFA5 ATP5F1A UQCRQ NDUFV1 PDHB COX5A NDUFA13 NDUFA9 UQCRC2 UQCRC1 TIMM8A COX5B COX6C PDHX COX6B1 PDHA1	5.9E-04
GO:0098800 inner mitochondrial membrane protein complex	2.2	16	188	8.5%	HSPA9 ATP5F1D NDUFS8 ATP5F1B NDUFA5 ATP5F1A UQCRQ NDUFV1 COX5A NDUFA13 NDUFA9 UQCRC2 UQCRC1 COX5B COX6C COX6B1	1.4E-03
GO:0098803 respiratory chain complex	2.4	12	110	10.9%	NDUFS8 COX6B1 NDUFA5 UQCRQ NDUFV1 COX5A NDUFA13 NDUFA9 UQCRC2 UQCRC1 COX5B COX6C	3.5E-03
GO:0005759 mitochondrial matrix	1.9	21	520	4.0%	TSFM PDHB OAT ATP5F1B HSPA9 LRPPRC NDUFA9 OGDHL NFS1 OGDH PDHX GLS DLST PDHA1 ATP5F1D ACO2 NDUFS8 SUCLA2 ATP5F1A ALDH7A1 GFM1	4.1E-03
GO:1990204 oxidoreductase complex	2.1	15	154	9.7%	OGDH PDHX NDUFS8 NDUFA5 UQCRQ NDUFV1 PDHB NDUFA13 OGDHL DLST PDHA1 NDUFA9 UQCRC2 UQCRC1 GMPR	7.3E-03
GO:0005739 mitochondrion	1.4	51	1830	2.8%	UQCRC1 MAOB HSP90AB1 ACO2 ATP5F1B HSPA9 DLST SLIRP TIMM8A PDHA1 SUCLA2 UQCRC2 ATP5F1A PRKCA ATP5F1D OGDH PDHX NDUFS8 TSFM NDUFAF4 COX6B1 NDUFA5 BBOX1 NDUFA9 UQCRQ NDUFV1 PDHB GFM1 COX5A NDUFA13 OGDHL TGM2 NFS1 OAT HSP90AA1 GSTP1 CPNE3 GLS LGALS3 COX5B LRPPRC ALDH7A1 COX6C SLC25A10 ACOT7 MAPK1 ASS1 SQSTM1 CAPN2 PLEC ANXA6	1.0E-02
GO:0005746 mitochondrial respirasome	2.2	12	114	10.5%	NDUFS8 NDUFA5 UQCRQ NDUFV1 COX5A NDUFA13 NDUFA9 UQCRC2 UQCRC1 COX5B COX6C COX6B1	1.1E-02
GO:0070469 respirasome	2.2	12	121	9.9%	NDUFS8 COX6B1 NDUFA5 UQCRQ NDUFV1 COX5A NDUFA13 NDUFA9 UQCRC2 UQCRC1 COX5B COX6C	1.1E-02
GO:0030016 myofibril	2.0	15	250	6.0%	AHNAK CSRP1 PDLIM5 SYNM SRI FERMT2 HSPB1 SLC2A1 FLNC BAG3 SQSTM1 CTNNB1 PLEC FLNA TPM3	1.4E-02
GO:0043292 contractile fiber	2.0	15	260	5.8%	AHNAK CSRP1 PDLIM5 SYNM SRI FERMT2 HSPB1 SLC2A1 FLNC BAG3 SQSTM1 CTNNB1 PLEC FLNA TPM3	1.4E-02

Appendices

Table A11. GO KEGG pathways enrichment in the substantia nigra of PSP cases using differentially expressed proteins

Pathways	Fold Enrichment	Protein count	Total Pathway proteins	%	Proteins	enrichment false discovery rate
Path:hsa01100 Metabolic pathways	1.9	53	1538	3.4%	NAMPT ALDH1L1 PLCD3 COX5B COX6B1 COX6C DLST AK1 ESD FAH PGLS GBE1 UQCRQ GLS GMPR GSTM2 GSTP1 GYG1 PSAT1 HNMT LTA4H MAOB ASS1 N NDUFA9 NDUFV1 NDUFS8 OAT OGDH ATP5F1A ACO2 ALDH7A1 ATP5F1B LAP3 NDUFA13 ATP5F1D PDHA1 PDHB PGAM2 PLCD1 OGDHL PYGL UQCF PDHX BBOX1 AKR1C3 SUCLA2 SYNJ1 SELENBP1 NFS1 COX5A ENTPD2	1.2E-09
Path:hsa05012 Parkinson disease	2.4	16	266	6.0%	COX5B COX6B1 COX6C UQCRQ MAOB NDUFA5 NDUFA9 NDUFV1 NDUFS8 ATP5F1A ATP5F1B NDUFA13 ATP5F1D UQCRC1 UQCRC2 COX5A	4.6E-05
Path:hsa05415 Diabetic cardiomyopathy	2.3	19	203	9.4%	COX5B COX6B1 COX6C UQCRQ NDUFA5 NDUFA9 NDUFV1 NDUFS8 ATP5F1A ATP5F1B NDUFA13 ATP5F1D PDHA1 PDHB PRKCA SLC2A1 UQCRC1 UQCRC2 COX5A	4.6E-05
Path:hsa05016 Huntington disease	2.3	17	306	5.6%	COX5B COX6B1 COX6C UQCRQ NDUFA5 NDUFA9 NDUFV1 NDUFS8 ATP5F1A ATP5F1B NDUFA13 ATP5F1D SLC1A2 TGM2 UQCRC1 UQCRC2 COX5A	1.6E-04
Path:hsa00190 Oxidative phosphorylation	2.2	16	134	11.9%	COX5B COX6B1 COX6C UQCRQ NDUFA5 NDUFA9 NDUFV1 NDUFS8 ATP5F1A ATP5F1B NDUFA13 ATP5F1D LHPTP UQCRC1 UQCRC2 COX5A	3.0E-04
Path:hsa05020 Prion disease	2.1	17	273	6.2%	COX5B COX6B1 COX6C UQCRQ NCAM1 NDUFA5 NDUFA9 NDUFV1 NDUFS8 ATP5F1A ATP5F1B NDUFA13 ATP5F1D MAPK1 UQCRC1 UQCRC2 COX5A	6.2E-04
Path:hsa04932 Non-alcoholic fatty liver disease	2.4	12	155	7.7%	COX5B COX6B1 COX6C UQCRQ NDUFA5 NDUFA9 NDUFV1 NDUFS8 NDUFA13 UQCRC1 UQCRC2 COX5A	7.8E-04
Path:hsa05014 Amyotrophic lateral sclerosis	2.0	18	364	4.9%	COX5B COX6B1 COX6C UQCRQ NDUFA5 NDUFA9 NDUFV1 NDUFS8 ATP5F1A ATP5F1B NDUFA13 ATP5F1D PFN1 SLC1A2 UQCRC1 UQCRC2 VAPB COX5A	8.9E-04
Path:hsa04260 Cardiac muscle contraction	2.4	9	87	10.3%	COX5B COX6B1 COX6C UQCRQ ATP1A3 ATP1B1 TPM3 UQCRC1 UQCRC2	9.1E-03
Path:hsa05208 Chemical carcinogenesis-reactive oxygen species	1.8	19	223	8.5%	COX5B COX6B1 COX6C EPHX4 UQCRQ GSTM2 NDUFA5 NDUFA9 NDUFV1 NDUFS8 ATP5F1A ATP5F1B NDUFA13 ATP5F1D MAPK1 UQCRC1 UQCRC2 AKR1C3 COX5A	9.2E-03